

Identification of manual control behaviour to assess rotorcraft handling qualities

Yilmaz, Deniz

DOI

[10.4233/uuid:00fadafa-0e24-4176-b533-d4b908c91a73](https://doi.org/10.4233/uuid:00fadafa-0e24-4176-b533-d4b908c91a73)

Publication date

2018

Document Version

Final published version

Citation (APA)

Yilmaz, D. (2018). *Identification of manual control behaviour to assess rotorcraft handling qualities*. [Dissertation (TU Delft), Delft University of Technology]. <https://doi.org/10.4233/uuid:00fadafa-0e24-4176-b533-d4b908c91a73>

Important note

To cite this publication, please use the final published version (if applicable). Please check the document version above.

Copyright

Other than for strictly personal use, it is not permitted to download, forward or distribute the text or part of it, without the consent of the author(s) and/or copyright holder(s), unless the work is under an open content license such as Creative Commons.

Takedown policy

Please contact us and provide details if you believe this document breaches copyrights. We will remove access to the work immediately and investigate your claim.



**IDENTIFICATION OF
MANUAL CONTROL BEHAVIOUR
TO ASSESS ROTORCRAFT
HANDLING QUALITIES**

Deniz Yilmaz

**IDENTIFICATION OF MANUAL CONTROL BEHAVIOUR
TO ASSESS ROTORCRAFT HANDLING QUALITIES**

Deniz YILMAZ

ISBN 978-94-6186-966-1

Printed by Ipskamp Printing, Enschede, The Netherlands

Laura van Arkelen - van As (Vakker-Design)

Copyright © 2018 2018 by Deniz Yılmaz. All rights reserved. No part of this publication may be reproduced, stored in a retrieval system, or transmitted, in any form or by any means, electronic, mechanical, photocopying, recording, or otherwise, without the prior permission in writing from the proprietor.

IDENTIFICATION OF MANUAL CONTROL BEHAVIOUR TO ASSESS ROTORCRAFT HANDLING QUALITIES

Proefschrift

ter verkrijging van de graad van doctor
aan de Technische Universiteit Delft,
op gezag van de Rector Magnificus prof. dr. ir. T.H.J.J. van der Hagen,
voorzitter van het College voor Promoties,
in het openbaar te verdedigen op vrijdag 2 november 2018 om 15.00 uur

door

Deniz YILMAZ

ingenieur luchtvaart en ruimtevaart, Technische Universiteit van het Midden-Oosten,
Turkije
geboren te Samsun, Turkije

Dit proefschrift is goedgekeurd door de promotor:

prof. dr. ir. M. Mulder

Copromotoren:

dr. ir. M. D. Pavel

dr. ir. D. M. Pool

Samenstelling promotiecommissie:

Rector Magnificus,
Prof. dr. ir. M. Mulder,
Dr. ir. M. D. Pavel,
Dr. ir. D. M. Pool,

voorzitter
Technische Universiteit Delft, promotor
Technische Universiteit Delft, copromotor
Technische Universiteit Delft, copromotor

Onafhankelijke leden:

Prof. dr. ir. L.L.M. Veldhuis,
Prof. dr. ir. D.A. Abbink,
Prof. dr. P. Masarati,
Assoc. Prof. dr. I. Yavrucuk,

Technische Universiteit Delft
Technische Universiteit Delft
Politecnico di Milano
Technische Universiteit van het Midden-Oosten



Dit onderzoek is gefinancierd door het the European Union 7th Framework - ARISTOTEL (Aircraft and Rotorcraft Pilot Couplings - Tools and Techniques for Alleviation and Detection) project.

Keywords: Rotorcraft; Handling Qualities; Adverse Rotorcraft Pilot Couplings; Manual Control Behaviour Identification; Pilot Modeling; Pilot Induced Oscillations...

Printed by: Ipskamp Printing, Enschede, The Netherlands

Front & Back: Designed by Laura van Arkelen - van As (Vakker-Design).

ISBN 978-94-6186-966-1

An electronic version of this dissertation is available at
<http://repository.tudelft.nl/>

Copyright © 2018 by Deniz Yilmaz. All rights reserved. No part of this publication may be reproduced, stored in a retrieval system, or transmitted, in any form or by any means, electronic, mechanical, photocopying, recording, or otherwise, without the prior permission in writing from the proprietor.

to my wife and family

SUMMARY

Identification of Manual Control Behaviour to Assess Rotorcraft Handling Qualities

Deniz Yilmaz

Flight safety has been a fundamental aspect of aircraft, and the future demand for wider usage of aerial operations leads to more focus on the flight safety. Particularly rotorcraft require high standards of flight safety due to their inherent features, such as complicated rotary mechanisms, close-to-ground operations, and complex aerodynamic environment. Consequently, rotorcraft pilots need to exert relatively high workload to safely operate these vehicles. An understanding of the interaction between the rotorcraft and the pilot is essential for improving flight safety. This interaction is elaborated by the Handling Qualities (HQ) discipline, which aims to identify and, if possible predict any deficiency in HQ that could potentially jeopardize safe flight.

A typical (and potentially catastrophic) example of a HQ deficiency are the Aircraft / Rotorcraft Pilot Couplings (A/RPC), formerly referred to as Pilot Induced Oscillations (PIO). A/RPC is defined as the involuntary and adverse interaction between the *pilot* and the *vehicle* under control. Generally for rotorcraft, the '*vehicle*' part of this interaction is evaluated by objective HQ criteria and online Rotorcraft Pilot Coupling (RPC) detection tools, whereas the '*pilot*' part is assessed with subjective pilot ratings. Using subjective ratings has several disadvantages, such as being used at very late stages of the design when a prototype vehicle is already built. Addressing a serious HQ deficiency after this late design stage then requires immense effort to re-design the vehicle systems and repeat the flight tests.

Considering the involvement of the '*pilot*' aspect of the HQ and RPC at an earlier stage of the design, some HQ criteria explicitly include 'paper pilot' models, which are essentially calculated models to meet predefined criteria requirements (e.g., the closed-loop resonance peak in the Neal-Smith criterion). However, these criteria are solely originated from dedicated fixed-wing flight tests, and the paper pilot models of these criteria could considerably deviate from the actual pilot behaviour due to the predefined criteria constraints.

Considering the limitations of the objective HQ criteria in terms of pilot modeling, and the drawbacks of the subjective pilot ratings of HQ and RPC, there is a scientific gap in the 'objective' pilot model considerations, especially for determining rotorcraft HQ deficiencies and RPC tendencies at an early design phase. This thesis targets this scientific gap by introducing the identification of the manual control behaviour (i.e., through a cybernetic approach) into the HQ and RPC domains. A new methodology, called as the Manual Control Identification Method (MCIM), was developed to achieve this objective. This thesis presents how to utilize the MCIM to obtain objective measures (e.g., iden-

tified pilot model parameters) while correlating with the HQ assessments and the RPC susceptibility of a rotorcraft model.

In MCIM, there are two important independent variables: the ***added time delay*** and the ***task difficulty***. The ***added time delay*** is a typical linear RPC trigger, which can lead the pilot to exhibit control behaviour that can cause the Pilot Vehicle System (PVS) to become out-of-phase. If the pilot continues to apply a tight-control during such a situation, the initiated RPC may quickly proceed to a become severe RPC event. A remedy to avoid further development of an initiated RPC event is the ‘back-off’ control strategy, during which the pilot reduces his/her control compensation to let the PVS to return to a more stable state. Another condition that would require the pilot to exhibit such a ‘back-off’ control strategy is the *crossover regression*. This phenomenon occurs during a human-in-the-loop control task, when the ***task difficulty*** is increased (e.g., increased task bandwidth). Consequently, human operators may need to regress the open-loop crossover frequency, which is fundamentally important while analysing closed-loop piloting tasks. Since the system stability is determined by the open-loop gain and phase characteristics near this frequency, a noticeable reduction of the crossover frequency can be interpreted as a HQ measure, such that the PVS could not achieve the same performance as before the crossover regression happened.

Considering the two independent variables (i.e., the added time delay and the task difficulty), there are five development steps of the MCIM. First, a rotorcraft model is developed with the capability of simulating the added time delay. At the second step, a compensatory task is designed to be used for the identification of the manual control behaviour, with various task difficulties. The third step is preparing a simulator experiment campaign to identify the manual control behaviour, such that human operators are subjected to experiment conditions with varied combinations of task difficulties and added time delays. The fourth step is analysing the measured data gathered from the manual control identification experiments, and compare parameters of identified human operator models and observe deviations between configurations. At this step of the MCIM, frequency and time domain identification techniques are utilized, namely the Fourier Coefficients Method with Optimization and the Maximum Likelihood Estimation, respectively. The fifth step is using RPC detection tools, which are the Realtime Oscillation Verifier (ROVER) and the Phase Aggression Criteria (PAC), to investigate the correlations between the observed manual control behaviour changes and the RPC tendencies.

To test the applicability of the MCIM, two preliminary identification experiments were designed, conducted and analysed. During these experiments, task difficulty was kept constant, while solely focusing on the changes in the manual control behaviour when additional time delay was inserted to the rotorcraft model. The first experiment was conducted in TU Delft’s SIMONA Research Simulator (SRS) with a roll-axis rotorcraft model during a disturbance-rejection task. In addition to the added time delay, the sensitivity of the control manipulator (i.e., the cyclic inceptor) was doubled. Identification results showed that human operators simply adapted their control gains while the remaining identified parameters did not show any significant variation between the same added time delay conditions. However, there was a noticeable reduction of the crossover frequency between the added delay conditions. Identified pilot parameters indicated that the pilot visual gain, and the neuromuscular natural frequency were de-

creased, whereas the lead compensation was increased.

The second preliminary experiment was conducted in the HeliFlight Helicopter Simulator (HHS) at the University of Liverpool (UoL) with a pitch-axis rotorcraft model with three levels of added time delay conditions (i.e., none, medium and high values of added delays). Between the none added and the medium added time delay conditions, crossover regression was not observed, however, the high added delay condition resulted in regression behaviour. When the added time delay was increased, the identified pilot model parameters showed that pilots had lower visual gain and neuromuscular natural frequency, and higher lead compensation. In both identification experiments, RPC detection tools in the MCIM (i.e., ROVER and PAC) indicated higher RPC susceptibility with increased added time delay, and correlated well with the identified manual control behaviour. Moreover, RPC tools also indicated the signatures of the ‘back-off’ control strategy, such that the trend of the increased RPC susceptibility between the none to the medium added time delay was not followed for the condition that showed a crossover regression (i.e., the high added time delay). These preliminary identification experiments demonstrated the applicability of the MCIM, and indicated that **only** added time delay can already lead human operators to exhibit a crossover regression strategy, and also that the corresponding RPC susceptibility can be determined by the MCIM.

Based on the MCIM results of the preliminary identification experiments, a follow-up computer simulation study was performed. The aim of these simulations was to investigate the manual control behaviour, which yields the optimum task performance during the conditions in which the added time delay and the task difficulty were combined. Based on the design of the MCIM, the developed simulation framework contained a pilot model, and a rotorcraft model as a Controlled Element (CE) in a compensatory task. While keeping the pilot limitation parameters (i.e., the pilot delay and neuromuscular system parameters) constant, both pilot equalization parameters (i.e., visual gain and lead compensation) were varied. Pilot remnant was either neglected or added to the pilot control signal, based on the simulation conditions. In the simulation, high and low bandwidth forcing functions were utilized to represent the task difficulty, as a part of the MCIM. For each task difficulty condition, that is with any Power Spectrum Density distribution, the added time delay generally required lower pilot visual gain and higher lead time constant to achieve the optimum performance.

This trend of parameter variation matches well with the results obtained from the preliminary identification experiments. Furthermore, added time delay and increased task difficulty also generally lead to crossover regression in the simulation. Despite the matching general trend, it was also observed that measurement data obtained in preliminary experiment show slightly higher tracking errors, with higher visual gains and lower lead compensation as compared to the optimum performance. In other words, ‘real’ pilots may have aimed for considerably lower lead compensation than the simulation pilot model with the optimum performance. This situation resembles the drawback of the ‘paper pilot’ models in HQ, such that the constraints (i.e., yielding the theoretically minimum tracking error in this simulation study) could deviate from the actual pilot behaviour. Therefore, a set of pilot model identification experiments were conducted as a following step to this simulation framework, with the usage of the complete MCIM.

The MCIM experiment was conducted in the SRS at TU Delft with nine participants,

who were subjected to nine experiment configurations as combinations of added time delay (i.e., none, medium, high) and task difficulty (i.e., easy, medium, hard) conditions. As described in the MCIM, the task difficulty was varied by increasing the bandwidth of the disturbance forcing function, and the time delay was implemented as a transport delay in the CE. Identified parameters of the manual control behaviour showed that the visual gain and the lead time constant were the most important parameters that indicated the adaptation of the exhibited manual control behaviour for different task configurations. A recognizable change in the trend of decreasing visual gain and increasing lead time constant characterized the major adaptation of the manual control strategy among experiment task conditions. Moreover, crossover frequencies showed three clear regression tendencies. An example of a 'classical' crossover regression due to increased task difficulty, and two examples of crossover regression due to added time delay.

The most interesting crossover regression occurred during the medium task, between medium and high levels of added time delay. At this condition, identification results showed a clear reduction in the visual gain, and an increase in the lead compensation, such that the human operators reduced the open-loop crossover frequency noticeably. This condition could be considered as a 'back off' control strategy, during which human operators could be avoiding to apply any tight control due to limited PVS stability. Furthermore, phase margins also indicated a recognizable deviation at this condition. In addition, RPC susceptibility of the rotorcraft model remarkably increased between none and medium added time delay conditions. However, further added time delay (i.e., high time delay) demonstrated a reduction of the RPC tendency. During this 'back-off' condition, human operators might have changed their control strategy to avoid any further increased RPC susceptibility of the PVS.

Considering the objective of this thesis, the MCIM successfully demonstrated its ability to detect the configurations where the HQ and the RPC susceptibility of a designed rotorcraft recognizably deviate, by using **objective** measures such as the identified parameters of manual control behaviour. Therefore, it would be possible to determine time delay and task difficulty combinations which could result in a noticeable change of HQ and RPC susceptibility. Such objective measures could be used at an earlier stage of rotorcraft design, and both the added time delay and task difficulty limitations could be determined objectively without requiring any subjective rating or any constrained 'paper pilot' models.

Due to its Linear Time Invariant (LTI) structure, MCIM is not able perform well with strong non-linearities, such as a transition from a steady condition to a fully developed RPC event. Thus, this structure limits the applicability of the MCIM to the conditions before and after an RPC event. However, enhancing the MCIM with Linear Time Varying (LTV) capabilities (e.g., LTV pilot modeling) could allow to investigate the transition conditions of an RPC event. Another aspect of the MCIM to be investigated further could be the task design, which is limited to the single-axis in the MCIM. Although such a task design is easy to analyse, extending it to multi-axis tasks could be an important improvement, particularly for rotorcraft, which mainly contain multi-axis control during their regular operations. Moreover, adding physical motion of the simulator to the MCIM task could lead to a more realistic task, and allow MCIM to extend its capabilities to examine the manual control behaviour for RPC with the physical motion feedback.

SAMENVATTING

Bepaling van de besturingseigenschappen van hefschroefvliegtuigen door het identificeren van menselijk stuurgedrag

Deniz Yilmaz

Veiligheid is een cruciaal aspect in het ontwerp en gebruik van vliegtuigen en krijgt alleen maar meer aandacht vanwege de groeiende toekomstige vraag naar vliegen en luchtoperaties. Het garanderen van de vliegveiligheid is vooral ook van belang voor hefschroefvliegtuigen¹ (Engels: rotorcraft, een woord dat we in het vervolg hier gebruiken), die vanwege hun inherente eigenschappen, zoals een gecompliceerd rotormechanisme, maar ook door hun gebruik dichtbij de grond en in zeer complexe aerodynamische omgevingen, relatief risicovol zijn in het gebruik. Een direct gevolg daarvan is dat rotorcraft-vliegers vaak een hoge werkbelasting ervaren bij het uitvoeren van hun vluchten. Een goed begrip van de interactie tussen het voertuig en de vlieger is daarom essentieel voor het verbeteren van de vliegveiligheid. Traditioneel wordt deze interactie onderzocht in het onderzoeksveld van de besturingseigenschappen², wat zich richt op het aan het licht brengen, en zo mogelijk vroegtijdig voorspellen, van eventuele tekortkomingen in de besturingseigenschappen die het veilig gebruik in gevaar zouden kunnen brengen.

Een typerend en soms catastrofaal voorbeeld van problemen met besturingseigenschappen zijn zogeheten Aircraft/Rotorcraft Pilot Couplings (A/RPC, “vliegtuig/rotorcraft-piloot koppelingen”), in de wat oudere literatuur veelal Pilot-Induced Oscillations (PIO, “piloot-geïnduceerde oscillaties”) genoemd. Onder de definitie van A/RPC vallen alle onbedoelde en ongewenste interacties tussen de *vlieger* en het bestuurd *voertuig*. Voor rotorcraft wordt het ‘voertuig’ deel van deze interactie veelal geëvalueerd met objectieve hanteringscriteria en online tests voor de detectie van specifieke RPC symptomen. Het ‘vlieger’ deel wordt in het algemeen bepaald via subjectieve beoordelingen door ervaren vliegers. Vooral de afhankelijkheid van deze laatste, *subjectieve*, beoordelingen leidt tot verschillende beperkingen, met de meest in het oog springende het feit dat een volledig prototype voertuig beschikbaar moet zijn voordat er langs deze weg voor mogelijke RPC getest kan worden. Als in een dergelijk laat stadium van een ontwerptraject nog ernstige problemen met de besturingseigenschappen worden blootgelegd, is het herontwerp en het herhalen van de benodigde vliegproeven financieel bijna niet meer op te brengen.

Om de invloed van de vlieger op de besturingseigenschappen en RPC in vroegere fasen van het ontwerpproces te kunnen meenemen, hanteren enkele bekende criteria voor het beoordelen van besturingseigenschappen een zogenaamd ‘papieren’ vlieger-model: een wiskundig model van het stuurgedrag van een vlieger, ingesteld om te voldoen aan bepaalde vooraf gedefinieerde eisen (zoals bijvoorbeeld de resulterende resonantiepiek

¹De Engelse term “rotorcraft” is vertaald in “hefschroefvliegtuig” of “helikopter” in het Nederlandse.

²De Engelse term “handling qualities” is vertaald in “besturingseigenschappen” in het Nederlandse.

in het zogenaamde “Neal-Smith criterium”). Deze criteria zijn echter bepaald uit specifieke vliegproeven met vliegtuigen met vaste vleugels, waardoor zowel de limieten van deze criteria, maar ook de -modellen die gebruikt worden voor vliegerstuurgedrag, aanzienlijk zouden kunnen afwijken van het besturen van een hefschroefvoertuig zoals een helikopter

Gezien deze beperkingen van de beschikbare vlieger-model-gebaseerde objectieve criteria voor besturingseigenschappen en de nadelen van subjectieve methoden voor het evalueren van besturingseigenschappen en RPC, bestaat er een wetenschappelijk hiaat in onze kennis over het ‘objectief’ modelleren van het stuurgedrag van vliegers voor het voorspellen van problemen met besturingseigenschappen en RPC voor rotorcraft, vroeg in het ontwerptraject. Dit proefschrift pakt dit hiaat direct aan door de identificatie van het handmatige besturingsgedrag (via een cybernetische, model-gebaseerde benadering) toe te passen binnen de domeinen van de besturingseigenschappen en RPC, waarvoor een nieuwe methodologie, de “Manual Control Identification Method” (MCIM, de “identificatie methode voor menselijk stuurgedrag”), is ontwikkeld. Dit proefschrift beschrijft hoe de MCIM gebruikt kan worden om objectieve meetdata te verzamelen en te analyseren (bijvoorbeeld in de vorm van de geïdentificeerde parameters van een vliegermodel) en te bewijzen hoe deze data correleren met subjectieve beoordelingen van de besturingseigenschappen en de RPC gevoeligheid van een bestuurd rotorcraft-model.

Binnen de MCIM wordt gewerkt met twee belangrijke onafhankelijke variabelen: (1) de aan de voertuigdynamica **toegevoegde tijdsvertraging**, en (2) de **moeilijkheid van de besturingstaak**. **Toegevoegde tijdsvertraging** is een bekende oorzaak van lineaire RPC doordat de vlieger stuurgedrag kan gaan vertonen waardoor het “Pilot Vehicle System” (PVS, het “piloot-voertuig systeem”) uit fase kan raken. Als vliegers in zo’n geval met een hoge bandbreedte blijven sturen kan een beginnende RPC zich snel ontwikkelen tot een ernstige, volledige RPC. Verdere ontwikkeling van een geïnitieerde RPC kan worden voorkomen als de vlieger zijn of haar besturingsbandbreedte vermindert om de PVS naar een stabielere staat terug te brengen, een zogenaamde ‘back-off’ stuurstrategie. Een tweede geval waarin vliegers een dergelijke ‘back-off’ stuurstrategie aannemen wordt in de literatuur ook wel *crossover-regressie* genoemd. Dit verschijnsel doet zich voor tijdens handmatige stuurtaken wanneer de **moeilijkheid van de besturingstaak** wordt verhoogd tot een bepaald niveau (bijvoorbeeld via verhoogde opgelegde taakbandbreedte). Boven een bepaalde taakmoeilijkheid zullen menselijke bestuurders gedwongen worden de open-lus crossover-frequentie te verlagen, een situatie die van fundamenteel belang is bij het analyseren van stuurtaken in gesloten lus. Aangezien de stabiliteit van het gesloten-lus systeem wordt bepaald door de versterkings- en fasekarakteristieken van de open lus dynamica in de buurt van de crossover-frequentie, kan een merkbare verlaging van de crossover-frequentie worden geïnterpreteerd als een maat voor verslechterde besturingseigenschappen, aangezien deze aanpassing nodig is om vergelijkbare acceptabele PVS prestaties te halen als onder nominale condities.

De ontwikkelde MCIM bestaat uit vijf onderzoeksstappen, waarin de twee bovengenoemde onafhankelijke variabelen een belangrijke rol hebben. Eerst wordt een nominaal rotorcraft-model gekozen en geïmplementeerd met de mogelijkheid een extra tijdsvertraging aan het model toe te voegen. In de tweede stap wordt een “compensa-

tory tracking"-taak ontworpen om het handmatige stuurgedrag van vliegers te kunnen identificeren met verschillende taakmoeilijkheden. De derde stap is het uitvoeren van simulator experimenten om menselijke stuurdata te verzamelen voor verschillende combinaties van de moeilijkheid van de taak en de toegevoegde tijdsvertraging. De vierde stap bestaat uit het analyseren van de verzamelde experimentele gegevens, om op basis van geschatte parameters van geïdentificeerde menselijke stuurmodellen veranderingen in stuurgedrag tussen verschillende configuraties te kunnen detecteren. Hier worden zowel frequentiedomein- (bijvoorbeeld de Fourier Coëfficiënten Methode) als tijdsdomein-identificatietechnieken (bijvoorbeeld de Maximum Likelihood Estimation) toegepast. De vijfde stap bestaat uit het toepassen van gangbare RPC detectietechnieken, dwz. Realtime Oscillation Verifier (ROVER) en Phase Aggression Criteria (PAC), om de geïdentificeerde aanpassingen in stuurgedrag te kunnen correleren met het neigen naar de ontwikkeling van een RPC.

Om de toepasbaarheid van de MCIM te testen zijn twee voorbereidende identificatie experimenten ontworpen, uitgevoerd en geanalyseerd. Bij deze eerste experimenten is de moeilijkheid van de taak niet gevarieerd en lag de focus op het meten van stuurgedragsveranderingen als gevolg van toegevoegde tijdsvertraging in het rotorcraft-model. Het eerste experiment is uitgevoerd in de SIMONA Research Simulator (SRS) van de TU Delft en instrueerde test-vliegers om een verstoringstaak om de rol-as van een rotorcraft-model uit te voeren. Naast het variëren van de toegevoegde tijdsvertraging werd in dit experiment ook de gevoeligheid van het stuurorgaan (d.w.z. de "laterale cyclic" van een rotorcraft) verdubbeld. De identificatieresultaten toonden aan dat vliegers simpelweg hun eigen stuurversterkingfactor aanpassen aan de verhoogde gevoeligheid van het stuurorgaan, terwijl de andere geïdentificeerde stuurparameters geen merkbare verschillen tussen condities met dezelfde toegevoegde tijdsvertraging lieten zien. De verschillende instellingen van de tijdsvertraging lieten een duidelijke verlaging van de crossover-frequentie zien bij een verhoogde toegevoegde tijdsvertraging. De geïdentificeerde stuurparameters lieten verder zien dat de visuele versterkingsfactor van de vliegers en de natuurlijke frequentie van hun neuromusculaire systeem waren afgenomen, terwijl door de vliegers meer "lead"-compensatie werd toegepast.

Het tweede voorbereidende experiment is uitgevoerd in de HeliFlight Helicopter Simulator (HHS) van de University of Liverpool (UoL). In dit experiment bestuurden vliegers de dwars-as (pitch) van een rotorcraft-model met drie waarden van toegevoegde tijdsvertraging: geen, een gematigde en een hoge toegevoegde vertraging. Bij het toevoegen van een gematigde tijdsvertraging werd geen crossover-regressie waargenomen, maar de hoge toegevoegde tijdsvertraging resulteerde duidelijk in een regressie in het stuurgedrag. De geïdentificeerde stuurparameters lieten zien dat met toenemende toegevoegde tijdsvertraging de vliegers ook in dit experiment een lagere visuele versterkingsfactor, een lagere natuurlijke frequentie van hun neuromusculaire systeem en een verhoging van hun "lead"-compensatie verkozen. In beide voorbereidende experimenten bevestigden de binnen MCIM gebruikte RPC detectietechnieken (d.w.z., ROVER en PAC) de hogere ontvankelijkheid voor RPC bij condities met toegevoegde tijdsvertraging. Bovendien lieten deze RPC detectietechnieken ook de kenmerkende effecten van de 'back-off'-stuurstrategie die door vliegers bij hoge tijdsvertraging werd toegepast zien: de ontwikkeling richting verhoogde RPC gevoeligheid die zichtbaar was tussen condities zon-

der en met een gematigde tijdsvertraging werd niet doorgezet voor de hoogste toegevoegde vertraging, waarbij de vliegers crossover-regressie toepasten. Deze voorbereidende experimenten bewezen de toepasbaarheid van de MCIM en lieten verder zien dat zelfs alleen toegevoegde tijdsvertraging al tot crossover-regressie kan leiden en dat de onderliggende RPC-gevoeligheid met succes gekarakteriseerd wordt door de MCIM.

Op basis van de met de MCIM behaalde resultaten uit de twee voorbereidende experimenten is vervolgens een computersimulatie-studie uitgevoerd. Het doel van deze computersimulaties was om te onderzoeken hoe vliegers hun stuurgedrag mogelijk aanpassen aan variaties in zowel toegevoegde tijdsvertraging als de moeilijkheid van de taak, om telkens toch tot het optimale niveau van stuurprecisie te komen. In overeenkomst met de MCIM, was het ontwikkelde simulatieprogramma opgezet als een compensatory stuurtaak waarin een vliegermodel in gesloten lus een rotorcraft-model bestuurdde als het Controlled Element (CE, "bestuurde element"). In de simulaties waren de parameters die natuurlijke stuurgedragsbeperkingen modelleren (d.w.z., de tijdsvertraging van de vlieger en neuromusculaire systeemdynamica) constant gehouden, terwijl de twee parameters die de compensatie van de vlieger voor een bepaald CE beschrijven (d.w.z., de visuele versterkingsfactor en de "lead" tijdsconstante) vrij werden gevarieerd. De niet-lineaire deel ("remnant") van het vlieger stuurgedrag werd ofwel verwaarloosd of toegevoegd aan het gesimuleerde vlieger stuursignaal in twee verschillende gekozen instellingen voor de simulaties. Om de moeilijkheidsgraad van de taak te variëren werden in de simulaties verstoringssignalen op het CE met hoge en lage bandbreedte getest. De computersimulaties lieten zien dat om met oplopende tijdsvertraging nog steeds optimale prestaties te bereiken vliegers een lagere visuele versterkingsfactor en een hogere "lead" tijdsconstante moeten aannemen en dat dit effect vrijwel onafhankelijk is van de moeilijkheid van de taak, d.w.z., de bandbreedte van het toegepaste verstoringssignaal.

De voorspelde stuurgedragsaanpassingen uit de computersimulaties komen erg goed overeen met de experimentele resultaten verkregen voor echte vliegers uit de voorbereidende simulatorexperimenten. Bovendien voorspellen de simulaties voor zowel toegevoegde tijdsvertraging als verhoogde moeilijkheid van de taak het optreden van crossover-regressie. Ondanks het goed voorspellen van relatieve veranderingen werd ook duidelijk dat de meetgegevens uit de voorbereidende experimenten iets grotere stuurfouten lieten zien dan de simulaties, met hogere visuele versterkingsfactoren en lagere "lead"-tijdsconstanten dan wat zou leiden tot optimale prestaties. Met andere woorden, 'echte' vliegers passen aanzienlijk minder "lead"-compensatie toe dan voorspeld door het simulatiemodel dat optimale prestaties nastreeft. Dit resultaat is consistent met een bekend probleem met de 'papieren' vlieger modellen die vaak worden toegepast in onderzoek naar besturingseigenschappen, namelijk dat de gestelde randvoorwaarden (d.w.z., het selecteren van de instelling die leidt tot de theoretisch minimale volgfout in de simulatiestudie) kunnen afwijken van de voorwaarden die het gedrag van echte vliegers bepalen. Om deze reden is volgend op de simulatiestudie een laatste identificatie-experiment uitgevoerd, waarbij de volledige MCIM in de praktijk is toegepast.

Het MCIM experiment werd uitgevoerd in de SRS aan de TU Delft met negen deelnemers, die werden onderworpen aan negen verschillende combinaties van toegevoegde tijdsvertraging (d.w.z., geen, gemiddeld of hoog) en moeilijkheidsniveau (d.w.z., makkelijk, gemiddeld of moeilijk). Het raamwerk van de MCIM volgend, werd de moeilijk-

heid van de taak gevarieerd met verschillende bandbreedtes voor het toegepaste verstoringssignaal en werd de toegevoegde vertraging geïmplementeerd als een vertraging in het CE. Geïdentificeerde stuurgedragsparameters lieten zien dat de aanpassingen in het toegepaste handmatige stuurgedrag over de verschillende taakconfiguraties het best zichtbaar waren in de visuele versterkingsfactor en de “lead”-tijdscontante. Een herkenbare discontinuïteit in de trends van afnemende visuele versterkingsfactor en een toenemende “lead”-tijdscontante kenmerkten de meest karakteristieke aanpassing in stuurgedrag over de verschillende experimentele condities. Bovendien liet het verloop van de crossover-frequentie drie duidelijke gevallen van crossover-regressie zien: de ‘klassieke’ crossover-regressie die optreedt bij hoge moeilijkheidsniveaus van de stuurtaak en twee voorbeelden van crossover-regressie door de extra tijdvertraging.

De meest interessante instantie van crossover-regressie vond plaats tijdens de taak van het gemiddelde moeilijkheidsniveau, tussen de gemiddelde en hoge toegevoegde tijdsvertragingscondities. Tussen deze twee condities lieten de identificatieresultaten een duidelijke verlaging van de visuele versterkingsfactor en een toename in “lead”-compensatie zien, waarmee de proefpersonen de open-lus crossover-frequentie merkbaar omlaag brachten. Deze gedragsverandering is kenmerkend voor de eerder genoemde ‘back-off’ stuurstrategie, waarbij menselijke bestuurders vermijden om echt strak te sturen vanwege de beperkte stabiliteit van het PVS. De bijbehorende fasemarges lieten ook een duidelijke afwijking zien bij dezelfde conditie. Bovendien nam ook de gemeten RPC-gevoeligheid van het rotorcraft-model duidelijk toe tussen de condities met geen en gemiddelde toegevoegde tijdsvertraging. Verdere toename in tijdsvertraging (d.w.z., de conditie met hoge tijdsvertraginginstelling) leidde echter tot een vermindering van de RPC-gevoeligheid. Dus, met deze ‘back-off’ strategie kiezen menselijke bestuurders ervoor om in dit soort kritieke gevallen de verdere toename in de RPC-gevoeligheid van het PVS te voorkomen.

Reflecterend op het doel van dit proefschrift, heeft de MCIM in de uitgevoerde studies laten zien het vermogen te hebben om configuraties waarin de besturingseigenschappen en de RPC-gevoeligheid van een rotorcraft herkenbaar afwijken met succes te detecteren, door te werken met objectief bepaalde metrieken zoals geïdentificeerde stuurgedragsparameters. Het is dus mogelijk om met deze methode de combinaties van toegevoegde tijdsvertraging en taakmoeilijkheid te bepalen die zullen resulteren in een merkbare verandering van de besturingseigenschappen en de gevoeligheid voor RPC. Deze objectieve aanpak zou nu in een eerder stadium van het rotorcraft-ontwerp kunnen worden toegepast om de voor het voertuig geldende beperkingen wat betreft tijdvertraging en taakmoeilijkheid objectief te bepalen, zonder dat daar subjectieve beoordelingen of een beperkte ‘papieren’ vlieger studies voor nodig zijn.

Vanwege het gebruik van Lineaire Tijds-Invariante (LTI) stuurgedragsanalyse is de MCIM niet toepasbaar op scenario’s met sterke niet-lineariteiten, zoals een instantane overgang van een stabiele toestand naar een volledig ontwikkelde RPC. Dit beperkt de toepasbaarheid van de MCIM tot analyse van situaties voor en na een echte RPC-gebeurtenis. Het uitbreiden van de MCIM met Lineaire Tijds-Variërende (LTV) analysetechnieken (d.w.z., LTV vliegeridentificatie) zou het expliciet onderzoeken van de overgangscondities rond een RPC-gebeurtenis mogelijk maken. Een tweede aspect van de MCIM dat verder moet worden uitgebouwd is de stuurtaak, die in de ontwikkelde MCIM beperkt

is tot het besturen van een enkele graad van vrijheid van het voertuig. Hoewel voor een dergelijke taak de analyse van het stuurgedrag eenvoudig is, is uitbreiding naar taken waar meerdere assen gelijktijdig worden bestuurd erg belangrijk, aangezien vooral ook bij rotorcraft in werkelijkheid altijd besturing op meerdere assen wordt uitgevoerd. Als laatste kan ook het toevoegen van de fysieke voertuigbeweging aan de MCIM taak leiden tot verbeterde toepasbaarheid op meer realistische taken en helpen bij het onderzoeken van het handmatige stuurgedrag van vliegers rond een RPC in aanwezigheid van fysieke bewegingsterugkoppeling.

CONTENTS

Summary	vii
Samenvatting	xi
1 Introduction	1
1.1 Handling qualities and adverse rotorcraft pilot couplings	1
1.1.1 Rotorcraft Pilot Couplings	2
1.1.2 RPC detection	3
1.1.3 Elements of a RPC	4
1.2 A closer look at pilot modeling	8
1.3 The scientific gap and the unique approach	10
1.4 Research question and methodology	11
1.5 Assumptions and limitations	13
1.6 Thesis Outline	13
2 Review: The link between rotorcraft HQ, pilot modeling and RPC	15
2.1 Introduction	15
2.2 Rotorcraft Handling Qualities	16
2.2.1 General definitions of handling and flying qualities	16
2.2.2 ADS-33 for the rotorcraft HQ.	18
2.3 Pilot modeling from Handling Qualities perspective	25
2.3.1 Control-theoretic pilot modeling.	25
2.3.2 Pilot models in HQ Criteria	30
2.4 Adverse Rotorcraft Pilot Couplings	34
2.4.1 Categories of RPC	35
2.4.2 Pilot Models in RPC events.	36
2.5 Time delay and Task Difficulty with HQ and RPC prospects	37
2.5.1 Effect of the time delay on HQ and RPC	37
2.5.2 Effect of the task difficulty on HQ and RPC.	41
2.5.3 Combined effect of the time delay and the task difficulty on HQ and RPC	45
2.6 Conclusions.	48
3 Methodology	51
3.1 Introduction	51
3.1.1 MCIM development	53
3.1.2 MCIM outline	55

3.2	Step 1: Rotorcraft model with added time delay in MCIM	58
3.2.1	Simplification I : Rigid Body/Rotor Couplings	61
3.2.2	Simplification II : Longitudinal/Lateral Couplings	63
3.2.3	Simplification III : Pitch(Roll) response	64
3.2.4	MCIM Rotorcraft model in ADS-33 terminology	66
3.3	Step 2: Task difficulty by forcing function bandwidth in MCIM	68
3.4	Step 3: Disturbance rejection task in MCIM	72
3.4.1	Display size and scale	73
3.4.2	Control Inceptor	73
3.4.3	Execution of identification experiments	74
3.5	Step 4: PVS analysis in MCIM	75
3.5.1	Pilot model in MCIM	76
3.5.2	Identification methods in MCIM	76
3.5.3	Pilot Model parameter and ω_c comparisons	79
3.6	Step 5: RPC detection in MCIM	80
3.6.1	RPC detection with ROVER	80
3.6.2	RPC detection with PAC	85
3.7	Conclusion	87
4	Preliminary Experiments on Manual Control Identification	89
4.1	Introduction	89
4.2	Preliminary Experiment I	91
4.2.1	Task Design	92
4.2.2	Independent variables	96
4.2.3	Experiment procedures	96
4.2.4	Dependent measures	97
4.2.5	Hypotheses	97
4.2.6	Methods used for analysing the experiment data	98
4.2.7	Results	99
4.2.8	Discussion on the first experiment	107
4.3	Preliminary Experiment II	109
4.3.1	Task Design	109
4.3.2	Independent variables	112
4.3.3	Experiment Procedures	112
4.3.4	Dependent Measures	112
4.3.5	Hypothesis	113
4.3.6	Methods Used for analysing the experiment data	113
4.3.7	Results	114
4.3.8	Discussion on the second experiment	120
4.4	Conclusions	121
5	Simulation Framework	123
5.1	Introduction	123
5.1.1	Methodology of the Simulation Framework	124

5.2	Simulation framework development	126
5.3	Simulation results.	129
5.3.1	Discrete PSD and The pilot model without remnant	130
5.3.2	Discrete PSD and pilot model with remnant	139
5.3.3	Comprehensive Results	143
5.3.4	Comparison to Experiment Conditions	144
5.4	Conclusions.	146
6	Manual Control Identification Method (MCIM) Experiment	149
6.1	Introduction	150
6.2	Task Design	150
6.2.1	Pitch Control Task	150
6.2.2	Rotorcraft model.	151
6.2.3	Apparatus and participants	152
6.2.4	Pilot model.	153
6.3	Independent variables	153
6.4	Experiment procedures	154
6.5	Dependent measures	155
6.6	Hypothesis	155
6.7	Methods used for analysing the experiment data	156
6.7.1	Identification methods.	156
6.7.2	Statistical analyses	157
6.7.3	RPC Detection	157
6.8	Results	158
6.8.1	Sample time histories	158
6.8.2	Task performance and Control activity.	160
6.8.3	Identified Pilot model parameters	161
6.8.4	Crossover frequencies and Phase Margins	165
6.8.5	ROVER and PAC results	167
6.9	Discussion	169
6.10	Conclusions.	171
7	Conclusions and Recommendations	173
7.1	Conclusions.	173
7.1.1	Theory	173
7.1.2	Development of the MCIM.	174
7.1.3	Application of the MCIM.	174
7.1.4	Conclusions on the MCIM steps	177
7.1.5	General conclusion	180
7.2	Recommendations	180
7.2.1	Step 1: Rotorcraft model	180
7.2.2	Step 2: Task difficulty.	181
7.2.3	Step 3: Disturbance-rejection task	182
7.2.4	Step 4: PVS analyses	183
7.2.5	Step 5: RPC Detection	183

References	185
A Subjective Rating Scales	197
A.1 Handling Qualities Rating Scale	198
A.2 Pilot Induced Oscillations Rating Scale	199
A.3 Adverse Pilot Coupling Scale	200
A.4 Workload Rating Scale	201
Acronyms	203
Nomenclature	206
Acknowledgements	207
CV	211
Publications	213

1

INTRODUCTION

1.1. HANDLING QUALITIES AND ADVERSE ROTORCRAFT PILOT COUPLINGS

Safety aspects of any flying machine consume an immense amount of effort and budget in aircraft development programs²³. With increased aviation activity in the last century, safety aspects have been integrated into the aircraft development programs starting from the initial design to the final operational phase of the vehicle⁵⁸. Although there has been extensive technological development in safety-aid tools, such as ground collision detection devices and fault-tolerant flight control systems¹⁴¹, flight safety remains a crucial issue in commercial and military vehicle certifications, regulations, flight test programs and regular operations⁸⁵.

In general, helicopters possess a high risk of flight safety due to complexity of the rotorcraft system. For instance, the main rotor of the rotorcraft is responsible of both propulsion and directional control of the vehicle, and any malfunction in the main rotor potentially creates a dangerous situation. In addition to the complex aerodynamic environment created by both main and tail rotors, nap-of-the-earth flying mission profiles also contribute to the flight safety risks of rotorcraft²⁹. Such flight safety risks have been addressed by safety regulation authorities and institutions. For example, the consortium of the International Helicopter Safety Team (IHST) has set a challenging goal of reducing the civil helicopter accident rate by 80% between 2006 and 2016⁸⁶. Although this goal was not completely achieved, the accident rate in key regions has decreased within a range of 40% to 60%, while the worldwide civil helicopter fleet has grown by 30% and the number of accidents has decreased up to 50%¹. Despite the encouraging worldwide efforts, which have resulted in international flight safety interventions (e.g., safety toolkits for helicopter operators¹³⁷), there is still a demand for improved helicopter flight safety¹.

Accident investigation reports of safety regulation and inspection authorities, such as IHST, show that *pilot loss of control* is, similar to fixed-wing aircraft, the most pronounced factor that threatens helicopter safety^{137,138}. There are numerous reasons for the loss of pilot control, such as inappropriate piloting techniques and rotorcraft malfunctions. Undoubtedly, the response characteristics of rotorcraft play a vital role in flight safety prospects. The interaction between the pilot control and the vehicle response is the essence of a broad and challenging research field in both fixed-wing and rotorcraft: Handling Qualities (HQ).

The common definition of HQ provided by Cooper and Harper¹⁹ is as follows; “*Handling qualities are those qualities or characteristics of an aircraft that govern the ease and precision with which a pilot is able to perform the tasks required in support of an aircraft role (p.6)*”. Considering this definition, which is also applicable to rotorcraft, deficiencies in HQ can potentially expose safety issues and require careful considerations.

1.1.1. ROTORCRAFT PILOT COUPLINGS

Among many possible HQ deficiencies threatening flight safety, one particular persistent and hazardous phenomenon has been troubling pilots, designers and flight program managers: Aircraft / Rotorcraft Pilot Couplings (A/RPC) formerly referred as Pilot Induced Oscillations (PIO). Briefly, A/RPC are ‘*unintended*’ and ‘*unfavourable*’ interactions between the pilot and the vehicle under control, and this phenomenon has been occurring since the first powered flight of mankind⁸⁵.

As an example inside a cockpit, a pilot comment in such an A/RPC event was²² “... *the airplane had never done anything like that before. It surprised me, it really shocked me... I thought something had broken and I didn't see any warning lights (p. 53)*”. Another example, a FedEx MD-11 experienced a PIO event while climbing out of Newark, New Jersey on 25th of November 2000¹⁰⁶. The first officer was manually flying and at a certain altitude the aircraft began to pitch up and down at a fast rate. The PIO continued until the autopilot was engaged. Post event analysis found a fault in one of the electronically-controlled hydraulic actuators that essentially gave the Stability Augmentation System (SAS) more authority than it was designed to have, leading to the undesired and unintended oscillations¹⁰⁶.

Another example is the low frequency lateral A/RPC encountered during flight experiments of the prototype tilt-rotor V-22 Osprey, which led to a ground collision¹¹⁰ as shown in Figure 1.1.

When compared to aircraft, rotorcraft are more prone to A/RPC due to their complexity which arises safety critical concerns, starting from the design phase¹¹⁵. For example, when a rotorcraft pilot exerts a control input during a manoeuvre, the main rotor responds to this control input and changes its orientation. During this transition of orientation, a time delay between the pilot control and vehicle response may occur, when combined with gyroscopic effects on the main rotor. In addition to this time delay, software delays and filter lags may contribute to high values of ‘effective’ time delay which

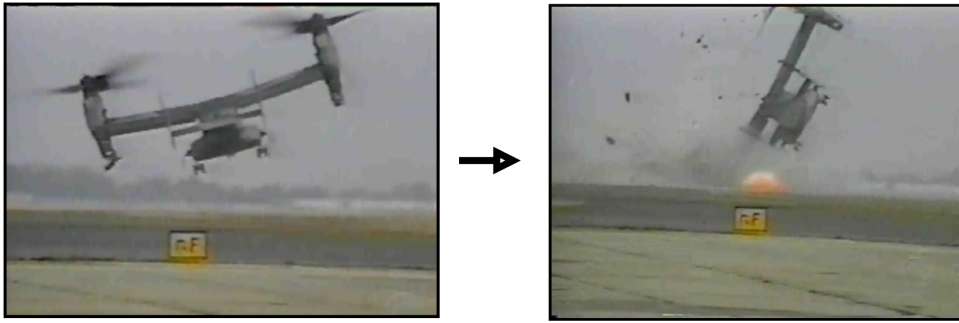


Figure 1.1: Crash of the prototype V-22 Osprey in 1991 during its initial test flight, pictures are taken from Ref. 73.

can be up to 250ms¹³⁴. It is worth mentioning that this amount of time delay is considerably higher when compared to typical delay values of fixed-wing aircraft. Moreover, the time delay is also known to be a trigger for RPC, such that a pilot may get into out-of-phase control with the vehicle response. For example, Ockier¹⁰⁸ investigated the effects of added time delay during a slalom-tracking task with an in-flight simulator rotorcraft (Bo-105 of German Aerospace Center (DLR)). Figure 1.2 illustrates a pronounced RPC situation observed in the mentioned study.

As it can be seen from the results of slalom-tracking task shown in Figure 1.2-a, with added time delay (160ms) in the roll control path (Figure 1.2-b) a RPC situation was pronounced between 20 and 25 seconds (Figure 1.2-c). A peak-to-peak pilot control behaviour was observed in this RPC event with a sort of see-saw like time traces which are a typical RPC symptom. In this example, combinations of the time delay and the demanding task lead to a RPC event to occur. The pilot commented “... *very poor HQ configuration (p. 239)*” for this particular flight sortie, and he perceived that the vehicle response was out-of-phase³⁵. In general, poor HQ is a candidate condition for high RPC tendency, especially when high pilot activity is required¹¹³.

1.1.2. RPC DETECTION

Since RPC events come as a surprise to pilots, detection of an RPC event as early as possible is crucial for rotorcraft safety. Several RPC tools have been developed and recognized by the aviation community to reveal the incipience and continuation of a potential RPC event. These detection tools solely use real-time flight test data, and they inherently aim to capture the out-of-phase control behaviour as early as possible. Then, any installed A/RPC suppression device in the cockpit activates, or the pilot in control is informed about the detected event. How to compensate for the A/RPC after detection depends on the integrated tool, or the pilot's technique within the specific task conditions^{85,92}.

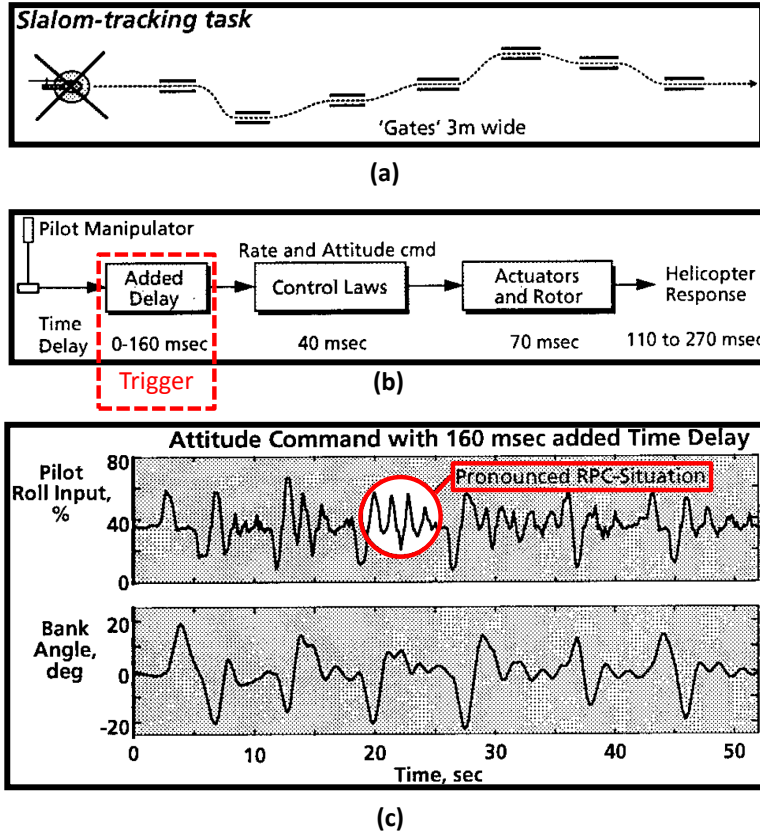


Figure 1.2: The slalom-tracking task (a), the added time delay to the pilot control manipulator (b) and time trace of a pronounced RPC , adapted from Ref. 35.

In principle, RPC detection tools aim to find peak pilot control inputs, and corresponding vehicle responses, and estimate the time difference between these two. Then, while running real-time during the flight, they evaluate the pilot control activity, vehicle response, severity of the delay and frequency of possible out-of-phase candidates. Two different RPC detection tools, Realtime Oscillation Verifier (ROVER)⁸⁸ and Phase Aggression Criteria (PAC)⁵² will be applied in this thesis as offline analysis tools to determine the RPC tendency. Details of these RPC detection tools will be covered in the methodology chapter (i.e., Chapter 3 of this thesis). It must be noted that these detection tools only function between input and output of the vehicle, and do not contain any information about the pilot's control strategy.

1.1.3. ELEMENTS OF A RPC

There are four main elements in a typical RPC event⁸⁵: the pilot, the vehicle, the task and the trigger. In an RPC scenario, the pilot should be controlling the vehicle in a demanding task, and the trigger should initiate a RPC event. The four elements of an RPC event

and their interactions are shown in Figure 1.3. Simulation and analysis of all elements shown in Figure 1.3 are important to understand the necessary dynamics behind a possible RPC event. The roles of the four elements can be summarized as:

- **The trigger:** Initiation of the RPC event.
- **The vehicle:** Flight dynamics response of the rotorcraft.
- **The task:** The operational conditions that unmask the HQ deficiency/RPC tendency.
- **The pilot:** Closing the control loop to achieve required performance and stability.

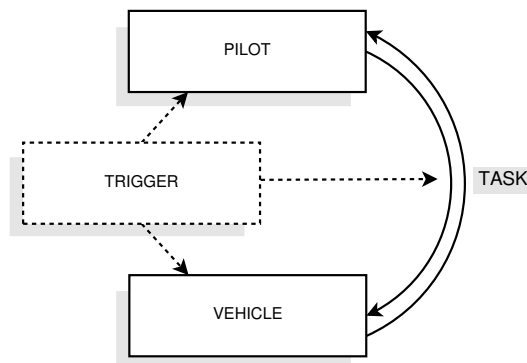


Figure 1.3: Four necessary elements of an RPC event.

① Trigger as an RPC element

Triggers are the factors that induce the A/RPC condition during a flying task containing a vehicle and a pilot in command. The primary effect of a trigger is unmasking the RPC potential of the PVS in a flying task. Triggers could be a sudden change in the vehicle dynamics, a hidden HQ deficiency that could be apparent in a demanding task or a change in the task. In all situations, they have the surprise effect on pilots such that they generally comment on an ‘unexpected’ response of the vehicle²².

The linearity of the trigger defines three categories of RPC. CAT I is the linear RPC which can be triggered by excessive lags, e.g., time delay. CAT II is the semi-linear RPC which can be initiated by rate-limiting in the control actuator. CAT III is the nonlinear RPC that can be triggered by a nonlinear element in the rotorcraft system, such as mode shifts in the flight director software⁸⁵. Only the CAT I category RPC will be investigated in this thesis.

② Vehicle as an RPC element

Primarily, the design of the vehicle determines its capability to perform a flying task. In principle, HQ aspects of the vehicle reflect this capability. If HQ deficiencies accumulate during a demanding rotorcraft task, it could quickly lead to a catastrophic danger to the

flight crew and the rotorcraft. Thus, understanding the vehicle HQ is crucial for preventing such occurrences.

In the rotorcraft community, the ADS-33 is the most widely used HQ qualifications. ADS-33 was used in the design stages of some recent rotorcraft development programs, such as the RAH-66 and NH-90 helicopters¹¹². ADS-33 utilizes different flight tasks, so-called Mission Task Element (MTE), with predefined task performance boundaries. Per each task, HQ charts show designated HQ by applying certain criteria. For example, like for the fixed-wing aircraft, one of the most widely used ADS-33 criteria is the Bandwidth Phase Delay (BPD). BPD is calculated by the response dynamics of the vehicle in the frequency domain. Basically, BPD determines two parameters of the vehicle model. First, the frequency at which the vehicle has sufficient stability to perform a selected MTE. Second, the available phase of the vehicle response at this frequency which is necessary to maintain the stability. BPD can be used to predict HQ of a rotorcraft if the frequency response is known or estimated during the design. Thus, a degradation in BPD criteria (i.e., a change in the vehicle dynamic response) may indicate an HQ deficiency and RPC proneness.

③ Task as a RPC element

Task is the element which keeps the pilot and the vehicle 'busy'. Demanding rotorcraft flying tasks possess a potential to drive the PVS into a dangerous instability¹¹¹. For example, a landing task on a helipad of a moving ship deck is a demanding task, and an additional gusty weather with lower visibility could drastically increase the RPC probability. If the vehicle has some HQ deficiencies, such a demanding task may unmask the unfavourable HQ characteristics which could be hidden during regular operations. Thus, the task difficulty can be considered as the operational template to bring the PVS into its performance and stability limit.

When the task difficulty is changed, pilots can exhibit different control strategies while flying an MTE. For example, in the Aircraft and Rotorcraft Pilot Couplings – Tools and Techniques for Alleviation and Detection (ARISTOTEL) project¹¹⁵ (a seventh framework European Union project dedicated to RPC research by using flight simulators), pilots exhibited different control strategies when the precision hover MTE of ADS-33 was changed with a more demanding task setup. With increased task difficulty, HQ deficiencies and RPC tendency of the rotorcraft became more pronounced, and pilots adjusted their control strategies accordingly.

④ Pilot as a RPC element

HQ and RPC assessments include two conventional methods to approach the pilot component of a PVS. These methods are the subjective pilot ratings and the mathematical pilot model considerations.

1. Subjective Pilot Ratings

Coherent to ADS-33 standards, the most common practice in HQ assessments is using subjective pilot ratings, such as Cooper-Harper Handling Qualities Ratings (HQR)¹⁹ for

HQ and Pilot Induced Oscillations Ratings (PIOR)¹³⁶ for PIO. Subjective ratings require pilots to assess the HQ of a flight test vehicle or a simulation model after completing a predefined task. Pilots award HQR and/or PIOR depending on how well the requirements of the task are met with the corresponding pilot workload. In principle, a rotorcraft with good HQ is awarded level-1, which reflects that the task at hand can be completed with a predefined desired performance with minimal pilot compensation. A level-2 HQ implies that the task can be completed just with adequate performance with great amount of pilot workload. At this level, HQ deficiencies warrant improvements. Finally, a level-3 HQ shows that there are major HQ deficiencies and the pilot can not attain adequate performance or need to apply intense pilot compensation or even abandon the task. Similarly, the PIOR indicates how much undesired oscillatory behaviour is experienced during the evaluation task. The higher the subjective ratings, the worse the RPC tendency.

Although using the subjective pilot ratings is a direct approach to assess the HQ of a rotorcraft, there are some drawbacks of this method. First, this evaluation is mainly applied at later stages of the design, such that there is already a prototype vehicle or a high fidelity simulation model. Bringing HQ considerations into the earlier stages of the rotorcraft design has been a quest for many researchers¹¹¹. If the rotorcraft is almost finalized with the complete design, and then if HQ are not awarded good enough, this would lead to additional budget cost and efforts to find a remedy and redesign the vehicle. Another drawback of using HQR is the need of proper training of the pilots to interpret the HQ evaluation tests. This kind of training requires specialized skills and experience to properly point out the possible HQ deficiency of the test vehicle³². As a result, only few pilots are available for such dedicated HQ experiments. Consequently, obtained results are generally statistically poor due to the limited number of participants. Related to this condition, another drawback is the variability of the HQR due to pilot subjectivity. This subjectivity issue has been reported in several test programs and flight simulator campaigns. For example, Mitchell⁸⁷ provides examples of a wide spread of pilot ratings for the same vehicle models with the same flight conditions, while conducting an RPC study.

II. Mathematical Pilot Model Considerations

Considering the critical role of the pilot in the HQ concept, several HQ criteria aim to model the pilot control behaviour mathematically for offline HQ predictions. Not only the vehicle response characteristics, but also mathematical pilot models are explicitly included in such HQ criteria. Two well-known HQ criteria using mathematical pilot models are the Neal-Smith¹⁰³ and the Handling Qualities Sensitivity Function (HQSF) criteria³⁹. The Neal-Smith criterion assumes a simple pilot model to represent the pilot control behaviour. This simple pilot model (so-called 'paper' pilot⁶⁶) is used in conjunction with the vehicle model and the HQ of the vehicle is determined according to the calculated PVS parameters. The Neal-Smith criterion have been mainly utilized for fixed-wing aircraft^{25,94}. The HQSF contains a similar approach to model the pilot but uses a more sophisticated pilot model. For example, the pilot neuromuscular dynamics are included in pilot model of the HQSF criteria³⁹.

Mathematical pilot models used in HQ criteria are theoretical models which contain general descriptions of the pilot with constrained parameters or adjusted settings. For example, the Neal-Smith criteria consider the pilot compensation at a predefined bandwidth frequency, and the HQSF assumes a constant crossover frequency and a constant neuromuscular setting of the pilot model. These kind of pilot models can be considered as adjustable controllers to achieve a predefined stability and performance of the PVS in a designed task.

Despite the pronounced simple and predictive form of mathematical pilot models of the Neal-Smith and HQSF criteria, representing an actual manual control strategy of a pilot requires a closer look. The next section will describe the overall pilot modeling concept in more details.

1.2. A CLOSER LOOK AT PILOT MODELING

Even at the later stages of the design phase, a simulation model of the vehicle can be available to be elaborated by engineering methods. However, human pilots are not designed to be vehicle controllers from birth. As a result, mathematically modeling a human pilot, who could be considered to be a superior controller with a complicated system of sensors, information processing, decision making and adaptive controlling, is an almost impossible task when considering the physiological and psychological complexities as well³⁹.

Despite this naturally highly non-linear human control behaviour, it has been delineated in the literature that pilots establish so-called 'behavioural control laws' in order to achieve a good (or adequate) performance with a given vehicle dynamics during a certain control task⁸⁰. These behavioural control laws benefits from quasi-linear describing function theory⁸⁰, which models the non-linear human control behaviour with a dominant linear part and a remaining non-linear counterpart which can not be captured by linear modeling techniques.

McRuer and Jex⁸⁰ defined several quasi-linear manual control behaviour models depending on the displayed information to the human operator. One of the most widely used models is obtained in the compensatory task, during which human operators only respond to the displayed error between the commanded reference signal and the current state of the vehicle response. A single axis compensatory task is illustrated in Figure 1.4.

As illustrated in Figure 1.4, a designed input signal, which is the target signal in this example, excites the closed-loop system. Then, the displayed error between this signal and the vehicle response causes the human operator to apply control inputs which result in a vehicle response. The input signal, which excites the closed-loop system, is called the forcing function which directly affects the task difficulty by its power spectrum. For example, when a multi-sine forcing function is used, powered frequencies of each sine signal define the Power Spectral Density (PSD) of this forcing function. Some human identification techniques, e.g., methods based on Fourier Coefficients¹⁴⁰, use these frequencies to identify the linear human operator control behaviour ($H_p(j\omega)$ in Figure 1.4). However, these techniques require low remnant levels, as high remnant indicates signs

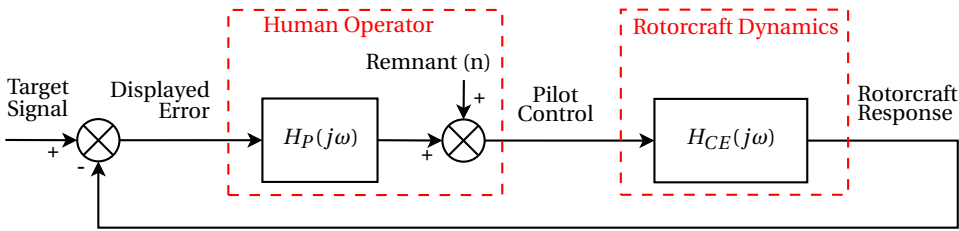


Figure 1.4: Schematic representation of a compensatory task. The human operator is modelled as the summation of the linear behaviour ($H_p(j\omega)$) and the remnant (n), which represents the non-linear control anticipation. The CE is represented by the linear rotorcraft dynamics which are shown as $H_{CE}(j\omega)$. Adapted from Refs. 26, 81, 83

of non-linearities and randomness in the control behaviour.

In order to obtain a mathematical control model of a human operator with minimized remnant during a compensatory task, an identification experiment is required. During such an experiment, data of the displayed error and the resulting pilot control anticipation (input and output of $H_p(j\omega)$ in Figure 1.4) are measured and processed. Various identification methods can be applied to the measured data. For example, the Fourier Coefficients¹⁴⁰ is a non-parametric frequency-domain identification technique, and the Maximum Likelihood Estimation (MLE)⁵⁷ is a parametric time-domain identification method. These methods will be discussed in detail in the next chapter.

By using the measured data, the result of a manual control identification process is a mathematical expression of a pilot model with parameters representing pilot compensation such as the pilot visual gain or the neuromuscular system. With all parameters combined, the identified pilot model aims to describe the relation between the input to the pilot, e.g., the displayed error, and the corresponding pilot input, e.g., cyclic manipulator input. By using this identified model, one can investigate the control behaviour changes between varied conditions and correlate these conditions with the change of pilot parameters.

In this identification context, the open-loop response of the combined human operator and the vehicle dynamics ($H_p(j\omega) * H_{CE}(j\omega)$ in Figure 1.4) can be used to analyse the stability of the PVS. One important feature of this open-loop response is the frequency region around the crossover frequency, where the open-loop amplitude response is 1 (or 0 dB). The system stability is determined by the open-loop characteristics near this crossover frequency. Moreover, the nature of the open-loop system near the crossover frequency determines the closed-loop modes and response⁸³.

1.3. THE SCIENTIFIC GAP AND THE UNIQUE APPROACH

McRuer et al.⁸⁰ found out that on certain conditions, a high power in the forcing function (i.e., high bandwidth of the target signal in Figure 1.4) can lead pilots to regress the crossover frequency of the open-loop PVS. This phenomenon is referred to as *crossover regression*, and it shows a noticeable change in pilot control behaviour. Several studies investigated this change, e.g., Damveld²⁰ used the crossover regression behaviour (achieved by changing the bandwidth of the forcing function) to assess the HQ of aeroelastic aircraft models in a pursuit tracking task. This thesis is based on the same principle idea: Human operators will change their control strategies when exposed to difficult tasks, and we can identify these changes using identification methods.

Considering the crossover regression phenomenon, McRuer and Jex⁸⁰ stated that under certain conditions when the manual control task becomes very difficult “... *the pilot regresses to a low gain technique and simply ignores the high-frequency input components (p. 238).*” Similarly, for A/RPC situations, Prouty¹²¹ describes the pilot control strategy for RPC prone conditions as: “*To avoid PIO, the pilot must 'back off' and operate at lower frequency-one that might not produce the precision he would like for compensating for turbulence or for tracking an enemy aircraft (p. 350).*” It can be seen that both crossover regression and RPC prone conditions suggest that human controllers try to limit their control anticipation to avoid unfavourable task conditions. Mainly, crossover regression studies focus on task difficulty, i.e., forcing function bandwidth, and HQ deficiency studies include vehicle originated instabilities, e.g., added time delay.

Subjective HQ rating studies of Smith et al.⁵ with fixed-wing aircraft showed that the combination of the trigger and the task difficulty lead to different results than their individual effects. Awarded HQR indicated a quicker degradation of HQ with added time delay when the task is more demanding. One of the drawbacks of this study was that it used subjective ratings which were prone to being scattered, i.e., the same condition was awarded good and poor HQ by different pilots, during demanding tasks⁸⁷. Another drawback was the determination of task difficulty, such that depending on the landing task in their study, task difficulties were arranged as ‘high’ and ‘low’ stress, which were not quantified measures^{47,120}.

Changing both the added time delay and the task difficulty could reveal the HQ deficiencies and the RPC tendency of the rotorcraft around a boundary which depends on both contributors. Current HQ assessments have not been used to **objectively** determine such boundary conditions formed by both task difficulty and added time delay. Regardless of such a demanding condition, limitations in theoretical pilot models in HQ criteria and pilot evaluations with possible subjectivity issues are known to be some of the drawbacks of current HQ assessment methods. For instance, the equivalent BPD criteria of fixed-wing aircraft have boundaries for PIO susceptibility, whereas there is no widely accepted PIO boundaries for rotorcraft yet. Moreover, Blanken et al.¹³ mention that one of the biggest issues of ADS-33 is the lack of information when the rotorcraft becomes RPC prone in HQ charts. In addition, Padfield¹¹¹ points out that the effect of task difficulty, i.e., task bandwidth, on HQ and RPC evaluations should be researched in

conjunction with available methods in ADS-33.

Hence, there is a scientific gap on the **objective** assessment of the HQ deficiency and RPC susceptibility of rotorcraft. The essential idea of this thesis is using identification of manual control behaviour as an objective method to observe the changes of PVS characteristics via varied manual control model parameters. This idea of combining objectivity of the manual control behaviour identification as in crossover regression phenomenon, with the vehicle triggered HQ deficiencies is summarized in Figure 1.5.

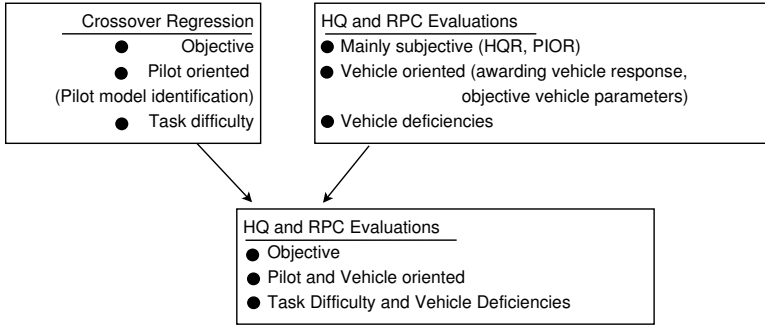


Figure 1.5: Using the crossover regression and vehicle oriented HQ deficiencies to develop a new approach to be used objectively.

By using the manual control behaviour identification, any changes in the estimated manual control model parameters could be studied when the PVS is subjected to a task with varied task difficulty and added time delay. In this way, already at early stages of the rotorcraft design an objective assessment of the HQ and RPC tendency could be obtained, rather than using subjective HQR ratings that often require an already developed flight test vehicle.

1.4. RESEARCH QUESTION AND METHODOLOGY

The main research question of this thesis can be stated as:

How can we objectively assess the HQ deficiency and RPC susceptibility of a rotorcraft at an early design stage?

In order to answer this question, HQ deficiency and RPC susceptibility are elaborated by changing **the task difficulty** and **the added time delay**. These conditions (individually and combined) are used in closed-loop manual control tasks that are designed to unmask the HQ deficiency and RPC susceptibility of the PVS. When such conditions possess HQ deficiencies and high RPC tendencies, human operators will try to adapt their manual control strategy accordingly. Through identification of the human operators manual control behaviour, an objective assessment can be done. A methodology,

referred to as the Manual Control Identification Method (MCIM), has been developed in this thesis to accomplish this goal. The following steps summarize the methodology;

- Step 1: Development of a rotorcraft model with the capability to simulate the added time delay.
- Step 2: Development of a forcing function design that can exhibit various task difficulties by changing the forcing function bandwidth.
- Step 3: Development of a disturbance-rejection task to be used in a manual control identification experiment campaign in a simulator, such that human operators are subjected to experiment conditions with varied combinations of task difficulties and added time delays.
- Step 4: Analyse the measured data gathered from the manual control identification experiments, and compare parameters of identified human operator models and observe deviations between configurations.
- Step 5: Use RPC detection tools to investigate the correlations between the manual control behaviour changes and RPC tendencies.

An example usage of these MCIM steps for the comparison of an identified manual control parameter by using the MCIM experiment setup (i.e., Step 3) in two scenarios (basis and RPC-prone) is illustrated in Figure 1.6.

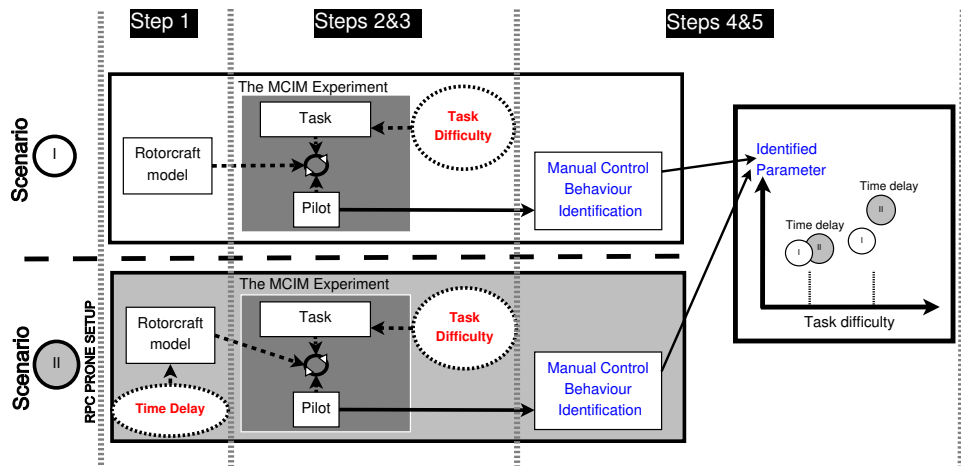


Figure 1.6: Graphical representation of the steps of the MCIM methodology for a basis (I) and a RPC prone (II) scenario in order to compare a sample identified manual control parameter.

As exemplified in Figure 1.6, the ultimate output of the MCIM allows for comparing the variation of manual control behaviour parameters (and corresponding RPC tendencies) for various task difficulties and time delay combinations.

1.5. ASSUMPTIONS AND LIMITATIONS

There are some assumptions and limitations considered in this thesis, as listed below:

- Identification procedures are carried out with Linear Time Invariant (LTI) models only. Thus, any non-linearities in the experiment setup are aimed to be minimized. For example, control loading systems in the identification experiments are utilized to exhibit linear behaviour, e.g., breakout forces are discarded.
- Since LTI models have been used, only CAT. I (i.e., linear) RPC are investigated.
- Simple, but yet still usable for HQ applications, on-axis rotorcraft models are considered. High frequency response of the main rotor is simplified by added time delay, and all cross-coupling and off-axis responses are neglected.
- Only compensatory displays, which are scaled-up attitude indicators, are used without any out-of-the-window visual cues for identification purposes.
- There is no physical motion in the identification experiments performed in the simulator, such that the compensatory task used in the identification experiment campaign is only a visual task.
- Since the task is a simple compensatory task, manual control behaviour of the non-pilot subjects is assumed to be close to professional pilot responses.
- Especially for the highly demanding task conditions, linear manual control behaviour is assumed to be achieved after five to six experiment runs with steady task performance.
- This thesis does not aim to identify the manual control behaviour in a fully-developed RPC event. The main scope is to identify the manual control behaviour when exposed to RPC-prone configurations, and investigate the corresponding manual control adaptation to these configurations.

1.6. THESIS OUTLINE

A schematic representation of the thesis is shown in Figure 1.7. Chapter 2 provides a comprehensive literature review of the rotorcraft HQ, correlated pilot modeling techniques, listing RPC categorizations, criteria and detection tools. Chapter 3 continues with the description of the new methodology, MCIM. All steps of the MCIM are provided in detail in this chapter. Chapter 4 explains the preliminary identification experiments, which mainly investigated the effects of added time delay on HQ, RPC and manual control behaviour. Both roll and pitch axes with varied rotorcraft models and added time delay configurations are investigated in this chapter. Next, chapter 5 continues with an offline simulation study, using the results of the preliminary identification experiments

and introduces the effect of increased task difficulty accompanying added time delay. Chapter 6 describes the final identification experiment campaign in which results of the simulation study are used as a basis. The MCIM is applied such that both the task difficulty and the added time delay are varied in experiment conditions. Results of the identified parameters, crossover regression tendencies and RPC susceptibility are provided. Finally, chapter 7 concludes on the main findings of the MCIM.

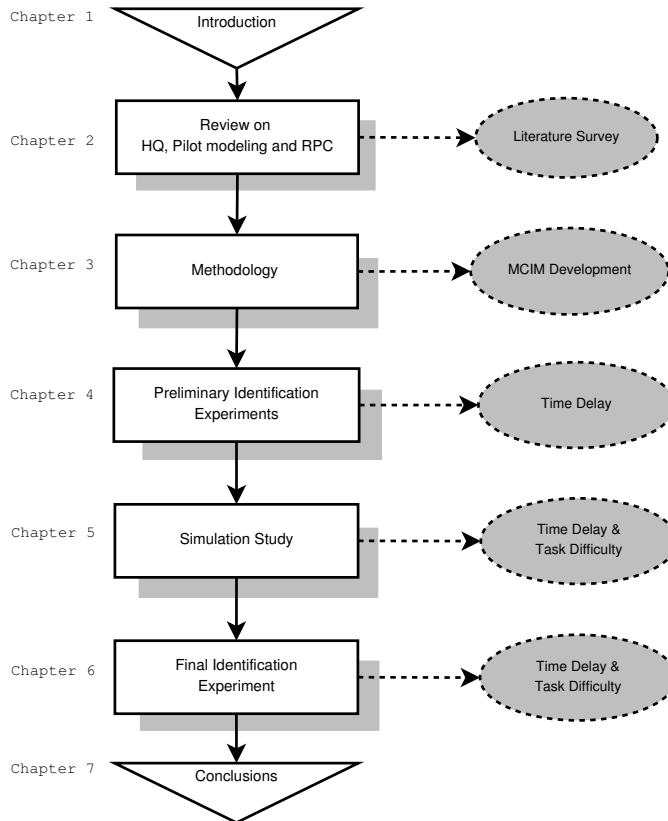


Figure 1.7: Graphical representation of the thesis.

2

REVIEW: THE LINK BETWEEN ROTORCRAFT HQ, PILOT MODELING AND RPC

The previous chapter introduced the scientific gap on 'objective' pilot model considerations during determination of rotorcraft HQ deficiencies and RPC tendencies. In this chapter, HQ and RPC aspects of rotorcraft will be discussed in more detail from the perspectives of HQ criteria and available pilot models to describe the manual control behaviour of human operators. Particularly, effects of the task difficulty and the added time delay on HQ and RPC susceptibility will be reviewed.

2.1. INTRODUCTION

HQ aspects of any manually controlled aerial vehicle play a fundamental role in operational safety and achievable task performance. It is worth recalling the classical HQ definition of Cooper and Harper¹⁹: '... Those qualities or characteristics of an aircraft that govern the ease and precision with which a pilot is able to perform the tasks required in support of an aircraft role (p. 2)'. Good HQ means that the vehicle follows pilot commands as expected with a low level of workload with a good task performance. On the other hand, bad HQ implies that the pilot needs to exert additional control effort, and yet he/she may not be able to achieve an adequate task performance, even get into safety critical flight conditions.

There are many HQ related flight accidents in aviation history, starting with the first flight⁴ of the Wright brothers, whose 1902 glider showed a tendency to pilot induced oscillation in tight tracking tasks⁶⁵. Although new technologies and methodologies have been developed to mitigate HQ deficiencies, such as complex control law implementations with adaptive capabilities¹²⁰, they also bring about new HQ issues which have not been foreseen. Fly By Wire (FBW) systems in aerial vehicle controls are a good example. Gibson³⁰ points out that new generation fly by wire aircraft has exhibited unexpected and often extremely serious handling quality problems due to dominated computer control. Kun et al.⁶³ investigated the flight control law reduction in fly by wire aircraft systems and concluded that such electronic flight control systems can lead to downgraded handling qualities, compromising effectiveness in fulfilling flight tasks. Therefore, instead of increasing the complexity of the control automation by computer powered systems, understanding the basic HQ characteristics of an aerial vehicle in an early design stage can be argued to be a proper step to achieve better flight safety.

This thesis aims to pursue the HQ deficiency issue by pilot model identification methods with a cybernetic approach, which will be discussed in the next chapter in detail. Briefly, the variation in pilot control behaviour is hypothesized to be an indication of HQ, and objective assessment by identified pilot model parameters is aimed to be achieved. In this thesis, HQ deficiencies will be mainly introduced by;

- the additional **time delay** in the vehicle control path, and
- the variation in the **task difficulty** in a closed-loop task.

These two factors will be discussed in detail in this chapter. Moreover, as being a sign of degraded HQ⁴⁹, will be reviewed as well. Furthermore, a detailed review will be provided on the modeling of pilot control behaviour which are utilized with the HQ and RPC criteria. This chapter will briefly summarize the state of the art in these fields as far as these are related to the goals set out in this thesis.

The outline of this chapter is as follows. First, Section 2.2 aims to provide a review on HQ, mainly focused on rotorcraft applications. Next, the role of the pilot in HQ studies, and HQ oriented modeling techniques for pilot control behaviour will be reviewed in Section 2.3. Following, Section 2.4 will describe the adverse RPC as an important example of a HQ deficiency, and associated pilot modeling approaches with this phenomenon will be briefly described. Next, Section 2.5 will focus on reviewing the effects of the added time delay and the task difficulty on HQ and RPC. Finally, the conclusion section will wrap up the reviewed aspects of the HQ and RPC.

2.2. ROTORCRAFT HANDLING QUALITIES

2.2.1. GENERAL DEFINITIONS OF HANDLING AND FLYING QUALITIES

In aviation terms, there is, and probably will continue to be, a definition debate between HQ and flying qualities⁹⁶. Several definitions will be listed below in order to illustrate the main differences and similarities on how the aerial vehicle community aim to describe

handling and flying qualities.

Cooper and Harper¹⁹ mention that their HQ definition is similar to the generally accepted meaning of flying qualities. Padfield et al.¹¹³ highlight flying qualities as the synergy between internal and external influencing factors. Internal factors can be grouped as the vehicle response, controls/displays settings and cockpit ergonomics, and external factors are the MTE, the level of urgency and the external environment. Carlson¹⁶ mentions that '*... Acceptable handling qualities meant good enough for the average, properly trained individual for the nominal missions flown (p. 14).*' Phillips¹¹⁷ interprets the flying qualities as the stability and control characteristics that have an important bearing on the safety of flight and on the pilots.

According to the United States Air Force - Test Pilot School (USAF-TPS)⁷: '*... Flying qualities are the characteristics, or the dynamics, of the airplane. Handling qualities are the characteristics, or the dynamics, of the pilot plus airplane.*' Gray³², who provides an extensive review on the evaluation of HQ in the USAF-TPS, mentions that '*... Handling qualities evaluation requires some understanding of the entire closed-loop, starting with the aircraft from forces and moments, to control systems and displays, and finishing with the human system from perception to computation to action (p. 5).*'

Cook¹⁷ defines flying qualities as '*... The pilot's perception of flying qualities is considered to comprise a qualitative description of how well the aeroplane carries out the commanded task. The pilot's perception of handling qualities is considered a qualitative description of the adequacy of the short-term dynamic response to controls in the execution of the flight task (p. 3).*' On the other hand, Key⁴ has a different definitions as phrased by Padfield¹¹² '*... the flying qualities are the vehicle stability, control and maneuvering characteristics, and the handling qualities are the combination of these and the mission task, the visual cues and atmospheric environment (p. 3).*'

It can be seen from these definitions of handling and flying qualities, that the majority of the definitions include two common core elements: **the vehicle response** and inherently **the pilot**. Differences between definitions mainly arise from the involvement of **the task**. For example, this difference can easily be noticed between definitions of Cook¹⁷ and Key⁴, as illustrated in Figure 2.1.

The **task** element in Figure 2.1 is responsible for representing the required performance, definitions and limitations of the flying mission and sometimes the environmental conditions.

In this thesis, the flying task will be defined as a disturbance-rejection task. A disturbance-rejection task demands human operators to keep a state of the vehicle as steady as possible under disturbance conditions, e.g., keeping a helicopter in hover during a gusty weather. In this example, the task difficulty can be considered as the severity of the gust. The concepts of disturbance-rejection tasks and the task difficulty will be discussed in more detail in the next chapter.

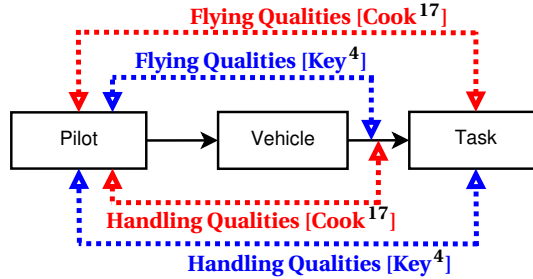


Figure 2.1: Differences between handling and flying qualities definitions. Adapted and simplified from Ref. [17] and Ref. [4].

Throughout this thesis, the term HQ will be used, without any intention to interfere with previous definitions and concepts of HQ and flying qualities, but rather to keep the consistency within the content of the thesis. Detailed historical reviews on HQ and flying qualities can be found in Refs. [96, 117].

2.2.2. ADS-33 FOR THE ROTORCRAFT HQ

EVOLUTION OF ADS-33

Rotorcraft inherently pose significant HQ challenges, due to their multi-axis and cross-coupled control structure, complex main and sub-systems, aerodynamically idiosyncratic environment, and generally demanding operation envelopes with great variability. Hoh⁴⁴ mentions that ‘... *Helicopter pilots have historically been willing to put up with considerably more degraded handling qualities than have fixed wing pilots (p. 6).*’ Considering the complexity of a rotorcraft within an operational flying role, HQ characteristics are, not surprisingly, one of the most important concerns from the beginning of rotorcraft history. Despite this, rotorcraft HQ evaluations were mainly considered in military applications, which can be arguably generalized to be more related to the task performance slightly more than the safety¹¹¹. With the rising demands on the complex mission profiles for rotorcraft, more civil and military fixed-wing HQ considerations were applied to rotorcraft. Carlson¹⁶ provides a descriptive time line for critical improvements in HQ evaluation for rotorcraft flight dynamics and simulation developments, as summarized in Figure 2.2.

As it can be observed from Figure 2.2, the evolution of rotorcraft HQ consideration is coupled with the developments of the control and stability methods, in-flight or ground simulation, a large number of flight tests and corresponding research efforts. Padfield provides an extensive historical review on the evolution of the rotorcraft HQ in Ref. [112].

As depicted in Figure 2.2, the current rotorcraft HQ standard is the ADS-33, with the latest version ADS-33E-PRF, published in 2000⁶. ADS-33 was a remarkable improvement in HQ assessment philosophies, such that for the first time specific tasks (i.e., Mission

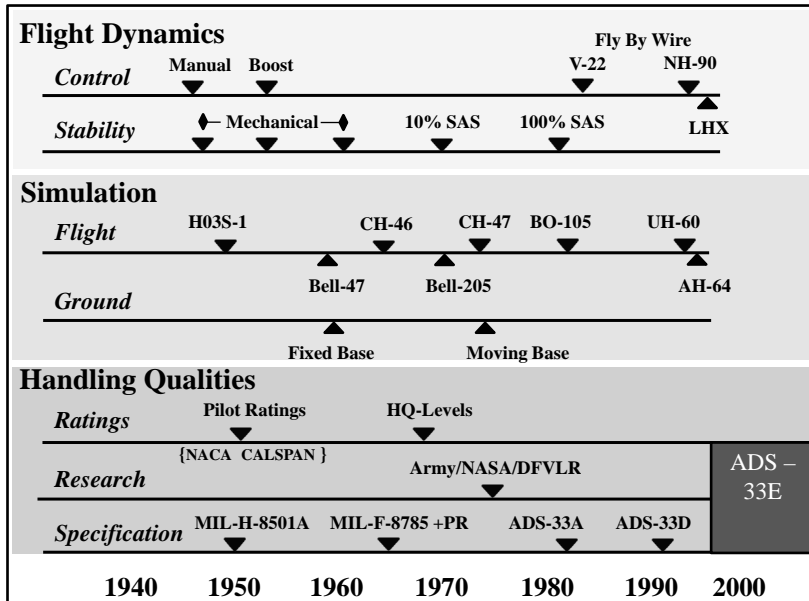


Figure 2.2: Timeline of rotorcraft handling qualities, adapted from Ref.16.

Task Element MTEs) were introduced to evaluate the HQ characteristics of rotorcraft for agility. Mitchell et al.⁹⁶ states the innovative attributes of ADS-33 as follows:

- Empirical methodology to describe the quality of visual cues.
- Specialized MTE for each helicopter category.
- Detailed descriptions of MTE for industry and evaluation pilots.
- Stabilization requirements that are graded according to visual environment.
- Control and maneuvering requirements that depend on the applicable MTE.
- New parameters to specify the short-term response to control (e.g., bandwidth).
- New parameters for large-amplitude control power (e.g., attitude quickness).
- New parameters for cross-coupling characteristics during aggressive manoeuvres.
- Incorporation of the tailoring process into the overall ADS-33 structure.

Throughout the years of ADS-33 development and application, many research institutes and rotorcraft industry partners aimed to validate and extend the usage of ADS-33 into their specific needs and new design programs. For example, Hoh and Heffley⁴⁸ used the ADS-33 to include slung load operations for HQ evaluations, and Mitchell et al.⁹⁷ investigated HQ in helicopter-ship operations. The NH-90 (shown in Figure 2.3) is one of the helicopters which had an extensive usage of ADS-33 during its design phase.



Figure 2.3: The NH-90 helicopter (Source: <http://www.airforce-technology.com/projects/nh90-nfh-asw>).

Considering the development of the NH-90 helicopter (Figure 2.3), Bellera and Varra¹⁰ mentioned that '... *The solution was a very rigorous development methodology based on ADS-33 approach and innovative design choices. For the first time in the world a helicopter was designed and qualified with the most demanding Handling Qualities military standards, ADS-33* (p. 8)' Several aspects that contributed to the success of ADS-33 can be listed as¹¹²: ① Clear and comprehensive description of requirements, ② Participation of the whole community, helicopter manufacturing industry, and possible users during the development and discussion phases of the standard, ③ Extensive usage of experimental facilities, flight test programs, in-flight and ground simulator facilities in several research centres, ④ Supervision of dedicated researchers who aim to generate database for criteria development, ⑤ Development of test and analysis methods to ensure engineers could effectively use the standard in design and qualification.

These factors regulated in agreement of **one set of criteria**, and such agreement does not exist in the fixed-wing community, where different criteria are applied during each activity⁴⁹. There are several HQ criteria in ADS-33, concerning the response type of the rotorcraft, axis (or axes) of interest, cross-couplings, short-term and mid-term responses. These criteria defined are in the time and frequency domains, and depend on the MTE, class of the rotorcraft, forward speed, visual cues, etc. Some of the major studies regarding the development of these criteria and their design perspectives can be found in Refs. [6, 21, 33, 44, 50, 112, 145].

BANDWIDTH PHASE DELAY CRITERION IN ADS-33

The BPD is one of the most well-known and extensively exercised criteria of ADS-33. Historical background on the development of the BPD can be found in Refs. [12,99], which include dedicated flight tests and flight simulator campaigns. Since BPD strongly correlates with two keywords of this thesis, the **time delay** and the **task**, a closer investigation of the BPD will be provided in this section. For the remaining criteria in ADS-33, the reader is advised to refer to the original ADS-33 document⁶.

The BPD criterion utilizes two descriptive parameters, *the bandwidth* and *the phase delay*. These parameters are obtained from the frequency domain characteristics of the

rotorcraft representing the vehicle attitude response to applied pilot control input. Determination of these parameters is illustrated in Figure 2.4.

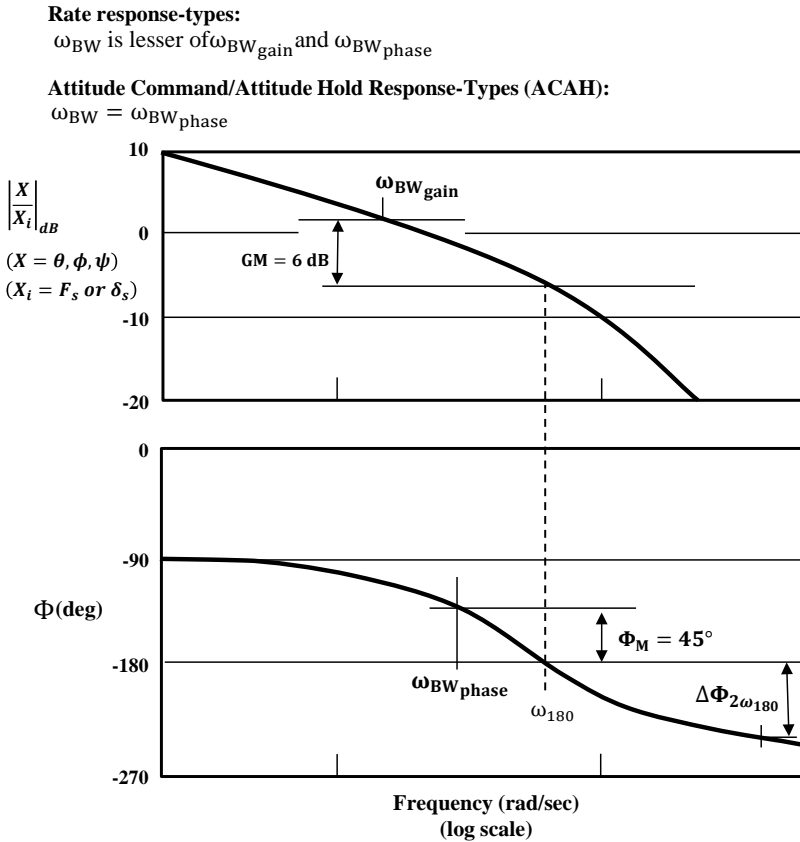


Figure 2.4: ADS-33 definitions of the bandwidth and the phase delay for Rate and ACAH response-types, adapted from Ref.6.

As shown in Figure 2.4, Rate and ACAH response-types are the two major rotorcraft response characteristics that are used by the BPD to define the bandwidth parameter ($\omega_{BW\theta}$). Rate-response types refer to direct control of the pilot (e.g., longitudinal cyclic) on the vehicle rate response (e.g., pitch rate q). In other words, when the pilot applies a constant control input in addition to the trimmed condition, the rotorcraft will keep on rotating. On the other hand, in a typical ACAH response-type, the same applied control will eventually result in a constant attitude, i.e., the rotorcraft will not continue rotating after a certain altitude is reached. ACAH response-types are generally more augmented (e.g., Stability Control Augmentation System (SCAS)) than the rate response-types¹¹. Discussions on the response-types will be given in the next chapter in more detail.

As shown in Figure 2.4, the BPD criterion can be applied in each on-axis response, i.e., pitch (θ), roll (ϕ) and yaw (ψ). Since primarily the pitch response will be examined in this thesis, descriptions of BPD in pitch will be given in this section. For the rate response-types⁶, the bandwidth parameter (ω_{BW_θ}) is the lesser of the gain bandwidth ($\omega_{BW_{gain}}$) and the phase bandwidth ($\omega_{BW_{phase}}$), which are defined as in Figure 2.4. Calculation of the phase delay parameter (τ_{p_θ}) is given in :

$$\tau_{p_\theta} = \frac{\pi}{180} \cdot \frac{\Delta\Phi_{2\omega_{180}}}{2\omega_{180}} \quad (2.1)$$

where $\Delta\Phi_{2\omega_{180}}$ (degrees), and $2\omega_{180}$ (rad/s) are depicted in Figure 2.4. The bandwidth parameter (ω_{BW_θ}) represents the boundary of a range of frequencies over which a pilot can exert good closed-loop control without excessive compensation⁸⁵. Beyond the ω_{BW_θ} frequency, the closed-loop stability is threatened. In practice, this frequency can be defined as¹¹¹ '... the highest frequency at which the pilot can double his/her gain or allow a 135° phase lag (p. 68)'. This is also the rationale behind choosing the ω_{BW_θ} as the lesser of $\omega_{BW_{gain}}$ and $\omega_{BW_{phase}}$ for rate-response types.

Although more details on rotorcraft modeling will be discussed in the next chapter, and adverse couplings between the pilot and the vehicle will be discussed in Section 2.4, it can be already interpreted that low values of ω_{BW_θ} can be an indication of an RPC tendency. For example, while flying a rotorcraft with a low ω_{BW_θ} , a pilot may prefer to apply high frequency inputs to minimize any small error during a demanding flying task. Consequently, low ω_{BW_θ} and these high frequency inputs of the pilot may bring the PVS into undesired oscillatory behaviour due to limited stability, i.e., low ω_{BW_θ} . This situation may force the pilot to lower his/her control anticipation, and to sacrifice the task performance, which is also a known RPC alleviation technique among pilots¹⁴³.

The phase delay parameter (τ_{p_θ}) quantifies the characteristics of the mid- and high frequency phase lag of the PVS, and defines the attainable closed-loop PVS bandwidth during a high precision task. Phase lags can originate from the high frequency rotor modes, actuator dynamics of the swash-plate, software filters on the control path, augmentation filters, computational delays, etc. In practice, τ_{p_θ} reflects the equivalent phase lag between the pilot control input and the resulting vehicle attitude response. Therefore, especially τ_{p_θ} is strongly correlated with the '**time delay**' effect in a rotorcraft system, as the available open-loop phase margin quickly reduces if τ_{p_θ} has a high value. Moreover, a high τ_{p_θ} also reduces the $\omega_{BW_{phase}}$ because -135° phase starts to occur at lower frequencies. Thus, a small increase in pilot gain can more easily drive the PVS into instability.

PVS instability due to added time delay, and the corresponding pilot control anticipation are crucial elements of this thesis, and they will be discussed in Sections 2.3 and 2.4 in more detail. Two examples of HQ assessments by using the BPD criterion on sample vehicle responses, which are prone to PVS instability, are shown in Figure 2.5.

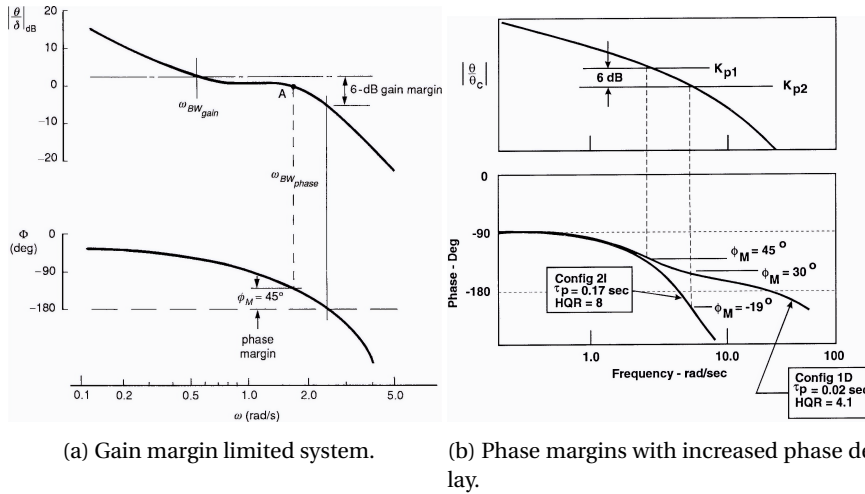


Figure 2.5: BPD determination of (a) gain-margined limited system (from Ref. [45]) and (b) increased phase lag configurations, adapted from Refs. [49, 103]).

From a BPD perspective, the vehicle configurations with a flat-like amplitude characteristics around possible crossover frequencies are prone to PVS instability, as illustrated in Figure 2.5a. The danger here is that any small increase in pilot gain, which can be interpreted as a shift-up of magnitude response in Figure 2.5a, immediately consumes available phase margin in PVS, i.e., a transition to instability. As a result, these configurations force pilots to apply very careful compensations. Consequently, pilots may prefer to keep a lower gain control strategy to avoid such 'suddenly appearing' system instability.

Another critical condition for such an instability can be introduced by increased $\tau_{p\theta}$, as illustrated in Figure 2.5b. It can be observed that the magnitude responses of two configurations are exactly the same, whereas there is a considerable difference between phases. Phase delay values are 0.17 sec and 0.02 sec, as shown in Figure 2.5b. It is worth noting that the phase delay is calculated in 'seconds', and it can be confused with the equivalent time delay or the added time delay, which possesses the same phase roll-off. However, a small deviation in phase delay value may represent a recognizable deviation in HQ⁴⁹. High values of $\tau_{p\theta}$ limit the available bandwidth at which the pilot can still sustain stable control of the vehicle.

The BPD criterion inherently considers these instabilities, and aim to provide a phase margin of 45° to the pilot, such that any change in his/her gain can be tolerated without threatening PVS stability in a high precision task. If this phase margin is decreased during the task, the critical -180° phase limit causes a fully out-of-phase response for the applied pilot control. This condition is an adequate set-up of an RPC incipience, which will be discussed in detail in Section 2.4.

In order to assess the HQ using BPD criterion, calculated ω_{BW_θ} and τ_{p_θ} values are plotted in a HQ levels chart. A sample BPD chart for rotorcraft pitch response is illustrated in Figure 2.6, in which fixed-wing boundaries are also additionally shown for comparison purposes.

In Figure 2.6, the boundaries that separate different levels of HQ of rotorcraft and fixed-

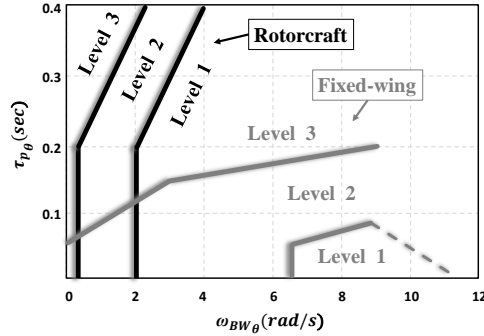


Figure 2.6: Pitch attitude BPD boundaries with comparison of rotorcraft and fixed-wing aircraft for high precision tasks (target acquisition and tracking MTE and Category A flight phases, respectively), adapted from Ref. [111].

wing aircraft are shown in terms of BPD parameters, especially for high precision demanding tasks for both aerial vehicles. These boundaries were defined after extensive flight tests and (ground and in-flight) simulator campaigns¹¹². While setting the boundaries, mainly pilot subjective ratings were used in order to evaluate the HQ. The most classical HQR scale is the Cooper-Harper scale¹⁹, and its application to HQ evaluations and resulting levels are described in Appendix A.

In Figure 2.6, it is apparent that rotorcraft and fixed-wing aircraft have very distinct HQ boundaries, such that a level-1 (good HQ) rotorcraft can easily be considered as level-3 (bad HQ) in fixed-wing aircraft constraints. The differences in bandwidth and phase delay boundaries stem from fundamental differences between rotorcraft and fixed-wing aircraft, e.g., vehicle aerodynamics extended with rotor dynamics, control systems and MTE that defines the vehicle task to evaluate HQ. This HQ comparison in Figure 2.6 is provided to highlight the dissimilarities of HQ applications between two types of aerial vehicles, even though they are subjected to the same criterion (BPD) in this example. More details on HQ comparisons between rotorcraft and fixed-wing aircraft are discussed in Ref. [111].

HQ boundaries in BPD charts plotted in ADS-33 are 'task' dependent, i.e., MTEs. One of the most aggressive tasks in ADS-33 is the 'target acquisition and tracking' task. Unlike the other MTEs, there is not a description of the task in ADS-33. The main rationale behind this task class is to provide high precision, tight control within a high gain task in order to reveal system instabilities around mid- and high frequencies. Tischler et al.¹³⁵ provide examples of acquisition and tracking tasks such as slope landings, air-to-air tracking, running landings, 60 knots quickstop and compensatory tracking tasks.

2.3. PILOT MODELING FROM HANDLING QUALITIES PERSPECTIVE

The previous section provided some insight on the rotorcraft HQ, assessed by BPD criterion which depends on the vehicle response and the required task. Both the vehicle and the desired task requirements are 'relatively' deterministic starting from the design phase, when compared to the most adaptive element in the PVS: **the pilot**. Similar to HQ studies, pilot modeling is also a very broad discipline which will not be fully reviewed in this thesis. However, major techniques of pilot modeling from a HQ perspective will be introduced in this section. McRuer and Jex⁸⁰ published a famous review on quasi-linear pilot models, which played a vital role in the development of pilot models in closed-loop tracking tasks. Lone and Cook⁶⁸⁻⁷⁰ provides reviews of pilot modeling techniques, targeted HQ challenges caused by unsteady aerodynamics and aeroelasticity. Mitchell et al.⁹⁶ briefly cover the topic of pilot modeling for HQ applications mainly for fixed-wing aircraft.

Physiological pilot models mainly focus on modeling the human perception and control activation mechanisms. Many of these studies use generally open-loop tasks to measure and validate the models of physiological perception organs and muscle models of the pilot, as illustrated in Refs. [102, 152]. This thesis, however, focuses on identifying the *manual control behaviour* by using control-theoretic pilot modeling applied to closed-loop control task measurements. The next section will review the pilot modeling aspects dedicated to manual control behaviour.

2.3.1. CONTROL-THEORETIC PILOT MODELING

McRuer et al.⁸³ introduced the essence of the crossover model, which became a baseline for several other approaches of control-theoretic pilot modeling techniques. Fundamental data for the development of the crossover model were obtained from single-loop visual compensatory (and pursuit) target tracking tasks with a random-appearing forcing function⁸³. A schematic representation is shown in Figure 2.7.

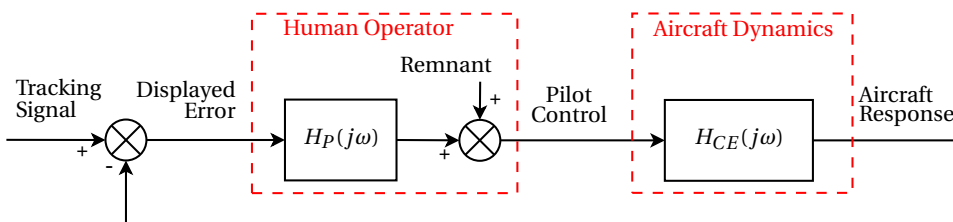


Figure 2.7: Schematic representation of a single-loop target-tracking task. The human pilot is modelled as the summation of the linear behaviour ($H_P(j\omega)$) and the remnant, which represents the non-linear control anticipation, random noise, etc. Adapted from Ref. [26, 81, 83].

In a compensatory task, human pilots are required to minimize the displayed error, which is the difference between the provided tracking signal and the aircraft response originated from human pilot control effort, as illustrated in Figure 2.7. Based on con-

ducted compensatory tracking experiments by McRuer et al.⁸³, a *Primary Rule of Thumb for Frequency Domain Synthesis* was stated as⁷⁹: ‘... At frequencies just within and beyond the input bandwidth, seek or create (by equalization) a fair stretch of -20 dB/decade slope for the amplitude ratio and adjust the loop gain so as to put the unity-amplitude crossover frequency near the higher edge of this region, while maintaining adequate stability margins (p. 5).’ Consequently, McRuer et al.⁸³ formulated the crossover model as given in equation 2.2.

$$H_P(j\omega)H_{CE}(j\omega) = H_{OL}(j\omega) \approx \frac{\omega_c}{j\omega} e^{-j\omega\tau_e} ; \text{ near } \omega_c \quad (2.2)$$

where $H_P(j\omega)$, $H_{CE}(j\omega)$, $H_{OL}(j\omega)$ are the pilot, the CE and the open-loop linear dynamic responses, respectively. ω_c is the crossover frequency and τ_e is the effective pilot time delay, which represents the phase lag of $H_P(j\omega)$ around ω_c due to internal delays caused by the pilot decision and activation. Determination of ω_c and the phase margin φ_m is illustrated in Figure 2.8.

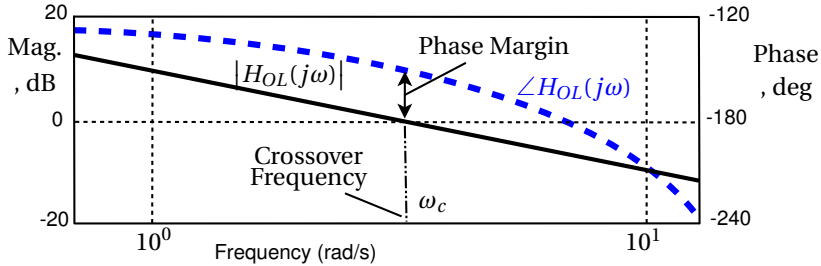


Figure 2.8: Determination of the open-loop crossover frequency and the phase margin according to the crossover model, adopted from Ref. [79]

As shown in Figure 2.8, ω_c is the frequency at which the open-loop transfer function has a 0dB magnitude, and φ_m is the phase difference between -180° and the phase of the open-loop transfer function at ω_c .

From a HQ perspective⁸⁵, ‘... The crossover model effectively describes how a human pilot can adapt to the **response characteristics** of various aircraft (p. 121).’. McRuer’s experiments⁷⁹ resulted in such human control behaviours that the open-loop magnitude $|H_{OL}(j\omega)|$ showed an integrator like ($K/(j\omega)$), i.e., -20dB/decade amplitude slope, around the crossover frequency (ω_c) for all examined CE configurations ($H_{CE}(j\omega)=K_c$, $K_c/(j\omega)$ and $K_c/(j\omega)^2$, where K_c is the CE gain).

The crossover model is perhaps the simplest, but probably the most profound, approach to pilot modeling⁸⁵. In order to improve the accuracy of the crossover model, McRuer et al.⁸⁰ further proposed the ‘*extended crossover model*’. The extended crossover model introduced the ‘ α effect’ to account for the low frequency lag, mainly experienced with conditionally stable systems. The extended crossover model is given by⁸⁰:

$$H_P(j\omega)_{\alpha \text{ model}} \approx K_v \frac{(\tau_L j\omega + 1)}{(\tau_I j\omega + 1)} e^{-j(\tau_e\omega + \alpha/\omega)} \quad (2.3)$$

where K_v is the pilot gain, τ_L and τ_I are the lead and the lag time constants, respectively, which depend on the CE to be compensated in the closed-loop system. Although the additional α parameter improves the low frequency lag, still the neuromuscular system and the manipulator feel characteristics are not covered in the extended crossover model. A good example of the usage of the extended crossover model can be found in Ref. [8] in which Aponso et al. investigated pilot performance in rotorcraft tracking experiments.

In order to improve the accuracy of the model to contain a wider frequency range, in which the neuromuscular system and the manipulator dynamics are included, a higher fidelity pilot model was proposed by McRuer et al.⁸³ as the '*the precision model*', given by equation 2.4:

$$\begin{aligned}
 H_p(j\omega) = & K_v \underbrace{\left(\frac{\tau_L j\omega + 1}{\tau_I j\omega + 1} \right)}_{\text{Pilot Equalization terms}} \underbrace{\left(\frac{\tau_K j\omega + 1}{\tau'_K j\omega + 1} \right)}_{\text{Low-frequency lead-lag terms}} \\
 & \times \underbrace{\frac{\omega_{nms}^2}{(\tau_N j\omega + 1) [(j\omega)^2 + 2\zeta_{nms}\omega_{nms}j\omega + \omega_{nms}^2]}}_{\text{Neuromuscular system}} \underbrace{e^{-j\omega\tau_p}}_{\text{Pilot time delay}} \quad (2.4)
 \end{aligned}$$

Fundamental differences between the precision and the extended crossover models (equations 2.3 and 2.4, respectively) are:

- Low-frequency lead-lag terms
- Presence of the neuromuscular system model
- Differences between time delay terms

Low-frequency lead-lag terms are generally included to compensate for matching the very low-frequency pilot describing function obtained from measurement data. The dynamics that the low-frequency lead-lag terms represent exhibit very few occurrences in the measured signal (i.e., very high periods). Thus, it exerts a low reliability while modeling a certain behaviour, but instead practised to match the pilot model with the very low-frequency content. Unlikely, the presence of the neuromuscular system strongly influence the modeling accuracy, especially at frequencies beyond ω_c . Moreover, the neuromuscular system model changes the definitions of the time delays in the pilot describing function model. The 'pure' pilot delay τ_p includes the perception, central nervous activity (e.g., decision making), and transmission of muscle activation signals. On the other hand, τ_e includes additionally phase lags, mainly caused by the neuromuscular system. In this thesis, a modified version of the precision model is utilized, and described in the next chapter.

STRUCTURAL PILOT MODEL

Starting from the crossover model, various control-theoretic models have been developed. The '*structural pilot model*' of Hess³⁹ is one of the famous models which has been widely used in aircraft and rotorcraft HQ studies. The block diagram of the structural pilot model is shown in Figure 2.9.

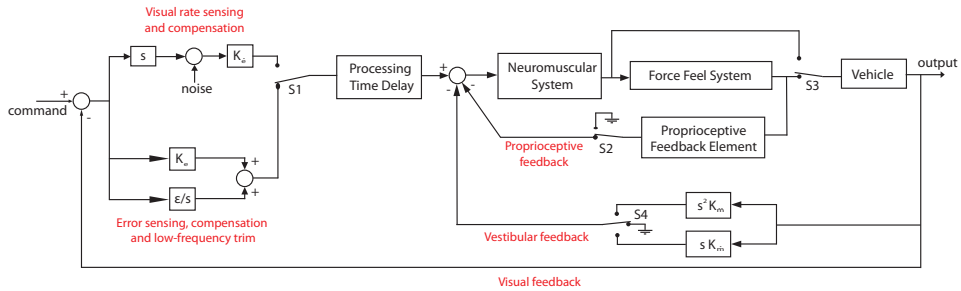


Figure 2.9: Compensatory structural model of the human pilot as proposed by Hess³⁹, adopted from Ref. [69].

As can be seen from Figure 2.9, there are several switches in the structural model to be set according to the specific application. For example, S3 can be used for assigning the manipulator feel characteristics between position and force sensing models. The innovative approach of the structural model is the combination of the proprioceptive feedback concept and Optimal Control Model (OCM) principles. The proprioceptive feedback modeling originated from Smith's¹²⁷ pilot opinion rating concept, and inherently includes the pilot compensation model of the extended crossover model. OCM principles will be discussed later in this section, but briefly, the structural model aims to implicitly include the minimization of a cost function idea of the OCM. Details of the structural model can be found in Ref. [39]. Hess³⁸ investigated the usage of structural pilot model for rotorcraft performance and HQ analysis with varied rotorcraft dynamics. Another application of the structural pilot model for rotorcraft HQ is presented in Ref. [40] during a ADS-33 hover task with multi-loop control. Prasad and Perhinschi¹¹⁶ utilized the structural pilot model for rotorcraft HQ with varied control sensitivity and flight speed, accompanying the BPD criterion. Weber et al.¹⁴² used the structural pilot model for the development of longitudinal HQ criteria in a pitch tracking task.

OPTIMAL CONTROL PILOT MODEL

Another widely used pilot model applied in HQ prospects is the Optimum Control Model (OCM). Kleinman et al.⁵⁹ introduced the OCM with the idea that a well-trained and motivated pilot behaves in an optimal manner while remaining properties are subjected to inherent physiological and physical limitations, which can be summarised as time delay, motor and observation noises. A schematic representation of the OCM is shown in Figure 2.10.

As indicated in Figure 2.10, a Kalman filter and a predictor are used to produce optimal estimates of the values of the state variables at each instant of time given noisy measurements of linear combinations of these variables³⁸. With parameters shown in

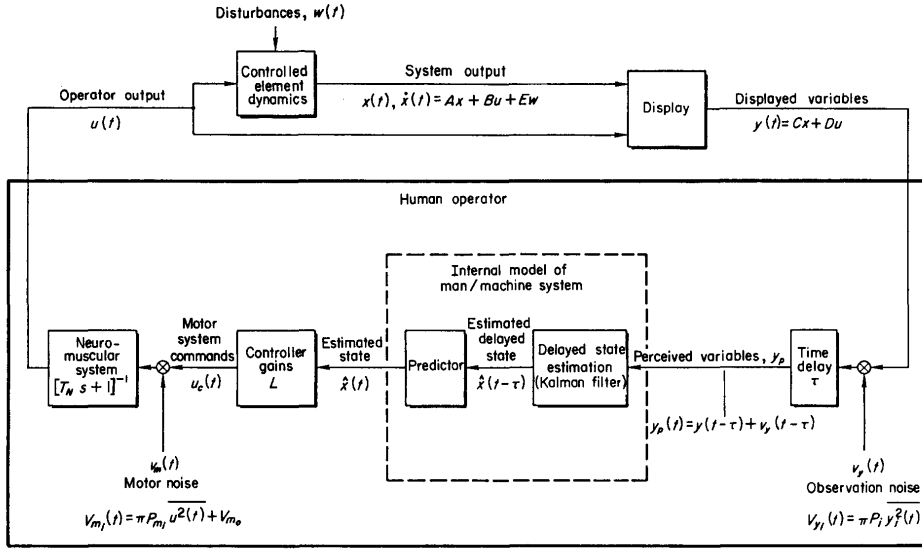


Figure 2.10: Block diagram of the OCM, adapted from Ref. [77].

Figure 2.10, a generic cost function of the optimization to be minimized can be given by

$$J(\underline{u}) = E \left\{ \lim_{\tau \rightarrow \infty} \frac{1}{\tau} \int_0^{\tau} \left(\underline{y}^T \mathbf{Q} \underline{y} + \underline{u}^T \mathbf{R} \underline{u} + \dot{\underline{u}}^T \mathbf{G} \dot{\underline{u}} \right) dt \right\} \quad (2.5)$$

where \mathbf{Q} , \mathbf{R} and \mathbf{G} are weightings of the displayed system output, pilot control input and control rates, respectively. By defining various optimization weights, optimal pilot control behaviour to satisfy the 'required' PVS response can be achieved. Thus, by changing the weighting gains, the optimization can represent various control behaviour types for the task. This is in close correlation with the principle of the crossover model, such that pilots adapt their control behaviour in order to achieve $1/(j\omega)$ open-loop response around the crossover frequency, independent of the exposed CE dynamics in the same task. McRuer et al.⁷⁷ state that for a simple single-axis control situation, excellent agreement with experimental measurements has been obtained with a very simple OCM cost function form:

$$J(\underline{u}) = E \left\{ \lim_{\tau \rightarrow \infty} \frac{1}{\tau} \int_0^{\tau} (e^2 + g\dot{u}^2) dt \right\} \quad (2.6)$$

where e is the displayed system error, \dot{u} is the human control rate, and g is the weighting factor which can be selected to yield an appropriate neuromuscular lag⁷⁷. Hence, for a single-axis compensatory task, it can be interpreted that the pilot aims to find the best trade off between maximizing system performance (e.g., e displayed error) and minimizing control activity (e.g., \dot{u}). The OCM finds the 'best' pilot model settings to achieve this goal. From HQ perspective, this resembles the compromise between the required task performance and the applied pilot workload. Detailed descriptions of the

OCM can be found in Ref. [77, 153].

McRuer et al.⁸⁴ applied the OCM to research the pilot modeling for flying qualities applications, mainly focused on divided attention operations during multi-axis tasks. They found that OCM has a potential for the development of subjective HQ ratings estimates, when it is 'calibrated'. Further, Thompson and McRuer¹³² compared the crossover model and OCM, and concluded that the crossover model is similar to the OCM by approximating very high order terms of the OCM by an effective delay in the crossover model. It must be noted that pilot model in the OCM can not be identified by using measurement data because it is over-parametrized for pilot model identification purposes^{61,144}.

2.3.2. PILOT MODELS IN HQ CRITERIA

Some of the pilot models have been applied in HQ criteria development and applications progress. This section briefly covers some of the most relevant applications of pilot models for HQ evaluations with respect to the contents of this thesis.

PILOT MODEL IN THE BPD CRITERION

The BPD criterion was described in Section 2.2.2 in detail. From a pilot modeling perspective, one can interpret the BPD as the stability and performance characteristics resulting from a pure **gain pilot** model in the PVS⁴⁹, as shown in Figure 2.11.

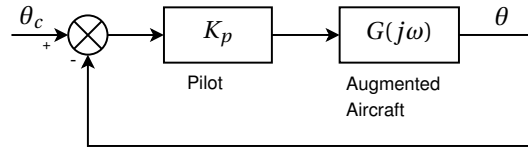


Figure 2.11: Interpretation of the BPD with a pure gain pilot, where θ_c is the commanded tracking signal. Adapted from Ref. [49].

According to Figure 2.11, the open-loop transfer function and the stability limit for this case are given as follows⁴⁹:

$$H_{OL}(j\omega) = K_p G(j\omega) \quad (2.7)$$

$$\underbrace{1 + H_{OL}(j\omega)}_{\text{stability limit}=0} \Rightarrow K_p = \frac{-1}{|G(j\omega)|} \quad (2.8)$$

It can be noted in Equation 2.8 that regardless of the dynamics of the aircraft ($G(j\omega)$), the pilot is modelled as a pure gain K_p which is the inverse of the amplitude of the aircraft dynamics at the open-loop stability limit. Unlike the crossover model, this pure gain pilot model does not include any phase information of the aircraft frequency response. The idea of setting an '**unequalized**' gain pilot in BPD is to define the bandwidth frequency (ω_{BW_θ}) as the highest frequency where the gain pilot can still achieve stable closed-loop response^{49,82}. Stability margins for the gain pilot model to sustain the stable closed-loop were quantified as 45° of phase margin or a $6dB$ of gain margin.

Thus, in practice, $\omega_{BW_{gain}}$ and $\omega_{BW_{phase}}$ reflect the available stability margins for a pure gain pilot in the PVS. The lesser is assigned as the bandwidth frequency in order to keep the closed-loop system as stable as possible, either from gain or phase limitations.

Although this simple pure gain pilot model benefits from the ease of analysis, it is highly limited without the phase compensation of the pilot model to interact with the phase characteristics of the vehicle response. In other words, the phase of the open-loop response of the PVS is exactly same as the phase response of the vehicle. When the vehicle phase response varies noticeably around possible piloting frequencies (e.g., up to 15 rad/s), this pure gain representation could be incorrect from a pilot modeling perspective, considering active pilot compensation.

PILOT MODEL IN THE NEAL-SMITH CRITERION

One of the HQ criteria with a described pilot model in its foundation is the Neal-Smith criterion¹⁰³, which has extensive use in fixed-wing aircraft but limited applications in rotorcraft studies. It is not intended to discuss the details of the criteria here, but instead, to illustrate the possibilities of integrated pilot modeling prospects into HQ assessments.

The basic idea behind the Neal-Smith criterion is to represent the pilot in a simple form such that any deviation in parameters of this 'paper' pilot can be related to HQ of the vehicle at hand. By conducting extensive flight tests with NT-33 variable stability aircraft with various selection of configurations, Neal and Smith obtained pilot ratings and measurement data to correlate with the paper pilot model¹⁰³. The pitch attitude tracking task is shown in Figure 2.12.

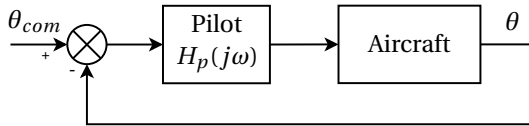


Figure 2.12: Pitch attitude tracking task, where θ_{com} is the commanded tracking signal. Adopted from Ref. [103].

In the illustrated pitch attitude tracking task in Figure 2.12, the pilot model is as follows:

$$H_p(j\omega) = \underbrace{K_v}_{\text{gain compensation}} \underbrace{\left(\frac{\tau_{LEAD}j\omega + 1}{\tau_{LAG}j\omega + 1} \right)}_{\text{phase compensation}} \underbrace{e^{-j\omega\tau_e}}_{\text{effective time delay}} \quad (2.9)$$

As given in Equation 2.9, the paper pilot model contains both a gain and a phase compensations, and a time delay as pilot limitation. This pilot model is a version of the McRuer's extended crossover model (see Section 2.3.1).

In order to assign the pilot model, three adjustment parameters for the closed-loop PVS are introduced. The **bandwidth** parameter is the frequency at which the closed-loop

phase response becomes -90° . The **closed-loop resonance** parameter is the magnitude of the maximum peak in the closed-loop response. This parameter represents the oscillatory behaviour of the PVS in a closed-loop task. The last parameter is the **droop**, which defines the deviation of the closed-loop magnitude below 0dB for frequencies smaller than the bandwidth parameter. These adjustment parameters are subjected to constraints stated by Neal and Smith, after analysing flight test data accompanying pilot HQ ratings. The constraints are listed below, and depicted in Figure 2.13.

- minimum bandwidth: 3.5 rad/s ,
- achieve minimum droop, maximum droop limit: -3dB , and
- after the bandwidth and the droop limit are satisfied, achieve minimum closed-loop resonance peak.

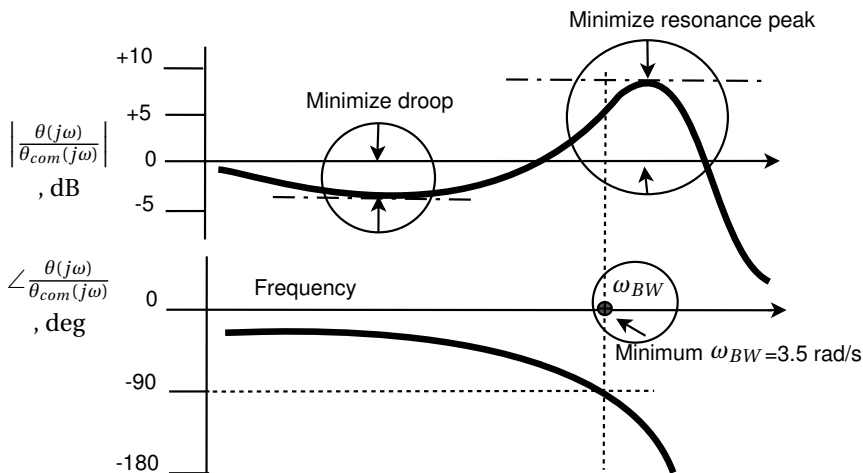


Figure 2.13: Neal-Smith constraints, adopted from Ref. [103].

In practice, the Neal-Smith criterion can be considered as an optimization problem, which has 'minimum bandwidth' and 'maximum droop' as constraints and 'closed-loop resonance peak' as the cost function to be minimized, all depicted in Figure 2.13. This can be related to the OCM from a conceptual pilot modeling point of view. The final step of the Neal-Smith criterion assessment is to plot the PVS **closed-loop resonance peak** and the corresponding **compensation of the mathematical pilot** model. This two-dimensional chart is given in Figure 2.14.

The boundaries of the Neal-Smith HQ chart in Figure 2.14 were obtained from awarded HQR for the NT-33 variable stability aircraft in many hours of flight testing¹⁰³. These boundaries are not validated for rotorcraft applications, but they still can be used for relative referencing purposes. For example, Mariano and Guglieri⁷⁴ used the Neal-Smith criterion for HQ assessment while elaborating other HQ and RPC criteria for rotorcraft. Sebastien and Mathieu¹²⁴ approached the problem of PIO susceptibility of UH-60 rotorcraft while utilizing the Neal-Smith criterion for HQ evaluation.

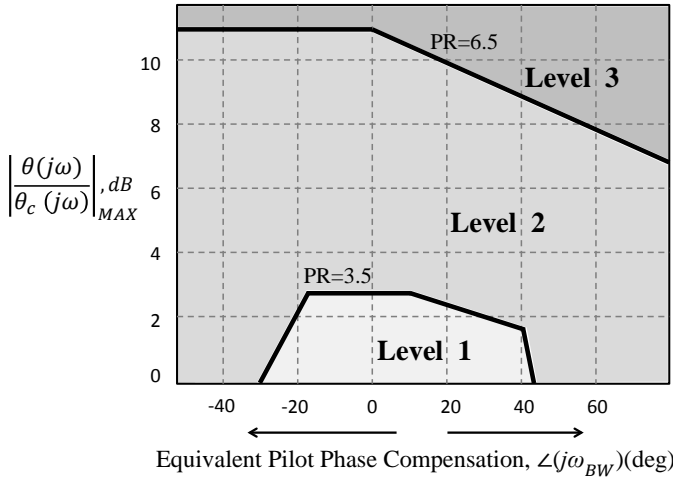


Figure 2.14: Neal-Smith criterion chart, adapted from Ref. [103]. PR: Cooper-Harper HQR.

PILOT MODEL IN THE HQSF CRITERION

Another well known HQ criteria with an internal pilot model is the HQSF criterion^{39,142}. The HQSF is based on the PSD of the proprioceptive feedback signal of the structural pilot model, which was described in Section 2.3.1. By using the simplified structural pilot model as shown in Figure 2.15, the procedure of obtaining the HQSF can be summarized as depicted in Figure 2.16.

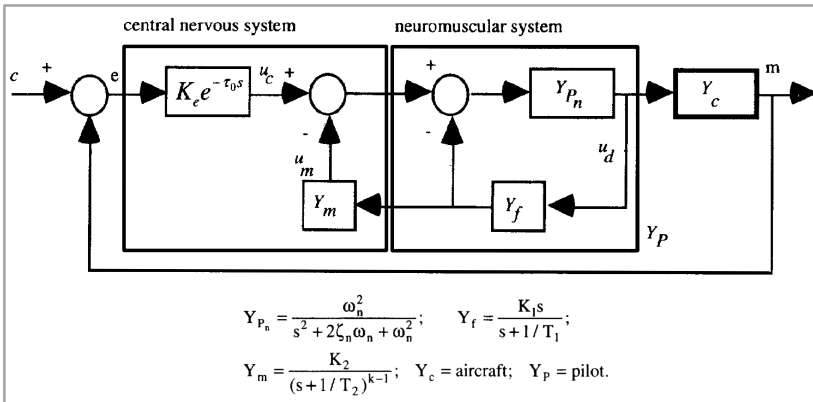


Figure 2.15: Simplified structural pilot model with associated transfer functions, adopted from Ref. [39]

Hess³⁹ utilized HQSF with HQ boundaries with awarded HQR obtained from HAVE PIO flight tests which refer to a series of experiments that collected important PIO data during flight experiments with aircraft in various configurations⁸⁵. For rotorcraft HQ applications, boundaries can be considered as tentative, and relative comparisons can still provide insight in the HQ. Hess⁴¹ used the HQSF for Bo-105 helicopter model during a

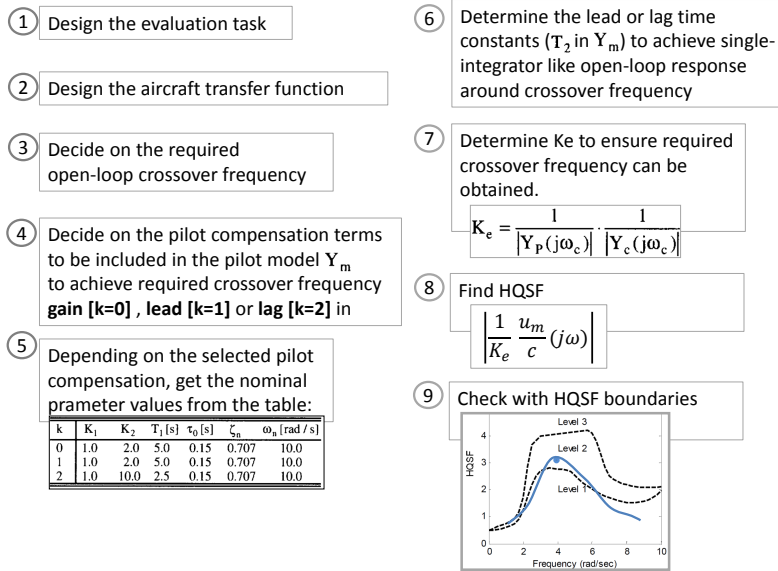


Figure 2.16: The routine to obtain the HQSF, adapted from Ref. [116].

ADS-33 hover task. Prasad¹¹⁶ used the HQSF for UH-1H helicopter, particularly focused on effects of flight speed and control sensitivity on rotorcraft HQ. It was concluded that the HQSF parameter and BPD bandwidth were consistent such that high bandwidth improves the handling qualities. In addition, variation of the HQSF with forward speed suggested different HQ boundaries of BPD for different flight speeds.

2.4. ADVERSE ROTORCRAFT PILOT COUPLINGS

Historically, the first famous terminology for the adverse coupling between the air vehicle and the pilot was PIO⁸⁵. In principle, PIOs are instabilities of the PVS which result in undesired oscillatory response. They can be severely safety-critical and several fatal flight accidents have been associated with this coupled behaviour⁸⁵. According to Pavel et al.¹¹⁵, '... PIO occur when the pilot inadvertently excites divergent vehicle oscillations by applying control inputs that are in the wrong direction or have phase lag with aircraft motion (P. 3).' There are also Pilot Assisted Oscillations (PAO) which are more related to higher frequency involuntary bio-dynamic coupling between the body of the pilot and the vehicle motion response¹¹⁵. After 1995, the term PIO (and PAO) started to be recalled as Aircraft (and Rotorcraft) Pilot Couplings. The change of terminology deemed from two main reasons: ① The phrase 'pilot induced' somehow blames the pilot, whereas these couplings are more recognized to be a HQ deficiency of the vehicle, and ② There are also non-oscillatory behaviours as well in the adverse couplings history. There is, and will probably continue to be, a debate between PIO and RPC terminology^{85,92}. Moreover,

Mitchell and Klye mention 10 different PIO definitions in the literature⁹². Nevertheless, the following definition of RPC will be used in this thesis:

A RPC event exists when the airplane attitude, angular rate, normal acceleration, or other quantity derived from these states is approximately 180 degrees out of phase with the pilot's control inputs and both the vehicle response and the pilot's control expose considerable activity regarding the flying task.

The terms RPC and PIO will be used interchangeably in this thesis since the category that is relevant to the research in this thesis is a 'RPC type PIO', which will be described in this section.

2.4.1. CATEGORIES OF RPC

In 2010, an international European Union project (European Commission-7th Framework Programme), ARISTOTEL was initiated in order to investigate the RPC phenomena from various perspectives, such as criteria, simulator applications, design guidelines to prevent RPC, prediction and detection tools. This project can be considered as a continuation of great number of RPC related GARTEUR projects¹¹⁵. The progress in this thesis was mainly achieved during the activities of the ARISTOTEL project. The general classification of RPC used in the ARISTOTEL project is illustrated in Figure 2.17.

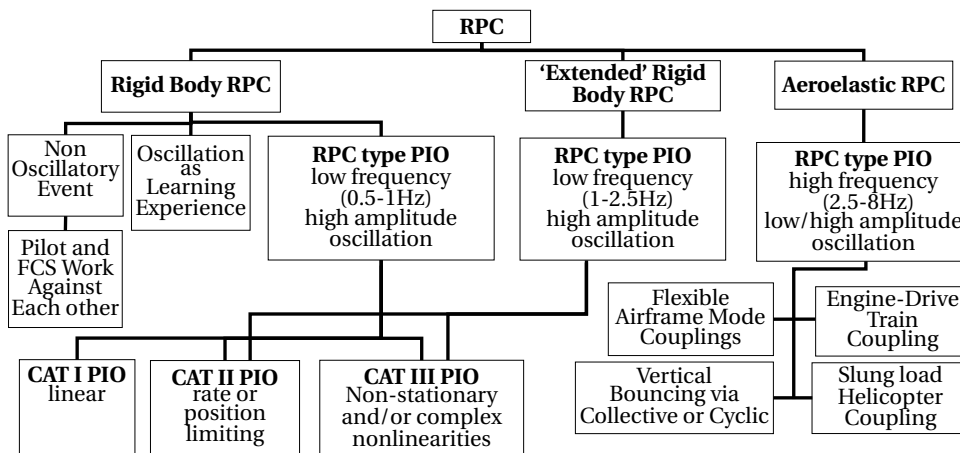


Figure 2.17: Classification of RPC, adopted from Ref. [115].

The main three categories of RPC are rigid body, extended rigid body and aeroelastic RPC as shown in Figure 2.17. For detailed descriptions of these RPC categories, the reader is advised to refer to Ref. [85, 115]. The RPC type in this thesis belongs to relatively low-frequency PIO, up to 1Hz, as will be discussed later in this thesis. In the 'RPC type PIO' class, there are three subcategories mainly described by the linearity of the RPC, as depicted in Figure 2.17.

CAT I category PIOs generally originate from excessive phase lags in the PVS, such as additional time delays, and they expose linear characteristics. CAT II category PIO manifest quasi-linear characteristics, such that most of the RPC occurrences can be modeled linearly with an extra identifiable non-linear element which can be separately handled. A classical example of this category is the RPC originated from actuator position and/or rate limiting. CAT III category PIO are non-linear couplings that can occur from sources like flight mode shifts and random flight control malfunctions.

Since this thesis will utilize LTI systems for manual control behaviour identification, the added time delay was chosen to be applied as a CAT I RPC trigger to represent the RPC susceptibility of the PVS.

The remaining RPC elements (the pilot model, the vehicle model and the task) used in this thesis will be discussed in the next chapter. In order to provide a general insight on these RPC elements, the following subsections will cover the general pilot modeling approach in RPC events, effects of the task difficulty and the time delay on HQ and RPC prospects.

2.4.2. PILOT MODELS IN RPC EVENTS

When considering the CAT I RPC, which is the relevant category for this thesis, there are primarily two pilot modeling methods⁸¹. The first one is the compensatory model, which is identical to the one described in Section 2.3.1. In short, here pilot applies a feedback loop to control the rotorcraft such that the open-loop exhibits a $1/(j\omega)$ -like response around the crossover frequency. In the ideal case, the pilot prefers a sufficient amount of phase margin to sustain a stable control of the vehicle. However, in a high precision tracking task, when the available phase margin drastically reduces due to a trigger (e.g., rate limiting) then the PVS can get into a RPC event rapidly.

The second pilot modeling method is a precognitive approach such that the pilot exerts control inputs depending on his/her previously experienced control behaviour. As a result, the pilot control behaviour simply becomes a gain, so-called 'Synchronous' pilot model⁸¹, following the vehicle response with a perfect synchronization without any time delay. For example, if the system inputs are of a sinusoidal shape, the pilot shows a pure gain response, matching the frequency of the sine wave without any time delay. This simple gain behaviour is a famous approach that fits with high accuracy to several recorded fully developed RPC⁸¹. It should be noted that this simple gain approach in RPC is essentially the rationale behind the pilot model in the BPD criterion described in Section 2.3.2.1.

Mitchell⁸⁷ investigated several actual PIO events and concluded that pilots **do not** show such a synchronous pilot behaviour in compensatory tasks. Instead, compensatory pilot behaviours were observed during PIO events. This agrees with the first type of pilot modeling method (the compensatory model), as introduced in this section. McRuer et al.⁸⁵ mention that PIO frequencies are around 1 Hz when the pilot is operating in a compensatory manner, whereas in a fully-developed synchronous operation it can

be as high as 2.5 Hz. Therefore, compensatory pilot control behaviour during an PIO can be expected around the crossover region. It is worth noting that this thesis does not aim to identify the pilot in a fully-developed RPC event. The main scope is to identify the manual control behaviour when exposed to RPC-prone configurations and investigate the pilot control adaptation to these configurations.

2.5. TIME DELAY AND TASK DIFFICULTY WITH HQ AND RPC PROSPECTS

As introduced at the beginning of this chapter, two key variables of this thesis are **the added time delay** and **the task difficulty**. In this section, the primary known effects of manipulating these variables on the HQ and RPC are investigated.

2.5.1. EFFECT OF THE TIME DELAY ON HQ AND RPC

Rotorcraft inherently exhibit delayed response, simply between the commanded pilot control input and the resultant vehicle response. Hamel³⁵ provides an analysis of the sources of the time delay in a rotorcraft control system, as shown in Figure 2.18.

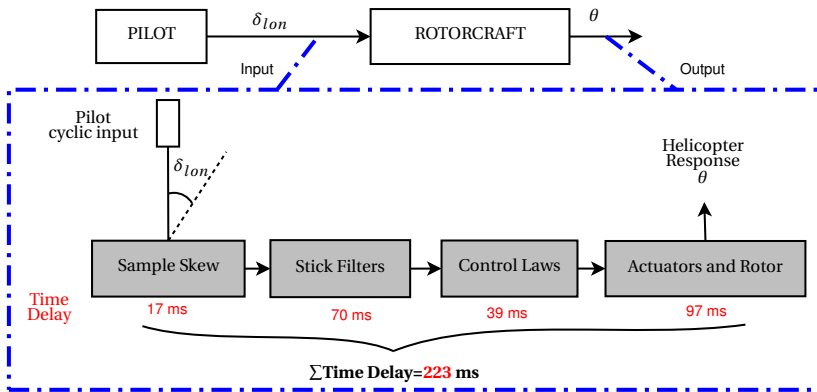


Figure 2.18: Response time analysis for the advanced digital optical control system demonstrator, adapted from Ref. [35].

As can be seen from Figure 2.18, the control command transmission from the cyclic input to the swash plate actuators generates a considerable amount of time delay (for example, a total delay of 223 ms in the Figure 2.18). The rotorcraft in this analysis of Hamel³⁵ is a FBW research rotorcraft, which does not include classical mechanical delays present in conventional helicopter systems. However, the sophisticated control laws and actuation technologies, such as FBW with notch filtering for flexible rotorcraft modes, lead to additional time delays as a side effect⁸⁵.

From a HQ perspective, an additional time delay results in phase roll-off at mid- and high frequencies, i.e., lower ω_{BW_θ} and higher τ_{p_θ} in BPD terms, as discussed in Section 2.2.2. For the pilot, the amount of time delay is directly related to a degradation of the 'perceived' HQ. By using the subjective pilot ratings, such as the Cooper-Harper

HQR in Appendix A, Hodgkinson et al.⁴³ investigated the primary effects of equivalent (effective) time delays on perceived HQ, as illustrated in Figure 2.19.

2

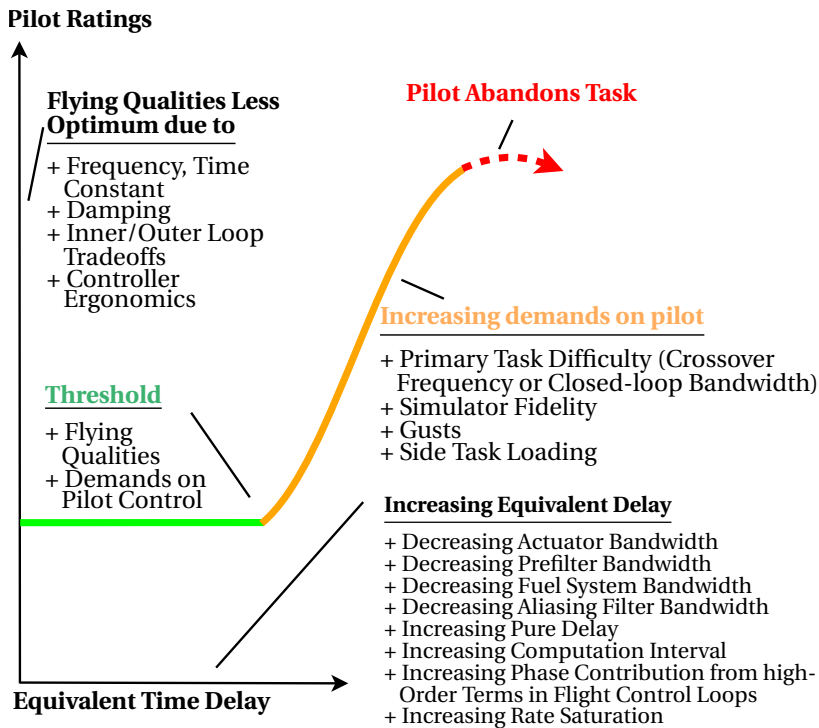


Figure 2.19: Generic rating variation with equivalent time delay, adapted from Ref. [43].

As shown in Figure 2.19, up to a certain amount of added time delay, pilots do not perceive any HQ degradation. This threshold depends on the HQ tolerance of the vehicle engaged in the task, such that the available gain and phase margins can still provide sufficient stability and task performance. After this amount, additional time delays cause quick HQ degradation with increased pilot demand, as indicated in Figure 2.19. This threshold value is also known as the 'HQ Cliff'⁴³, after which the HQ quickly deteriorate with increasing time delay.

After the start of the 'HQ Cliff', HQ degradation continues up to a time delay value beyond which the task is impossible to complete and the pilot abandons the task. Thus, the pilot HQR results shown in Figure 2.19 suggest that not only the HQ criteria such as BPD, but also the pilot as an operator is directly adversely affected by the additional time delay in the system.

Mitchell et al.⁹³ investigated the effect of added time delay (and motion) on rotorcraft HQ by using a flight simulator. The HQ evaluation was performed using subjective pilot ratings, HQR. Their results of the hover and vertical translation tasks of ADS-33 are depicted in Figure 2.20.

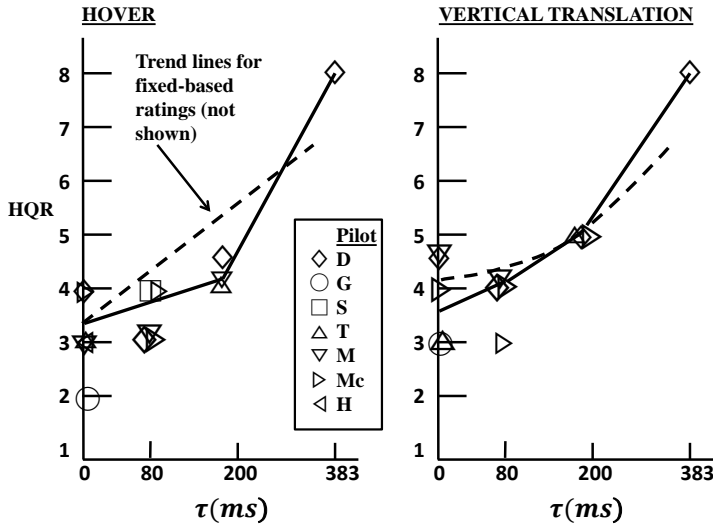


Figure 2.20: Effects of added time delay on HQR for the hover and vertical translation MTE in fixed-based and motion based simulator, adapted from Ref. [93].

As can be observed in Figure 2.20, additional time delay in the system caused pilots to award worse HQR, both for the hover and the vertical translation MTE. Moreover, this HQ degradation was observed in both the fixed-based and the motion-based configurations of the flight simulator⁹³.

Hess³⁷ conducted a set of experiments which utilized a compensatory task with basic controlled elements with various amounts of added time delays. The results of the open-loop response, i.e., $H_p(j\omega)H_{CE}(j\omega)$, is shown in Figure 2.21 for the $H_{CE}(j\omega) = K/(j\omega)$.

Figure 2.21 shows that increasing added time delay resulted in lower ω_c and higher φ_m . These variations arise from the pilot's effort to compensate for the additional phase lag originated from added time delay. When exposed to an additionally delayed CE, the pilot has to generate extra lead to compensate for the reduced phase margin. As a result, even though the dynamics of the CE do **not** require any pilot lead equalization (e.g., $Y_C = K/(j\omega)$) in Figure 2.21), additional pilot lead causes a relatively flat open-loop magnitude response around the crossover frequency. This can be observed in Figure 2.21b, in which the -20dB/decade slope can not be obtained. Thus, the fundamental rule of the classical crossover model can not be satisfied, since the open-loop does not exhibit $1/(j\omega)$ -like behaviour around crossover frequency. Moreover, it is worth recalling the BPD (Section 2.2.2.2), especially the vehicle model illustrated in Figure 2.5a. As dis-

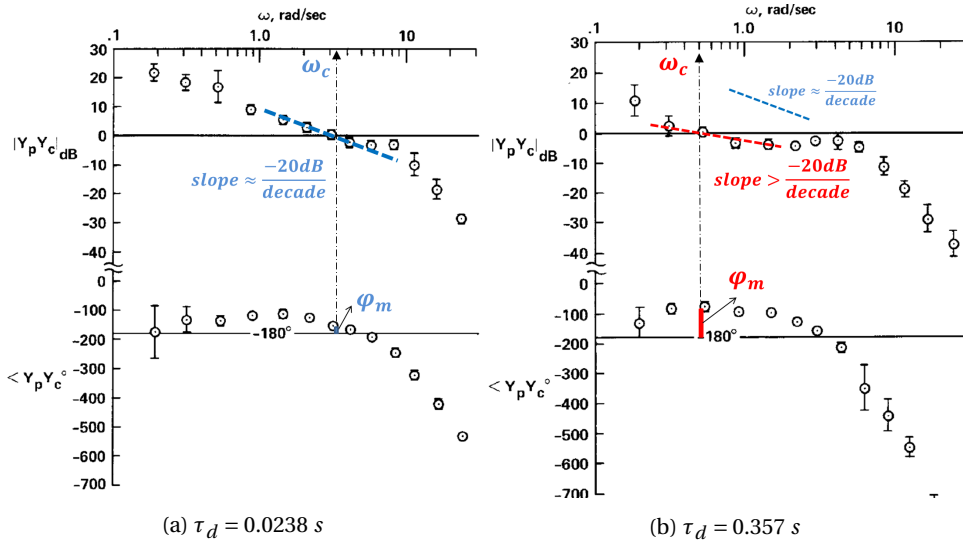
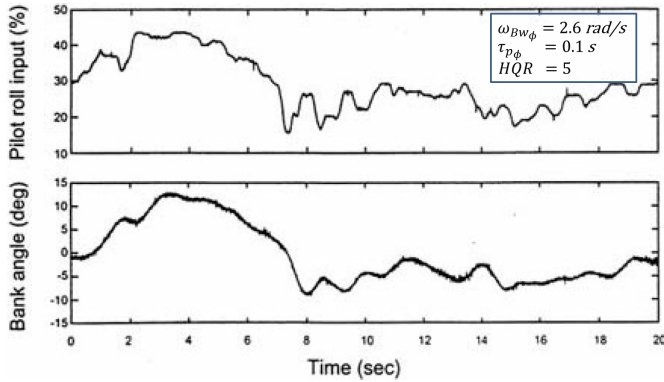


Figure 2.21: Bode plots of measured open-loop describing functions for the controlled element $Y_C = K/(j\omega)$, with two distinct values of added time delay; (a) 0.0238s and (b) 0.357s, adapted from Ref. [37]. Crossover frequencies, phase margins and the slope of open-loop magnitude responses are emphasized in the figure.

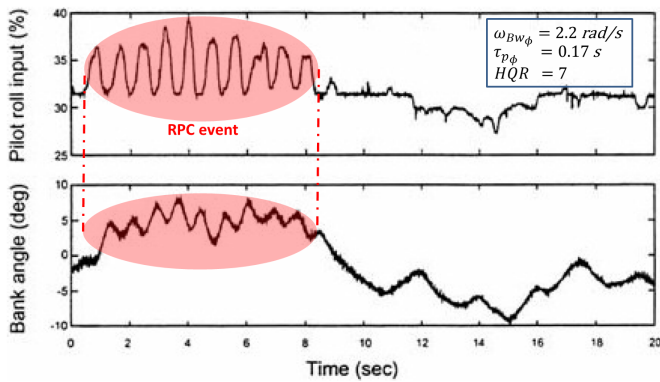
cussed in Section 2.2.2.2, flattened open-loop dynamics mean that any slight change in pilot gain can rapidly consume the available phase margin. This is a perfect catalyst for an RPC incipience.

As discussed in Section 2.4.1, additional time delay is a well-known CAT I RPC trigger. For example, Ockier¹⁰⁷ conducted a flight test campaign with a Bo-105 helicopter in a lateral-position task with varied added time delay. Sample data with and without added time delay are shown in Figure 2.22.

The results shown for the added time delay, as depicted in Figure 2.22, is a typical CAT I RPC. The saw-like pilot manipulator activity and oscillatory vehicle response, which is not required by the task, are both signatures of a RPC event. As given in Figure 2.22, the BPD criterion indicates a reduction in the bandwidth and an increase in the phase delay parameters. This deviation with added time delay was already discussed in Section 2.2.2.2. In addition, the increase of HQr (from 5 to 7) shows that pilots also noticed the degradation of HQ, and 'bang-bang' style control is already an indication of a HQ deficiency from a piloting perspective, as reflected in the awarded HQr¹⁰⁷.



(a) No added time delay



(b) 100 ms of added time delay

Figure 2.22: Pilot lateral cyclic and vehicle roll attitude of Bo-105 in a lateral-position task without (a) and with 100 ms of added time delay (b), adapted Ref. [107]. BPD parameters and awarded HQR are listed in the figure.

2.5.2. EFFECT OF THE TASK DIFFICULTY ON HQ AND RPC

One can interpret that the added time delay threatens the stability of the rotorcraft and limits the available performance (and safety) of the required task. This reduced stability may not be equally dangerous for all tasks that may need to be performed with the vehicle. For instance, the difficulty of the task also defines the achievable task performance with the capabilities of the vehicle. In any closed-loop task, the interaction between the pilot and the vehicle depends on the required task performance, which inherently depends on the definition of the task itself. Therefore, changing the task difficulty consequently forces the pilot to compensate accordingly to achieve the same performance. This pilot adaptation can reveal response characteristics of the vehicle within this varied task difficulty. Thus, the task difficulty has the potential to unmask any HQ deficiency of the vehicle via coupled pilot compensation to complete the task.

A typical example of the deviation of pilot control with varied task difficulty is the classical 'crossover regression' phenomenon described by McRuer et al.⁸¹. This phenomenon will be discussed in more detail in the next chapter. McRuer and Jex⁸⁰ found that for certain CEs in a compensatory tracking task, pilots adapt their control strategy such that the open-loop crossover frequency quickly decrease when the task bandwidth was increased after a certain value. This crossover regression is illustrated in Figure 2.23.

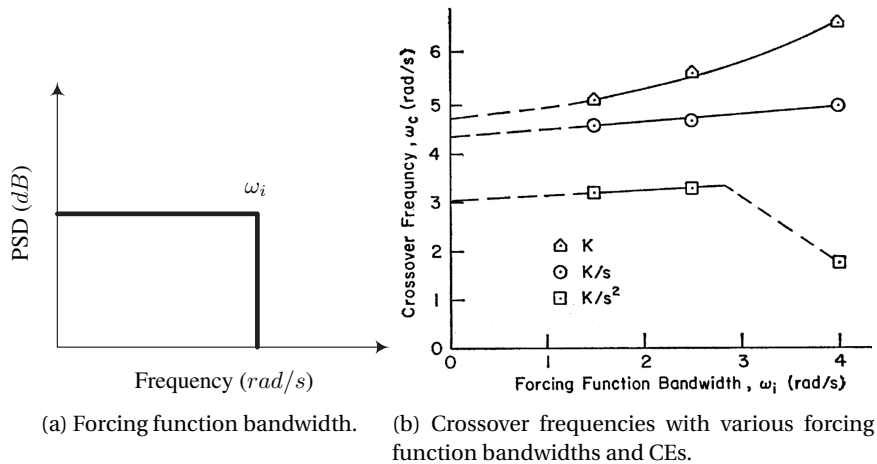


Figure 2.23: Definition of the forcing function bandwidth (a) and the crossover frequencies with varied forcing function bandwidth for three basic CE, adapted from Ref. [80].

The forcing function bandwidth, as shown in Figure 2.23a, characterizes the available frequency content in the tracking signal, and can be used to set the task difficulty in a compensatory tracking task. When different CEs are utilized, a clear crossover regression was observed with double-integrator dynamics ($H_{CE}(s) = K/s^2$) when task difficulty increased from $\omega_i \approx 2.5 \text{ rad/s}$ to $\omega_i \approx 4 \text{ rad/s}$, as depicted in Figure 2.23b. This shows that task difficulty can force the pilot to adapt his/her control strategy to certain conditions, in such a way that the PVS can exhibit considerably different task performance and stability characteristics. This situation suggests a close link between the task difficulty and the HQ. A good example of this link is the HQ research of Damveld²⁰ who focused on HQ assessments of fixed-wing aircraft models in a pursuit tracking task with various task bandwidths. In addition to the task difficulty, aeroelastic characteristics of the aircraft models were also varied to investigate the crossover regression tendencies based on the task bandwidth and aeroelastic aspects of the aircraft. In the present thesis, a similar methodological approach is followed, and a detailed comparison of both methodologies will be discussed in the next chapter.

As discussed in Section 2.2.2, in the field of HQ standards, ADS-33 is one of the most unique because of being explicitly 'task oriented', among other reasons mentioned in Section 2.2.2. There have been, and continue to be, many flight tests in several research

institutes and flight laboratories to elaborate the desired and adequate task performance boundaries of MTEs in ADS-33⁹⁶. For example, Figure 2.24 shows awarded pilot HQR during a sidestep manoeuvre conducted with various sidestep durations and roll response bandwidths.

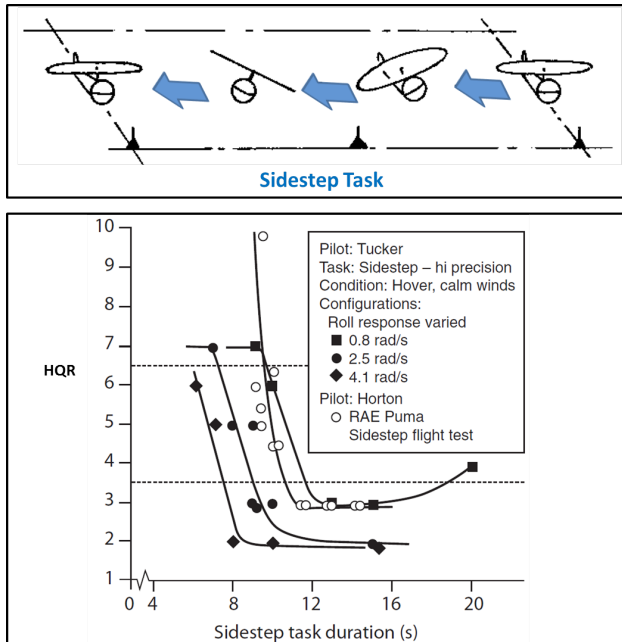


Figure 2.24: Rotorcraft agility with pilot ratings in a side-step MTE with varied task duration and roll responses, adapted from Ref. [111].

It can be clearly seen in Figure 2.24 that at a certain increased level of difficulty, which is correlated to sidestep duration, pilot HQR rapidly increased, representing a big degradation of HQ. Similar to the crossover regression phenomena, the HQ degradation occurs faster with different CEs, which are different roll bandwidths in this example. In Figure 2.24 it is shown that high roll bandwidth configurations can achieve shorter task durations (i.e., higher agility) before showing the 'cliff-like' degradation of HQ. Here, one can make the analogy with the crossover regression behaviour observed for the double integrator dynamics, i.e., $H_{CE}(s) = K/s^2$.

Akin to added time delay, task difficulty is also a contributor to the RPC characteristics of a vehicle. Mitchell et al.⁹⁶ state that the task should be sufficiently hard enough to unmask RPC susceptibility of the rotorcraft. A high gain task demands pilots to exert a tight control strategy with careful compensation and high precision. McRuer et al.⁸⁵ highlight the importance of pilot stress as a source of adverse coupling between the vehicle and the pilot, and he refers to the task difficulty issue as '... *Stress can also be task-induced when the pilot attempts a high-gain, high-stress task, such as aerial refueling or aircraft-carrier landing (p. 54).*'

The Handling Qualities During Tracking (HQDT) method for HQ evaluation for fixed-wing aircraft used very high-gain tracking tasks, with a strict demand on pilot to eliminate any displayed small error, consequently investigating PIO tendencies in high-gain tasks³². Although a great amount of research has been conducted with this HQ method in the USAF-TPS, the required 'zero-error' for high-gain tasks lead pilots to exhibit almost open-loop like high frequency corrective inputs, which is reported to be unnatural for pilots¹²⁵. Moreover, a lack of performance standards (only subjective PIOR were used) makes it hard to compare the results of HQDT with existing HQ assessment methods.

Nevertheless, high-gain tasks, which exhibit high potential to unmask susceptibility of adverse couplings between the pilot and the vehicle, have been used in many studies. McRuer et al.⁸⁵ stated that '*... The committee¹ believes that a desirable way to generate high gains is to simulate real aircraft tasks that emphasize precision PVS performance because realistic high-gain tasks make problems more credible. However, it is useful to include some tasks that naturally maximize pilot gain but that may not be typical of normal flight operations. These tasks should stress the PVS to its limits, thereby ensuring that it is not susceptible to APC phenomena under even the most extreme conditions (p. 98).*' Suggested high-gain tasks for unmasking A/RPC susceptibility can be summarized as⁸⁵:

- Aggressive Acquisition Maneuvers
- Aggressive Tracking Maneuvers
- Mode Transitions
- Formation Flying
- Aerial Refuelling (an example is shown in Figure 2.25)
- Approach and Landing
- Special Tracking Tasks with Random Forcing Functions

One can imagine the required precision and acquisition to perform a high-gain task such as aerial refuelling, as exemplified in Figure 2.25, under serious safety critical boundaries such as collision of the main rotor with the fuel probe while subjected to air-wake of the fuel carrier aircraft. This task is surely a difficult task such that if there is any RPC tendency, which could not be observed in a regular operational task, safety of the rotorcraft and the crew is highly threatened if the RPC gets triggered. Therefore, it is crucial to examine the RPC susceptibility of a rotorcraft for 'difficult' and demanding tasks to minimize the possibility of safety critical RPC occurrences.

¹The committee on the Effects of Aircraft-Pilot Coupling on Flight Safety, authors of the book 'Aviation Safety and Pilot Control: Understanding and Preventing Unfavorable Pilot-Vehicle Interactions'⁸⁵



Figure 2.25: A CH-53 helicopter performing an aerial refueling task. (Source: www.defenseimagery.mil)

2.5.3. COMBINED EFFECT OF THE TIME DELAY AND THE TASK DIFFICULTY ON HQ AND RPC

As being two key variables in this thesis, both the time delay and the task difficulty can be effective in revealing possible HQ deficiencies and the RPC susceptibility of the rotorcraft, as discussed in previous sections. This section will focus on the 'combined' effect of these two major variables as evaluated in previous investigations. For example, Smith and Sarrafian¹²⁸ presented pilot HQR for F-8 and NT-33 aircraft flight and simulator tests, with varied effective time delays and task stresses, as shown in Figure 2.26.

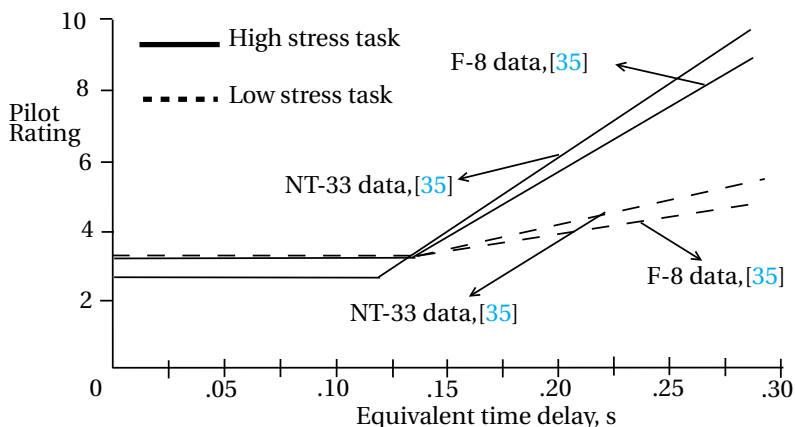


Figure 2.26: Pilot HQRs for low and high stress flying tasks with different levels of equivalent time delays, adapted from Ref. [128].

Figure 2.26 indicates two important observations. First, the 'HQ Cliff', which was discussed in Section 2.5.1, can be clearly seen for both aircraft in both stress level tasks. Second, high and low stress tasks showed different tendencies to expose HQ degradations with increasing equivalent time delay. As highlighted in Figure 2.26, high stress tasks have a sharper HQ degradation than low stress tasks, which confirms the impor-

tant role of 'the task difficulty' on HQ accompanying equivalent time delay.

During the ARISTOTEL project, the precision hover task, a MTE defined in ADS-33, was flown by four professional rotorcraft pilots in SIMONA Research Simulator (SRS) and HeliFlight-R Helicopter Simulator (HFR) full motion simulators. In addition to the original hover task, an important element of the task was modified to achieve a more demanding task, such that the vehicle under control, a high fidelity simulation model of Bo-105 helicopter, could reveal it's HQ characteristics accompanying it's RPC proneness. The altered task element was the location of the hover ball, which is illustrated in Figure 2.27.

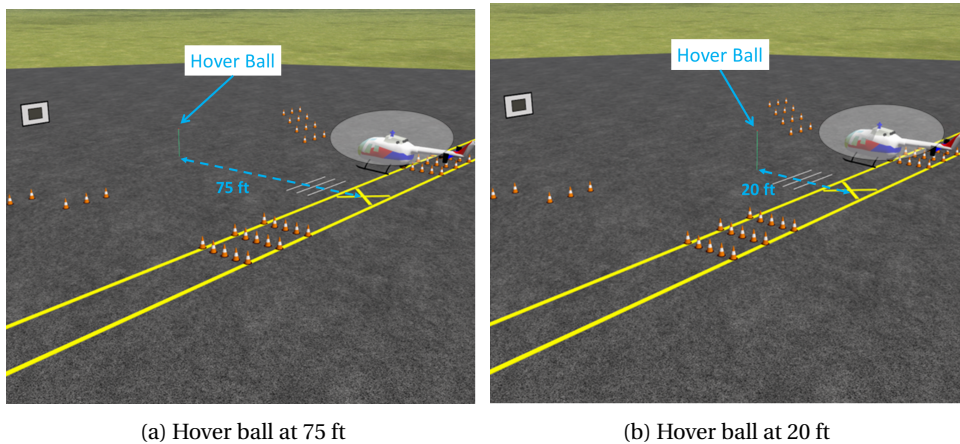
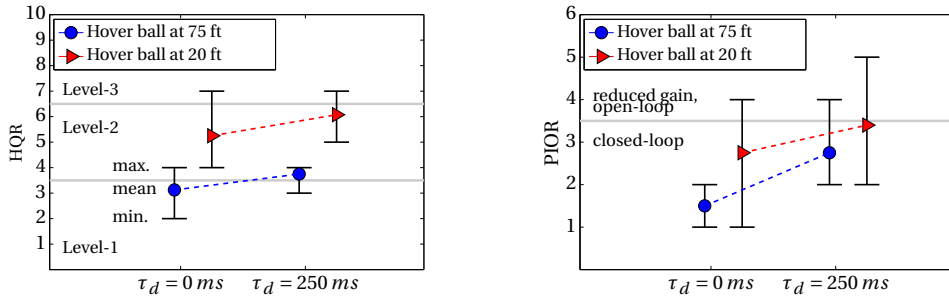


Figure 2.27: Outer view of the precision hover task MTE with hover ball at 75 ft (a) and 20 ft (b).

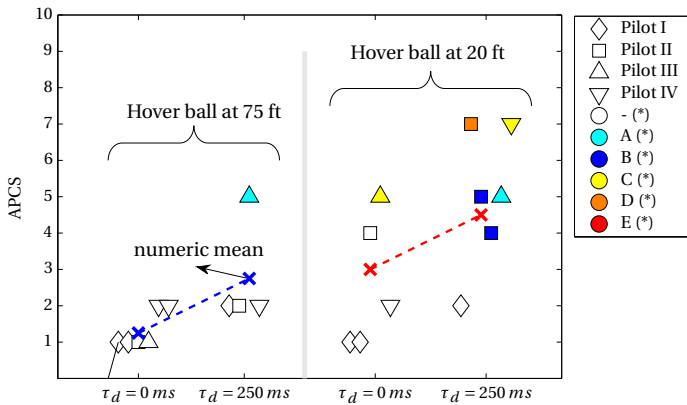
During the capture and stabilisation phases of the hover MTE, a relocated hover ball (Figure 2.27) lead to a higher precision task which demanded tighter pilot control. This is equivalent to increasing task difficulty. When combined with the added time delay, this task modification also increased the RPC tendency of the PVS. Figure 2.28 shows pilot ratings of the precision hover task with original (75 ft) and closer (20 ft) hover ball configurations with and without the presence of the additional time delay, in HFR simulator. Recorded pilot ratings were HQR, PIOR and Adverse Pilot Coupling Scale (APCS), which are provided in Appendix A.

It can be seen from Figure 2.28a that pilots awarded worse handling qualities ratings when the task difficulty was increased, i.e., hover ball located at 20 ft. This degradation of HQ due to task difficulty was observed with added time delay configurations as well. For each task difficulty, added time delay degraded the HQ, such that original task (75 ft) shifted from Level-1 to Level-2, whereas the harder task showed a deviation from Level-2 to the border of Level-3 HQ. A similar trend can be seen in the PIOR, as depicted in Figure 2.28b. Although the between-subject variability is relatively high for the awarded PIOR, still a trend of increased RPC tendency with increased task and the added time



(a) Awarded HQR.

(b) Awarded PIOR.



(c) Awarded APCS. *: Oscillation rating letters in APCS, see Appendix A.3.

Figure 2.28: Awarded pilot ratings for original (75 ft) and closer (20 ft) hover board location without and with the additional time delay (250 ms); a) HQR, b) PIOR and c) APCS.

delay can be observed. Especially, the harder task resulted in dangerous RPC boundary (PIOR 3.5 boundary in Figure 2.28-b) after which pilots need to severely reduce their gain and switch into open-loop control. It is worth mentioning that during the total four simulator test campaigns conducted in SRS and HFR for the ARISTOTEL project, the PIOR were found to be somewhat of confusing for the pilots, such that the numeric numbering and the corresponding text description found be not directly descriptive of the experienced RPC condition⁵⁴. Instead, a new subjective rating scale was developed and used during the test campaign. This rating scale is called⁵⁴ and presented in Appendix A.

The fundamental improvement of the APCS is categorizing the pilot compensation effort and the adversely coupled conditions separate, by utilizing numeric and alphabetic ratings assigned with clear descriptions. Pilots commented the positive contribution of the APCS to assesses the RPC tendency of the rotorcraft. For detailed information, reader is advised to refer to Ref. [54]. As shown in Figure 2.28c, APCS tendencies show a clear difference between the task difficulties. The harder task configuration exposed more RPC prone responses than the original hover, for both no time delay and added time delay conditions. Moreover, the added time delay clearly increased the RPC susceptibility of the rotorcraft, both in the original and the harder task configurations. However, added time delay caused highly RPC prone conditions for the hard task, whereas it has not experienced such a strong RPC susceptibility in the normal hover task. Especially the oscillatory characteristics, which are awarded by apathetic ratings (see Figure 2.28c), indicate the RPC problem of the rotorcraft for that configuration.

From a practical point of view, increased task difficulty brings the pilot to his/her edge of the precise control. Then, reducing the stability of the rotorcraft, like adding a time delay, strongly effects the closed-loop PVS response characteristics, which are already on their boundaries due to the engaged high-precision task. Thus, a joint effect of the task difficulty and the added time delay can actually benchmark the PVS better than the individual effects of the task bandwidth and the added time delay.

2.6. CONCLUSIONS

A brief review on rotorcraft HQ was provided, highlighting the innovative task-oriented ADS-33 HQ evaluations, with a particular interest in the BPD criterion. The importance of the BPD is the inherent capability of the composing parameters to address PVS stability. Pilot modelling techniques, which are utilized in HQ studies, were briefly introduced. Furthermore, pilot model structures used in HQ criteria were reviewed. Unfavourable couplings between the pilot and the rotorcraft were introduced, with definitions of categories and involved pilot modeling approached to RPC phenomenon.

Principles of McRuer's crossover model found to be a fundamental approach to describe pilot control behaviour, and serve as an origin to various pilot modeling techniques used in HQ and RPC studies.

As being two major factors in the thesis, the added time delay and the task difficulty were reviewed in terms of their individual and combined effects on rotorcraft HQ and RPC. It is concluded that the combination of both factors has a high potential to unmask RPC susceptibility, which can actually be hidden if each factor has been applied individually.

In this chapter, two drawbacks of the current HQ and RPC criteria and assessment methods are discussed. First drawback is the lack of pilot modeling with parameters to describe the manual control behaviour. The review on the pilot modeling in HQ and RPC shows that 'paper' pilot models (e.g., Neal-Smith), simplified pilot models (e.g., synchronous simple gain pilot) and more complicated models (e.g., structural pilot model)

have application constraints and limitations, and they do not contain any identified pilot model with parameters. Thus, understanding the manual control behaviour on the detail of pilot model parameters is missing. Second drawback is the scatter of subjective pilot ratings during some HQ and RPC assessments. As shown in this chapter, subjective ratings can have a high variety on certain conditions, and this variety can cause unclear determination of the HQ and RPC susceptibility of the vehicle. The next chapter will summarize these drawbacks, and propose a new methodology to address these drawback with an objective HQ determination by using a parametrized and identified manual control behaviour model.

3

METHODOLOGY

The previous chapter provided a review on rotorcraft HQ and RPC, and pilot modeling prospects of these two elements of rotorcraft performance. Individual and combined effects of added time delay and increased task difficulty on rotorcraft HQ and RPC tendency were discussed. Moreover, it was summarized that during the assessment of HQ and RPC susceptibility, pilots award subjective ratings (e.g., HQR and PIOR) and mathematical pilot models are utilized in HQ criteria (e.g., Neal-Smith criteria) or RPC studies (e.g. synchronous pilot model). In order to overcome drawbacks of subjective ratings and current theoretical math pilot approaches, this chapter introduces a new methodology to be used for objective HQ assessment, by using manual control behaviour identification techniques. Details of this new methodology, referred to as the MCIM, will be thoroughly described, including descriptions of the RPC detection tools to be used in the MCIM.

3.1. INTRODUCTION

The previous chapter presented a review on HQ and RPC prospects of rotorcraft, and provided some typical pilot modeling approaches being used to assess these elements. Based on this review, two important drawbacks of the current HQ and RPC assessment methods can be summarized:

① **Limitations of the theoretical pilot models**

As discussed in the previous chapter, the BPD criterion in ADS-33 can be interpreted as a stability measure of the PVS with a pure gain pilot with assigned phase and gain limitations of the open-loop. In addition to this simple gain pilot model, Neal-Smith criteria utilize a theoretical pilot model with gain, lead and lag compensation with a certain closed-loop bandwidth restriction. Similarly, the majority of the theoretical pilot models

in HQ assessment methods such as BPD, Neal-Smith and HQSF criteria are subjected to such predefined restrictions. These restrictions in HQ and RPC criteria could lead to improper (or lacking) modeling of the pilot control behaviour^{20,69}. For example, Lone and Cook⁷¹ stated that the major contribution of the Neal-Smith criteria is successfully linking pilot compensation to handling qualities, not pilot model development.

② High variety in subjective pilot HQ and RPC ratings for the same flying task

A general practice of evaluating rotorcraft HQ and RPC tendency is using subjective pilot assessments, e.g., HQR and PIOR. Pilots require dedicated training to apply proper HQ and RPC assessment methods¹⁴⁶. Using HQR, HQDT and PIOR directly reflects the 'perceived' HQ and the RPC tendency by trained pilots. However, these assessment methods are often prone to high subjective variability for the same flying task^{46,146}. Flynn and Lee²⁷ illustrated this HQR diversity as shown in Figure 3.1. As exemplified

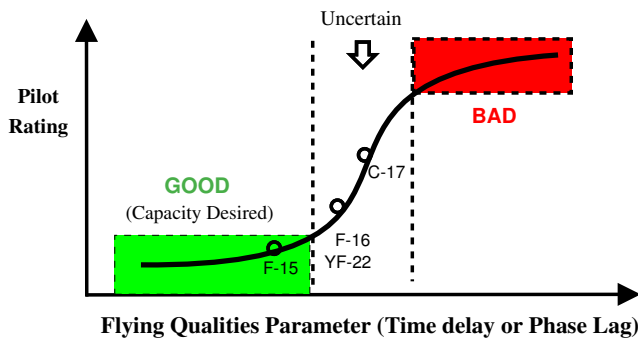


Figure 3.1: Pilot rating versus HQ correlation, adapted from Ref. [27].

in Figure 3.1, subjective ratings for very good or very bad HQ are generally well captured by subjective pilot ratings. However, under certain conditions, a region of pilot subjective ratings shows considerable variation²⁷, as illustrated by the uncertain region in Figure 3.1. This high variety in subjective pilot ratings suggests that awarded HQR in such conditions should be carefully examined before any qualitative HQ assessment^{46,146}.

These two drawbacks (i.e., limitations of theoretical pilot models and the diversity in awarded pilot ratings) bring a new opportunity for a novel HQ and RPC assessment research that utilizes objective manual control behaviour. The new methodology proposed in this thesis, MCIM, originates from this idea.

Section 3.1.1 will describe the development of the MCIM. Next, Section 3.1.2 will provide the outline of the MCIM. The following sections will describe each element of the MCIM in detail. Section 3.2 will explain the selection of rotorcraft model and applied additional time delay to be used in MCIM. Section 3.3 will provide information about the selection of forcing function bandwidth as a measure of task difficulty in MCIM. Next, the forcing function to be used in simulator experiments for manual control identification in MCIM will be described in Section 3.4. As a fourth step, Section 3.5 will describe

the techniques to be used for PVS analysis in MCIM. Next, RPC detection tools to be utilized in MCIM will be provided in Section 3.6. Finally, Section 3.7 will conclude on the development and methodology of the MCIM.

3.1.1. MCIM DEVELOPMENT

In 2009, Damveld²⁰ developed a methodology which utilizes the identification of the pilot control behaviour for HQ assessments of fixed-wing aircraft with various aeroelastic characteristics. This method, the so-called Experimental Behavior Measurement Method (EBMM), evaluates the crossover regression as an indication of HQ when the task difficulty is altered for tracking tasks. After a certain level of task difficulty is reached, pilots noticeably changed their control strategies which were determined by using identification of pilot control behaviour.

MCIM adapts a similar rationale of the EBMM, such that HQ of an aerial vehicle can be assessed by investigating the manual control behaviour in an objective manner, e.g., manual control identification. However, there are several differences between EBMM and MCIM. First, EBMM focuses on the pilot control behaviour for fixed-wing aircraft with different aeroelastic characteristics in a tracking task with various task difficulties. Whereas the MCIM focuses on the manual control behaviour for **rotorcraft** with added **time delays** and varied task difficulties. As discussed in the previous chapter, added time delay and varied task difficulty are two linked contributors of HQ deficiencies and **RPC susceptibility**, which are considered in MCIM. In other words, whereas the EBMM focuses on the determination of the HQ of the aircraft, the MCIM also considers the RPC proneness of the rotorcraft, and provides information about the relation between the RPC susceptibility and the changes in manual control behaviour. A second difference between EBMM and MCIM is the **parametrization of the identified manual control behaviour**. EBMM mainly uses the open-loop crossover frequency to assess the HQ of the aeroelastic aircraft. Pilot describing functions are obtained but a pilot model structure has not been used. The MCIM utilizes not only crossover frequencies, but also identified parameters of the estimated pilot model structure. Finally, EBMM primarily targets high-frequency aspects of the pilot control behaviour correlated with aeroelastic modes, whereas the MCIM focuses on low and mid-frequency manual control during which pilots exhibit cognitive controls. Advantages and disadvantages of both EBMM and MCIM, and other typical HQ assessment methods are listed in Table 3.1.

Table 3.1: Summary of advantages and disadvantages of some HQ evaluation methods including MCIM. The original table is adapted from Ref. [20].

	HQ method	Advantages	Disadvantages
Theoretical analysis	Neal-Smith	<ul style="list-style-type: none"> • Correlates handling qualities to only two parameters (phase compensation and resonance peak) • Quantifiable measures 	<ul style="list-style-type: none"> • Prediction can be erroneous • Limited human operator model • Fixed bandwidth • Restricted to simple tasks • No feel-system present
	BPD	<ul style="list-style-type: none"> • Correlates handling qualities to only two parameters (bandwidth and phase delay) • Quantifiable measures 	<ul style="list-style-type: none"> • Prediction can be erroneous • Limited human operator model • Fixed stability margins • Restricted to simple tasks • No feel-system present
Pilot evaluation	Cooper-Harper	<ul style="list-style-type: none"> • Real pilot behaviour and opinion • Evaluates all aspects of realistic tasks 	<ul style="list-style-type: none"> • Lack of stress or anxiety • Lack of insight in cause • Quasi-quantitative (subjective)
	HQDT	<ul style="list-style-type: none"> • Reveals hidden deficiencies due to forced high-bandwidth control behaviour 	<ul style="list-style-type: none"> • Pilots regard piloting technique highly unnatural • No quantifiable measures
Control behaviour measurement	EBMM	<ul style="list-style-type: none"> • Reveals hidden high bandwidth deficiencies • Real pilot behaviour • Correlates handling qualities to a few behavioural parameters (open-loop crossover frequency, phase margin, pilot describing function) • Feel-system present • Pilots can use natural piloting technique 	<ul style="list-style-type: none"> • Restricted to simple tasks • Does not evaluate all aspects of realistic tasks
	MCIM	<ul style="list-style-type: none"> • Correlates handling qualities to a few behavioural parameters • Feel-system present • Quantifiable measures (open-loop crossover frequency, phase margin, pilot describing function) • Identified pilot model parameters • Time delay and Task difficulty and their combined effects on HQ and RPC tendency • Utilized RPC detection tools 	<ul style="list-style-type: none"> • Restricted to simple tasks • Does not evaluate all aspects of realistic tasks

3.1.2. MCIM OUTLINE

In MCIM, a single-axis disturbance-rejection task is utilized with visual cues only. The schematic representation of a disturbance rejection task is shown in Figure 3.2.

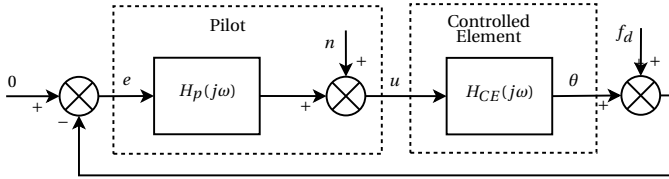


Figure 3.2: Block diagram of the compensatory disturbance-rejection task in MCIM.

As shown in Figure 3.2, in a compensatory single-axis disturbance-rejection task in the pitch (or roll) channel, human operators try to minimize the displayed error (e) which is originated from the difference between the disturbance forcing function (f_d) and the vehicle pitch θ (or roll ϕ) response due to applied pilot control (u). In Figure 3.2, quasi-steady pilot model is given as the linear behaviour model ($H_p(j\omega)$) summed with pilot remnant (n) accounted for nonlinear control inputs. The rotorcraft represented as the CE is a linear on-axis frequency response of the rotorcraft ($H_{CE}(j\omega)$).

Considering the task in MCIM, adding a time delay to the CE causes a phase margin reduction, and results in an open-loop instability which occurs at lower frequencies than no delay conditions, as discussed in the previous chapter. In addition, increasing the bandwidth of the forcing function causes the task to become harder. Thus, the human operator may need to exhibit a crossover regression strategy to maintain performance at a sufficient level, as outlined in the previous chapter. Individual and combined effects of these two contributors, i.e., added time delay and forcing function bandwidth (here also referred to as task bandwidth), can determine the tolerance of the rotorcraft model under manual control to complete a given task. MCIM identifies manual control behaviour of human operators subjected to rotorcraft models with these individual and combined conditions. MCIM proposes that the conditions at which control strategies of human operators noticeably change, e.g., the crossover regression, can be used as a measure of the HQ and RPC proneness. MCIM A schematic overview of the MCIM is shown in Figure 3.3.

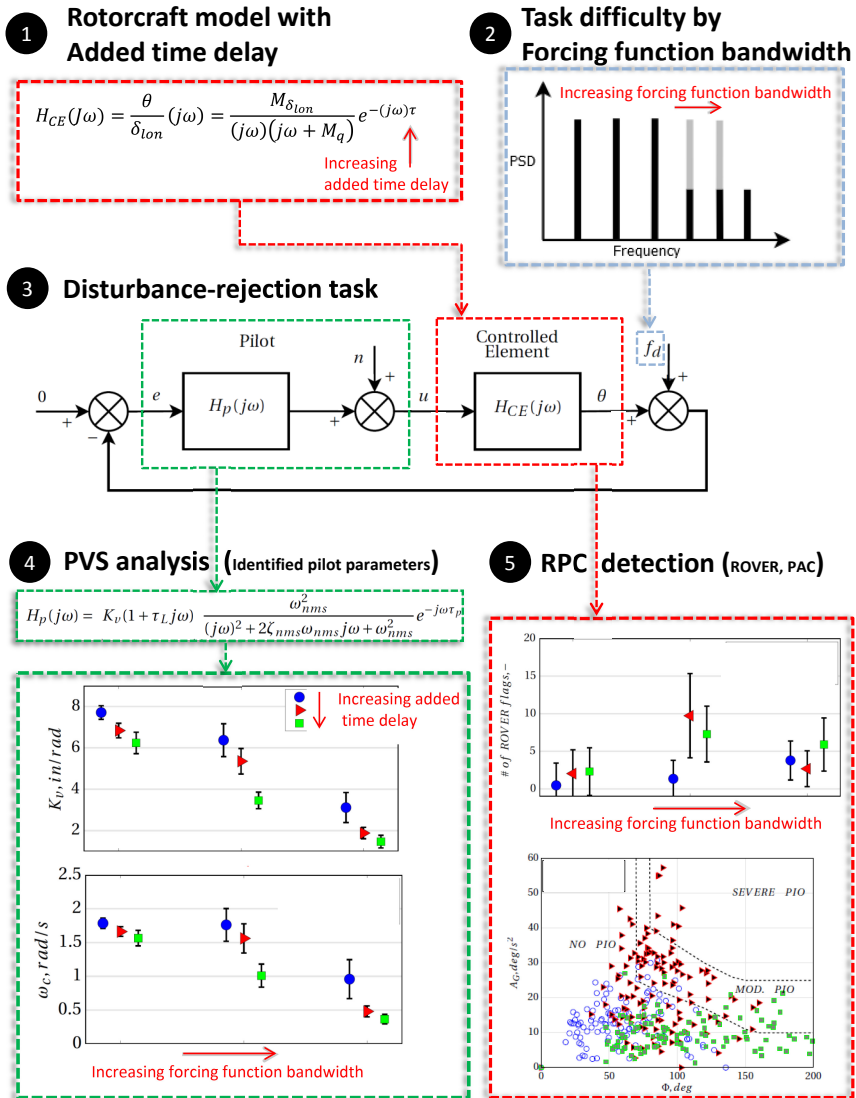


Figure 3.3: A schematic overview of the MCIM, with five steps of the methodology.

The outline of this chapter coincides with the proposed steps of the MCIM in Figure 3.3. Brief descriptions of these steps are given as follows:

- **Step 1: Rotorcraft model with added time delay**

The first step consists of the rotorcraft model to be used in the MCIM. The model should be able to significantly represent the vehicle characteristics, especially around the possible crossover frequency region which can be considered as low and

mid-frequencies when rotorcraft dynamics are taken into account. In addition, the rotorcraft model should be able to include additional time delay, which is used here to vary the HQ deficiencies and RPC tendencies. Details of this step will be further described in Section 3.2.

- **Step 2: Task difficulty by forcing function bandwidth**

As a part of the MCIM, human operators are exposed to a random appearing forcing function, i.e., disturbance, which excites the PVS. In this thesis, the bandwidth of the forcing function represents the difficulty of the task that human operators have to compensate with the given rotorcraft model. It can lead the human operator to adopt a 'regressed' control strategy, which can be observed by the classical crossover regression. This step of determination the forcing function will be described in detail in Section 3.3.

- **Step 3: Disturbance-rejection task**

As shown in Figure 3.3, MCIM utilizes a compensatory disturbance-rejection task to be used in identification experiments. In this task, a disturbance signal is injected to the PVS and human subjects aim to null the displayed error originated from the difference between the disturbance and the response of the rotorcraft model. By using this compensatory task, it is possible to identify the manual control behaviour. Details of this task will be described in Section 3.4.

- **Step 4: PVS analysis**

Measured data from the disturbance-rejection task are analysed in this step. Measured time traces of the displayed error (input to the human operator) and corresponding pilot control activity (output of the human operator) are processed. With the LTI assumption, the output-to-input relation of the human operator defines the control behaviour, which can be determined by identification techniques. Therefore, variations in manual control strategies for combinations of added time delay and task difficulty can be examined. Measured errors, manual control activities, open-loop crossover frequencies, phase margins and identified pilot model parameters are analysed in this step. Detailed description of this PVS analysis process will be given in Section 3.5.

- **Step 5: RPC detection**

This step consists of applying two RPC detection tools; ROVER and PAC. These tools are used on the data obtained from identification experiments. Particularly, the conditions in which human operators exhibit crossover regression tendencies are checked with the detected RPC occurrences. As a result, correlations between the change of pilot control strategy and RPC susceptibility of the rotorcraft model in these conditions can be obtained. Section 3.6 will describe the application of RPC detection tools in MCIM.

3.2. STEP 1: ROTORCRAFT MODEL WITH ADDED TIME DELAY IN MCIM

In this thesis, the Bo-105 helicopter (Figure 3.4) is chosen to be simulated. An interesting feature of Bo-105 is the hingeless rotor mechanism which allows the rotor moments to be transferred to the rotorcraft body. Thus, it exhibits higher manoeuvrability than rotorcraft with conventional articulated rotor. As a result, it provides an interesting research field for HQ and RPC studies. Moreover, Bo-105 is a well-known helicopter in HQ and RPC researches due to extensive flight test and identification data which are publicly available⁵⁶. Particularly, DLR conducted many flight tests with Bo-105, dedicated to HQ and RPC research. For instance, Ockier¹⁰⁸ investigated the effect of added time delay on HQ of Bo-105 during a side-step task.

3



Figure 3.4: Bo-105 helicopter (www.dlr.de).

Development of rotorcraft simulation models has several challenges. Some of the major challenges arise from inherent rotorcraft characteristics such as nonlinear and coupled responses depending on the flight speed and manoeuvre, aerodynamically challenging environment with the wake of both main and tail rotors, cross-coupled flight controls, interacting fuselage and rotor modes, and high demand on operational performance and safety with nap-of-the-earth mission profiles³⁶. Considering these challenges, a common follow-up question in the rotorcraft simulation community can be addressed as: 'What would be the appropriate simulation fidelity of a rotorcraft simulation model?'. The answer to this question solely depends on the 'aim' of the simulation effort. Depending on the aim, rotorcraft models with various fidelities have been developed, and continue to be evolved¹¹¹. For example, a decoupled and linearised model can be considered as a simple model, whereas a sophisticated aeroelastic simulation model with non-linear wake features can be an example of a complex model.

Pavel¹¹⁴ investigated the necessary Degree of Freedom (DoF) to be simulated in helicopter (and wind turbine) models by using critical pole distance criterion, which mainly determines the couplings between the rotorcraft body and the main rotor modes. Prior to the development of this criterion, a literature survey was conducted on rotorcraft DoF as a measure of model complexity, as shown in Table 3.2.

Table 3.2: Simulation model complexity for various helicopter applications, adapted from Ref. [114].

Model Complexity		6 DoF	8 DoF	9 DoF	10 DoF	12 DoF	16 DoF
Basic aircraft							
Low frequency maneuver	articulated	■					
	hingeless	▲	▲	▲			
High frequency maneuver	articulated		▲	▲			
	hingeless		■	▲	▲		
Helicopter+SCAS system							
Fuselage feedback	articulated	▲	▲				
	hingeless	▲	■	▲			
Fuselage/Rotor feedback	articulated			▲	▲	▲	▲
	hingeless			▲	▲	▲	▲
Full HHQ Basic aircraft							
Within Envelope		▲			▲		▲
At the Boundary					▲		■
Specific HHQ							
		▲			▲		▲

■ : model used in most of the cases	6 DoF: Fuselage + Quasi-static Rotor
▲ : model used for some cases	8 DoF: Fuselage + First-order Disc-Tilt Dynamics
HHQ : Helicopter Handling Qualities	9 DoF: Fuselage + Second-order Disc-Tilt Dynamics
	10 DoF: Fuselage + Rotor Flap +rpm
	12 DoF: Fuselage + Rotor Flap +Rotor Lead/Lag
	16 DoF: Fuselage + Rotor Flap + Rotor Lead/Lag + Pitch + rpm

Table 3.2 shows that rotorcraft simulation community chooses the required DoF for their specific needs per application. In addition, Padfield¹¹¹ provides a summary of simulation fidelities depending on the rotor modeling and corresponding applications, as shown in Table 3.3. As Table 3.3 illustrates, Level 1 and Level 2 simulation fidelities of rotor modeling are appropriate for parametric HQ research studies.

It is worth noting that this thesis mainly focuses on the manual control behaviour, instead of achieving high fidelity rotorcraft models. Thus, instead of a sophisticated rotorcraft simulation model, a simple (yet still representative) form of a rotorcraft response model is utilized. Moreover, this form has to be a linear model since this thesis contains LTI identification methods, which will be described in Section 3.5. With a linear rotorcraft model, a state-space representation of the coupled body and rotor equations of motion can be achieved¹²², as shown in Eq. (3.1).

Table 3.3: Rotorcraft simulation fidelity based on rotor modelling and corresponding applications, taken from Ref.[111].

	Level 1	Level 2	Level 3
<i>Aerodynamics</i>	<ul style="list-style-type: none"> •linear 2-D dynamic inflow •local momentum theory •analytically integrated loads 	<ul style="list-style-type: none"> •non-linear(limited 3-D) dynamic inflow •local momentum theory •local effects of BVI •unsteady 2-D compressibility •numerically integrated loads 	<ul style="list-style-type: none"> •non-linear (full 3-D) wake analyses (free or prescribed) •unsteady 2-D compressibility •numerically integrated loads
<i>Dynamics</i>	<ul style="list-style-type: none"> •rigid blades (1) quasi-steady motion (2) 3 DoF flap (3) 6 DoF flap + lag (4) 6 DoF flap + lag + quasi-steady torsion 	<ul style="list-style-type: none"> (1) rigid blades with as in Level 1 (2) limited number of blade elastic modes 	<ul style="list-style-type: none"> •detailed structural representation as elastic modes of finite elements
<i>Applications</i>	<ul style="list-style-type: none"> •parametric trends for flying qualities and performance studies well within operational flight envelope •low bandwidth control 	<ul style="list-style-type: none"> •parametric trends for flying qualities and performance studies up to operational flight envelope •medium bandwidth appropriate to high gain active flight control 	<ul style="list-style-type: none"> •rotor design •rotor limit loads prediction •vibration analysis •rotor stability analysis up to safe flight envelope

$$\begin{array}{c}
 \begin{array}{l}
 \text{Fuselage} \\
 \left[\begin{array}{c} \dot{u} \\ \dot{v} \\ \dot{w} \\ \dot{p} \\ \dot{q} \\ \dot{r} \\ \dot{\theta} \\ \dot{\phi} \end{array} \right] \\
 \\
 \text{Rotor} \\
 \left[\begin{array}{c} \dot{a}_0 \\ \dot{a}_1 \\ \dot{b}_1 \\ \vdots \end{array} \right]
 \end{array}
 =
 \begin{array}{c}
 \text{State Matrix} \\
 \left[\begin{array}{|c|c|}
 \hline
 \text{rigid body} & \text{body /rotor coupling} \\
 \hline
 \text{rotor /body coupling} & \text{rotor} \\
 \hline
 \end{array} \right]
 \end{array}
 \begin{array}{c}
 \text{States} \\
 \left[\begin{array}{c} u \\ v \\ w \\ p \\ q \\ r \\ \theta \\ \phi \\ a_0 \\ a_1 \\ b_1 \\ \vdots \end{array} \right]
 +
 \begin{array}{c}
 \text{Control Matrix} \\
 \left[\begin{array}{|c|c|}
 \hline
 \text{dark shaded} & \text{light shaded} \\
 \hline
 \text{light shaded} & \text{dark shaded} \\
 \hline
 \end{array} \right]
 \begin{array}{c}
 \text{Controls} \\
 \left[\begin{array}{c} \delta_0 \\ \delta_x \\ \delta_y \\ \delta_{TR} \end{array} \right]
 \end{array}
 \end{array}
 \quad (3.1)
 \end{array}$$

where the state vector contains the three translational velocity components u, v and w , the three rotational velocity components p, q and r , the Euler angles ϕ and θ , longitudinal δ_x and lateral δ_y cyclic inputs, collective δ_0 and pedal δ_{TR} inputs, longitudinal (a_0, a_1) and lateral b_1 rotor states. Rotor states in Eq. (3.1) can be extended with flapping, lead-lag, inflow and torsion modes, with required order of harmonics. As indicated by the dark-shaded regions in Eq. (3.1), both rigid body and rotor have their state and control matrix partitions directly responsible for their state derivatives. In addition, cou-

plings between the body and the rotor introduce body/rotor or rotor/body coupled state matrix terms which are indicated by the light-shaded regions in Eq. (3.1).

In order to obtain the Bo-105 rotorcraft model to be used in MCIM, three simplifications are considered starting from the coupled linearized model (Eq. (3.1)). Section 3.2.1 will describe the first simplification, which is on the rigid body and rotor mode couplings. Then, Section 3.2.2 will continue with discussing the longitudinal and lateral axes responses and their interaction. Finally, Section 3.2.3 will describe the simplification on the on-axis response.

3.2.1. SIMPLIFICATION I : RIGID BODY/ROTOR COUPLINGS

In MCIM, couplings between the body and the rotor are neglected.

A high fidelity rotorcraft model generally includes the main and tail rotors, the body (i.e., fuselage), and their coupled modes, as McRuer⁷⁸ exemplified in a roll axis model, shown in Figure 3.5.

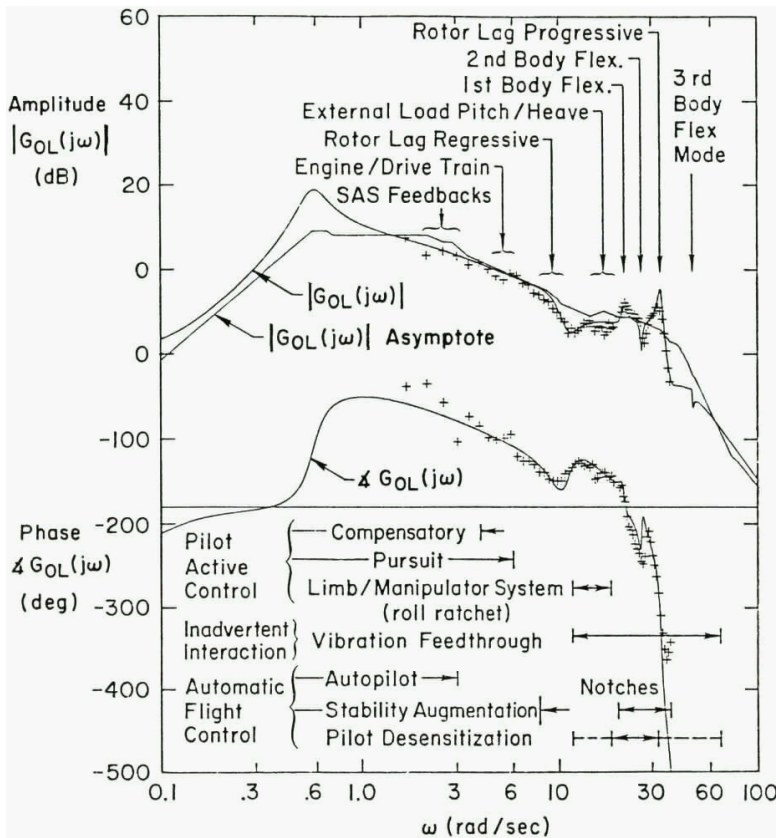


Figure 3.5: Bode plot of a helicopter roll response, adopted from Ref. [78].

As illustrated in Figure 3.5, rotor lag (regressive and progressive) and flexible body modes can be beyond mid-frequency with high order dynamics. This thesis focuses on the pilot active control in compensatory tracking, and this activity occurs at relatively lower frequencies than rotor modes and body flexibility modes⁷⁸, as shown in Figure 3.5. Another high fidelity rotorcraft (Bo 105) simulation model, which is a 7th order transfer function of the roll response, is provided by Tischler and Remple¹³⁴ as follows;

$$\frac{\phi}{\delta_{lat}} = \frac{\overbrace{2.62 [0.413, 3.07]}^{\text{Roll-yaw}} \overbrace{[0.0696, 16.2]}^{\text{Lead-lag to control}} \overbrace{e^{-0.0225s}}^{\text{Actuator}}}{\underbrace{[0.277, 2.75]}_{\text{DutchRoll}} \underbrace{[0.509, 13.7]}_{\text{Roll-flap}} \underbrace{[0.0421, 15.]}_{\text{Lead-lag}}} \text{rad/\% - lat} \quad (3.2)$$

where notation $[\zeta, \omega]$ represents the damping and the natural frequency of a second order system ($s^2 + 2\zeta\omega s + \omega^2$). In Eq. (3.2), one can see the second order oscillatory couplings of body roll and rotor lateral flapping modes, body Dutch roll and rotor lead-lag modes. Although this kind of high order models can represent the characteristics of a rotorcraft with a high fidelity¹³⁴, the aim of this thesis is more into the compensatory pilot control behaviour which does not solely depend on high frequencies characteristics of the controlled element.

By decoupling the rigid body and the rotor modes, the state-space representation of the rotorcraft generally reduces to a 6 DoF model (i.e., classical coupled body modes) with an equivalent time delay accounted for the high-frequency rotor dynamics. Although this simplification significantly downgrades the fidelity of the simulation model, examples of such simple models are present in the literature, specifically addressed for HQ studies. For example, Kaletka et al.⁵⁶ conclude that models of Bo-105 with 6 DoF including equivalent time delay, which represents the rotor dynamics, are satisfactory for HQ applications and piloted simulations. In an AGARD report dedicated to identification of rotorcraft systems, it is concluded that 6 DoF models of Bo-105 with rotor dynamics approximated by equivalent time delays are well suited for the lower and mid-frequency range, where HQ aspects of the vehicle are effective⁵⁶. Moreover, Tischler and Cauffman¹³³ state that 'A quasi-steady formulation in 6 DoF is commonly used in rotorcraft system identification for application to simulations or handling qualities that do not require high-frequency validity (p.9).' Kaletka and Gimonet⁵⁵ conclude that a 6 DoF model is sufficient to simulate the hovering Bo-105 to be used in piloted simulations and HQ applications. Similarly, Rohlfs et al.¹²² states that a 6 DoF model with main rotor dynamics approximated by equivalent time delays for the controls provide a reliable representation of the Bo-105 rotorcraft dynamics in low and mid-frequency range, and this approach is appropriate and useful for applications for HQ evaluations and less demanding control system designs.

3.2.2. SIMPLIFICATION II : LONGITUDINAL/LATERAL COUPLINGS

In MCIM, couplings between longitudinal/heave and lateral axes are neglected.

After achieving the 6 DoF state-space form of the rigid body dynamics, lateral and longitudinal (with heave) partitions of stability and control matrices can be grouped³⁶, as shown in Eq. (3.3).

$$\begin{array}{c}
 \begin{array}{c} \text{State} \\ \text{Derivatives} \end{array} \\
 \begin{array}{c} \text{Longitudinal} \\ \dot{u} \\ \dot{w} \\ \dot{q} \\ \dot{\theta} \\ \text{Lateral} \\ \dot{v} \\ \dot{p} \\ \dot{r} \\ \dot{\phi} \end{array} \\
 = \\
 \begin{array}{c} \text{State Matrix} \end{array} \\
 \begin{array}{cc}
 \begin{array}{c} \text{Long.} \end{array} & \begin{array}{c} \text{Long. /Lat.} \\ \text{coupling} \end{array} \\
 \begin{array}{c} \text{Lat. /Long.} \\ \text{coupling} \end{array} & \begin{array}{c} \text{Lat.} \end{array}
 \end{array} \\
 + \\
 \begin{array}{c} \text{States} \end{array} \\
 \begin{array}{c} u \\ w \\ q \\ \theta \\ v \\ p \\ r \\ \phi \end{array} \\
 + \\
 \begin{array}{c} \text{Control Matrix} \end{array} \\
 \begin{array}{c} \delta_0 \\ \delta_x \\ \delta_y \\ \delta_{TR} \end{array} \\
 \end{array} \tag{3.3}$$

where the classical state matrix and state derivatives are the same as the ones given in Eq. (3.1), without the contribution of the rotor dynamics. In other words, the state matrix in Eq. (3.3) is the 'rigid body' partition of the state matrix which was shown in Eq. (3.1). Longitudinal and lateral partitions of the 6 DoF rigid body are highlighted in Eq. (3.3).

Rotorcraft, particularly hingeless rotor configurations like Bo-105, exhibit strong pitch-roll cross-couplings. Ockier and Pausder¹⁰⁹ states that '*... this coupling is inherent to the stiff rotor system and large hinge offset required to generate the large rotor moments needed for agility and responsiveness (p. 4-12)*'. However, there are examples of decoupling longitudinal and lateral axes responses as well, particularly used in HQ and RPC studies, controller designs and system identification efforts. For example, Lawler et al.⁶⁴ conducted a research on identification of the longitudinal/heave-axis bare-airframe dynamics for the heavy gross weight hover configuration of CH-47F helicopter, as a part of the Digital Automatic Flight Control System development program. Bottasso et al.¹⁵ investigated the Galerkin Projection method to be used in computing optimal trajectories for rotorcraft systems, which was demonstrated by a longitudinal model only. Kumar et al.⁶² developed a Stability Augmentation System, by utilizing Linear Quadratic Regulator (LQR) approach, used for helicopter longitudinal and lateral axes individually, particularly in conjunction with ADS-33 metrics.

3.2.3. SIMPLIFICATION III : PITCH (ROLL) RESPONSE

In MCIM, pitch (and roll) responses are chosen to be only the pitch (and roll) subsidence modes.

This final simplification reduces the rotorcraft model into one DoF model, only effective in one axis, longitudinal or lateral in this thesis. Considering the inherent complexity of rotorcraft response characteristics, this state-space model can only be representative of rotorcraft dynamics in low and mid-frequencies in a single axis task in a HQ related study. From a practical perspective, this simple model simulates the short-term dynamics of the vehicle after a pilot input in a single axis task. The baseline model structure in this thesis is a single axis quasi-steady state model for longitudinal and lateral axes, so-called 'conceptual handling qualities model'¹¹¹, as given in Eq. (3.4) and Eq. (3.5).

$$\text{Pitch Model: } \frac{\theta}{\delta_{lon}}(j\omega) = \frac{M_{\delta_{lon}}}{j\omega(j\omega + M_q)} e^{-\tau_s(j\omega)} \quad (3.4)$$

$$\text{Roll Model: } \frac{\phi}{\delta_{lat}}(j\omega) = \frac{L_{\delta_{lat}}}{j\omega(j\omega + L_p)} e^{-\tau_s(j\omega)} \quad (3.5)$$

where $M_{\delta_{lon}}$ and $L_{\delta_{lat}}$ are control derivatives, M_q and L_p are the aerodynamic pitch and roll dampings, q and p are the pitch and roll rates, θ and ϕ are the pitch and roll Euler angles, δ_{lon} and δ_{lat} are the longitudinal and lateral cyclic inputs and τ_s is the inherent delay accounting for the high-frequency rotor dynamics.

In Bo-105, as having a hingless rotor, the body pitch mode and the longitudinal flapping mode are distinct real roots, unlike the coupled roll and flapping oscillations. The main reason is the considerable difference between rotorcraft pitch and roll moment of inertias in corresponding axes. Therefore, the rotor can be considered as an actuator in series with the quasi-steady rigid body mode in pitch axis¹³⁴. In addition, Cooke and Fitzpatrick¹⁸ state that for the short-term or pitch (subsidence) mode: '*... when the pilot wishes to manoeuvre the aircraft he will be only be concerned with the response in the short-term and therefore the short-term dynamic modes along with the control derivatives can be used to predict the handling qualities of the helicopter. The time constant of the pitch subsidence mode is dependent solely on the value of M_q (p. 160).*'

Several studies considered the single-axis state-space models for pitch and roll axes, i.e., conceptual handling qualities models, for low and high bandwidth rotorcraft, e.g., with articulated and hingeless rotors. For example, Blanken et al.¹⁴ used first-order state-space models without time delay on each axis of four different class of helicopters in a piloted simulation study focusing on ADS-33 HQ research. Ockier and Puauder¹⁰⁹ used both pitch and roll state-space models in a HQ study with Bo-105 helicopter, mainly investigating the effects of additional cross-coupling terms on HQ evaluations with ADS-33. Mitchell et al.⁹⁸ used pitch and roll quasi-state models (i.e., Eq. (3.4) and Eq. (3.5) without any time delay as rotor dynamics $\tau_s = 0$), and investigated the pilot control adaptation to added dynamics to these baseline models.

Heffley³⁶ provides a general trend of on-axis pitch and roll damping for teetering, articulated and hingeless rotors, as shown in Figure 3.6.

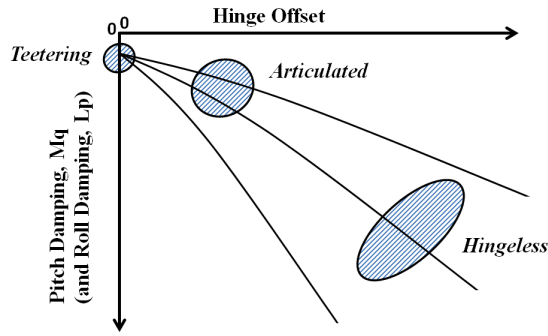


Figure 3.6: Pitch and roll dampings with hinge offsets for various types of rotor systems, adapted from Ref.[36].

As a general trend, M_q and L_p are correlated with the effective hinge offset, as it can be seen in Figure 3.6. This trend is highly coherent with the degree of transfer of blade moments to the rotor hub, such that hingeless rotors with high equivalent hinge offset values exhibit the largest aerodynamic damping values.

Blanken and Pausder¹² used the same state-space models (i.e., M_q and L_p) as baseline rate command vehicle models for their HQ research. Their HQ assessment criterion was the BPD criterion in the ADS-33. The BPD criterion is thoroughly discussed in the previous chapter, Section 2.2.2.2. Briefly, BPD determines two parameters based on the frequency response of the rotorcraft; the bandwidth and phase delay. Bandwidth parameter (e.g., ω_{BW_ϕ} in roll-axis) represents the possible highest frequency which allows the pilot to double his/her control gain or to attain a 135% phase lag¹¹¹. Phase delay parameter (e.g., τ_{p_ϕ}) quantifies the phase lag characteristics of the vehicle at mid- and high- frequencies. By using the BPD criterion, Blanken and Pausder¹² investigated the sensitivity of HQ with additional time delay and varied roll aerodynamic damping term, L_p , as shown in Figure 3.7.

Figure 3.7 is a typical roll BPD chart, in which right-down direction (i.e., high bandwidth and low phase delay) represents good HQ, whereas left-up direction (i.e., low bandwidth and high phase delay) is towards worse HQ. It can be seen in Figure 3.7 that decreasing L_p in the quasi-steady roll rate command model resulted in lower rotorcraft bandwidth and higher phase delay for low bandwidths. Similarly, increasing added time delay resulted in both reduced bandwidth and increased phase delay. Due to the combined effect of reduced bandwidth and increased phase delay, it can be seen in Figure 3.7 that added time delay cause a more rapid HQ degradation when compared to effects of decreased L_p .

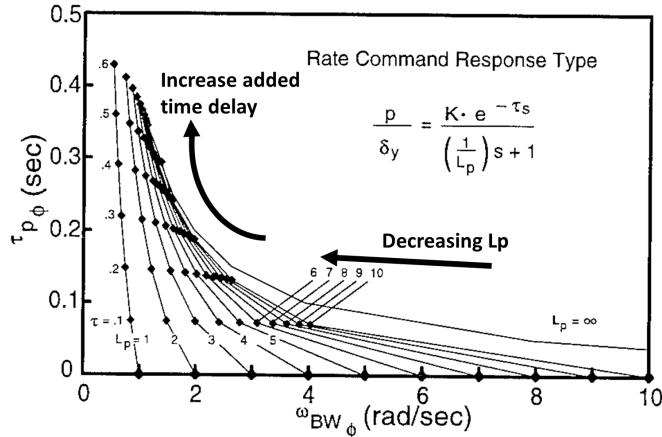


Figure 3.7: Effects of time delay and roll damping (L_p) on roll BPD, adapted from Ref. [12].

It is worth noting that **added time delay** is one of the two independent variables used in the MCIM. As illustrated in Figure 3.7, if an inherent time delay (τ_s) is included in the model describing function, then added time delay can be simply added to the τ_s , representing the new transport delay between the pilot input and the vehicle response. Therefore, by changing the values of τ_s in Eq. (3.4) and Eq. (3.5), added time can be included in the single-axis state-space model. In MCIM, this approach is used to increase the added time delay.

3.2.4. MCIM ROTORCRAFT MODEL IN ADS-33 TERMINOLOGY

COMMAND RESPONSE-TYPE OF THE MCIM ROTORCRAFT MODEL

In ADS-33, several Response-Types are defined⁶. Particularly, Attitude, Translational Rate and (rotational) Rate Command Response-Types are the most important types to discuss for the MCIM. Attitude Command Response-Types in ADS-33 means that a step cockpit input (e.g., longitudinal cyclic) shall produce a proportional attitude change (e.g., pitch), and this attitude shall remain essentially constant for a certain time. In Translational Rate Command Response-Types, constant cockpit input shall produce a proportional steady translational rate, with respect to the Earth, in the appropriate direction. In ADS-33, a Rate Command Response-Type is classified if a response fails to meet the requirements defining the characteristics of an Attitude Command or a Translational Rate Command Response-Type. A basic requirement of Rate Command Response-Types is that the initial and final cockpit controller force shall be the same sign, following an attitude change. Furthermore, Rate Command Response-Types do not require a specific shape of the attitude response to control inputs⁶, but it contains the proportional control of the attitude rate response of the rotorcraft (inherently including the acceleration command). Figure 3.8 illustrated typical attitude responses to a step control input, for different Response-Types.

As it can be seen Figure 3.8, a step control input results in a continuous attitude change (e.g., pitching) in a Rate (and Acceleration) Command Response-Type. On the contrary,

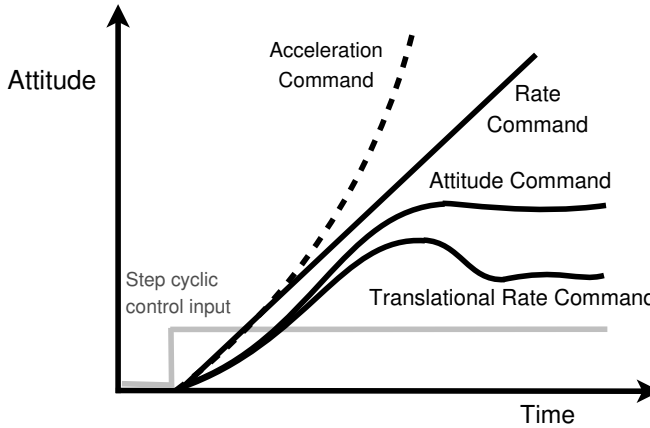


Figure 3.8: Several attitude responses to a cockpit step control input for various Response-Types, adapted from Ref. [111]. The acceleration command is added for completeness.

Attitude and Translational Rate Command Response-Types bring the rotorcraft to a ‘demanded’ attitude, and they aim to maintain this attitude steady. This attitude stabilization generally requires high levels of outer-loop augmentation¹¹¹, whereas Rate Command Response-Types are generally regarded as the simplest practical type found with conventional helicopters. In Figure 3.8, the Acceleration Command Response-Type was added for completeness, and in ADS-33 terms, it belongs to the Rate-Response Types category.

The rotorcraft model that is used in the MCIM (i.e., Eq. (3.4)) is a Single Input Single Output (SISO) system, which can be represented in the state-space form as :

$$\ddot{\theta} = M_q \dot{\theta} + M_{\delta_{lon}} \delta_{lon}(t - \tau_s) \quad (3.6)$$

where the parameters were described in Eq. (3.4), and the only observation term is the pitch attitude (θ). From both Eq. (3.4) and Eq. (3.6), it can be seen that the pitch attitude stabilization loop behaves like an integrator up to the frequency $-M_q$. This means that the pitch angle rate $\dot{\theta}$ (i.e., q in this SISO form) is proportional to the control input δ_{lon} , which is applied with the inherent time delay (τ_s). Beyond this $-M_q$ frequency, the vehicle response transforms into a double-integrator type, which means that the pilot controls the pitch acceleration $\ddot{\theta}$ (i.e., \dot{q}). Therefore, the rotorcraft model in the MCIM can be considered as a Rate Command Response-Type, which is essentially a combination of rate and acceleration command types switching at the frequency defined by the pitch aerodynamic damping (i.e., $-M_q$).

PIO PREDICTION OF THE MCIM ROTORCRAFT MODEL

The only PIO consideration in the ADS-33 is : ‘... For Attitude Command Response-Types, if the bandwidth defined by gain margin is less than the bandwidth defined by phase margin, or is undefined, the rotorcraft may be PIO prone. In this case flight testing

shall be performed to determine acceptability (p. 10).' A detailed discussion on this PIO statement can be found in Ref. [45]. In summary, the reason is the risk of a sudden reduction of the PVS phase margin due to an abrupt change of the pilot gain, in Attitude Command Response-Types. A similar characteristics was exemplified in Section 2.2.2, as an example of a gain margin limited system (Figure 2.5). Since the MCIM rotorcraft model is a non-augmented Rate Command Response-Type (i.e., not an Attitude Command Response-Type), this PIO consideration in ADS-33 is not applicable to the MCIM analysis. Therefore, ADS-33 is solely used for HQ predictions in this thesis, and PIO (i.e., RPC) susceptibility will be determined by RPC detection tools, which will be described in Section 3.6.

Some of the fixed-wing applications of ADS-33 indicate boundaries of PIO proneness¹²⁵, which are based on fixed-wing flight test data. On the contrary, rotorcraft applications of ADS-33 do not have such globally accepted PIO boundaries on BPD charts. Despite this lack, several rotorcraft research and development projects have used these fixed-wing PIO boundaries, but only as a reference¹¹⁵. In this thesis, such PIO boundaries are plotted on ADS-33 charts as well, but only to provide an insight on PIO predictions based on 'fixed-wing' considerations. As it was exemplified in Section 2.2.2, rotorcraft and fixed-wing BPD characteristics could differ significantly, thus, fixed-wing PIO boundaries shall not be taken quantitatively for rotorcraft interpretations.

3.3. STEP 2: TASK DIFFICULTY BY FORCING FUNCTION BANDWIDTH IN MCIM

In MCIM, the disturbance signal (f_d in Figure 3.2) defines the 'flying task', and it is used in the manual control identification process. This task is in the form of a disturbance-rejection task, during which human operators aim to minimize the vehicle attitude error due to the applied disturbance. This task is equivalent to a tracking task since it is only a visual task in this thesis, as shown in Figure 3.2. Controlling the attributes of the forcing function allows various flying tasks to be designed by mastering the frequency content and the resultant time history of the disturbance signal.

The aim of the disturbance forcing function is to provide sufficient excitation to the PVS such that the manual control behaviour can be identified. If the power of the forcing function is too low, then the human operator would not respond with sufficient control activity to be identified, since the error (e) to be minimized would be too small. Such insufficient excitation limits the application of system identification techniques. If the power of the forcing function would be too high, then the human operator would be exposed to violently changing error, and he/she would not show much active compensation in this 'chaotic' turbulence-like task. Therefore, disturbance functions should be chosen considering the main elements of the compensatory task: the pilot and the CE, and the power spectra should be carefully designed.

Forcing functions can be classified according to their power spectra distribution as continuous and discrete, as demonstrated in Figure 3.9.

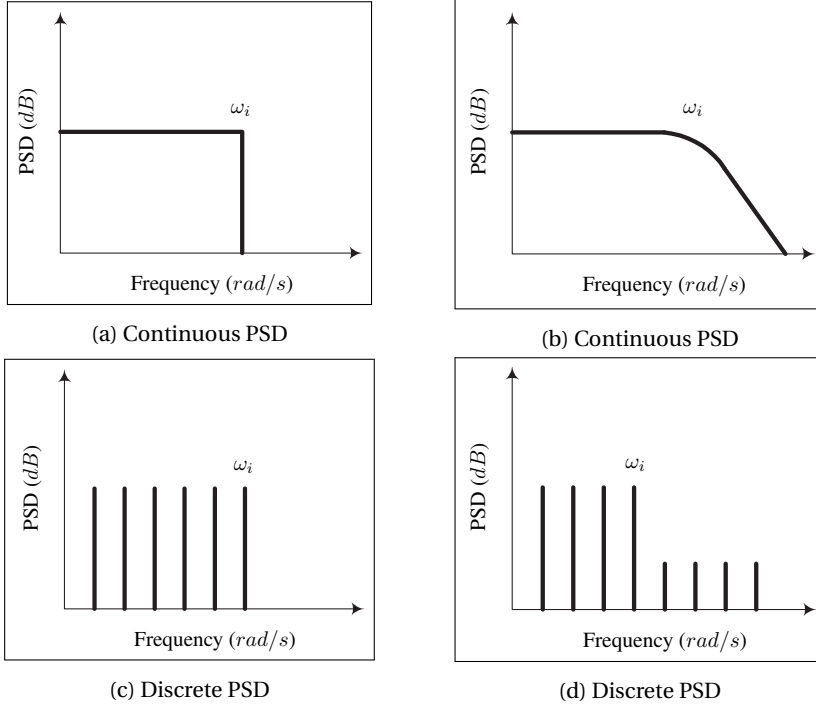


Figure 3.9: Continuous spectra (a and b), discrete (multi-sine) spectra (c), and spectra of multi-sine with high-frequency low-amplitude shelf (d), taken from Ref.[20].

After sampling, forcing functions with continuous-spectra can be considered as discrete with the frequency resolution depending on the sampling rate²⁰. In MCIM, a discrete PSD forcing function with sharp power cut-off is used, as illustrated in Figure 3.9-d. In MCIM, the forcing function should be able to:

- trigger a crossover regression strategy, and
- be used in identification of manual control behaviour at a wide frequency range.

The forcing function should exhibit a Gaussian magnitude distribution. Pintelon and Schoukens¹¹⁸ state that a non-linear system will be best approximated to a linear system when subjected to Gaussian input signal. Slack¹²⁶ mentions that five or more sines in a multi-sine signal can be enough to provide a quasi-Gaussian distribution. A discrete-spectrum multi-sine, so-called '*sum of sines*' can be defined as;

$$f_d(t) = \mu_{f_d} + \sum_{j=1}^N A_j \sin(\omega_j t + \phi_j) \quad (3.7)$$

where μ_{f_d} is the mean, N is the number of sines, A_j , ω_j and ϕ_j are amplitudes, frequencies and phases of the sines respectively. In order to design the forcing function according to the requirements of the identification method, parameters of the multi-sine signal should be carefully considered. In MCIM, both in pitch and roll axes, applied

forcing functions have zero mean. The number and frequencies of the sines in the forcing function are generally defined by the required range of frequencies and their spacing in frequency axis. Since only these frequencies have power in the signal, distributing this power plays a vital role in the identification of manual control behaviour. Frequencies in the multi-sine should cover the required range with a small enough frequency spacing, such that any important response characteristics of the human operator is not missed⁸². Amplitudes of the sines define the power in the signal, thus, they should be carefully designed. Since identification is only possible with powered frequencies, some power is required to identify the human operator response *beyond the crossover frequency*. However, this generally results in crossover regression because the bandwidth of the forcing function exceeds the crossover frequencies⁸¹.

As a solution, amplitudes of the sines at high-frequencies are lowered and a low-frequency high-amplitude region and a high-frequency low-amplitude shelf is formed, as shown in Figure 3.9-d. The former region contains most of the power in the signal, and the latter shelf is used for identification of the higher frequency response of the pilot. It is assumed that the high-frequency content of the forcing function does not affect the low-frequency manual control behaviour of the human subject²⁰. In MCIM, disturbance forcing functions are designed to contain the same total signal power and the same frequency resolution with various forcing function bandwidths (ω_i). Thus, the task difficulty can be expressed by ω_i in MCIM. Increasing ω_i corresponds to more high-frequency content in the low-frequency high-amplitude region, hence, a harder task for the human operator.

Another parameter of the forcing function is the set of phases of the sines in the forcing function. Phase characteristics of a multi-sine signal determine the signal in the time-domain. If the phases of the sines lead sine signals to collapse or integrate with a recognizable period, then the forcing function may appear step-like. Consequently, considerable peaks in the forcing function may lead to 'predictable' excitation. The human operator can recognize the peak occurrences and adapt the control behaviour accordingly. Damveld²⁰ used peak-minimization by using a crest factor, and proposed to select the phases in such a way that the maximum absolute forcing function and its first and second derivatives match the median of the corresponding distributions.

In MCIM, a previously used forcing function is selected and adjusted per application. The selected 'baseline' forcing function in the MCIM has been used in several manual control identification experiments. Nieuwenhuizen et al.¹⁰⁴ have used the structure of the baseline forcing function in a pilot control behaviour identification study in a roll-lateral helicopter hover task. Zaal et al.¹⁵¹ have used the 'baseline' forcing function in a simulator experiment campaign of multi-modal pilot model identification with alternative target signals like step-like ramp signals. In a similar study, Pool et al.¹¹⁹ have used the structure of the baseline forcing function in the disturbance function during identification experiments to identify the pilot control behaviour with varying ramp steepness in tracking signals. While keeping the same structure, amplitudes of the sine signals can be scaled all together depending on the application, e.g., the compensatory display size

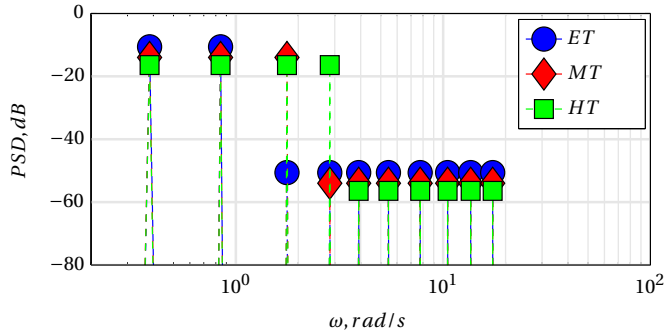
may require higher (or lower) resolution for the error to be displayed. One can argue that such scaling of forcing function amplitudes can alter the total power of the signal. However, McRuer et al.⁸³ showed in an experiment with single and double integrator dynamics that the pilot describing function is invariant with the power of the forcing function.

In a multi-sine forcing function, the power is included at only the multiples of the base frequency ω_b , which is defined by the measurement time T_m according to $\omega_b = 2\pi/T_m$. This prevents power leakage between frequencies. In addition, it is preferable to have frequency components *without* being integer multiple of other frequency components to avoid the risk of predictable trace for the human operator¹⁰⁰. The baseline forcing function duration is to $T_m = 81.92$ seconds, yielding a base frequency of $\omega_b = 0.0767$ rad/s. In order to be used in wide frequency identification, a -20 dB amplitude difference is used between low-frequency high-amplitude region and the high-frequency low-amplitude shelf.

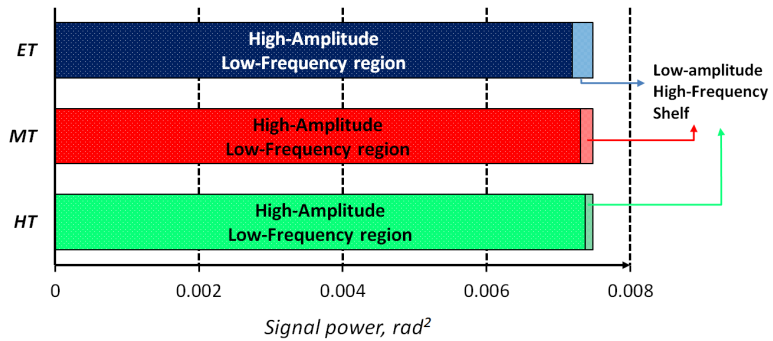
Attributes of the forcing function with three task difficulties in given in Table 3.4. The Easy Task (ET), the Moderate Task (MT) and the Hard Task (HT) configurations are defined by forcing function bandwidth values of $\omega_i \approx 0.8, 1.8$ and 2.8 rad/s, respectively, which are marked with grey shades in Table 3.4. The corresponding PSDs of the forcing function with varied task difficulty are shown in Figure 3.10.

Table 3.4: Attributes of the disturbance forcing functions with three bandwidths, i.e., task difficulties. The shaded frequencies indicate the forcing function bandwidth and corresponding amplitudes in the sines signal up to that bandwidth.

<i>Disturbance forcing function</i>						
j	k_j	$\omega_j, rad/s$	ϕ_j, rad	A_j, rad	A_j, rad	A_j, rad
				ET	MT	HT
1	5	0.3850	-0.2690	0.0848	0.0698	0.0607
2	11	0.8437	4.0160	0.0848	0.0698	0.0607
3	23	1.7641	-0.8060	0.0085	0.0698	0.0607
4	37	2.8379	4.9380	0.0085	0.007	0.0607
5	51	3.9117	5.442	0.0085	0.007	0.0061
6	71	5.4456	2.274	0.0085	0.007	0.0061
7	101	7.7466	1.636	0.0085	0.007	0.0061
8	137	10.508	2.973	0.0085	0.007	0.0061
9	177	13.576	3.429	0.0085	0.007	0.0061
10	226	17.334	3.486	0.0085	0.007	0.0061



(a) PSDs of the disturbance forcing functions for three task difficulties: ET, MT and HT.



(b) Power compositions of high-amplitude low-frequency regions and low-amplitude high-frequency shelves of forcing functions used in MCIM.

Figure 3.10: PSDs (a) and signal power compositions (b) of forcing functions with three task difficulties: ET, MT and HT.

It can be seen from Figure 3.10 that increasing the bandwidth of the forcing function results in more high-frequency content and higher power in the high-amplitude low-frequency region of designed disturbance signals. Thus, the compensatory task becomes more demanding. The values of forcing function amplitudes will be given in each application of the forcing function in this thesis.

3.4. STEP 3: DISTURBANCE REJECTION TASK IN MCIM

This third step of the MCIM consists of conducting human-in-the-loop experiments to identify the manual control behaviour of human operators when subjected to various added time delays in the CE (step 1) and changes in the task difficulty (step 2).

3.4.1. DISPLAY SIZE AND SCALE

A visual compensatory task is prepared, as a disturbance-rejection task, as illustrated in Figure 3.3. The error (e) between the disturbance signal and the vehicle response is displayed in a compensatory display, e.g., the attitude indicator used in the SRS) as shown in Figure 3.11.

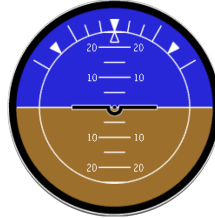


Figure 3.11: Attitude indicator used as a compensatory display in a disturbance-rejection task in the SRS experiments.

The size and scale of the attitude indicator is a factor to determine the maximum available disturbance signal to be displayed in an identification experiment. Moreover, it must be kept in mind that, in a typical MCIM application, human operators can get into RPC occurrences, and degraded HQ configurations may cause the attitudes to archive higher values than injected by the disturbance function. Therefore, a safety margin should be considered in the compensatory display size and scale for such additional attitudes. In MCIM, the scaling of the display size is performed when the identification experiment is designed in the simulator facility prior to actual experiment campaigns. Not only the size of the display, but also the power in the disturbance function, and the general attitude response of the CE with the control inceptor in the simulator cockpit are all taken into account to scale the attitude indicator while designing manual control identification experiments in MCIM.

3.4.2. CONTROL INCEPTOR

The inceptor, which is a rotorcraft cyclic for pitch and roll in this thesis, should be available for human subject to control the CE. Since MCIM uses LTI assumptions, any non-linearity in the inceptor dynamics should be avoided. For example, the breakout force and friction should be removed from the feel system, whereas the force gradient (linear) can be modelled in order to provide a sufficient feeling of the control loading. In MCIM, the deflection of the control inceptor is used as an input to the vehicle model, thus, it can be interpreted as a position command control system, instead of force command feel system (i.e., direct measurement of applied force on the inceptor). The sensitivity of the inceptor control with respect to the vehicle response is included in the control derivative parameters $M_{\delta_{lon}}$ and $L_{\delta_{lat}}$ in Eq. (3.4) and Eq. (3.5), respectively. These parameters contain the transmission of the pilot control inputs (deflection in inches) to inputs to the main rotor swashplate deflections. For example, doubling these parameters would require half of the stick deflection to obtain the same vehicle response. Thus, if the deflection scale of the control inceptor needs to be changed, e.g., due to cockpit

limitations, these parameters also should be adjusted for comparison purposes.

3.4.3. EXECUTION OF IDENTIFICATION EXPERIMENTS

PARTICIPANTS

Although rotorcraft piloting requires extensive training, the flying task (i.e., disturbance-rejection task) in MCIM does not require a high experience level of piloting techniques because of the simplicity of the task. The task is a compensatory task with a single axis response model with only attitude indicator as a display, without outer world visuals or motion cues. Although manual control of human operators and professional pilots could be similar in such simple tasks, when the complexity of rotorcraft systems and tasks increases, piloting techniques become more important. Throughout the identification experiment related sections of the thesis, the term 'pilot' will be used to represent the human operator, not necessarily a professional pilot, in control of the vehicle model. However, professional helicopter pilots participated in the second preliminary identification experiment, which will be discussed in the next chapter. In each experiment in MCIM, more information about the participants will be provided.

MEASUREMENT DATA

Each experiment run consists of 91.92 seconds, from which the first 10 seconds are not used in the measurement, because this run-in time segment includes the initial transient response which originates from participant's efforts to stabilize the PVS. Measurement data should be logged at the frequency of the data recording system of the simulator facility, e.g., in this thesis it is 100 Hz for both SRS and University of Liverpool (UoL) simulators.

EXPERIMENT RUN PHASES

There are two main phases in MCIM identification experiments in MCIM :

1. Familiarization phase

All conditions (combinations of added time delay and the task difficulty) are repeated twice. In this phase, human subjects get familiarized with the task and the simulator environment, e.g., cyclic forces to control with precision. No data need to be measured, and subjects are not informed about their performance by any quantifiable measure.

2. Training and measurement phase

Each human subject completes the task with given the condition. Participants are not informed about the condition to be experimented. A quantitative measure, the score (Equation 3.8), is used to provide information about the performance of the human subject after each run. The score is given as:

$$Score = \left(1 - \frac{\sigma_e^2}{\sigma_{fd}^2} \right) \times 100\% \quad (3.8)$$

where σ_e^2 and $\sigma_{f_d}^2$ are signal variances in the displayed error (e) and the applied forcing function (f_d), respectively. After each run, obtained scores are announced to participants to encourage them to improve their scores, i.e., minimize the error. In order to achieve a better performance, participants are motivated to select the best and steady control strategy for themselves by tracing the announced score after each run. Especially in MCIM, which manifests degraded HQ models in various task difficulties, it is important to give participants sufficient time and training to achieve steady performance for each condition. After achieving steady scores, participants are assumed to adapt a steady control response for the subjected task conditions, and a final five steady runs are recorded as measurement data. Time-averaging these measurement data increases the signal-to-noise ratio of all measurements for identification.

Depending on the total conditions to be investigated, inviting at least the same number of human operators to participate in the experiment can be beneficial for statistical analysis of the results, which are typically repeated-measures Analysis of Variance (ANOVA). The ANOVA provides a strong capability of detecting the effects of the experiment configurations on the dependent measures²⁰. The ANOVA requires several assumptions to be checked before its application. The tests of assumptions to be carried out are listed as²⁰:

- Homogeneity of variance tests: Levene's test.
- Sphericity tests: Mauchly's test.
- Interval scale checked per each dependent measure.
- Normality tests: Kolmogorov-Smirnov's test.

These assumptions of ANOVA should be satisfied, and the execution sequence of identification experiment conditions should be balanced among all participants. A common way of designing the test matrix for such an experiment is using a Latin square design²⁰.

3.5. STEP 4: PVS ANALYSIS IN MCIM

In this step of the MCIM, measured experiment data are analysed per subject and per condition, i.e., with the task difficulty and added time delay as our main independent variables. Then, trends in the dependent measures are obtained. Dependent measures are task performance, control activity, pilot model parameters and open-loop crossover frequency and phase margin.

Task performance and control activities can be calculated from time traces of displayed error and human control inputs, e and u respectively in Figure 3.2. Task performance can be formulated as:

$$\text{Task performance} = \frac{\sigma_e^2}{\sigma_i^2} \quad (3.9)$$

where σ_e^2 and σ_i^2 are the variances of displayed error and the forcing function, respectively. The task performance calculated by Eq. (3.9) determines how much of the power

of the injected disturbance signal is compensated by the participant. In MCIM, another time-domain dependent measure is the control activity which is calculated by the Root Mean Square (RMS) of the cyclic control input u per participant per experiment condition.

3.5.1. PILOT MODEL IN MCIM

As shown in Figure 3.2, the quasi-linear human operator control behaviour can be described by a linear pilot response ($H_p(j\omega)$) and the remnant (n). When LTI considerations are taken into account, manual control behaviour can be represented by $H_p(j\omega)$ while non-linear remnant n is assumed to be relatively small when compared to linear counterpart. In MCIM, control-theoretic pilot modeling techniques are considered, as discussed in the previous chapter. A simplified version of the 'precision model' is utilized in MCIM considering the CE models given in Eq. (3.4) and Eq. (3.5). The model of the manual control behaviour in MCIM is given as:

$$H_p(j\omega) = \underbrace{K_v(1 + \tau_L j\omega)}_{\text{Pilot Equalization}} \underbrace{\frac{\omega_{nms}^2}{(j\omega)^2 + 2\zeta_{nms}\omega_{nms}j\omega + \omega_{nms}^2}}_{\text{Pilot Limitation}} e^{-j\omega\tau_p} \quad (3.10)$$

where the pilot equalization parameters are the pilot visual gain (K_v) and the lead time constant (τ_L), and the pilot limitation terms are the pilot time delay (τ_p), the neuromuscular natural frequency (ω_{nms}) and the damping (ζ_{nms}). Thus, five pilot model parameters to be identified from the measurement data are:

$$\Theta = [K_v \quad \tau_L \quad \tau_p \quad \omega_{nms} \quad \zeta_{nms}] \quad (3.11)$$

When human operators are subjected to various conditions with different task difficulty and added time delay, they are assumed to adapt their control strategies according to the varied condition. Thus, the variation in the identified pilot model parameters (Eq. (3.11)) is proposed here to describe the adapted manual control behaviour. This allows the MCIM to detect which conditions lead pilots to noticeably change their control strategy. This objective method to identify pilot adaptation can be used in conjunction with subjective measures such as ratings.

3.5.2. IDENTIFICATION METHODS IN MCIM

Two LTI identification methods are used in MCIM, frequency-domain Fourier Coefficients Method with Optimization (FCMwO) and time-domain MLE for parametric identification, which will be discussed in Section 3.5.2.1 and Section 3.5.2.2, respectively. Both identification techniques have been utilized in conjunction while processing measurement data gathered from conditions with added time delay and varied task difficulty combinations of MCIM. This joint method is described in Section 3.5.2.3.

1. FREQUENCY-DOMAIN: FCMWO

Assuming high signal-to-noise ratios, an estimate of the pilot's describing function can be obtained by computing the quotients of the Fourier coefficients of the human operator's output and input signals at the frequencies that contain power injected by the

forcing function¹⁰⁰. The describing function simply provides the frequency response characteristics of the manual control behaviour, i.e., $output(u)/input(e)$ just at the frequencies of sines in the designed forcing function²⁰.

After obtaining the manual control describing functions, an optimization is performed to find the parameters (Θ) of the pilot model ($H_p(j\omega)$) that minimize the error between the measured and modeled response of the manual control behaviour. The optimization method that is utilized in MCIM is a nonlinear least squares solver, 'lsqnonlin' in MATLAB³. Figure 3.12 shows the estimate of the optimized pilot model ($H_p(j\omega)_{FCMwO}$) with respect to measured $H_p(j\omega)_{Measured}$.

2. TIME-DOMAIN: MLE

MLE is a time-domain identification method which has been used in estimating the manual control behaviour in similar identification experiments¹⁴⁷. The principle of MLE is to find the joint-probability density function for predicted error ϵ (error between the measured and the estimated u) which makes the parameter estimate $\hat{\Theta}$ 'most likely' by maximizing the likelihood function, given as:

$$L(\Theta) = f(\epsilon_1, \epsilon_2, \dots, \epsilon_N; \Theta) \quad (3.12)$$

This likelihood function is maximized by the parameter vector $\hat{\Theta}_{MLE}$, which is defined by:

$$\hat{\Theta}_{MLE} = \underset{\Theta}{\operatorname{argmin}} \left[\underbrace{\frac{m}{2} \ln \sigma_n^2 + \frac{1}{2\sigma_n^2} \sum_{i=1}^N \epsilon_i^2}_{\text{Optimization target}} \right] \quad (3.13)$$

where m is the measurement index, σ_n is the standard deviation of remnant with the zero-mean Gaussian white noise assumption, and ϵ is the residual, i.e., the predicted error. In Eq. (3.13), the optimization target is marked, and a convex Gauss-Newton optimization is used to find the optimum solution¹⁴⁷. While transforming the frequency response $H_p(j\omega)$ into state-space form during the calculations of MLE, a 5th order Pade approximation is used to model the pilot delay τ_p . A sample pilot describing function achieved by the MLE method is shown in Figure 3.12, which shows the MLE estimate of the pilot model ($H_p(j\omega)_{MLE}$), together with measurement Fourier coefficients, and the FCMwO estimation, $H_p(j\omega)_{Measured}$ and $H_p(j\omega)_{FCMwO}$, respectively.

It is demonstrated in Figure 3.12 that both identification methods are capable of finding pilot models which closely describe the measured describing functions. Next section will describe the joint identification method which is used in MCIM.

3. JOINT FCMwO AND MLE IDENTIFICATION

A typical method to check the accuracy of the estimated pilot model with the identified pilot parameters $\hat{\Theta}$, is the Variance Accounted For (VAF), which is given as;

$$VAF = \left(1 - \frac{\sum_{i=1}^N |u_{m(i)} - u_{sim(i)}|^2}{\sum_{n=i}^N u_{m(i)}^2} \right) \times 100\% \quad (3.14)$$

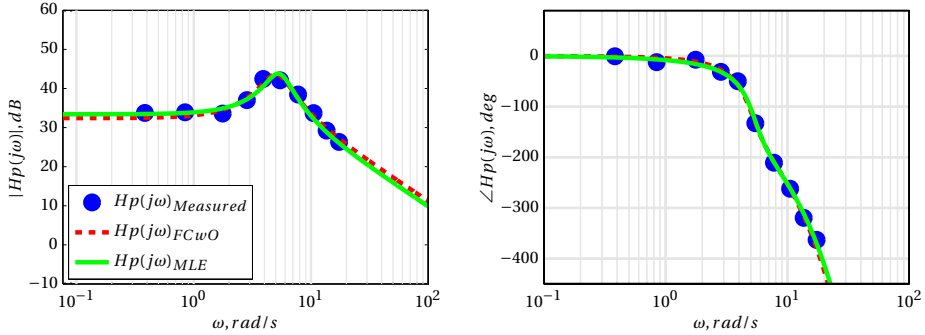


Figure 3.12: Pilot describing function ($H_p(j\omega)_{Measured}$) from a sample identification experiment run, and pilot models are fitted in magnitude and phase response by using identified parameters obtained by two identification techniques: FCMwO and MLE.

where u_m and u_{sim} are the measured and the modeled control inputs calculated from identified pilot models, respectively, and N is the sample number. High VAF values indicate that the simulated control behaviour, which is obtained by simulating the identified operator model, can fairly describe the measured control behaviour. In MCIM, after the identification procedure, the accuracy of the estimated pilot model should be checked with VAF. This accuracy highly depends on the structure of the pilot model and the convergence of the identification technique.

Since both FCMwO and MLE contains optimization routines, some well-known optimization issues can be encountered, such as converging to local minima, setting the initial conditions and parameter boundaries¹¹. Despite their differences in their defined domain, FCMwO and MLE share the same pilot model to describe the manual control behaviour ($H_p(j\omega)$). Thus, in order to handle the optimization issues, in case of low accuracy of estimation, e.g., $VAF < 60\%$, identification results of both methods are set as initial conditions to the other one. Therefore, probability of convergence to a global minimum is aimed to be improved. It must be noted that, this joint method does not guarantee a definite global minimum, but instead, it can be applied to overcome some local minima issues. The schematic of the determination of the pilot model parameter by the joint identification method is shown in Figure 3.13.

As shown in Figure 3.13 first the FCMwO was used to obtain the first parameter estimate of the optimization during the identification process. Then, these parameters are set as initial conditions to the MLE. Next, the resultant parameter set of the MLE is used again in FCMwO as initial condition. Finally, the results are fed into the MLE again. The final parameter set obtained by the MLE is compared with the final parameter set of the FCMwO. If they are close enough (i.e., VAF difference $< 3\%$), these parameters can be used in the identified control behaviour ($H_p(j\omega)$). This whole procedure is repeated four times with randomized initial conditions, and the resulting final parameters values are compared with each other. The parameter set, which provides the best VAF accuracy among these four processes, is selected as the final value of the pilot model parameter set (Θ).

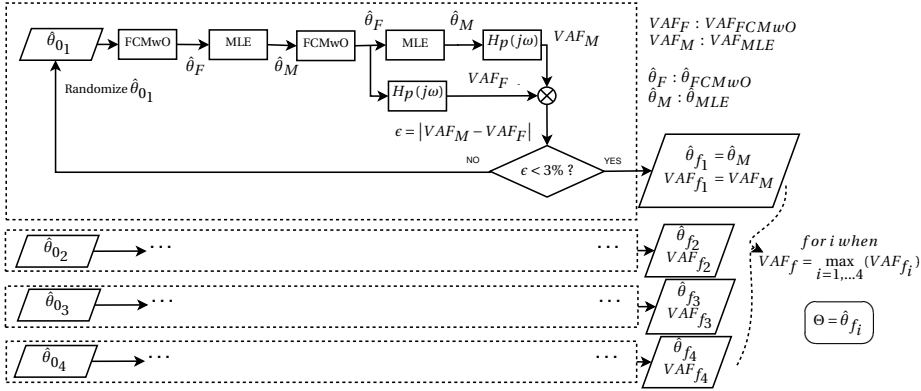


Figure 3.13: Flow chart describing the determination of the identified pilot model parameters ($\hat{\Theta}$) per each subject and configuration in MCIM.

3.5.3. PILOT MODEL PARAMETER AND ω_c COMPARISONS

After obtaining identified pilot model parameters (Θ) for all conditions per each participant, they are compared against each other to detect any recognizable deviation from general trends. In addition, the open-loop crossover frequency and phase margin trends can be showed as a function of the task difficulty and added time delay variations.

ESTIMATED ω_c REGRESSION TREND

ω_c comparisons is a crucial step in MCIM because it may show the occurrences of crossover regression between conditions. The classical crossover regression occurs with increasing task difficulty, when the closed-loop resonance peak starts to be more effective in the error signal. It can be interpreted that increasing the time delay may have a similar reduction in crossover frequency since the phase crossover frequency reduces. Therefore, not only the classical regression due to the task difficulty, but also another regression due to the added time delay can yield a 'combined' crossover regression trend together. This estimated ω_c trend is illustrated in Figure 3.14.

There are two main rationales of the estimated crossover regression trend in Figure 3.14 associated with shown independent variable directions, i.e., added time delay and task difficulty.

1. Classical crossover regression can be observed due to the task difficulty since the closed-loop error would be amplified by higher frequency forcing function bandwidth¹³². Thus, pilot may need to regress open-loop ω_c as in classical crossover regression condition (task difficulty direction in Figure 3.14).
2. Additional time delay in the CE causes a phase drop at lower frequencies; thus, the closed-loop instability of the PVS can start to occur at lower frequencies. Depending on the task, pilot may need to regress his/her control strategy drastically to avoid this instability (added time delay direction in Figure 3.14).

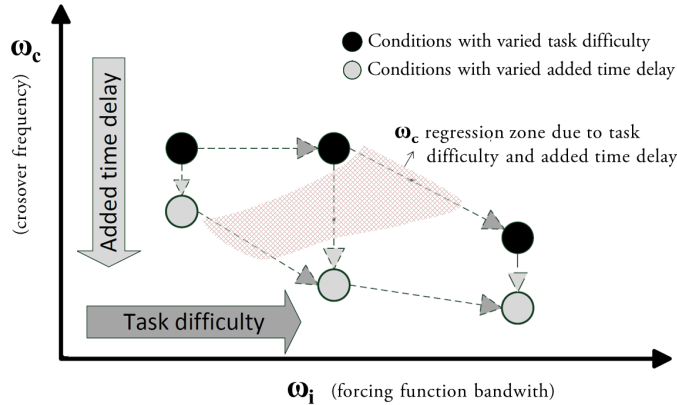


Figure 3.14: Estimated crossover regression trend with time delay and forcing function bandwidth deviations.

A combination of both the added time delay and the task difficulty originated regressions can form-up a crossover regression zone as indicated in Figure 3.14. High resolution of the added time delay and the forcing function bandwidth deviations between conditions can narrow down the ω_c regression zone. Similar zones for identified pilot parameters can be estimated to represent the crossover regression tendency.

3.6. STEP 5: RPC DETECTION IN MCIM

In the previous chapter, effects of the added time delay, the task difficulty and their combination on HQ degradation and RPC proneness were discussed. Considering these effects, MCIM aims to find the correlation between the identified manual control strategy and the RPC susceptibility. In order to detect RPC susceptibility, two detection tools are utilized in MCIM: ROVER and PAC. These RPC detection tools are described in the following subsections.

3.6.1. RPC DETECTION WITH ROVER

ROVER is a classical PIO detection tool, which scours real-time data of the pilot control input and the vehicle rate response. It was designed with the main goal of warning the pilot about the incipience of RPC events in real-time as early as possible⁹⁵. It is also possible to use the same algorithm as a post-run analysis tool to process the measured data for any signs of RPC occurrences. For example, ROVER has been used as a PIO detection tool while analysing historical flight accidents and ground simulation⁹⁰.

There are six general ground rules⁹¹ that were established while developing the ROVER;

- Assume every aircraft response is an oscillation
- Limit the search to a reasonable frequency range
- Focus on aircraft response, then look for a corresponding control input

- Check for phase differences between the aircraft response and pilot input
- Use an easily monitored aircraft state
- Check the amplitudes of peak angular rate and cockpit control inputs

Mitchel and Klyde explain these ground rules in detail in Ref. [91], and they provide a flowchart for the ROVER detection process, as shown in Figure 3.15.

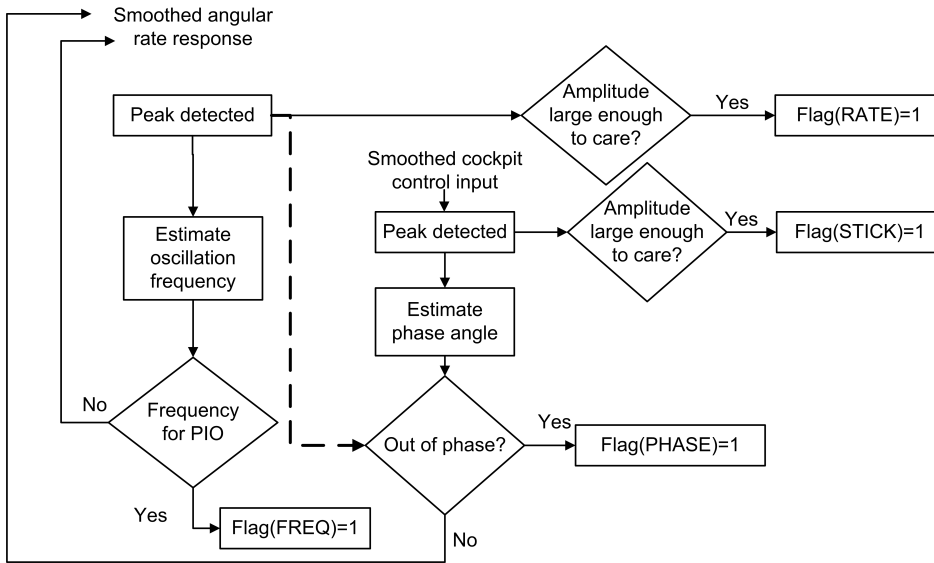


Figure 3.15: Flowchart of ROVER, adapted from Ref. [91].

As presented in Figure 3.15, outputs of the ROVER algorithm are four flags which are assigned based on threshold values:

- flag(FREQ): estimated oscillation frequency of vehicle angular rate response,
- flag(PHASE): phase between applied pilot control and corresponding vehicle rate response.
- flag(RATE): amplitudes of vehicle angular rate response, and
- flag(STICK): amplitudes of pilot cyclic input.

The threshold of the estimated oscillation frequency, i.e., flag(FREQ), is the interval of vehicle rate response frequencies at which ROVER evaluate as potential for RPC. flag(PHASE) is assigned if the phase exceeds a predefined threshold. In ROVER, phase is calculated from peak-to-peak values of control input and resultant vehicle rate response. Control input and vehicle rate response data are usually smoothed by low-pass filters which are capable of removing high-frequency noise and data spikes in measured

signals⁹¹. In MCIM, a 3rd order low-pass Butterworth filter² is utilized, and the resulting rate response and control input data are compared against predefined thresholds. Pilot control inputs that exceed the threshold are assigned as flag(STICK), and vehicle rate response is assigned as flag(RATE) based on a vehicle response rate threshold. In MCIM, an RPC detection is considered if four flags are encountered simultaneously at any analysed segment of measurement data. If consecutive three flags are detected, an RPC warning is declared.

3

One drawback of the ROVER approach is the assignment of thresholds, which defines the logic in diamond blocks in Figure 3.15. This threshold assignment is considered to be subjective because of the uncertainty while predicting the nature of the task to be flown, e.g., how much pilot control would be applied and from which point we should start to be concerned about RPC incipience. Threshold assignment must be done depending on the vehicle capabilities, and the task to be flown. Inappropriate thresholds could result in over/under predicted PIOs. Examples of threshold values used in different studies are given in Ref. [115].

In MCIM, ROVER is used as a post hoc analysis tool, which enables the investigation of measured data for all conditions and all participants of MCIM identification experiments. Therefore, thresholds are assigned according to the trends of variables in already available experiment data, instead of real-time detections. However, it must be noted that there is, and always will be, some uncertainty involved during the threshold assignment⁹¹. Nevertheless, using the ROVER method on already measured data diminishes the uncertainty and provides better prediction than a real-time detection scenario¹³⁰. In this thesis, ROVER thresholds will be provided for each MCIM experiment campaign.

Another drawback of the ROVER detection tool is the wrong phase calculation, even though high-frequency control inputs and vehicle response data are filtered. Especially in high-gain high-precision tasks, pilots need to constantly apply corrective inputs while controlling a demanding rotorcraft model. In such a demanding task with high control activity, relating the control peak to the vehicle response peak can be difficult which may lead to incorrect phase delay determination¹³⁰.

As a part of the ARISTOTEL project, the ROVER algorithm is improved with detection method of peak values. As a result, irregular phase detection cases of control input and associated vehicle rate response are reduced¹³⁰. For example, Figure 3.16 demonstrates the determination of the improved average peak while processing pilot control and rotorcraft rate response data.

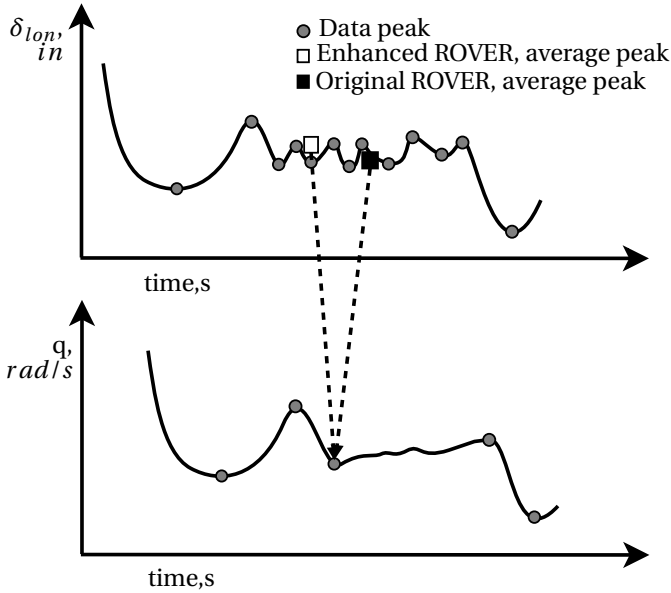
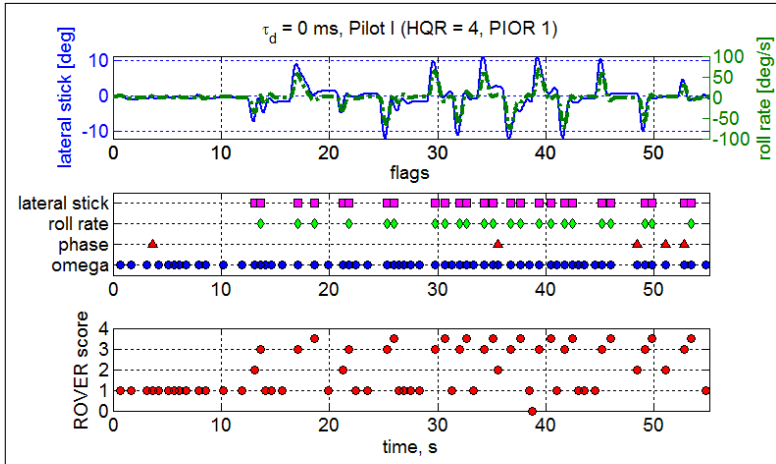


Figure 3.16: Improved average peak selection, adapted from Ref. [130].

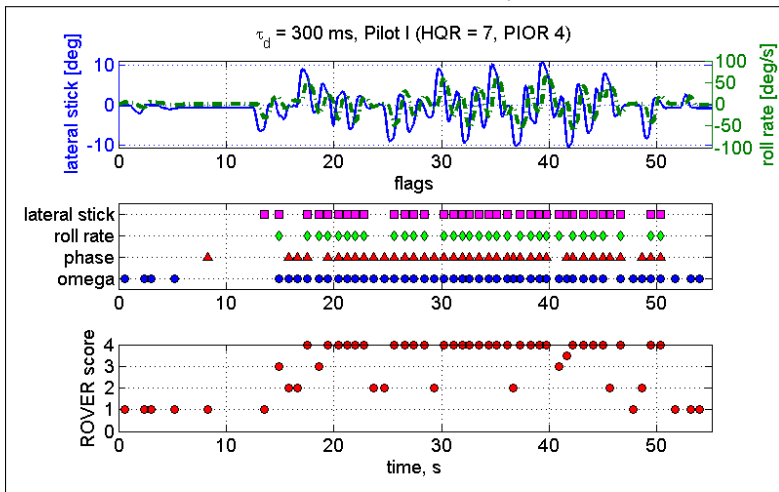
As illustrated in Figure 3.16, by using original ROVER, a peak of the control input responsible of a peak of the vehicle rate response can be wrongly determined, e.g., with a control input occurring later than the rate response which is physically impossible. In enhanced ROVER, the incipience of rate response, and the corresponding average peaks are calculated accordingly. Therefore, average control input is detected before the rate response. As a result, the phase delay between control input and the corresponding vehicle response can be determined with a better accuracy. More details about the phase detection improvements of the enhanced ROVER can be found in Ref. [130].

The enhanced ROVER was initially tested on SRS experiment data which were measured during a single-axis roll tracking task¹³¹. The vehicle model was a Bo-105 helicopter model with 0, 100, 200 and 300 ms added time delays, and two pilots participated in the experiment. Details of the experiment can be found in Ref. [131]. As a sample application of the enhanced ROVER, Figure 3.17 shows experiment data of one pilot lateral cyclic, the roll rate response of the vehicle, and corresponding ROVER flag determination, with 0 and 300 ms of added time delay conditions.

It can be seen in Figure 3.17-a that without any added time delay, there are 11 ROVER warnings (i.e., two consecutive ROVER scores of three, shown as 3.5) but there are no detected RPCs by ROVER, i.e., no ROVER score of four. This detection is well matched with the pilot subjective PIOR, which was awarded as one. The baseline simulation model without added time delay was awarded as HQR four, which corresponds to Level-2 HQ.



(a) No added time delay



(b) 300 ms of added time delay

Figure 3.17: Determined ROVER flags from experiment data of pilot lateral cyclic input, and roll rate response of a Bo-105 rotorcraft model with a) 0 ms, and b) 300 ms added time delay, adapted from Ref. [130].

When 300 ms of time delay was added the baseline model, performing the same task with the same pilot resulted in 28 occurrences of RPC detection, i.e., a ROVER score of four, as depicted in Figure 3.17-b. This noticeable increase in RPC tendency was also captured by the pilot PIOR, which was awarded to be four. Moreover, the HQR increased to 7, which corresponds the Level-3 HQ. This HQ degradation and increased RPC tendency are both caused by the added time delay. Results of this experiment showed that the enhanced ROVER to be used in MCIM is indeed capable of detecting the RPC tendency variations between configurations with different added time delays.

3.6.2. RPC DETECTION WITH PAC

PAC can be considered as an extension of the ROVER by using the Pilot Inceptor Workload (PIW) criterion which is originally developed by Gray³². Original PIW have two time-domain based parameters; the Duty Cycle (DC) and the Aggression term (A_G). The DC defines the percentage of time the pilot is applying control stick input. The A_G is the measure of the pilot control activity in terms of the magnitude of inceptor displacement and rate. The aggression (A_G) and the DC in PIW are illustrated in Figure 3.18.

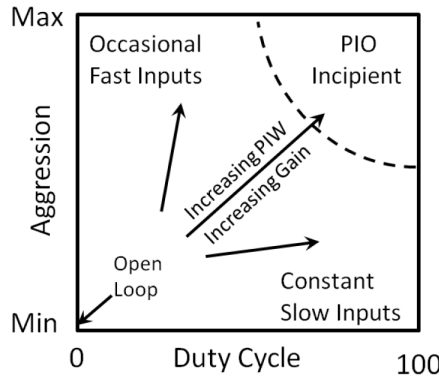


Figure 3.18: Duty Cycle and Aggression relationship to control activity, taken from Ref. [53].

As indicated in Figure 3.18, Gray³² proposes in an PIW criterion which entails that conditions with high aggression and high DC can lead to PIO occurrences. Based on principles of PIW, PAC extends it by introducing the phase difference between pilot input displacement and vehicle rate output⁵³. This phase difference parameter (Φ) is similar to the phase parameter in the ROVER algorithm. In PAC, two parameters (i.e., A_G and Φ) are coupled by the control input activity, and in longitudinal axis they are given as;

$$A_G = \frac{1}{T_{q_2} - T_{q_1}} \int_{T_{q_1}}^{T_{q_2}} H_s |\dot{\delta}_{long}(t)| dt \quad (3.15)$$

$$\Phi = 360 \left(\frac{T_{q_2} - T_{\delta_2}}{T_{\delta_2} - T_{\delta_1}} \right) \quad (3.16)$$

where the illustrations of how to determine pilot control input peaks (T_{δ_1} and T_{δ_2}) and rotorcraft rate response peaks (T_{q_1} and T_{q_2}) are depicted in Figure 3.19, H_s describes the vehicle attitude rate with respect to the pilot control input (i.e., H_s is the average gain response of the vehicle), and $\dot{\delta}_{long}$ is the rate of the cyclic control input.

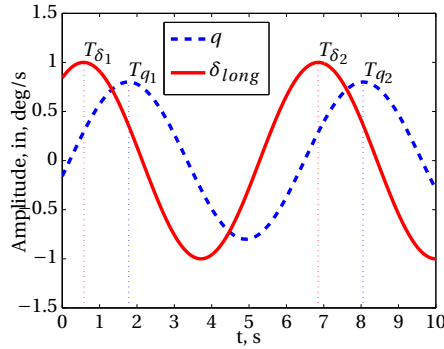


Figure 3.19: Illustration of the calculation of pilot input – vehicle response phase lag in the time domain for PAC calculations, adapted from Ref. [53].

When PAC is processed on measured pilot control input and vehicle response data, for each peak-to-peak detection a pair of A_G and Φ is calculated. Then, these calculated values are plotted on phase aggression plots. Examples of such PAC plots in longitudinal axis during a precision hover MTE, which was performed in HFR, are shown in Figure 3.20. Boundaries that define zones (No PIO, Moderate PIO and Severe PIO) are proposed after conducting several simulator experiments in HFR by using six helicopter pilots and a rate-commanded Bo-105 with added time delay and actuator rate limits. Details of these experiments are described in Ref. [53].

In Figure 3.20-a, it can be seen that PAC results are located in the NO PIO zone which was also confirmed by subjective pilot ratings⁵³. As shown in Figure 3.20-b, when exposed to added time delay configuration, higher frequency and higher amplitude control input activity were observed, as marked in the time trace of the cyclic input histogram. When combined with the phase difference coming from the added delay, the PAC plot resulted in a high number of detected PIOs in moderate and severe PIO zones.

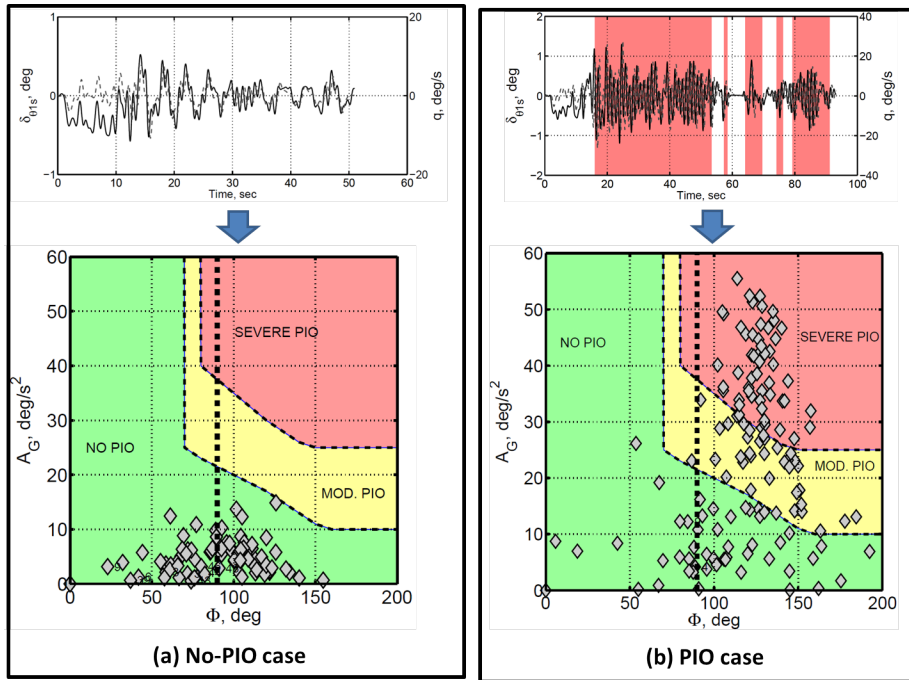


Figure 3.20: Pilot control input and rate response of an example time history without any PIO processed with PAC (a) and an example time history of pilot control and rate response with the presence of PIO and PAC results (b). Adapted from Ref. [53].

3.7. CONCLUSION

This chapter introduced a new method, the MCIM, to objectively assess the HQ deficiency and RPC susceptibility of a rotorcraft model by using manual control behaviour identification. Added time delay and task difficulty are the two independent variables used in this thesis to change the HQ and RPC proneness of the vehicle. MCIM utilizes a single axis pitch (or roll) subsidence rotorcraft model with an additional time delay term and a forcing function structure with adjustable bandwidths to simulate the task difficulty. These two variables are merged in a compensatory disturbance-rejection task to be completed in an experiment campaign conducted with human operators. Finally, manual control behaviour for combinations of added time delay and task difficulty conditions are identified from the measured data. Identification is performed by both frequency and time domain techniques. Identified pilot model parameters and the open-loop response dynamics of the PVS both provide information about conditions at which recognizable changes in the control strategy have occurred. In addition, two RPC detection tools are applied offline on the measured data to correlate the RPC susceptibility of the vehicle with the identified manual control behaviour.

The next chapter will describe applications of the MCIM on two preliminary identification experiments which were conducted in SRS at TU Delft and HeliFlight Helicopter

Simulator (HHS) at University of Liverpool. These experiments mainly focused on effects of the added time delay on manual control behaviour. In the first identification experiment, a roll-axis rotorcraft model was utilized with two configurations of added time delay. The second identification experiment consisted of a pitch-axis rotorcraft model with three levels of added time delay, and the participants were professional helicopter pilots. The next chapter will provide MCIM results of these experiments in terms of manual control behaviour changes, crossover frequencies and RPC tendencies.

4

PRELIMINARY EXPERIMENTS ON MANUAL CONTROL IDENTIFICATION

The methodology applied in this thesis, referred to as the MCIM, was described in the previous chapter. This chapter will provide results of two preliminary identification experiments that were designed, conducted and analysed to test the MCIM. In these experiments, task difficulty was not varied, and the main focus was on elaboration of changes in the manual control behaviour when time delay is added to the rotorcraft model. The first experiment was conducted in the SRS at TU Delft with a roll-axis rotorcraft model during a disturbance-rejection task. In addition to the added time delay in the rotorcraft model, the sensitivity of the cyclic inceptor was doubled, and the combined effects of the added time delay and the cyclic sensitivity on the identified manual control behaviour are discussed. The second preliminary experiment was conducted in the HHS at the UoL with a pitch-axis rotorcraft model with various added time delay conditions. Particularly, occurrences of the crossover regression due to the added time delay are investigated. As a part of the MCIM, RPC tendencies in both experiments are analysed, and the correlation between RPC susceptibility and corresponding identified manual control behaviour parameters are discussed.

4.1. INTRODUCTION

Additional time delay can cause rotorcraft HQ deficiencies, and is a well-known RPC trigger, as discussed in Chapter 2. When time delay is added to a vehicle under manual control, the additional phase lag causes reduced closed-loop stability of the PVS. As a result, human operators need to adapt their manual control strategies to compensate for this increased PVS instability. This manual control behaviour adaptation due to added time delay has been investigated in several studies, as discussed in Chapter 2. Some of these studies investigated changes in **pilot model parameters** when human operators are sub-

jected to various sources of time delays. Levison and Papizian⁶⁷ investigated the effect of transport delay between the pilot input and the vehicle response on manual control behaviour, by comparing subjective HQ ratings (i.e., HQR), task performance measures, and frequency domain analysis of pilot response characteristics. The pilot control behaviour was modeled using the OCM^{59,77}, and the results showed that the adapted manual control behaviour indicated tendencies of lower pilot gains, increased lead compensation, lower frequencies of neuromuscular resonance peaks, and increased remnant. Similarly, Hess³⁷ investigated pilot control behaviour in a compensatory task including various simple CEs with added time delays, as discussed in Chapter 2. The structural pilot model³⁹ was utilized to describe the manual control behaviour, and the relevant pilot model parameters were obtained for both baseline and additional time delay conditions. It was demonstrated that for an integrator-like CE (i.e., $K/(j\omega)$), pilots generated extra lead compensation that is not required according to the classical crossover model⁸³ of the human pilot. In addition to this lead, which is associated with PIOs and high pilot workload⁷⁵, both neuromuscular natural frequency and damping increased. In another study, Stegeman¹²⁹ introduced visual delay in the provided outer visual of a simulator screen, in a disturbance-rejection task with a roll-axis model of Citation II aircraft simulation, controlled by a side-stick manipulator. Identified pilot parameters showed that with the increased time delay, the crossover frequency, pilot control variance, pilot gain and task performance all decreased, whereas the lead time constant and phase margin increased. No significant deviation was observed for neuromuscular parameters and pilot time delay.

Given examples indicate that added time delay causes human operators to generate additional lead to compensate for the reduced phase of the vehicle model. This additional lead increases the positive slope of the Bode magnitude of the pilot model if the pilot model does not have a lead term before the added time delay condition. If the model already has a lead term before the added delay condition, then positive slope in the magnitude starts at lower frequencies (i.e., $1/\tau_L$). Thus, the pilot gain is reduced to provide adequate closed-loop response around the crossover frequency, as reported in given examples. As a result, the open-loop magnitude response near crossover becomes more flat than the classical open-loop response, which is a single integrator⁸¹ (i.e., $1/(j\omega)$). Due to a more flat open-loop response around crossover frequency, a small pilot gain change can rapidly affect the phase margin of the PVS. Although the manual control adaptation (i.e., generated lead and reduced gain for added time delay conditions) is common in the provided examples above, tendencies of neuromuscular system adaptations vary. It must be noted that the structure of the neuromuscular system can be lumped with the control manipulator dynamics, as discussed in the previous chapter. Considering the differences between control inceptors (e.g., side-stick, yoke, cyclic), the resultant neuromuscular system setting mainly depends on the inceptor characteristics.

In given examples, the open-loop crossover frequency (ω_c) is found to reduce with added time delay. However, a systematic approach to detect the crossover regression was not accomplished. In order to examine the effect of added time delay on crossover-regression and manual control behaviour, MCIM is utilized in two preliminary identifi-

cation experiments, without changing the task difficulty. Main features of preliminary identification experiments are summarized in Table 4.1.

Table 4.1: Main features of the first and the second preliminary identification experiments.

Preliminary Experiment	Axis	Independent variables	Added time delay (τ_d),ms	Damping derivative, s^{-1}	Simulator	Participants	Rating Scales
I	Roll	τ_d, K_g	0,300	$L_p(-10.94)$	SRS	Subjects*	N/A
II	Pitch	τ_d	0,100,200	$M_q(-3)$	HHS	Pilots	HQR, PIOR, WLR

* Human operators without professional helicopter pilot licence

As listed in Table 4.1, active axes, CE dynamics, the number of added time delay conditions, simulator environments, participant experience with rotorcraft piloting, and availability of using subjective rating data differ between the two preliminary identification experiments. The first experiment included a high-bandwidth roll model of a rotorcraft (e.g., Bo-105), with and without 300 ms of added time delay conditions. In addition to the added time delay, the control gearing (K_G) was varied to represent a higher sensitivity control manipulator, such that human operators could use half the deflection to get the same vehicle response. The second identification experiment was conducted with a focus on occurrences of crossover regression due to added time delay (three levels). A pitch-axis model with a break frequency of 3 rad/s (e.g., the Bo-105) was controlled in a disturbance-rejection task, as a part of the MCIM.

Details of the preliminary identification experiments will be provided in Section 4.2 and Section 4.3. Section 4.4 will provide the conclusions of both experiments.

4.2. PRELIMINARY EXPERIMENT I

In the first experiment, the primary goal was to investigate changes in manual control behaviour when human operators are subjected to **added time delay** in the vehicle model. The secondary goal of this experiment was to investigate the effect of control inceptor sensitivity on manual control, when combined with added time delay conditions. Although the control sensitivity is not a part of the MCIM design, effects of the cyclic sensitivity on the pilot behaviour in delayed CE conditions with varied RPC susceptibility were also examined.

In compliance with the structure of the MCIM introduced in the previous chapter, this section will describe the details of the first preliminary experiment.

In this thesis, the added time delay is an important variable to be used in the proposed methodology, i.e., MCIM, which is thoroughly described in the previous chapter. While keeping the task difficulty constant, two preliminary identification experiments were conducted to particularly focus on the effect of added time on manual control behaviour. Details of these experiments will be provided in Section 4.2 and Section 4.3. Based on the measured data gathered from these identification experiments, the pilot model described in the previous chapter was used to investigate the manual control behaviour change due to the added time delay in these identification experiments.

4.2.1. TASK DESIGN

As a part of the MCIM, this section delineates the design of the first preliminary experiment. In this section, details of the manual control task, the CE (i.e., the rotorcraft model), the pilot model to be identified from the measurement data, the apparatus, and information about the participants will be provided.

ROLL CONTROL TASK

A roll-axis disturbance-rejection task was considered in the experiment. The block diagram of this compensatory tracking task is shown in Figure 4.1.

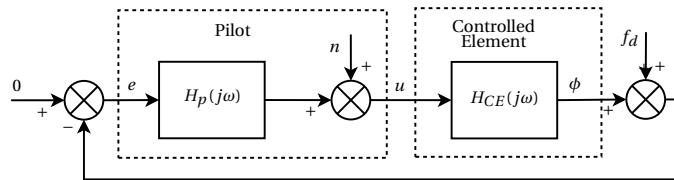


Figure 4.1: Block diagram of the roll-axis compensatory disturbance-rejection task used in the first preliminary identification experiment. The linear pilot control behaviour $H_p(j\omega)$ and the remnant n , which accounts for the nonlinear control, forms up the pilot control (u). $H_{CE}(j\omega)$ is the vehicle dynamics, and f_d is the disturbance forcing function.

The task was a single-axis disturbance-rejection task in the roll channel, and human operators were asked to minimize the displayed error (e in Figure 4.1). The displayed error is composed of the injected disturbance forcing function (f_d) and the vehicle roll response (ϕ) due to applied pilot control (u). The disturbance forcing function (f_d) has a discrete PSD designed as the MT (i.e., f_d bandwidth of $\omega_i \approx 1.8$ rad/s as given in the previous chapter). The PSD and a sample time trace of the forcing function are shown in Figure 4.2.

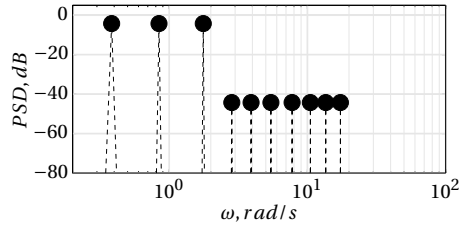
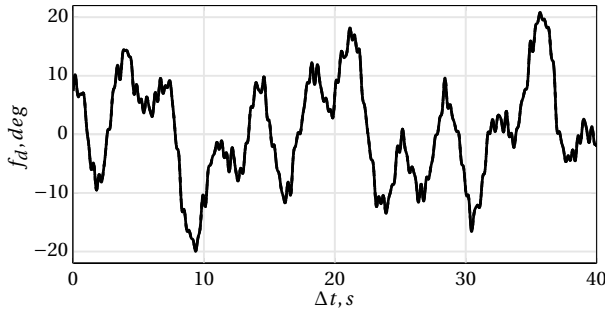
(a) PSD of the f_d .(b) Sample time trace of the f_d .

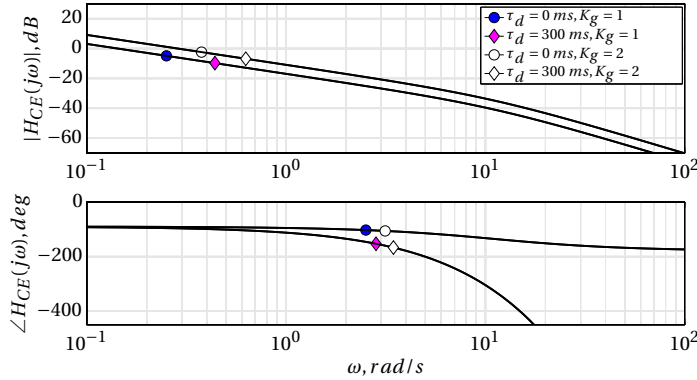
Figure 4.2: The PSD (a) and a sample time trace (b) of the disturbance forcing function.

ROTORCRAFT MODEL

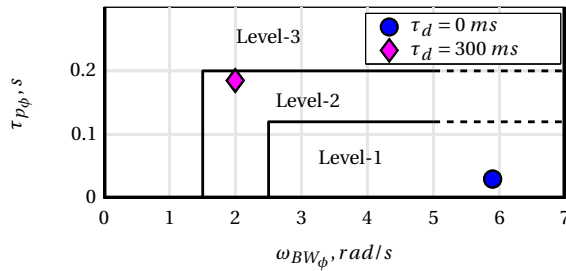
The controlled element (H_{CE} in Figure 4.1) was a roll-axis rotorcraft model. Discussions about the model structure of the CE was provided in the previous chapter as a part of the development of MCIM. In this experiment, the control gear gain (K_g) is added to change the control sensitivity, and the transfer function of the CE is given as:

$$H_{CE}(j\omega) = K_g \frac{L_{\delta_{lat}}}{(j\omega)(j\omega - L_p)} e^{-\tau_d(j\omega)}, \quad (4.1)$$

where the control authority term $L_{\delta_{lat}} = 1.5643 \text{ rad}/(\text{in} \cdot \text{s}^2)$, the aerodynamic roll rate damping derivative $L_p = -10.94 \text{ s}^{-1}$, ϕ is the roll attitude, δ_{lat} is the lateral cyclic input, τ_d is the added time delay. In a single-axis rate command system, the roll subsidence mode is characterised by the aerodynamic damping derivative L_p , and the value used in this experiment was taken from Bo-105 models (in hover condition) used in the ARISTOTEL project¹¹⁵. The $L_{\delta_{lat}}$ parameter models the transmission gain between the pilot control input to the vehicle response. Here, it was aimed to study the possible effects of changing this gearing, such that the sensitivity of the cyclic (K_g in Equation 4.1) was varied, and the corresponding manual control behaviour changes were analysed. Two cyclic sensitivity settings were applied, $K_g=1$ and $K_g=2$, the latter representing a higher control inceptor gearing. The frequency responses of the vehicle models are shown in Figure 4.3.



(a) Bode plot of CEs.

(b) Bandwidth phase delay criterion of ADS-33 for Target Tracking and Acquisition tasks⁶.Figure 4.3: Bode diagram (a) and bandwidth phase delay criterion (b) of CEs with 0 and 300 ms of added time delay, and two levels of control gearing sensitivity: $K_g = 1$ and $K_g = 2$.

L_p determines the break frequency of the CE, such that the vehicle response approximates a single integrator until this frequency, and becomes a double integrator beyond it, as depicted in Figure 4.3-a. According to the crossover model^{81,83}, the manual control equalization for a CE with single integrator dynamics is a pure pilot gain. On the other hand, a CE with double integrator dynamics requires a lead control around the crossover frequency to achieve an open-loop response that is a single integrator (i.e., $K/(j\omega)$). Thus, a high L_p provides a CE with an easier control for the human operator, because the transition from single to double integrator CE response occurs at higher frequencies. When the CE break frequency is high, it inherently exhibits a higher tolerance to HQ deficiencies caused by added time delay, since the double integrator dynamics starts at higher frequencies. Therefore, a 300 ms of time delay was applied in order to change the HQ of the rotorcraft model. 300 ms can be considered as a high delay for fixed-wing aircraft, but it is in fact a realistic value for rotorcraft systems, as discussed in

Chapter 2. In terms of HQ prediction, the BPD criterion of the ADS-33 for the developed models are depicted in Figure 4.3-b.

It can be seen from Figure 4.3-a that increasing added time delay results in a sharper phase roll-off, such that the bandwidth of the vehicle (i.e., frequency at which the phase is -180 deg) drastically reduces, as discussed in Chapter 2. The magnitude response does not vary with added time delay, however, it is directly affected by the increased control sensitivity. Changing K_g does not influence the phase response, as shown in Figure 4.3-a. By using the frequency response of vehicle models with and without the added time delay, the HQ of these models are assessed by the BPD criterion⁶, as shown in 4.3-b. It is clear that the HQ of the rotorcraft model with added time delay drastically degrades, from Level-1 to Level-2, even close to the boundary of Level-3. Changing the control sensitivity gain does not affect the BPD criterion, such that increased control sensitivity causes a shift in the magnitude response, and this shift does not change the BPD parameters⁶ (i.e., the phase and gain bandwidth).

APPARATUS

The first preliminary experiment was conducted in SRS (Figure 4.4-a) without motion. A scaled-up attitude indicator (Figure 4.4-b) was used as a compensatory display to show the roll tracking error. The control inceptor was a central cyclic stick from Moog FCS[®], shown in Figure 4.4-b, with a control loading system that is particularly designed for rotorcraft simulations. During the experiment, the breakout force and friction settings of the control loading system were set to zero in order to sustain the linearity in the control path of the CE. Only the roll-axis cyclic control was active during the experiment, and other axes were locked. The force gradient of the control loading system was set to 1.54 pound/in in order to provide sufficient feel of control loading system of a realistic central cyclic. This value also belongs to Level-1 in ADS-33 Handling Qualities specifications for allowable control force gradients⁶.

PARTICIPANTS

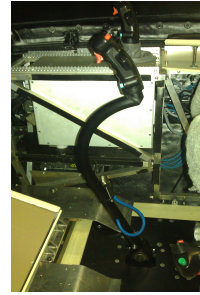
This experiment was performed by four participants, who were all Delft University of Technology students or staff members. All participants had prior experience with similar human-in-the-loop experiments and manual control tasks. All participants were male, and their ages ranged from 25 to 31 years, with an average age of 29 years. Two participants had private pilot licences for single engine fixed-wing aircraft.

PILOT MODEL

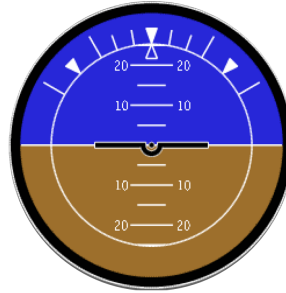
In this experiment, manual control behaviour was identified using a simplified version of the precision model, (i.e., the pilot model utilized in MCIM), as given in the previous chapter. After identification of manual control behaviour during conditions of the experiment (i.e., the added time delay and the control gear sensitivity), identified parameters of the pilot model were compared.



(a) The SIMONA Research Simulator (SRS) of Delft University of Technology.



(b) Cyclic control inceptor in the SRS simulator.



(c) Attitude indicator used for displaying roll angle error during the disturbance-rejection task.

Figure 4.4: The experiment was conducted in the SRS (a). Participants used a cyclic controller (b). The roll error was displayed to the human subjects on the scaled-up attitude indicator (c). The indicator outer and inner ring diameters were 13 cm and 9.5 cm, respectively. The display distance to eye design point of the pilot seat was approximately 85 cm.

4.2.2. INDEPENDENT VARIABLES

The experiment had two independent variables. First, an added **time delay** was added to the baseline CE model was varied. Second, the control gearing sensitivity was varied by changing the gain of the cyclic input. Two added time delay values were applied ($\tau_d = 0$ and 300 ms), and two control gearing gains ($K_g = 1$ and 2) were used in the experiment. Hence, there were four conditions in total.

4.2.3. EXPERIMENT PROCEDURES

Prior to the experiment, all participants were briefed on the task to be completed. The participants were instructed to minimize the displayed error (e) by using the lateral cyclic input (u). Details of the CE or the control gearing sensitivity were deliberately not a part of the briefing to the participants, in order to sustain compensatory control behaviour without pre-assigned control strategies.

The experiment was designed by considering the application of an ANOVA to the measured data, as described in the previous chapter, and status of ANOVA assumptions will be provided in Section 4.2.6. A Latin square design was used to ensure a balanced order such that each human subject experiences each condition in a different sequence¹⁰⁴. For this purpose, the number of conditions and number of participants were set as equal, and the experiment execution order is listed in Table 4.2.

Table 4.2: 4X4 Latin square experiment design with independent variables added time delay (τ_d) and control gearing gain (K_g).

Participants	Experiment Conditions (τ_d, K_g)			
	I	(0 ms,1)	(300 ms,2)	(0 ms,2)
II	(300 ms,1)	(0 ms,1)	(300 ms,2)	(0 ms,2)
III	(0 ms,2)	(300 ms,1)	(0 ms,1)	(300 ms,2)
IV	(300 ms,2)	(0 ms,2)	(300 ms,1)	(0 ms,1)

Procedures of the identification experiments were described in Chapter 3, as a part of the MCIM. All participants were exposed to all conditions in the familiarization phase. Next, participants continued to the training and measurement phases. During these phases, participants were informed about their performance scores after they complete an experiment run.

4.2.4. DEPENDENT MEASURES

During the experiment, the roll attitude (ϕ) of the CE, the displayed error (e) and the pilot control input (u) were recorded. By using these measured data, several dependent measures were calculated. First, the variances of the measured displayed error, and the control input were interpreted as indications of task performance, and control activity, respectively. Second, by using the identification methods explained in the MCIM in Chapter 3, pilot model parameters were identified from the measured data. Based on the variations on these dependent measures, the pilot control behaviour adaptation to experiment conditions is discussed. Then, open-loop crossover frequencies and phase margins were calculated. In addition, time traces of the pilot control input and the vehicle responses were used during the RPC detection processes by using ROVER and PAC, which were described in detail in the previous chapter.

4.2.5. HYPOTHESES

This experimental approach is the essence of the MCIM, and it was primarily aimed to investigate pilot control behaviour and PVS characteristics when subjected to variation of added time delay in the CE. Considering the HQ and RPC review provided in Chapter 2, a primary hypothesis can be formulated as '**added time delay in the CE will result in a lower crossover frequency**'. Based on given examples in Section 4.1, another primary

hypothesis can be stated about identified pilot parameters as ‘**added time delay in the CE will result in a lower pilot gain (K_v) and an increased lead time constant (τ_L)**’.

Human operators are able to adapt their gain (K_v) according to the gain of a controlled element ($|H_{CE}(j\omega)|$), as described by McRuer⁷⁶. Increased control sensitivity directly shifts the gain of the controlled element, and it was hypothesised that human operator could change his/her gain while maintaining a similar open-loop response, and a similar crossover frequency. Hence, our hypothesis is ‘**control gearing gain will not have any effect on crossover frequency**’. Moreover, this adaptation of K_v for varied control gearing could be independent of the added time delay, and the final hypothesis can be stated as ‘**interaction of control gearing sensitivity and the added time delay will not have any effect on crossover frequency**’.

4

4.2.6. METHODS USED FOR ANALYSING THE EXPERIMENT DATA

IDENTIFICATION METHODS

Two identification methods were utilized during the analyses of the measured data of the experiment: FCMwO and MLE. Details of these methods, which are inherently included in the MCIM, the order of their execution on the measured data, and the VAF for examining the accuracy of the identified manual control behaviour have all been described in the previous chapter. High values of the VAF indicate that the identified manual control behaviour can describe the actual control behaviour of the corresponding human operator participated in the experiment.

STATISTICAL ANALYSES

In order to analyse the statistical significance of the variations among configurations, a two-way repeated-measures ANOVA was applied to the results of the experiment, as described in the previous chapter. Measured data of this experiment showed that the interval scale assumption was satisfied for all dependent measures analysed with the two-way repeated-measures ANOVA. The normality assumption was rarely violated, but the ANOVA is fairly robust for such instances¹⁰⁵. If the sphericity assumption was violated, the Greenhouse-Geisser correction was applied²⁰.

RPC DETECTION TOOLS

As a part of the MCIM, two RPC detection tools were used: ROVER and PAC, which are described in the previous chapter. These detection tools were applied to investigate the correlation between identified manual control behaviour and RPC susceptibility of the PVS with added time delay. In the previous chapter, ROVER flags and their thresholds were described in detail for the pitch-axis, and for the first experiment, equivalent roll-axis flags and their thresholds are given in Table 4.3. PAC detects the control aggression and phase delay in the measured data, and locates these detected parameter pairs on a phase-aggression chart with PIO susceptibility boundaries, as described in the MCIM.

Table 4.3: ROVER variables and their threshold values used in the first experiment. Here, ω_p is the roll rate frequency, $\hat{\theta}_{lat}$ is the lateral cyclic stick deflection, p is the roll rate response of the rotorcraft, and ϕ_ϕ is the phase between pilot control peaks and resultant rotorcraft body rate response p .

Variables as ROVER flags		Threshold
Frequency	ω_p	8 rad/s
Stick amplitude	$\hat{\theta}_{lat}$	0.97 in
Roll rate	p	0.29 rad/s
Phase	ϕ_ϕ	85 deg

4.2.7. RESULTS

TASK PERFORMANCE AND CONTROL ACTIVITY

The task performance was measured by the normalized error variance (σ_e^2/σ_i^2), where σ_e^2 and σ_i^2 are the variances of the tracking error and the disturbance forcing function, respectively. Low values of the normalized error variance indicate good task performance. If normalized error variance values are above one, instead of attenuating the error, the operator actually amplifies the error. RMS of the control input was used as a measure of pilot control activity. Figure 4.5 depicts the task performance and the control activity.

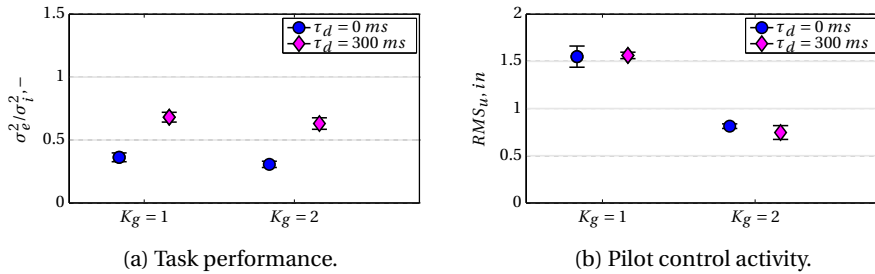


Figure 4.5: Mean and 95% confidence intervals of measured task performance (a) and control activity (b), all corrected for between-subject variability.

It can be seen from Figure 4.5-a that increasing added time delay resulted in increased error for both control gearing settings. Moreover, normalized errors for the same added time delay conditions were very similar regardless of the control gearing gains. The effect of control gearing on the control activity is clearly visible in Figure 4.5-b. When the control gear sensitivity is increased $K_g = 2$, the control activity reduced by approximately 50%, regardless of the added time delay. These observations were checked with an ANOVA analysis, see Table 4.4.

The ANOVA results show that the added time delay has a highly significant effect on the normalized error variance [F(1,3)=112.5, $p < 0.05$], whereas the control gearing gain has no significant effect [F(1,2)=9.23, $p \geq 0.1$]. On the other hand, the control gearing gain has a highly significant effect on control activity [F(1,3)=371.06, $p < 0.05$], and the added

Table 4.4: Two-way repeated-measures ANOVA results for the control activity and task performance, where ** is highly significant ($p < 0.05$) and - is not significant ($p \geq 0.1$).

Dependent measures	Independent variable factors								
	τ_d			K_g			$\tau_d \times K_g$		
	dF	F	Sig.	dF	F	Sig.	dF	F	Sig.
σ_e^2/σ_i^2	1,3	112.45	**	1,3	9.23	-	1,3	0.04	-
RMS_u	1,3	0.248	-	1,3	371.06	**	1,3	3.17	-

time delay has no significant effect on control activity [$F(1,2) = 0.248, p \geq 0.1$]. The combination of added time delay and the control gearing gain did not show any significant effect on both the normalized error and the control activity [$F(1,2) = 3.71, p \geq 0.1$].

IDENTIFIED PILOT MODEL PARAMETERS

Identification of manual control behaviour depends on the assumption that human operators exhibit a linear control behaviour, as discussed in the previous chapter. The linearity of the pilot control behaviour at the frequencies excited by the forcing function was checked by the squared correlation coefficient (ρ^2), defined by McRuer et al.⁸³ as:

$$\rho^2(j\omega) = 1 - \frac{S_{nn}(j\omega)}{S_{uu}(j\omega)} \quad (4.2)$$

where S_{nn} and S_{uu} are the periodgrams of the noise and the control signal, respectively, at the powered frequencies of the forcing function. S_{nn} was calculated based on the discussion in the previous chapter, such that the noise is accounted for the control nonlinearities which could not be modeled in an LTI model. In addition to the correlation coefficient, the VAF of the identified model can also be considered as evaluation of the linearity of the system, depending on the accuracy of the estimated pilot model. An example of the average correlation coefficient for one typical participant, and VAF values which were corrected for between-subject variability, are shown in Figure 4.6.

As illustrated in the Figure 4.6, the correlation coefficients were generally found to be close to one, which shows that manual control behaviour can indeed be considered linear in all experiment conditions. Moreover, VAF values obtained for all subjects were between 90% to 97%, with a grand average of 93.7%, as shown in Figure 4.6. In other words, the estimated describing function ($H_p(j\omega)$) with identified parameters captures the majority of the measured manual control behaviour in all experiment conditions.

This allows for high-accuracy identification using the pilot model proposed in the MCIM. Considering the estimated pilot model given in Section 4.2.1 describing the manual control behaviour of human operators, pilot equalization parameters were the pilot visual gain (K_v) and lead time constant (τ_L). Pilot limitation parameters were the pilot delay (τ_p), neuromuscular damping (ζ_{nms}) and natural frequency (ω_{nms}). Figure 4.7 depicts the estimates of these parameters with their means and 95% confidence intervals

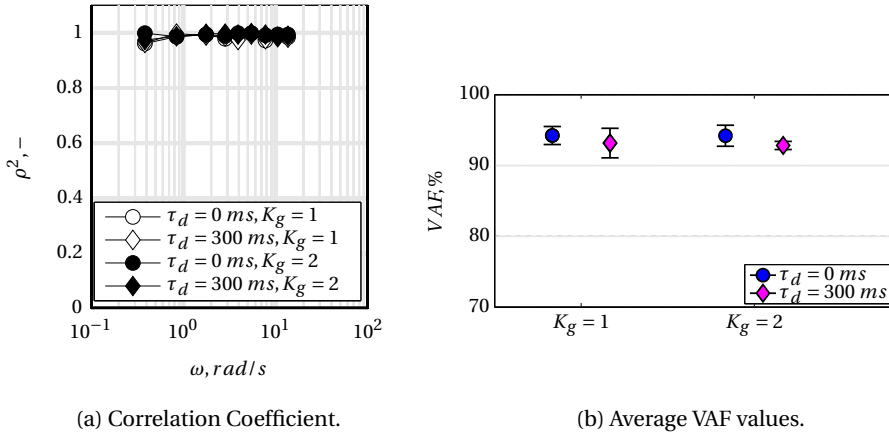


Figure 4.6: Average correlation coefficient values for Participant 3 (a), and mean and 95% confidence intervals of VAF values, corrected for between-subject variability (b).

for each condition of the experiment. Results of the two-way repeated-measure ANOVA performed on the pilot parameters are listed in Table 4.5.

Table 4.5: Two-way repeated-measures ANOVA results for the identified pilot model parameters, where ** is highly significant ($p < 0.05$), * is significant ($0.05 \leq p < 0.1$), and - is not significant ($p \geq 0.1$).

Dependent measures	Independent variable factors								
	τ_d			K_g			$\tau_d \times K_g$		
	dF	F	Sig.	dF	F	Sig.	dF	F	Sig.
K_v	1,3	10.52	**	1,3	12.55	**	1,3	0.941	-
τ_L	1,3	1.275	*	1,3	2.437	-	1,3	0.176	*
ω_{nms}	1,3	4.899	**	1,3	1.382	-	1,3	2.829	*
ζ_{nms}	1,3	0.07	-	1,3	3.292	-	1,3	0.233	-
τ_p	1,3	4.394	-	1,3	0.914	-	1,3	0.463	-

As can be seen from Figure 4.7-a, the added time delay caused a strong reduction in the visual gain of the pilot, in both control gearing conditions [$F(1,3)=10.52, p < 0.05$]. Moreover, increased control gearing resulted in reduced pilot gain (K_v) with a highly significant statistical effect [$F(1,3)=12.55, p < 0.05$]. However, the interaction of the added time delay and the control gear gain did not show a significant effect on the pilot visual gain, [$F(1,3)=0.941, p \geq 0.1$]. It can be observed in Figure 4.7-b that the confidence intervals in the lead time constant parameter (τ_L) for all conditions are large when compared to the confidence intervals of the pilot gain parameter. However, average-means of τ_L show a clear increase with the added time delay for all control gain conditions. Added

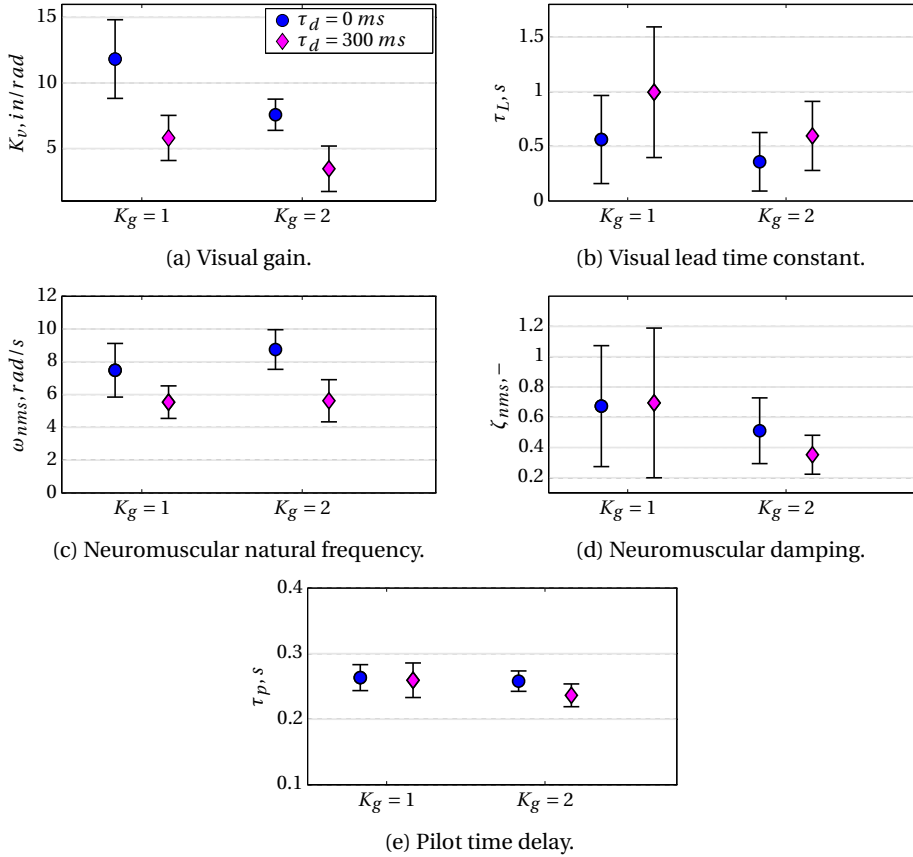


Figure 4.7: Mean and 95% confidence intervals of estimated pilot visual gain (a), lead time constant (b), neuromuscular natural frequency (c), neuromuscular damping (d), and pilot time delay (e) parameters, all corrected for the between-subject variability.

time delay showed a significant effect on τ_L [$F(1,3)=1.275, 0.05 \leq p < 0.1$], whereas the control gearing and its interaction with the added time delay do not show a statistically significant effect, [$F(1,3)=2.437, p \geq 0.1$] and [$F(1,3)=0.176, p \geq 0.1$], respectively. Added time delay caused the neuromuscular natural frequency (ω_{nms}) to decrease with a highly significant effect [$F(1,3)=4.899, p < 0.05$]. Varied control gear gain does not show a significant effect on ω_{nms} , [$F(1,3)=1.382, p \geq 0.1$]. The neuromuscular system damping (ζ_{nms}) possesses the highest relative confidence variation, as shown in Figure 4.7-d. Both ζ_{nms} and the pilot delay (τ_p) parameters were not significantly affected by either of the independent variables or their combinations. By using the means of the identified pilot model parameters, the average manual control behaviour for each independent experiment variable is depicted in Figure 4.8.

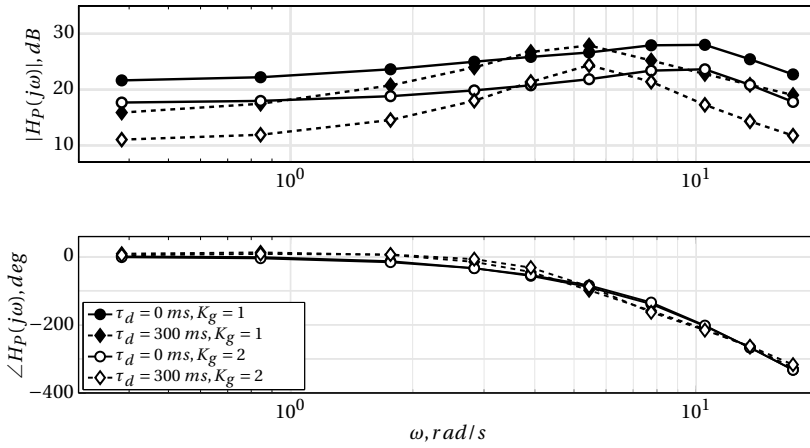


Figure 4.8: Manual control behaviour of human operators described by the pilot model using grand averaged identified parameters in 0 and 300 ms of added time delay and increased control gear gain, $K_g=1$ and 2.

Figure 4.8 illustrates the major differences between manual control behaviour over all tested conditions. Adaptation of the human operator to the increased control sensitivity is a matching shift in the magnitude response while the phase response is identical for both control gear conditions. However, the manual control adaptation to the added time delay has a number of characteristic deviations in the identified manual control response, as summarized in Table 4.6.

Table 4.6: Main observations and their indications from identified pilot parameters of manual control behaviour adapted to the added time delay condition.

Observations when $\tau_d \uparrow$	Relevant pilot parameter deviation	
Shift of magnitude response	Decrease in pilot visual gain at low and mid-frequencies	$K_v \downarrow$
Increased magnitude slope	Increase in lead time constant at low and mid-frequencies	$\tau_L \uparrow$
Increased phase response	Increase in lead time constant at low and mid-frequencies	$\tau_L \uparrow$
Decreased frequency of the magnitude peak	Decrease in neuromuscular natural frequency at mid- and high frequencies	$\omega_{nms} \downarrow$

As listed in Table 4.6, added time delay resulted in a lower plot gain at low and mid-frequencies, with an increased magnitude slope. This steeper magnitude slope is an indication of increased lead time constant, which is also coherent with the increased

phase response around low and mid-frequencies. Another observation is the reduction of the natural frequency of the neuromuscular system (ω_{nms}). This decrease of the natural frequency of the second order neuromuscular system model can be interpreted as adaptation of human operators to apply muscular activation at lower frequencies combined with linear control inceptor system, when subjected to degraded HQ conditions. In degraded HQ conditions human operators may inherently avoid to exhibit high frequency neuromuscular activity which would amplify the response of the degraded HQ .

CROSSOVER FREQUENCIES AND PHASE MARGINS

By using the identified pilot parameters from the previous section, the open-loop crossover frequencies and corresponding phase margins could be obtained, see Figure 4.9 with means and 95% confidence intervals, corrected for between-subject variability. In order to evaluate the statistical significance of the added time delay and the control gear on crossover frequencies and phase margins, a two-way repeated-measure ANOVA was applied, and the results are listed in Table 4.7.

4

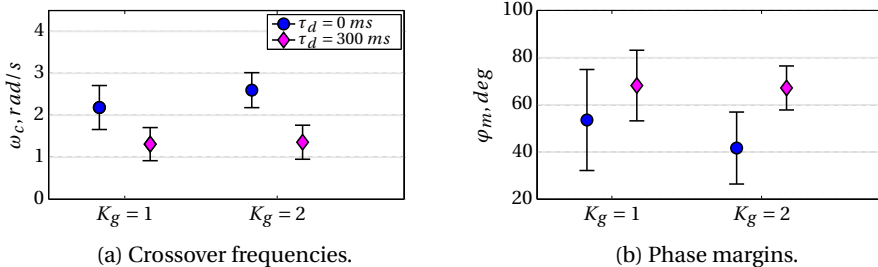


Figure 4.9: Mean and 95% confidence intervals of the crossover frequency(a) and the phase margin(b), all corrected for the between-subject variability.

Table 4.7: Two-way repeated-measures ANOVA results for the crossover frequencies and phase margins, where ** is highly significant ($p < 0.05$), * is significant ($0.05 \leq p < 0.1$), - is not significant ($p \leq 0.1$).

Dependent measures	Independent variable factors								
	τ_d			K_g			$\tau_d \times K_g$		
	dF	F	Sig.	dF	F	Sig.	dF	F	Sig.
ω_c	1,3	52.63	**	1,3	3.68	-	1,3	4.94	-
ϕ_m	1,3	2,45	*	1,3	0.22	-	1,3	14.34	-

Figure 4.9 shows that the crossover frequency (ω_c) decreased, with a highly significant effect of added time delay, [F(1,3)=52.63, $p < 0.05$]. Increased control gearing does not show a significant effect on the crossover frequency, even with the combination of the added time delay. Moreover, the control gearing does not effect the phase margin (ϕ_m) as well, whereas added time delay showed a significant effect on ϕ_m , [F(1,3)=2.45, $0.05 \leq p < 0.1$]. Combined effects of the added time delay and the control gear gain also did not show a significant effect on phase margin. Similar to the identified pilot parameter comparisons, the added time delay was the most effective independent variable that influenced the adaptation of the manual control behaviour, observed with the crossover frequency and the phase margin comparison as well. These results agree with the hypotheses given in Section 4.2.5.

ROVER AND PAC RESULTS

In order to investigate the correlation between the identified manual control behaviour and the RPC tendency, the measured data was processed with ROVER and PAC, as a part of the MCIM described in the previous chapter. ROVER results are shown in Figure 4.10, and corresponding two-way ANOVA statistical analysis table is given in Table 4.8.

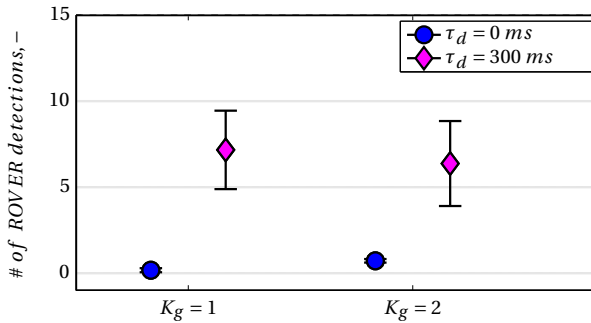


Figure 4.10: Mean and standard deviations of the detected ROVER flags for all experiment conditions.

Table 4.8: Two-way repeated-measures ANOVA results for the number of ROVER detections, where ** is highly significant ($p < 0.05$) and - is not significant ($p \leq 0.1$).

Dependent measures	Independent variable factors								
	τ_d			K_g			$\tau_d \times K_g$		
	dF	F	Sig.	dF	F	Sig.	dF	F	Sig.
<i>ROVER flags</i>	1,3	7.558	**	1,3	1.939	-	1,3	4.11	-

From Figure 4.10, it can be clearly seen that added time delay indeed increased the RPC susceptibility, such that the number of RPC detections (i.e., four simultaneously detected ROVER flags) significantly increased, $[F(1,3)=52.63, p<0.05]$. Both control gearing and combination of added time delay and control gearing do not show any significant effect on the number of ROVER detections, $[F(1,3)=1.939, p\geq 0.1]$ and $[F(1,3)=4.11, p\geq 0.1]$, respectively. It must be noted that the scope of this experiment was not to identify the manual control behaviour during a fully developed RPC event. Instead, manual control behaviour in RPC prone conditions were investigated by using the MCIM. Therefore, the identification of the manual control behaviour was performed on the human operator who could still maintain the control of the vehicle but with a change of his/her control behaviour to adapt to the RPC prone task. Similar to the ROVER, PAC was processed on the measured data and, its results are demonstrated in Figure 4.11.

4

It can be seen in Figure 4.11 that, added time delay caused pairs of phase-aggression detections in PAC to shift from the 'NO PIO' zone to closer to the 'Moderate PIO' zone, where the RPC susceptibility is higher, as described in the previous chapter. It is worth noting that the translation of these detections was mainly due to the phase parameter of the PAC. Moreover, it can be observed from Figure 4.11 that the average aggression parameter of the detected points became approximately its half value when the control gear gain was doubled, independent of the added time delay condition. This behaviour is highly correlated with the gain of the pilot model such that in order to attain a similar vehicle response, human operators adjusted their gain (i.e., shift the magnitude of the pilot response) when subjected to a higher control gearing gain.

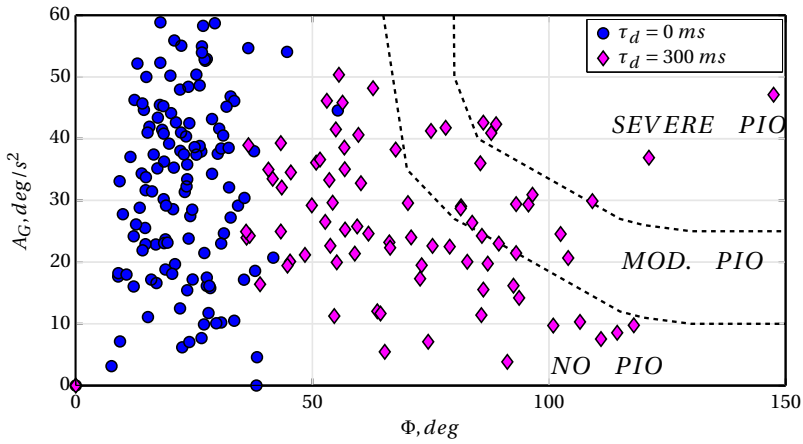
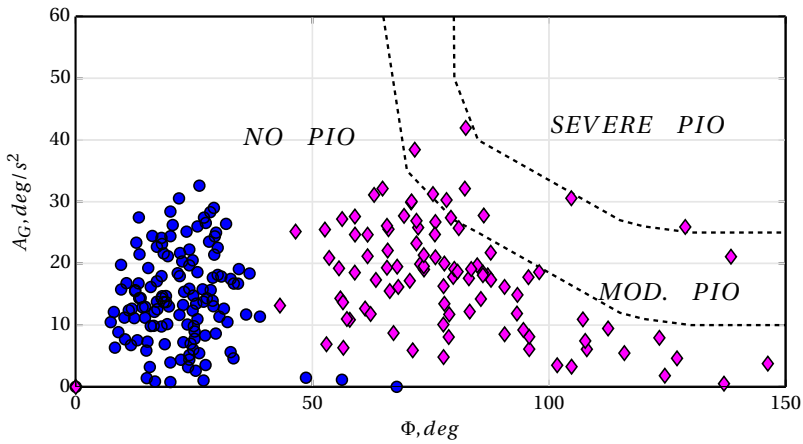
(a) $K_g = 1$ (b) $K_g = 2$

Figure 4.11: PAC detection results for Participant 2 in conditions with 0 and 300 ms of added time delays, for the two levels of control gearing values.

4.2.8. DISCUSSION ON THE FIRST EXPERIMENT

The first preliminary experiment investigated the effects of added time delay and increased control gearing on manual control behaviour. The MCIM, which was introduced in the previous chapter, was used in all its proposed stages except for changing the task difficulty. Two levels of added time delays ($\tau_d = 0$ and 300 ms) and two values of control gains ($K_g = 1$ and 2) were used. The rationale of the control gearing variation was to investigate the control behaviour changes if participants were exposed to a higher-sensitivity manipulator, e.g., different control manipulator gearings in different simula-

tors, in a test campaign with various conditions of added time delay in the vehicle model.

Four participants completed a roll-axis disturbance-rejection task. The primary scope was to investigate the adaptation of manual control behaviour for the added time delays, since literature shows that increased control gearing would only change the gain of the control behaviour accordingly, such that a similar open-loop response near crossover frequency is achieved. This result is a good example of one of the classical verbal adjustment rules of McRuer⁸⁰ (i.e., K_c - ω_c independence). This rule states that after an initial adjustment, any change in the CE gain (K_c) is offset by the pilot gain, thus, crossover frequency (ω_c) is invariant of the CE gain.

The CE was a single-axis steady-state roll model which was characterized by the roll subsidence. A high value of the roll subsidence (-10.94 s^{-1}) was used in order to simulate a high bandwidth rotorcraft, e.g., the Bo-105. After completing the first preliminary identification experiment, measured data were analysed and processed to identify the linear control behaviour of participants. Particular interest was given to the change of crossover frequency and the corresponding pilot model parameters. It was observed that control gearing did not change the crossover frequency, and there was no significant variation in the pilot model parameters due to K_g except for the pilot gain. Added time delay significantly changed the control behaviour, and decreased open-loop crossover frequencies and increased phase margins were obtained. Moreover, by using the RPC detection tools of the MCIM, it was observed that RPC susceptibility was increased with the added time delay. Identified pilot parameters showed that with the added time delay, human operators decreased their visual gains, increased their lead time constants, and reduced their neuromuscular natural frequencies. Neuromuscular damping and pilot delay parameters did not show a clear trend of change. Therefore, the first preliminary identification experiment showed how human subjects adapted their manual control strategies to cope with the reduced PVS stability caused by added time delay.

Although a reduction in crossover frequency with added time delay was observed, it was not clear whether it was a crossover regression or not. Crossover regression is a phenomenon that shows a clear regression between two conditions (e.g., forcing function bandwidths), as described by McRuer and Jex⁸⁰. In principle, human operators can reduce their crossover frequencies for stability reasons or due to the difficulty of the task⁸⁰. In addition, participants commented that the roll error in the display could not be perceived with high precision. Several studies also indicated a similar issue, for example Nieuwenhuizen et al.¹⁰⁵ also showed that in a multi-axis compensatory task (pitch and roll) pilots showed less noisy control anticipation for the pitch axis, and they aimed to minimize the pitch error with a higher precision and priority, rather than the roll error. The error of the roll attitude requires human operators to apply sideways cyclic input. The response of the neuromuscular system is less linear in this direction since the activated muscular system is less symmetrical when compared to longitudinal control⁵¹. Considering the demanding MCIM experiment conditions (e.g., degraded HQ and increased RPC susceptibility during possibly harder tasks), it was decided to use the pitch-axis model of the MCIM to result in a more linear human control behaviour when both

added time delay and task difficulty were proposed to be altered. As the next step, a second preliminary identification experiment was designed, and described in the next section.

4.3. PRELIMINARY EXPERIMENT II

The first experiment showed that when exposed to a CE with added time delay, significant changes in the pilot model parameters were: decreased pilot visual gain, increased lead time constant and the lower neuromuscular natural frequencies. Open-loop crossover frequency was decreased with added time delay, but the tested conditions were not sufficient to determine the crossover-regression tendency by comparing just two crossover frequencies. In order to detect the crossover regression better, the second preliminary experiment tested a higher resolution of the added time delay. Akin to the first preliminary experiment, the main goal of this experiment was investigating the effects of added time delay on manual control behaviour with a particular focus on the crossover regression determination, while keeping the task difficulty constant. In compliance with the structure of the MCIM introduced in the previous chapter, this section will describe the details of the second preliminary experiment.

4.3.1. TASK DESIGN

PITCH CONTROL TASK

In this experiment, the disturbance-rejection task of the MCIM in the pitch-axis was used, as described before. Moreover, task difficulty was not.

ROTORCRAFT MODEL

The controlled element (H_{CE}) was the single axis (pitch) rotorcraft model of the MCIM, as described in the previous chapter. In this experiment, the control authority term $M_{\delta_{lon}}$ was $4.095 \text{ rad}/(\text{in.}\cdot\text{s}^2)$, and the aerodynamic pitch rate damping derivative M_q was -3 s^{-1} . Three levels of added time delay (τ_d) were tested; 0, 100 and 200 ms. Considering the pitch subsidence which determines the break frequency of the CE, this rotorcraft model starts to behave like a double integrator at lower frequencies (3 rad/s) than the roll model ($\approx 10 \text{ rad/s}$) of the first experiment. Therefore, the added time delay values were chosen to be lower than 300 ms. The Bode plot of the CE is shown in Figure 4.12.

As can be seen from Figure 4.12, increasing the added time delay results in larger phase lag of the CE; whereas it does not affect the magnitude response. Corresponding BPD criterion assessments of the CE with added time delay are shown in Figure 4.3.

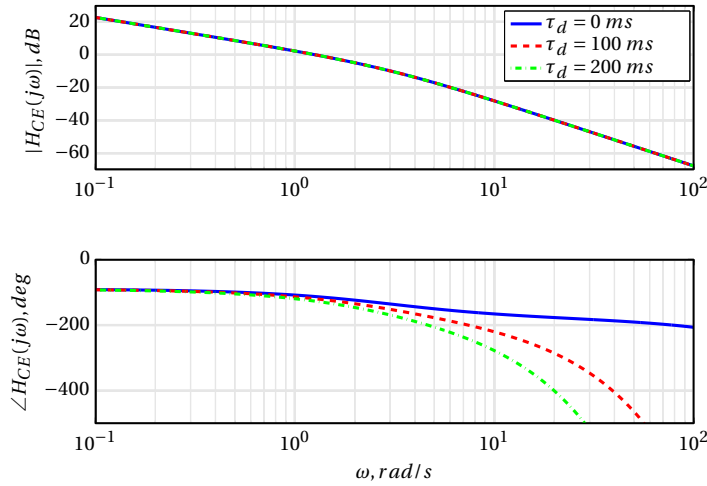


Figure 4.12: Bode diagram of the CE with 0, 100 and 200 ms of added time delay.

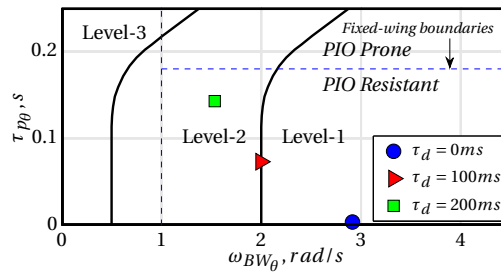
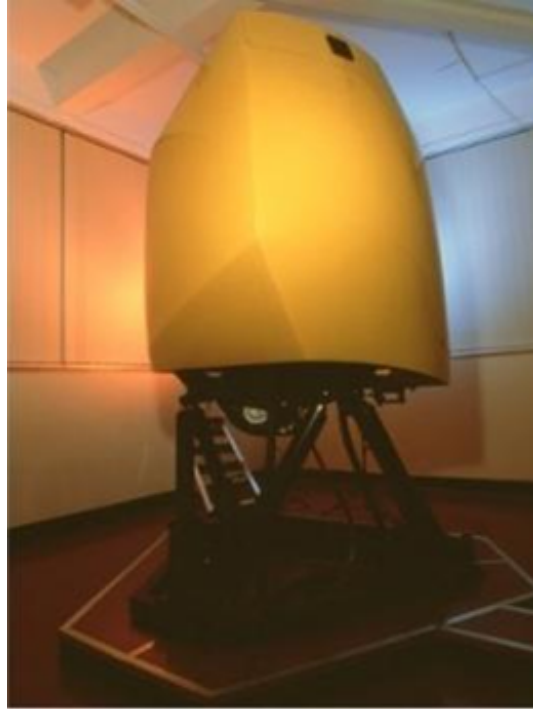


Figure 4.13: Bandwidth phase delay criterion of the CE with 0, 100 and 200 ms of added time delay.

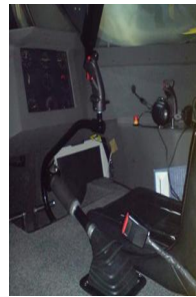
It can be observed from Figure 4.13 that the baseline model (i.e., $\tau_d=0$ ms) exhibits Level-1 HQ, whereas 100 ms of added time delay degrades the HQ to the border of Level-2 HQ. Furthermore, 200 ms of added time delay resulted in Level-2 HQ. In Figure 4.13, PIO boundaries of fixed-wing aircraft are superimposed on the BPD chart with dashed lines for comparison reasons, since boundaries for rotorcraft have not been determined yet¹¹⁵. According to the fixed-wing boundaries, all added time delay conditions were still predicted to be PIO resistant.

APPARATUS

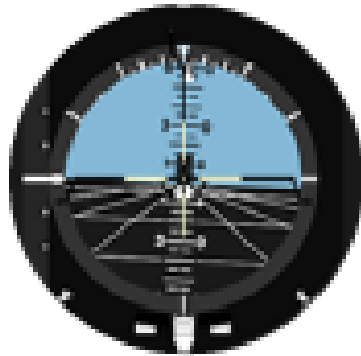
The experiment was conducted in the HHS (Figure 4.14-a) without motion. A scaled-up attitude indicator (Figure 4.14-c) was used as a compensatory display to show the pitch error. The control inceptor was a generic central cyclic stick (Figure 4.14-b) with a rotational spring, and without the breakout force and friction to sustain the linearity in



(a) The Heliflight Helicopter Simulator (HHS) of the University of Liverpool.



(b) Cyclic control inceptor in the HHS simulator.



(c) Attitude indicator used for displaying pitch error during the disturbance-rejection task.

Figure 4.14: The second preliminary identification experiment was conducted in the HHS. Participants used the cyclic controller(b). The pitch error was displayed to the pilots on the scaled-up attitude indicator (c). The indicator outer and inner ring diameters were 15 cm and 13 cm, respectively. The display distance to eye design point of the pilot seat was approximately 90 cm.

the control path of the CE. Only the longitudinal cyclic control was enabled during the experiment, while all other axes of control were locked.

PARTICIPANTS

This experiment was performed by three participants, all professional rotorcraft pilots. All pilots had prior experience with similar human-in-the-loop experiments with manual control tasks. All subjects were male and their ages ranged from 42 to 63 years, with an average age of 50.7 years. The same pilots also participated in the rigid body simulator test campaigns of the ARISTOTEL project, which focused on triggering RPC events in full motion simulator environments through added time delay and rate limiting in Bo-105 simulation models¹¹⁵.

Table 4.9: Flying and simulator experiences of the participant pilots in the second preliminary identification experiment. Listed flying hours belong to 2012, taken from Ref.[53].

Pilot	Job title	Rotary wing hours	Fixed-wing hours	Simulator hours
I	Senior First Officer for commercial airline/British Royal Navy	7800	8000	1300
II	Royal Netherlands Airforce Chinook Test Pilot	1500	200	230
II	Royal Netherlands Airforce Apache Test Pilot	2000	6150	400

4.3.2. INDEPENDENT VARIABLES

The only independent variable was the added time delay in the CE for 0, 100 and 200 ms (i.e., three conditions).

4.3.3. EXPERIMENT PROCEDURES

The experiment was designed and executed according to MCIM, such that all pilots were briefed on the task to be completed (i.e., minimize the displayed pitch error by using the longitudinal cyclic input). Scope of the experiment and any configuration details were not provided to pilots to avoid any pre-assigned control strategy.

Since the ANOVA was used while analysing the measured data, the execution order of experiment conditions was designed as a Latin square, as listed in Figure 4.10.

4.3.4. DEPENDENT MEASURES

Similar to the first preliminary identification experiment, the dependent measures were the task performance (i.e., the normalized error variance), the control activity, identified pilot model parameters, the crossover frequency, the phase margin and RPC tendencies that were detected by ROVER and PAC.

Table 4.10: 3x3 Latin square experiment design with the independent variable, i.e., added time delay (τ_d).

Participants	Experiment Condition		
	τ_d		
I	100 ms	0 ms	200 ms
II	200 ms	100 ms	0 ms
III	0 ms	200 ms	100 ms

Finally, pilots were asked to subjectively evaluate the HQ and RPC of experiment conditions by using HQR and PIOR, respectively. Details of these subjective ratings are given in Appendix A. For the HQR, $\pm 10^\circ$ pitch error was set as desired performance, and $\pm 15^\circ$ was set as adequate performance for the tracking task. Although these performance levels were not taken from a realistic task, experimental trial runs conducted with pilots resulted in these levels to be applicable in this experiment. It is worth noting that the complete simulator environment directly affects the execution of the task, such as the cyclic forces and the error display size. As a part of the ARISTOTEL simulator test campaigns, pilots, who also participated in this experiment, had already been familiarized with the rating scales and the simulator environment. Pilots awarded the HQ and RPC ratings of the configuration after each measurement run (last 4 runs with steady scores). Moreover, pilots also awarded Bedford pilot workload ratings (see Appendix A.4) to evaluate the change in the subjective workload between experiment conditions.

4.3.5. HYPOTHESIS

Human operators were expected to exhibit a noticeable change in their manual control behaviour after some value of added time delay, similar to the 'HQ cliff' occurrences^{5,5}, which were discussed in Chapter 2. Hence, it was hypothesized that '**added time delay would induce crossover regression**'. Such occurrences of manual behaviour changes will be captured by using the objective measures of MCIM, i.e., identified pilot model parameters.

4.3.6. METHODS USED FOR ANALYSING THE EXPERIMENT DATA

IDENTIFICATION METHODS

Akin to the first preliminary experiment, both FCMwO and MLE identification methods were used while analysing the measured data, as described in the MCIM.

STATISTICAL ANALYSES

In order to analyse the statistical significance of the variations among configurations, an one-way repeated-measures ANOVA was applied to the results of the second preliminary experiment. Measured data of this experiment showed that the interval scale assumption was satisfied for all dependent measures analysed. The normality assumption was rarely violated, but the ANOVA is fairly robust for such instances¹⁰⁵. If the sphericity assumption was violated, the Greenhouse-Geisser correction was applied²⁰.

RPC DETECTION TOOLS

ROVER thresholds were assigned according to the post-run analysis of the measured data of the experiment, as explained before, and they are given in Figure 4.11.

Table 4.11: ROVER variables and their threshold values used in the second experiment. Here, ω_q is the pitch rate frequency, $\hat{\theta}_{lon}$ is the longitudinal cyclic stick deflection, q is the pitch rate response of the rotorcraft, and ϕ_θ is the phase between pilot control peaks and resultant body rate response.

Variables as ROVER flags		Threshold
Frequency	ω_q	8 rad/s
Stick amplitude	$\hat{\theta}_{lon}$	0.49 in
Pitch rate	q	0.18 rad/s
Phase	ϕ_θ	85 deg

4

4.3.7. RESULTS

This section will provide the results of the dependent measures of the second preliminary experiment that were described in the previous section. Since the only independent variable was the added time delay, a one-way repeated measures ANOVA is used to analyse statistical significance of the added time delay in these dependent measures, and the ANOVA results are provided in Table 4.12.

Table 4.12: One-way repeated-measures ANOVA results for the dependent measures of the second preliminary experiment, where ** is highly significant ($p < 0.05$), * is significant ($0.05 \leq p < 0.1$), and - is not significant ($p \geq 0.1$).

Dependent measures	Independent variable		
	τ_d		
	dF	F	Sig.
σ_e^2 / σ_i^2	2,4	8.203	**
RMS_u	2,4	1.213	-
K_v	2,4	3.723	**
τ_L	2,4	12.328	**
ω_{nms}	2,4	1.865	*
ζ_{nms}	2,4	1.968	-
τ_p	2,4	0.685	-
ω_c	2,4	1.851	**
ϕ_m	2,4	1.748	*
ROVER flags	2,4	1.583	**

Following subsections will provide the results obtained from the experiment, and use Table 4.12 to provide statistical information about the observed variations of dependent measures.

TASK PERFORMANCE AND CONTROL ACTIVITY

Similar to the first identification experiment, task performance was measured by the normalized error variance (σ_e^2/σ_i^2), while the RMS of the control input was used as a measure of pilot control activity. Figure 4.15 depicts the task performance and the control activity, calculated from measurement data.

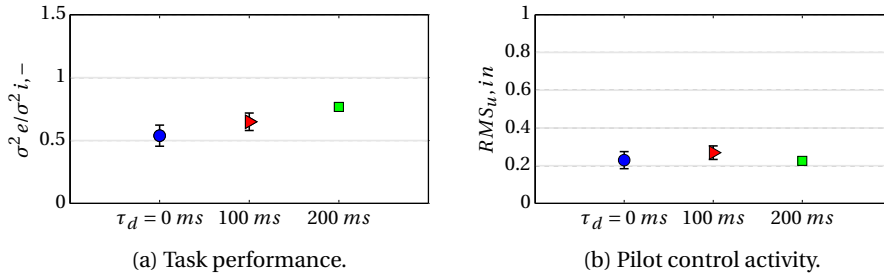


Figure 4.15: Mean and 95% confidence intervals of measured task performance (a) and control activity (b), all corrected for the between-subject variability.

It can be seen from Figure 4.15-a that increasing added time delay resulted in increased error. Moreover, ANOVA results in Table 4.12 also shows that added time delay has a highly significant effect on the normalized error variance, $[F(2,4)=8.203, p<0.05]$. However, added time delay did not show a clear deviation tendency in control activity, as shown in Figure 4.15-b, and statistically not effective as well ($[F(2,4)=1.213, p>0.1]$).

IDENTIFIED PILOT MODEL PARAMETERS

In order to check the linearity of the pilot control behaviour, the correlation coefficients and VAF values were examined, similar to the first identification experiment. VAF values represent the accuracy of the estimated pilot model behaviour when compared to the measured data. Since linear manual control models were considered in MCIM, high VAF values inherently may indicate the linearity of the control behaviour. The opposite argument is not true such that low VAF values do not strictly indicate the non-linearity of the measured response, but instead improper estimated pilot model structure can be a reason as well. An example of the average correlation coefficient for a pilot, and VAF values, which were corrected for between-subject variability, are shown in Figure 4.16.

As illustrated in Figure 4.16, the correlation coefficients were close to one. Moreover, VAF values obtained for all subjects were between 89% to 93%, with a grand average of 91.1%, as shown in Figure 4.16. Such high values of VAF indicates the good fit of the estimated linear control behaviour model to the measured data.

Since the linearity of the control response was checked, the identified pilot model can be considered to well describe the manual control behaviour of the participant pilots. Means and 95% confidence intervals of the identified parameters of the pilot model are depicted in Figure 4.17.

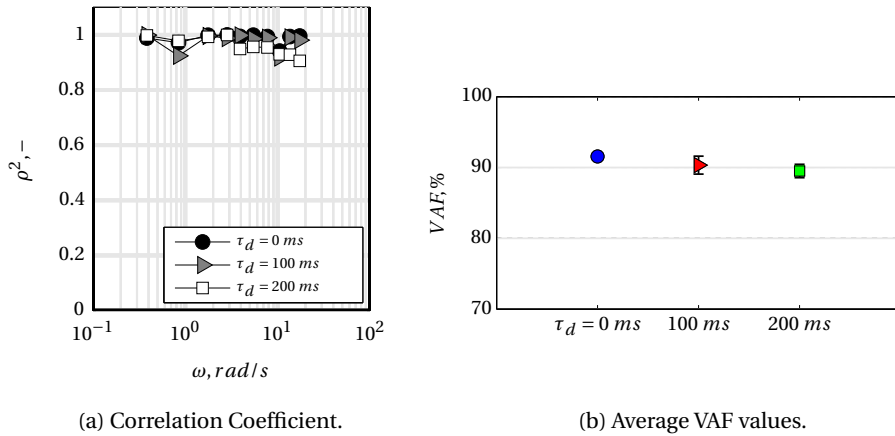


Figure 4.16: Average correlation coefficient values for Pilot 2 (a), and mean and 95% confidence intervals of VAF values, corrected for between-subject variability (b).

It can be observed from Figure 4.17-a that with increasing added time delay, pilots reduced their visual gain, which agrees with the highly significant effect of added time delay on the visual gain according to ANOVA results ($[F(2,4)=3.723, p<0.05]$ in Table 4.12). Particularly, the reduction was more noticeable when added time delay increased from 100 ms to 200 ms. In correlation with this trend, the lead time constant parameter increases with added time delay, which showed a statistically highly significant effect on the lead time constant [$F(2,4)=12.328, p<0.05$]. Similarly, for the 200 ms condition the increment was noticeably higher than the increase from 0 to 100 ms of added time delay. With increasing added time delay, natural frequency of the neuromuscular system was decreased [$F(2,4)=1.865, 0.05 \leq p<0.1$], and a noticeable change can be observed with 200 ms of added time delay. Both neuromuscular damping and the pilot delay did not show any noticeable trend with the added time delay.

In order to visualize the overall effect of the change in manual control behaviour, frequency responses of grand-average pilot models obtained from the mean values of the identified pilot models are depicted in Figure 4.18.

The grand-mean pilot model for 200 ms added time delay condition is noticeably different than the pilot models for the 0 and 100 ms added time delay conditions. This change of manual control behaviour suggests that between 100 and 200 ms of added time delay conditions, there could be a 'cliff-like' sudden change in HQ.

CROSSOVER FREQUENCIES AND PHASE MARGINS

Crossover frequencies and phase margins with their means and 95% confidence intervals, corrected for between-subject variability are depicted in Figure 4.19.

Figure 4.19 shows that with increasing added time delay, the crossover frequency stays

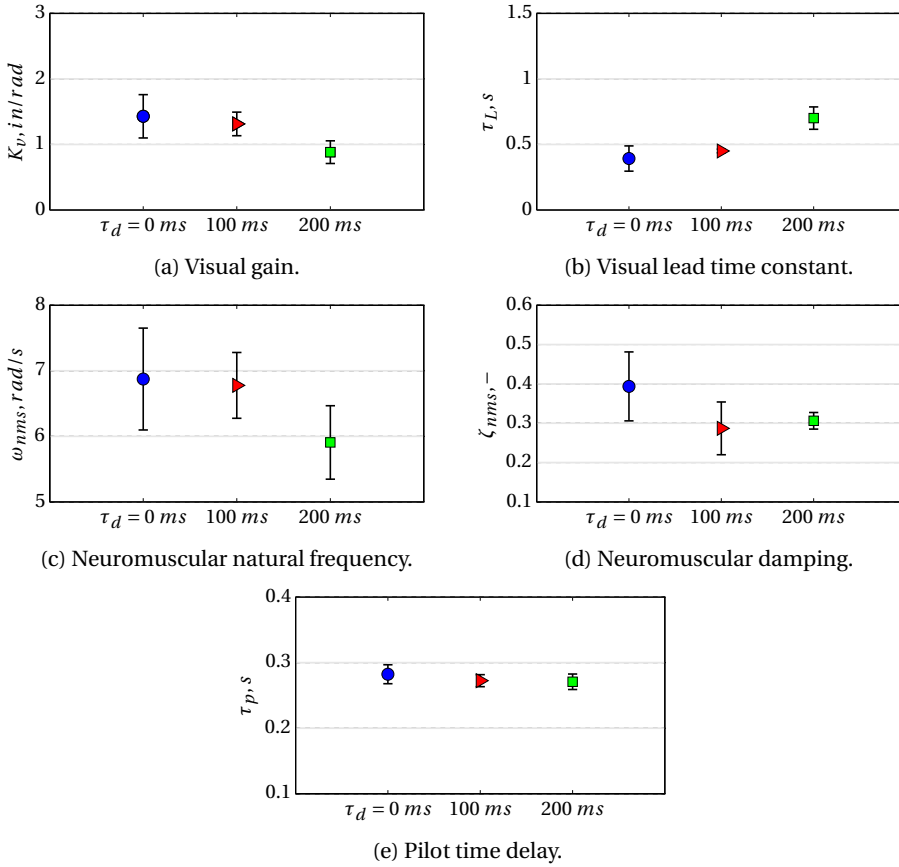


Figure 4.17: Mean and 95% confidence intervals of the estimated pilot visual gain (a), the lead time constant (b), the neuromuscular natural frequency (c), the neuromuscular damping (d), and the pilot time delay (e) parameters, all corrected for the between-subject variability.

almost steady from 0 ms to 100 ms. However, when the added time delay was increased to 200 ms, a clear crossover regression tendency ($\approx 30\%$) was observed. In addition, ANOVA results show that added time delay has a highly significant effect on crossover frequency ($[F(2,4)=1.851, p<0.05]$ in Table 4.12). Similarly, the phase margin values show a noticeable difference ($\approx 30\%$) when 200 ms of added time delay was applied. Added time delay showed a significant effect on the phase margin. Unlike the classical crossover regression^{81,83}, this regression due to added time delay did not require the change of the task difficulty, i.e., bandwidth of the forcing function. Instead, HQ degradation due to the added time delay can be interpreted as a harder task from a classical crossover regression perspective.

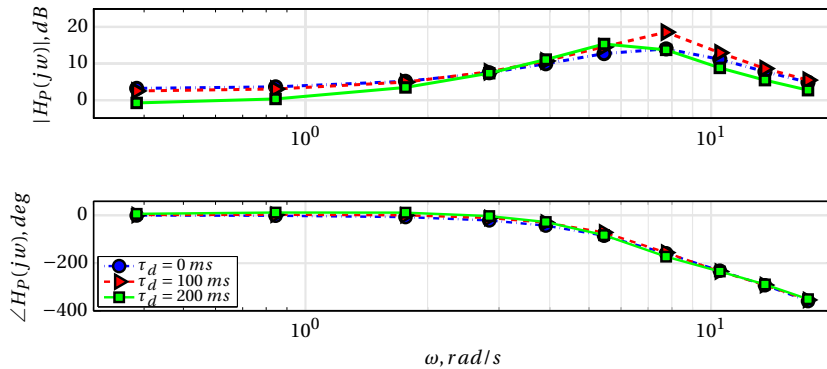


Figure 4.18: Manual control behaviour of human operators described by the pilot model using grand averaged identified parameters in 0, 100 and 200 ms of added time delay conditions.

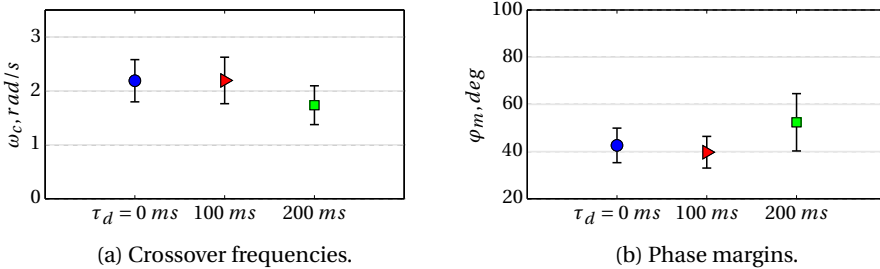


Figure 4.19: Mean and 95% confidence intervals of the crossover frequency(a) and the phase margin(b), all corrected for the between-subject variability.

ROVER AND PAC RESULTS

As a part of the MCIM, ROVER and PAC were used to investigate the correlation between occurrences of the crossover regression and the RPC susceptibility caused by the added time delay. Results are shown in Figure 4.20 and Figure 4.21, respectively.

The ROVER results in Figure 4.20 indicate that from 0 ms to 100 ms, detected RPC numbers increased from 0 to 10 detections. This deviation illustrates that the RPC tendency of the rotorcraft in the task increased considerably. However, when added time delay was increased to 200 ms, the detected RPC occurrences remained almost constant. It is suggested that pilots preferred to exhibit a 'back-off' strategy here, and consequently avoid any further RPC tendency between 100 ms and 200 ms of added time delay conditions. Added time delay showed a highly significant effect on the detected ROVER flags [$F(2,4)=1.583, p<0.05$]. Similarly, PAC results shown in Figure 4.21-b demonstrate that from 0 ms to 100 ms of added time delay, the detected PAC parameters shifted from 'NO PIO' to 'Moderate PIO' zone, by both increased aggression and phase detections. As depicted in Figure 4.21-b, PAC detections show that 200 ms of added time delay condition

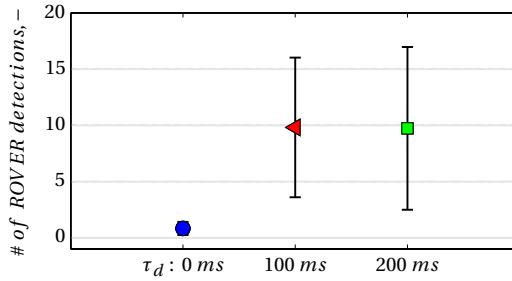


Figure 4.20: Mean and standard deviations of ROVER detections.

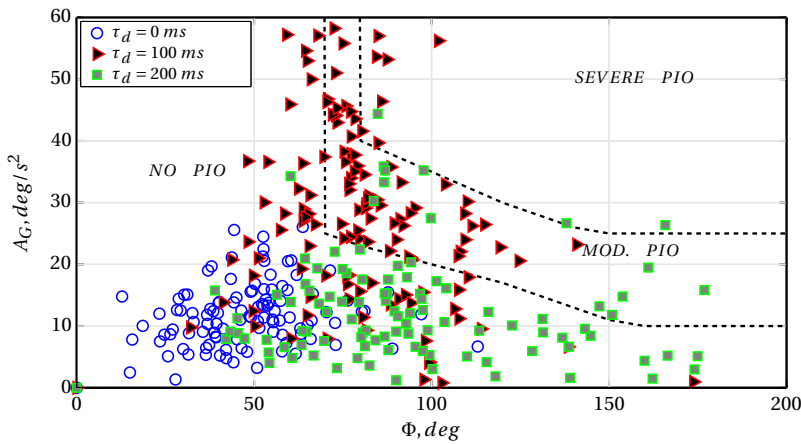


Figure 4.21: PAC results of subject 2 for 0, 100 and 200 ms of added time delay conditions.

resulted in 'NO PIO' zone, which again indicates that pilots preferred to avoid the increased risk of severe RPC tendencies as added time delay became 200 ms.

PILOT SUBJECTIVE RATINGS

As described in Section 4.3.2, three subjective pilot ratings were used in the second preliminary identification experiment by professional pilots. It must be noted that these subjective scales are not part of the MCIM, but they were used for comparison purposes. These three subjective pilot ratings were: the Cooper-Harper HQR for the HQ assessment, PIOR for the RPC susceptibility, and Bedford Work Loading Scale Ratings (WLR) , which are provided in Appendix A. Awarded ratings of these rating scales in the second preliminary identification experiment are depicted in Figure 4.22.

It can be seen from Figure 4.22 that all ratings got worse as the added time delay increased. HQ stayed in Level-2 (i.e., ratings from four to six in HQR), but 200 ms of added time delay was awarded on the border of Level-3. The PIOR indicated that for the baseline condition, mean of the PIOR was awarded two, which is described as (Appendix A.2) '*Undesirable motions tend to occur when pilot initiates abrupt maneuvers or attempts*

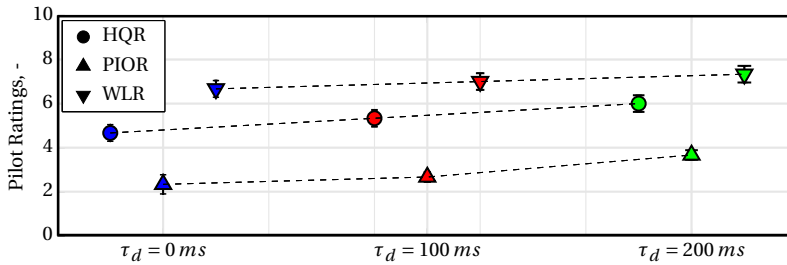


Figure 4.22: Awarded HQR, PIOR and WLR for 0, 100 and 200 ms of added time delay conditions.

tight control. These motions can be prevented or eliminated by pilot technique. For the 200 ms added time delay condition, the PIOR was awarded four, which is described as ‘Oscillations tend to develop when pilot initiates abrupt maneuvers or attempts tight control. Pilot must reduce gain or abandon task to recover.’ This PIOR deviation suggests that the 200 ms added time delay condition enforced pilots to exhibit precarious control to avoid potential RPC occurrences, and a reduced gain strategy was applied since pilots did not abandoned the task. These subjective ratings are in good agreement with the ROVER and PAC detections, such that they also indicated the change of RPC occurrences due to adapted control strategy. WLR was explicitly considered for comparison purposes only because such an identification experiment severely limits capacity for additional piloting tasks. It can be observed from WLR that pilots were already exerting high workload for the identification experiment, i.e., WLR in Level-3 (ratings between 7 and 9). Overall, awarded WLR showed a gradual increase in pilot workload with added time delay conditions during which degraded HQ required higher attention, as depicted in Figure 4.22. This result is also highly correlated with the identified parameters, for instance, increased lead time constant is an indication of increased pilot workload⁷⁵.

4.3.8. DISCUSSION ON THE SECOND EXPERIMENT

The second identification experiment was conducted with a focus on occurrences of **crossover regression** due to added time delay. During this experiment, human subjects were three professional helicopter pilots who also had participated in the ARISTOTEL project during RPC test campaigns. Three levels of added time delay were applied in order to expose possible crossover regression behaviour of pilots. A pitch-axis model with a break frequency of 3 rad/s, which is located in the expected crossover frequency range, was controlled in a disturbance-rejection task, as described in MCIM. Analyses on measured data showed that a similar pilot model adaptation as in the first preliminary identification experiment was observed in the second experiment as well. Moreover, a considerable occurrence of crossover regression ($\approx 30\%$) between 100 ms and 200 ms of added time delay conditions was observed. The change in pilot model parameters which were also the most effective parameters in the first experiment (i.e., K_v , τ_L , and ω_{nms}), became more apparent. Consequently, RPC tendencies indicated that from 0 ms to 100 ms of added time delay, RPC occurrences already drastically increased, whereas for 200 ms condition the RPC tendency remained almost the same as the 100 ms condi-

tion, as detected by both ROVER and PAC. Apparently, pilots tried to avoid any further RPC events to be triggered when the condition changed from 100 ms to 200 ms of added time delay.

In addition to objective HQ assessments and identified manual control behaviour, three subjective rating scales were used. Awarded HQR showed that HQ degraded gradually with added time delay, mainly staying in Level-2 regime of Cooper-Harper rating scale. Similarly, awarded WLR ratings indicated that pilots awarded higher workload with added time delay. PIOR results illustrated that RPC tendencies increase with added time delay, and awarded PIOR for the 200 ms added time condition indicate that pilots needed to reduce their gain to complete the task. This reduction was identified from the measured data as well. It is worth noting that RPC detection tools notify the occurrences of RPC insurances in the measured data, whereas PIOR show the RPC tendency of the vehicle in general. Thus, if pilots experience a general over-shooting response of the vehicle with moderate pilot control input, they may prefer to reduce their control efforts, i.e., reduce their gain. Therefore, they would award a high PIOR whereas detected RPC would be almost the same due to already reduced aggression. Moreover, fixed-wing PIO boundaries for the bandwidth phase delay criterion predicted all conditions to be PIO resistant, however subjective ratings showed that especially for the 200 ms added time delay condition, it was not verified. The need for adjusting the fixed-wing PIO boundaries for the rotorcraft already has been an ongoing process in literature¹¹⁵, while ADS-33 only provides a warning about the PIO tendency for attitude command systems¹³.

4.4. CONCLUSIONS

By using the MCIM discussed in the previous chapter, two preliminary experiments were conducted. A common goal of both experiments was to identify the adaptation of manual control behaviour when CEs included different levels of added time delay. Especially, possible crossover regression behaviour was examined. Even though the two experiments had several differences, e.g., different CE models in different axes, identification results of manual control behaviour in both experiments revealed that pilots showed lower visual gain and neuromuscular natural frequencies, and higher lead compensation, when the added time delay was increased. In addition, changed control gearing gain in the first experiment showed no effect on the manual control behaviour except for direct gain adaptation of human operators. The second experiment revealed the crossover regression due to added time delay. Furthermore, RPC detection tools showed the increased RPC susceptibility with increased added time delay, and correlated well with the identified manual control behaviour.

Using MCIM starting from the initial design to the final analyses phases of identification experiments successfully demonstrated its applicability for the added time delay conditions in different simulators, vehicle active axes, participant profiles, and added delay values. Adaptation of manual control behaviour to added time delay conditions were also successfully determined and correlated with the RPC susceptibility in both

preliminary identification experiments. Particularly the second experiment showed crossover regression tendency of human operators when exposed to added time delay conditions.

The results of the present chapter demonstrate the capability of the MCIM to detect crossover regression due to added time delay. The next chapter will introduce the second important variable of the MCIM: task difficulty. Crossover regression due to task difficulty is a well-known phenomenon, as discussed in Chapter 2. In addition to the classical occurrences, the MCIM aims to identify the control behaviour changes, when task difficulty *and* added time delay are varied individually and in combination. A fundamental follow-up question in such conditions can be stated as: '*What would be the optimum pilot parameters that could provide the best performance when task difficulty and added time delay are varied?*'. In the next chapter, a theoretical simulation study will be performed to address this question. Particularly, finding the optimum pilot parameters that can provide the best performance will be the main focus of the simulation. Then, corresponding PVS characteristics and signatures of crossover regression with these optimum pilot parameters will be further elaborated.

5

SIMULATION FRAMEWORK

*In the previous chapter, preliminary human-in-the-loop identification experiments, which were conducted in the SRS at Delft University of Technology, and HHS at University of Liverpool, were analysed. This chapter uses the results of these experiments and provides a follow-up computer simulation study in order to investigate the manual control behaviour model in a compensatory task with **additional time delay** in CE, and various **forcing function bandwidths**. In MCIM, various forcing function bandwidths represent different levels of ‘task difficulty’. Crossover regression tendencies in simulated manual control behaviours that yield optimum task performance will be emphasized, based on variation of additional time delay and the task difficulty. In the simulation study, discrete and continuous forcing functions will be used with and without the presence of pilot remnant.*

5.1. INTRODUCTION

In the previous chapter, the preliminary identification experiments showed that when human operators are exposed to CEs with added time delay, they exhibit a manual control behaviour to compensate for the reduced phase of the PVS due to the added time delay. From a handling qualities perspective, additional time delay plays a vital role in defining the available bandwidth of the vehicle from phase-drop restrictions, while the magnitude response remains same. As shown in Chapter 2, this information could already provide an indication of the HQ of the vehicle. For example, ADS-33 contains the BPD criterion, which only considers the transfer function between pilot input and the rotorcraft (i.e., CE) response. The effect of time delay can easily be noticed by increased phase delay and reduced bandwidth, as together these degrade HQ of the rotorcraft (e.g., from Level-1 to Level-2). Although this HQs degradation is a very useful measure to perform an initial assessment of the HQs deficiency of the vehicle, the ‘pilot’ is the ultimate element of the closed-loop PVS who perceives the handling qualities¹⁷. Therefore, investigation of the pilot control behaviour adaptation to various time delay conditions would likely bring a different perspective to the evaluation of HQ. Moreover, increased

time delay also provokes higher adverse A/RPC proneness, which consequently requires a pilot to adjust his/her control strategy.

In the previous chapter, preliminary identification experiments showed that human operators change their control strategy to retain satisfactory task performance when subjected to CEs with added time delay. This adaptation of the manual control strategy was clearly more recognizable after a certain level of added time delay in the second preliminary experiment. This kind of noticeable change in the control strategy for certain conditions resembles the well-known crossover regression strategy^{81,83} which is discussed in Chapter 3 in detail. Briefly, it can be summarized as a recognizable manual control change after exceeding a certain task difficulty (i.e., forcing function bandwidth). In this thesis, the proposed methodology, so-called the MCIM, is designed to investigate the changes in manual control behaviour based on these two crossover regression occurrences (i.e., due to the added time delay and the task difficulty), as provided in Chapter 3. Not only individual occurrences of these crossover regression tendencies, but also their combination is a part of the main research targets of the MCIM.

5

Considering the effects of the added time delay and varied task difficulty on manual control behaviour, several questions can be listed as a follow-up to the results presented in the the previous chapter:

- Which pilot compensation scheme would provide the *best performance* in MCIM tasks with varied added time delay and different task difficulties?
- What would be the *corresponding PVS characteristics* (e.g., crossover frequencies) with these pilot compensation schemes that provide the best performance?
- Would there be any trace of *noticeable change in these PVS characteristics* (e.g., crossover regression) due to the altered task difficulty and added time delay?

In order to address these questions, a computer simulation framework was set-up, utilizing by the general task design of the MCIM. This chapter describes the development of the simulation framework and provides the main results and conclusions of the simulation analysis.

5.1.1. METHODOLOGY OF THE SIMULATION FRAMEWORK

The general scheme of the methodology of the simulation framework is illustrated in Figure 5.1. The methodology can be summarized as:

1. Gather **baseline parameters** and values from the preliminary identification experiments.
2. Set-up a simulation framework that uses the gathered parameters. Then, change the pilot gain (i.e., K_p) and the lead time constant (i.e., τ_L) in the pilot model (i.e., $H_p(j\omega)$) to create control activity and task performance maps for various configurations of **forcing function** and levels of **additional time delay**.

3. Find the pairs of K_v and τ_L that provide **the optimal task performance**.
4. Investigate **crossover regression** tendencies and PVS characteristics of the optimal task performance configurations.

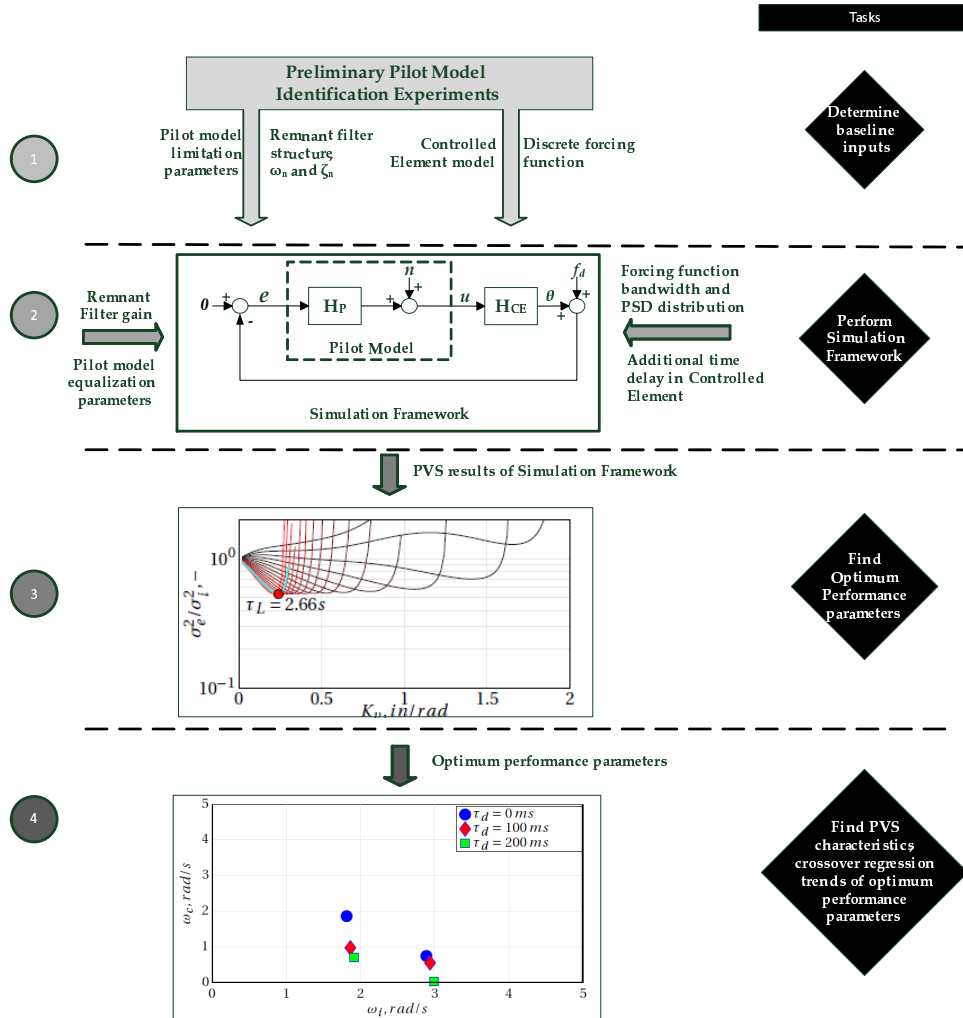


Figure 5.1: Methodology of the simulation framework

5.2. SIMULATION FRAMEWORK DEVELOPMENT

In the simulation framework, the compensatory disturbance-rejection task of the MCIM was used as the baseline, as explained in Chapter 3. Summarizing, in a disturbance-rejection task, the linear pilot describing function ($H_p(j\omega)$) and the pilot remnant (n) creates the pilot control signal (u) to the controlled element ($H_{CE}(j\omega)$). CE generates the pitch attitude (θ), and the displayed error (e) is generated by this θ and the injected disturbance forcing function (f_d). This error is the input of the pilot model, which is the summation of the $H_p(j\omega)$ and the remnant. The same task structure was used for the identification of the manual control behaviour in the previous chapter while analysing the preliminary identification experiments. Although the task structure was kept the same in the simulation framework as well, several task properties were varied during the simulation analysis: the forcing function bandwidth (ω_i), the added time delay (τ_d) in the CE, pilot model parameters and remnant properties.

In the simulation study, the disturbance forcing function contains sharp power cut-off on a certain frequency⁸¹, which defines the forcing function bandwidth (ω_i). As described in detail in Chapter 3, the forcing function bandwidth defines the transition between the high-amplitude low-frequency content and the low-amplitude high-frequency shelf in the signal⁸³. Hence, akin to the MCIM, the forcing function bandwidth is the crucial element that defines the task difficulty in this simulation framework. Two forcing function bandwidths were used: $\omega_i \approx 1.8 \text{ rad/s}$ and $\omega_i \approx 2.8 \text{ rad/s}$, which were given as the MT and the HT, respectively, with their attributes in Chapter 3. In this simulation framework, in order to comply with the MCIM, selection of the forcing function bandwidth was checked for two conditions stated in the MCIM (i.e., the forcing function should provide enough excitation without compromising the identification procedure, and it should allow the detection of possible crossover regression occurrences). The first condition of the ω_i selection was satisfied by the fact that the baseline forcing function had already been used in the preliminary identification experiments successfully. The second condition will be investigated in this chapter, since investigating the tendency of the crossover regression is the goal of the simulation study and the MCIM.

The simulation study was performed offline (i.e., without identification experiments with human operators), thus, it was possible to investigate the simulation results of the analysis with forcing functions with **continuous** PSD. Generally, forcing functions with continuous PSD have more applications in theoretical studies, whereas discrete PSD usually associates with experimental studies^{20,81,83,100}. Since MCIM utilizes a forcing function with a discrete PSD as discussed in Chapter 3, this chapter will provide results of the discrete PSD.

As described in Chapter 3, there is an amplitude reduction (-20 dB) at frequencies beyond bandwidths in forcing functions with discrete and continuous PSDs. Moreover, the total power of the forcing function was kept constant for all PSD distributions and bandwidths. Therefore, forcing functions with higher bandwidths have lower amplitudes in all frequencies. The simulation framework was designed to analyse the PVS characteristics essentially in the frequency domain. Therefore, the phase characteristics of the

forcing function has no impact on the simulation analysis.

In the simulation framework, the controlled element (i.e., $H_{CE}(j\omega)$ in pitch-axis) was taken from the second preliminary identification experiment, as provided in the previous chapter. Moreover, akin to the second preliminary identification experiment, three levels of added time delay were applied (i.e., 0, 100 and 200 ms). As a part of the MCIM, the BPD criterion was applied to assess the HQ of the CE. According to the BPD, HQ of the rotorcraft degrade from Level-1 to Level-2 with increasing add time delay, as discussed in the previous chapter.

In the simulation framework, the linear pilot model (i.e., $H_p(j\omega)$) of the MCIM was utilized, as it was used for the identification of manual control behaviour in the preliminary identification experiments described in the previous chapter. The main goal of this simulation framework was to investigate the optimal pilot equalization (i.e., K_v and τ_L pairs that result in the best task performance) for CEs with added time delay configurations in the task with various forcing function bandwidths. The simulation framework utilized a grid search method, such that K_v and τ_L were varied in the model, and resultant parameters (e.g., crossover frequency) were investigated in a grid made of K_v and τ_L pairs. Resolutions and limitations of the equalization parameters in the grid search is given in Table 5.1. Pilot limitation terms (i.e., pilot time delay (τ_p), neuromuscular natural frequency (ω_{nms}) and damping (ζ_{nms})) were kept constant in order to focus on the effects of the pilot equalization terms on the PVS. Values of the pilot limitations terms are based on the results of the second preliminary identification experiment, and these values are given in Table 5.1.

In experimental conditions (e.g., identification experiments described in the MCIM), human operators can exhibit non-linear control behaviour (i.e., the pilot remnant) which was described in Chapter 3 in detail. In order to simulate a similar behaviour in the simulation framework, the pilot remnant (n) was added to the linear pilot describing function ($H_p(j\omega)$), and the summation of the linear response and the remnant describe the final pilot control input (u) to the CE. Based on the PSD of the measured n from the second preliminary identification experiment, the structure of the noise was selected to be as a second-order system, as exemplified in Figure 5.2.

As shown in Figure 5.2, the remnant is modelled as a Gaussian white noise unattenuated by a second-order filter⁸¹ given as:

$$H_n(j\omega) = \frac{K_{un}}{(j\omega)^2 + 2\zeta_{un}\omega_{un}(j\omega) + \omega_{un}^2} \quad (5.1)$$

where K_{un} is the filter gain, ω_{un} and ζ_{un} are the filter natural frequency and damping respectively. It was observed that a second order filter structure ($H_n(j\omega)$) could represent the noise power distribution globally for all added time delay configurations in the experiment (see Figure 5.2). In the simulation framework, ω_{un} and ζ_{un} were kept constant (see Table 5.1) and K_{un} was calculated for each time delay, task difficulty, K_v and τ_L variation during the grid search, such that the remnant power was 10% of the simulated

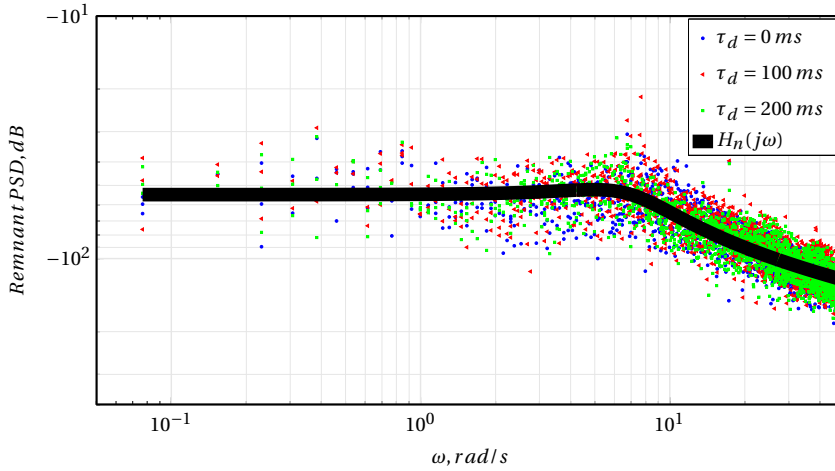


Figure 5.2: PSD of measured remnants of three pilots in preliminary identification experiments for pitch axis with 0, 100 and 200 ms of added time delays. The filter structure ($H_n(j\omega)$) used for pilot remnant modeling in simulation framework analysis was provided to illustrate the fit of selected filter structure to measured remnant PSDs.

control input power (i.e., $\sigma_n^2/\sigma_u^2=0.1$) based on the results of the preliminary identification experiments.

Table 5.1 provides the constant parameters, resolution and interval values of varying parameters in the simulation framework.

Table 5.1: Parameters used in the simulation framework.

Pilot Limitation terms			Pilot Equalization terms		Remnant filter terms		
ω_{nms} (rad/s)	ζ_{nms} (-)	τ_p (s)	K_v (in/rad)	τ_L (s)	ω_{un} (rad/s)	ζ_{un} (-)	K_{un} (-)
6.5	0.32	0.28	0.02 → 3	0 → 3	7	0.5	attain
			$\Delta K_v = 0.02$	$\Delta \tau_L = 0.02$			$\sigma_n^2/\sigma_u^2=0.1$

During the simulation framework development, integrations were handled numerically, and remaining calculations of the simulated PVS were performed analytically in the frequency domain. Throughout the simulation framework, pilot equalization parameters (K_v and τ_L) were varied as shown in Table 5.1, and some resultant parameters were analysed. One of the critical parameters was the normalized error variance (σ_e^2/σ_i^2) which is the task performance per forcing function. The optimum task performance is determined by the minimum value of this parameter for each condition. Another resultant parameter was the crossover frequency (ω_c) which inherently reflects the open-loop pilot vehicle system characteristics. In addition, the phase margin (PM) of the open-

loop system was considered as an indication of the system stability, and the RMS of pilot control activity (RMS_u) were analysed. Independent variables and dependent measures in the simulation framework are given in Table 5.2.

Table 5.2: Independent variables and dependent measures in the simulation framework.

Independent variables	Dependent measures
added time delay (τ_d)	normalized error variance (σ_e^2/σ_i^2)
forcing function bandwidth (ω_i)	crossover frequency (ω_c)
pilot gain (K_v)	phase margin (PM)
lead time constant (τ_L)	pilot control activity (RMS_u)
	optimal K_v and τ_L pair

5.3. SIMULATION RESULTS

This section provides the primary results of the simulation framework. First, pilot equalization terms (K_v and τ_L pairs) were varied independently within their parameter interval (see Table 5.1) for each combination of added time delay ($\tau_d \in \{0, 100, 200\}$ ms) and forcing function bandwidth ($\omega_i \in \{1.8, 2.8\}$ rad/s) for both discrete and continuous PSDs, as a part of the second step in Figure 5.1. Although this grid search approach depends on the parameter step resolution (e.g., 0.02 for K_v and τ_L in the simulation framework), it is computationally beneficial when compared to regular optimization for the global minimum, which could bring local minima issues. Each combination of K_v and τ_L was checked for the stability of closed-loop transfer functions and the availability of finding a remnant filter gain (K_{um}) which could provide 10% remnant power in total pilot control (u). If both conditions were satisfied, then a scheme of available pilot visual gain and lead time constant parameters for each τ_d and ω_i combination was generated. Then, the best performance achievable within the scheme (K_v and τ_L pairs) was determined by using the normalized error variance (σ_e^2/σ_i^2), as the third step in Figure 5.1. The minimum value of the normalized error variance determines the best task performance based on the K_v and τ_L pairs in each condition. Optimal pilot equalization parameters (K_v and τ_L pairs), which lead to this best performance point, were determined per condition. After achieving the optimal pilot equalization parameters, corresponding crossover frequencies, phase margins, pilot control activities and PSD distributions were determined, as the fourth step in Figure 5.1.

In this section, the visual gain (K_v) and dependent measure are plotted by showing the lead time constant (τ_L) isolines (i.e., lines on which τ_L is constant). Darker to lighter isolines represents 0 to 3s of τ_L with an increment of 0.1s in the figures in this section. Moreover, the optimal parameter pair (i.e., K_v and τ_L that provides the minimum error) is marked in the figures. Figure 5.3 exemplifies the description of τ_L isolines.

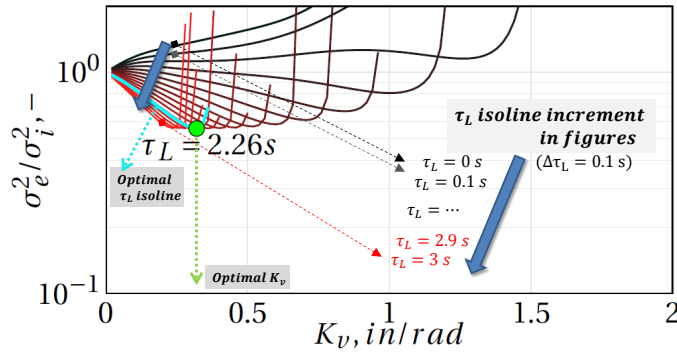


Figure 5.3: Description of τ_L isolines in simulation framework plots.

As demonstrated in Figure 5.3, figures in the following subsections will mark the optimal τ_L lines, and a circular marker to indicate the corresponding optimum K_v . Moreover, the optimal τ_L will be given in figures of all results (i.e., the dependent measure parameters) obtained by the grid search.

5

5.3.1. DISCRETE PSD AND THE PILOT MODEL WITHOUT REMNANT

The simulation framework was initially analysed with the discrete forcing function and without the pilot remnant ($n = 0$). Following the simulation settings described in the previous section, corresponding isoline plots of normalized error variance (σ_e^2/σ_i^2), RMS of pilot control activity (RMS_u), crossover frequency (ω_c) and phase margins (PM) for forcing function bandwidth $\omega_i \approx 1.8 rad/s$ and $\omega_i \approx 2.8 rad/s$ and CE time delay of $\tau_d = 0, 100, \text{ and } 200 ms$ are depicted in Figures 5.4 to 5.9.

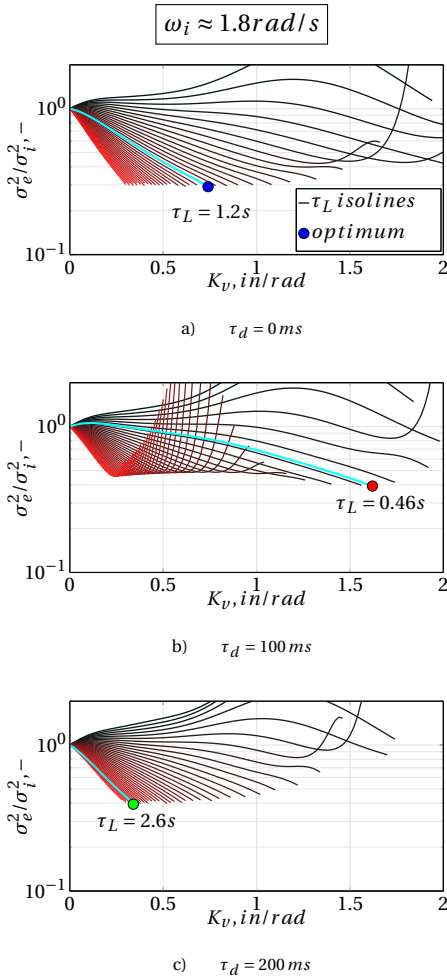


Figure 5.4: Normalized error variance for forcing function bandwidth $\omega_i \approx 1.8 \text{ rad/s}$ and discrete PSD and CE configurations of 0, 100 and 200 ms of time delays, without pilot remnant.

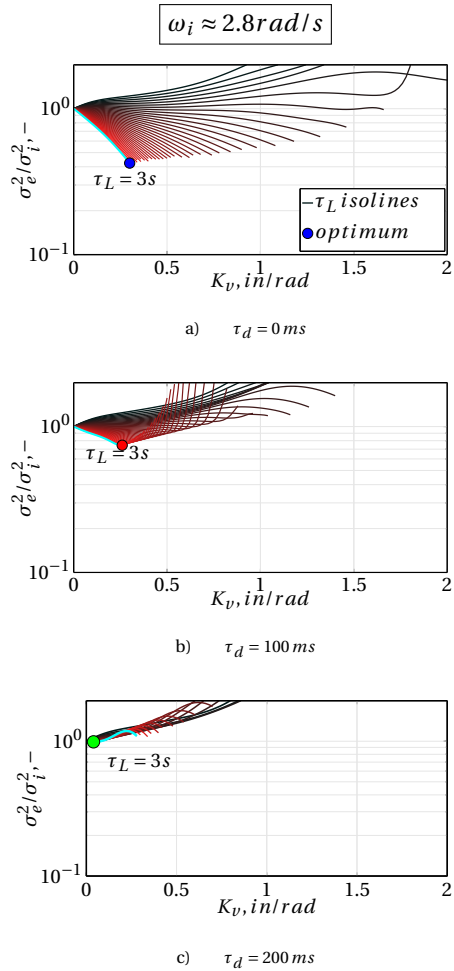


Figure 5.5: Normalized error variance for forcing function bandwidth $\omega_i \approx 2.8 \text{ rad/s}$ and discrete PSD and CE configurations of 0, 100 and 200 ms of time delays, without pilot remnant.

Figure 5.4 and 5.5 show the normalized error variance for three levels of additional time delay (0,100 and 200 ms) in the CE for two forcing function bandwidths: $\omega_i \approx 1.8 \text{ rad/s}$ and $\omega_i \approx 2.8 \text{ rad/s}$, respectively. Since the high forcing function bandwidth induces more frequency content in high amplitude-low frequency shelf (thus, results in a harder task), attainable performance is lower with $\omega_i \approx 2.8 \text{ rad/s}$ when compared to $\omega_i \approx 1.8 \text{ rad/s}$, regardless of the applied time delay. Increasing the time delay shows degraded performance (i.e., lower optimum σ_e^2/σ_i^2) for both forcing function bandwidths. The optimal performance operating points for the high forcing function bandwidth ($\omega_i \approx 2.8 \text{ rad/s}$) configurations demanded the maximum lead time constant ($\tau_L = 3 \text{ s}$) that

was set during the simulation. The area that covers the vicinity of the optimum point diminishes with increasing time delay. This trend implies that attaining good performance is more restricted in terms of possible K_v and τ_L pairs. Especially, the high forcing function bandwidth configuration reflects this behaviour in Figure 5.5. Although a similar trend (i.e., reduced area in the vicinity of the optimum point) was observed for the forcing function with low bandwidth, the optimum point had a higher pilot visual gain and a lower lead time constant for 100 ms time delay, when compared to 0 and 200 ms time delay conditions (see Figure 5.4). Values of the optimal pilot compensation terms, open- and closed-loop parameters are listed in Table 5.3.

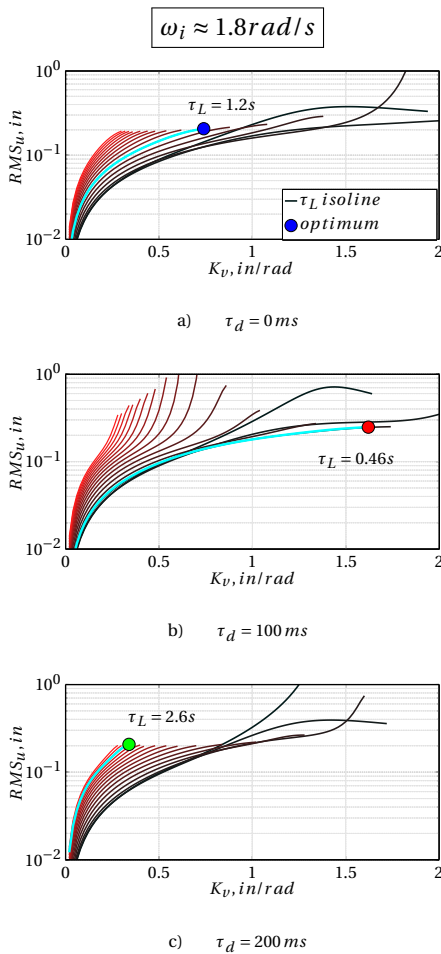


Figure 5.6: Root mean square of pilot control (RMS_u) for forcing function bandwidth $\omega_i \approx 1.8 rad/s$ and discrete PSD and CE configurations of 0, 100 and 200 ms of time delays, without pilot remnant.

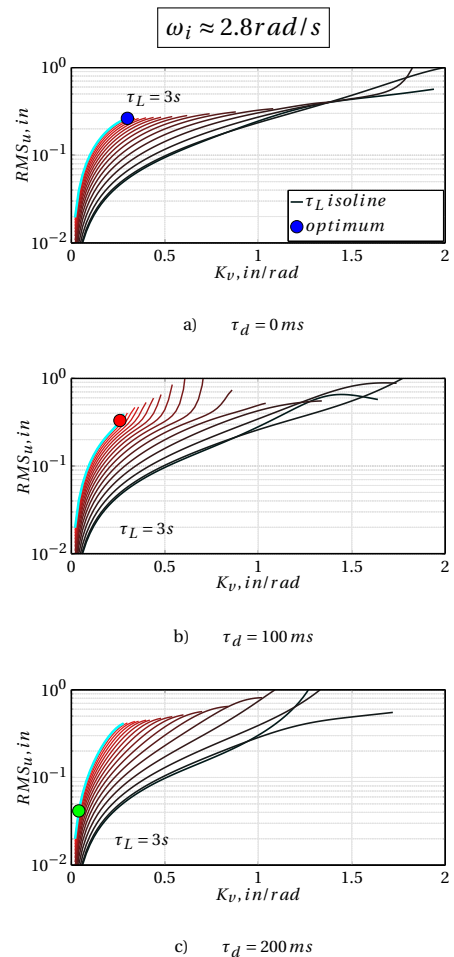


Figure 5.7: Root mean square of pilot control (RMS_u) for forcing function bandwidth $\omega_i \approx 2.8 rad/s$ and discrete PSD and CE configurations of 0, 100 and 200 ms of time delays, without pilot remnant.

RMS_u comparisons in Figures 5.6 and 5.7 show that the optimal performance was achieved for relatively high pilot control activity. Although the simulation framework can calculate any pilot activity, in experiment conditions actual application could depend on the control device characteristics, e.g., required deflections could be hard to expose due to the high forces required to move the manipulator. In the conditions without the remnant, the control activity for the high bandwidth forcing function was higher than the low bandwidth conditions, except 300 ms time delay configurations.

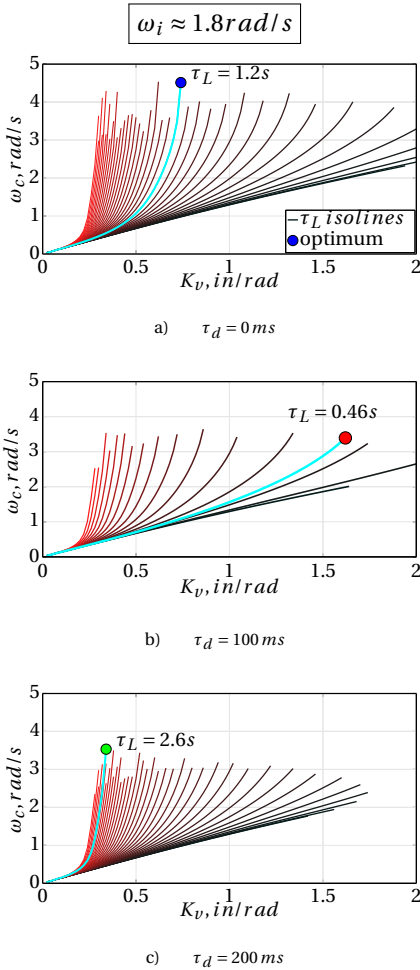


Figure 5.8: Crossover frequency (ω_c) for forcing function bandwidth $\omega_i \approx 1.8$ rad/s and discrete PSD and CE configurations of 0, 100 and 200 ms of time delays, without pilot remnant.

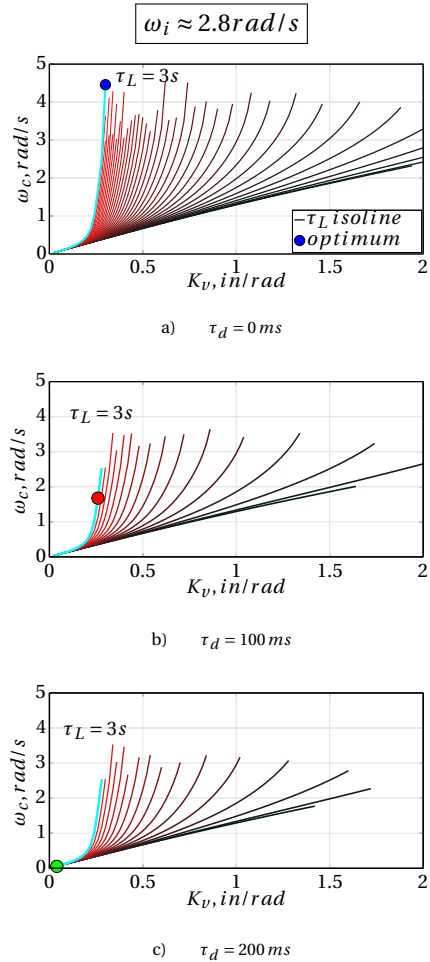


Figure 5.9: Crossover frequency (ω_c) for forcing function bandwidth $\omega_i \approx 2.8$ rad/s and discrete PSD and CE configurations of 0, 100 and 200 ms of time delays, without pilot remnant.

Since ω_c is determined by the open-loop magnitude response, the added time delay in the CE does not affect the shape of the τ_L isolines, as depicted in Figures 5.8 and 5.9. However, pairs of the available pilot equalization parameters (i.e., K_v and τ_L) reduced for increasing time delay, as can be seen by smaller total isoline areas in Figures 5.8 and 5.9. For $\omega_i \approx 1.8 \text{ rad/s}$, crossover frequencies of the optimum are close for all time delay values, and between 3.5 and 4.5 rad/s (see Figure 5.8). However, there is a drastic change in the crossover frequency of the optimum for the high forcing function bandwidth ($\omega_i \approx 2.8 \text{ rad/s}$) with increasing time delay. The main source of this difference is related to whether the frequency of the peak of the closed-loop system coincides with any powered frequencies of the forcing function. This effect, which also appears in phase margin plots in Figures 5.10 and 5.11, will be discussed in the closed-loop PSD comparisons later in this section.

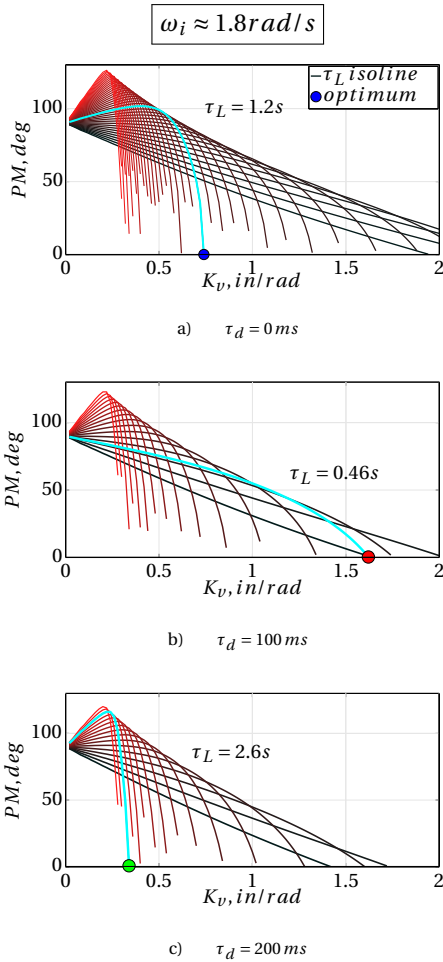


Figure 5.10: Phase margin (PM) for forcing function bandwidth $\omega_i \approx 1.8 \text{ rad/s}$ and discrete PSD and CE configurations of 0, 100 and 200 ms of time delays, without pilot remnant.

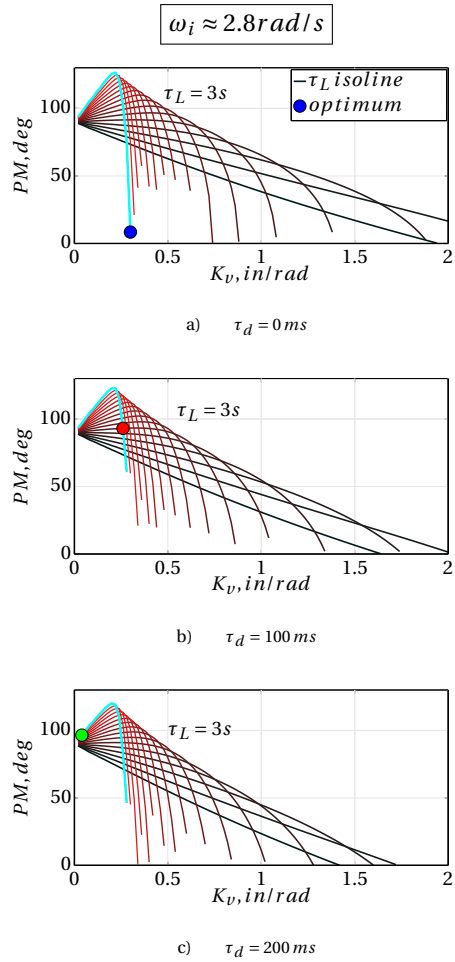


Figure 5.11: Phase margin (PM) for forcing function bandwidth $\omega_i \approx 2.8 \text{ rad/s}$ and discrete PSD and CE configurations of 0, 100 and 200 ms of time delays, without pilot remnant.

Figures 5.10 and 5.11 illustrate that for the settings resulting in optimal tracking performance, the phase margin for the low forcing function bandwidth ($\omega_i \approx 1.8 \text{ rad/s}$) is almost 0 degrees regardless of applied time delay, whereas the high forcing function bandwidth ($\omega_i \approx 2.8 \text{ rad/s}$) shows an increase up to 100 degrees with increasing time delay. Akin to the observed high crossover frequency (see Figure 5.8) with $\omega_i \approx 1.8 \text{ rad/s}$, almost 0 phase margin is actually a result of the closed-loop system response, which are only powered with the frequencies of the discrete forcing function. Thus, any resonance peak of the closed-loop system has no effect on the task error if the resonance peak does not coincide with one of the discrete frequencies of the disturbance forcing function. Hence, the optimum points could avoid these peaks, and they may result in optimum

performance while system stability as at its limits. Figure 5.12 illustrates this situation for the $\omega_i \approx 1.8 \text{ rad/s}$ condition by showing the PSD of error, and corresponding closed-loop error responses of CE with 0, 100 and 200 ms of time delays. Closed-loop transfer function between forcing function to error is given as;

$$H_{e,fd}(j\omega) = \frac{-1}{1 + H_{OL}(j\omega)} \quad (5.2)$$

where;

$$H_{OL}(j\omega) = H_p(j\omega)H_{CE}(j\omega) \quad (5.3)$$

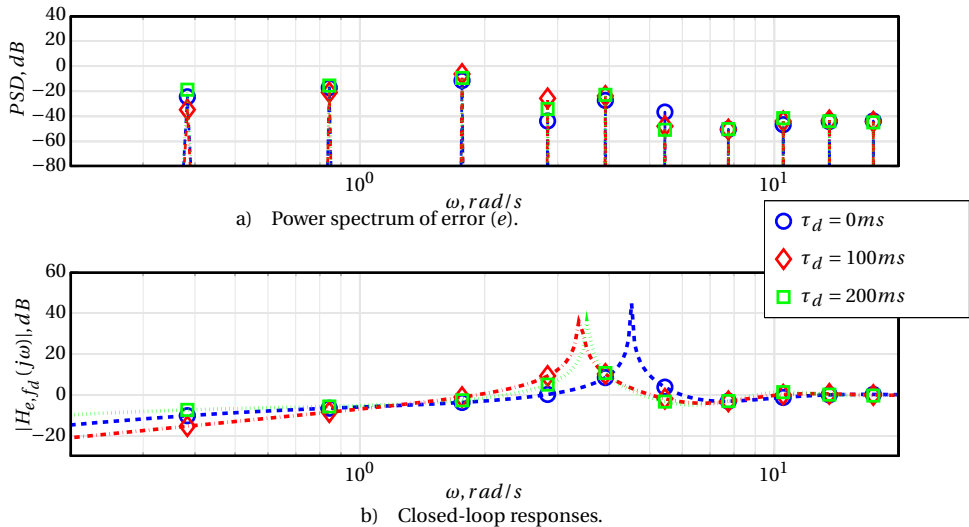


Figure 5.12: PSD of the minimum error (a) and closed-loop response (b), which shows the powered frequencies by markers, and the forcing function bandwidth $\omega_i \approx 1.8 \text{ rad/s}$.

As can be seen from Figure 5.12, PSD of the error(e) only has power at the frequencies of the forcing function, and the spectrum magnitudes depended on the corresponding closed-loop responses at the same frequencies. Since the forcing function was composed of two shelves, the resultant PSD of error was simply scaled by the closed-loop response according to ratios of these two shelves. It is clear from Figure 5.12 that even though there were considerable closed-loop resonance peaks in the response, the effective power spectrum (markers in the figure) just depends on frequencies of the applied forcing function. In this case, the closed-loop peaks were not reflected in the error. Thus, pilot parameters could achieve such values that closed-loop system could reach to instability limit, whereas performance still could be optimal. A slightly different situation is shown for the high bandwidth forcing function conditions in Figure 5.13.

As shown in Figure 5.13, when the forcing function with the high break frequency ($\omega_i \approx 2.8 \text{ rad/s}$) was used in the simulation framework, higher frequencies of the closed-loop response were transmitted into the error. Therefore, the resonance peak of the

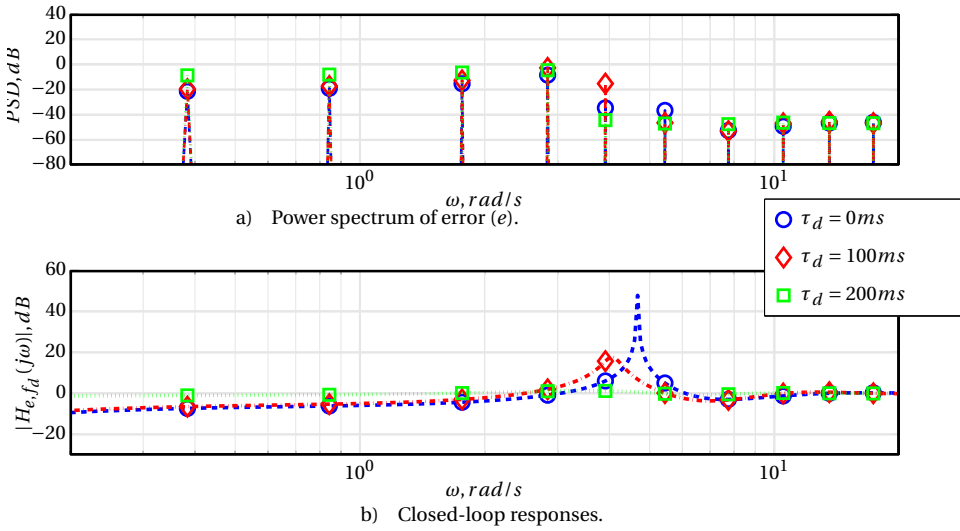


Figure 5.13: PSD of the minimum error (a) and closed-loop response (b), which shows the powered frequencies by markers, and the forcing function bandwidth $\omega_i \approx 2.8rad/s$.

closed-loop system had more effect on the development of the system error. Consequently, system stability could not be sacrificed easily like the case with the forcing function with low bandwidth, because neighbour frequencies towards the resonance peak would be amplified in the system error. When CE with 0 ms time delay condition was used, the closed-loop response was able to position the resonance peak between the powered frequencies, whereas 100 and 200 ms conditions could not manage to achieve the same. In return, a drastic drop of crossover frequencies, and considerably higher phase margins were obtained. It must be also noted that for the high break frequency and high time delay conditions, the closed-loop system could only provide limited options for pilot parameters to achieve the optimum performance (see Figure 5.5), such that on 200 ms time delay condition, almost all pilot equalization term combinations (K_v and τ_L) amplify the error ($\sigma_e^2/\sigma_i^2 \geq 1$).

As a summary, calculated parameters for the optimum performance points for both bandwidths of forcing function with discrete PSD, and 0, 100 and 200 ms of added time delay in CE are listed in Table 5.3.

When time delay increases in the CE, the phase of the CE drops in lower frequencies. Consequently, the phase crossover frequencies of the open-loop system decreases. Therefore, the closed-loop resonance peaks shift to lower frequencies. Thus, with the application of the high forcing function bandwidth, the peaks become more effective with increasing time delay. As a result, the pilot model should contain very high lead generation to shift the phase crossover frequencies to higher values in order to reduce the amplification of the closed-loop resonance with high bandwidth forcing function. It

Table 5.3: Parameters of optimum points for forcing function bandwidths $\omega_i \approx 1.8$ and 2.8 rad/s, and CE with 0, 100 and 200 ms time delays, while pilot model excludes remnant (n).

Parameter		$\omega_i \approx 1.8 \text{ rad/s}$			$\omega_i \approx 2.8 \text{ rad/s}$		
		τ_d 0 ms	τ_d 100 ms	τ_d 200 ms	τ_d 0 ms	τ_d 100 ms	τ_d 200 ms
σ_e^2/σ_i^2	-	0.29	0.39	0.39	0.42	0.74	0.99
K_v	in/rad	0.74	1.62	0.34	0.3	0.26	0.04
τ_L	s	1.2	0.46	2.6	3	3	3
RMS_u	in	0.21	0.25	0.21	0.30	0.38	0.05
ω_c	rad/s	4.51	3.39	3.53	4.46	1.67	0.05
PM	deg	0.08	0.37	0.72	8.48	93.11	96.54

can be seen in Table 5.3 that the lead time constant (τ_L) reached to three seconds, which is the upper boundary during the simulation analysis, for optimums of all values of time delay, with high forcing function bandwidth ($\omega_i \approx 2.8$ rad/s).

5

Crossover regression

In order to investigate the crossover regression tendencies, crossover frequencies of optimum performance points for CEs with 0, 100 and 200 ms of added time delay within a task excited by forcing functions with discrete PSD with two bandwidths are plotted in Figure 5.14.

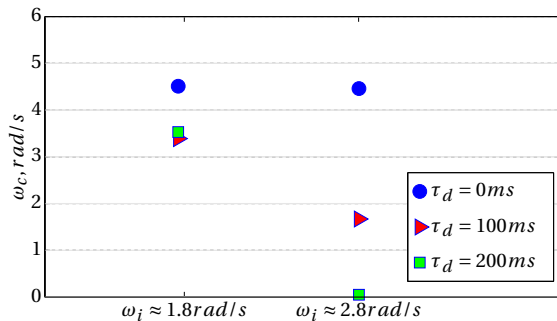


Figure 5.14: Crossover frequencies of open-loop systems with optimum performance pilot models and CEs with 0, 100 and 200 ms of time delays, when subjected to forcing function with discrete PSD with bandwidths of 1.8 and 2.8 rad/s.

Figure 5.14 shows that a crossover regression tendency is observed especially for the high bandwidth ($\omega_i \approx 2.8$ rad/s), when time delay of the CE is increased to 100 ms. For the low bandwidth, it must be noted that crossover frequencies were able to achieve high values while threatening closed-loop system stability up to its limits, when the forcing function with discrete PSD was utilized for $\omega_i \approx 1.8$ rad/s. It must be noted that in experiment conditions, it is unlikely for human operators to aim for such low phase margins

(i.e., high crossover frequencies in the simulation framework conditions for this configuration) due to the stability concerns. Besides, this simulation framework aimed for the numerically optimum performance obtained by pilot equalization term pairs.

5.3.2. DISCRETE PSD AND PILOT MODEL WITH REMNANT

In this section, the pilot remnant (n) was added to the pilot model output, and the same forcing function from the previous section was utilized (i.e., with the discrete PSD). As described in Section 5.2, the remnant model was modelled as white noise with a second order low-pass filter, and the remnant filter gain was adjusted to attain a remnant power of 10% of the total pilot control (u) power for each available active pilot parameter pair (K_v and τ_L) for all time delay configurations of the CE. Akin to the no remnant case (Section 5.3.1), isolines of available normalized error variance are plotted in Figures 5.15 and 5.16, and equalization parameters that result in the minimum error (i.e., optimum points) are marked. When compared with the case without remnant (Figures 5.4 and 5.5), higher errors were achieved, especially for the low bandwidth ($\omega_i \approx 1.8$ rad/s) forcing function. The similar trend of increasing error with bandwidth was also clear, with the condition including pilot remnant.

Pilot remnant introduces a new input signal to the PVS (i.e., a new contributor to error signal). The closed-loop transfer function, which relates the pilot remnant (n) to the error(e), is given in Equation (5.4) as:

$$H_{e,n}(j\omega) = \frac{-H_{CE}}{1 + H_{OL}(j\omega)} \quad (5.4)$$

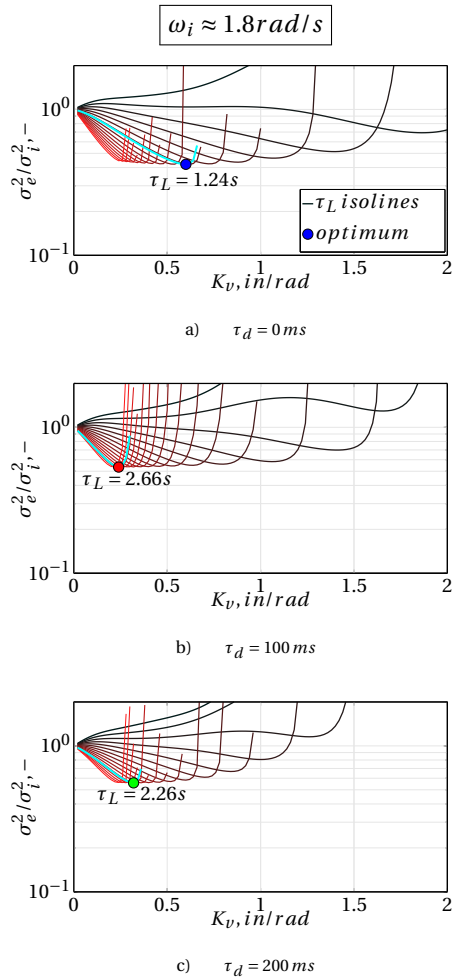


Figure 5.15: Normalized error variance for forcing function bandwidth $\omega_i \approx 1.8 \text{ rad/s}$ and discrete PSD and CE configurations of 0, 100 and 200 ms of time delays, with pilot remnant.

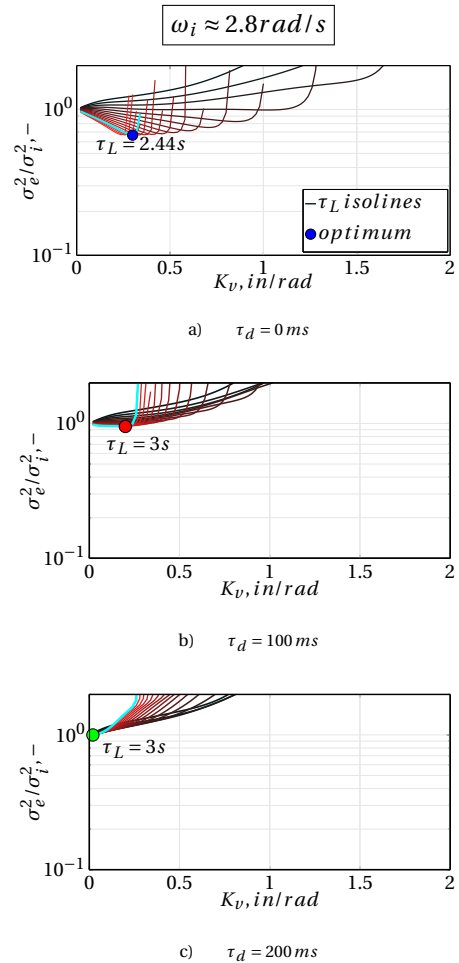


Figure 5.16: Normalized error variance for forcing function bandwidth $\omega_i \approx 2.8 \text{ rad/s}$ and discrete PSD and CE configurations of 0, 100 and 200 ms of time delays, with pilot remnant.

$H_{e,n}(j\omega)$ and $H_{e,f_d}(j\omega)$, Equations (5.4) for n and (5.2) for f_d , respectively, together compose the closed-loop error. Figure 5.17 shows magnitude responses of the closed-loop forcing functions and the PSD of the error of the optimum points for 0, 100 and 200 ms of time delays for the forcing function bandwidth $\omega_i \approx 1.8 \text{ rad/s}$.

Since the remnant was modelled as a second-order low-pass filter on a Gaussian white noise signal, the contribution of remnant to the error has power on each frequency. This remnant signal contained lower magnitudes than the contribution of the forcing function (see Figure 5.17-b). When comparing the PSD of the error without and with the remnant (Figures 5.12-a and 5.17-a, respectively), the major effect of the remnant is the

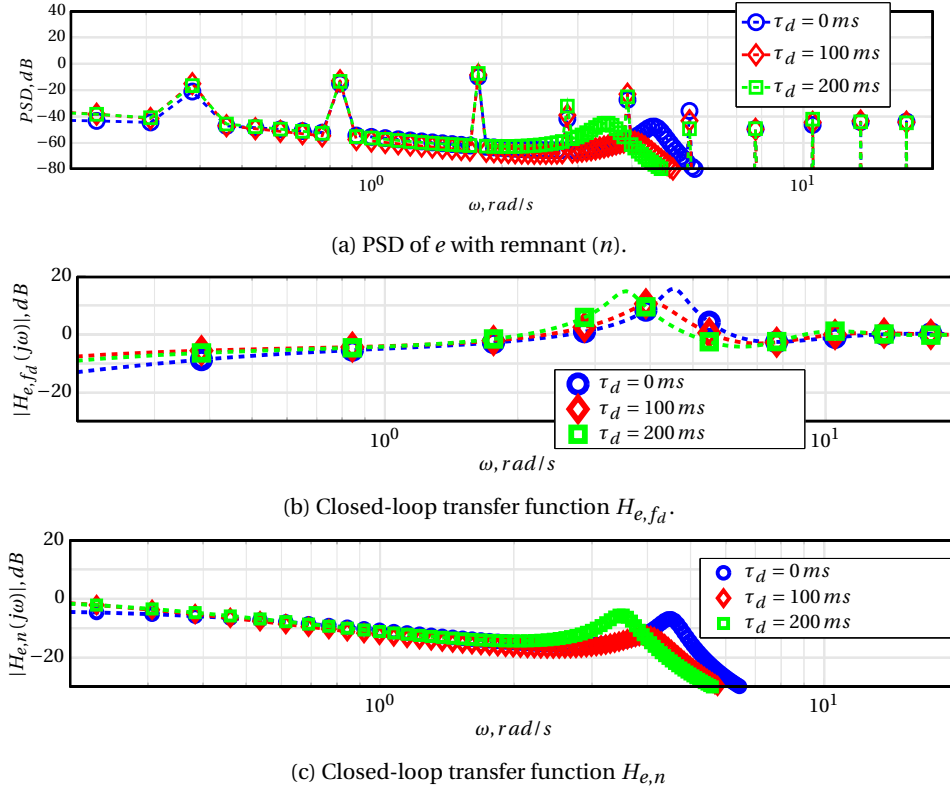


Figure 5.17: PSD of the error (a), and the closed-loop response (b and c) of the optimal performance points for 0, 100 and 200 ms of time delays, with $\omega_i \approx 1.8 \text{ rad/s}$. Markers indicate the frequencies with power and dashed lines indicate the closed-loop response.

amplification of power around the closed-loop system resonance peaks. As a result, the closed-loop systems of the optimum points cannot expose large resonance peaks like the ones for the no remnant configurations. This difference can be observed by comparing the dashed lines in Figure 5.12-b with Figure 5.17-b.

Table 5.4 summarizes the parameter values of the optimum points in the simulation framework with discrete PSD forcing function, CE with 0, 100 and 200 ms of added time delays, and the pilot model with remnant.

Table 5.4 shows that errors of the optimum points increase with increased time delay, regardless of forcing function bandwidth. The pilot visual gain shows a drastic decrease with increasing time delays for the low bandwidth forcing function condition, for the 0 and 100 ms conditions. For the low bandwidth forcing function, the lead time constant rapidly increases with the addition of time delay for the 100 ms case, and keeps around the same value for the 200 ms condition. However, the same change could not be observed with the high bandwidth forcing function, simply due to already severely

Table 5.4: Parameters of optimum points for forcing function bandwidths $\omega_i \approx 1.8$ and 2.8 rad/s, and CE with 0, 100 and 200 ms time delays, while pilot model includes remnant (n).

Parameter		$\omega_i \approx 1.8 \text{ rad/s}$			$\omega_i \approx 2.8 \text{ rad/s}$		
		τ_d 0 ms	τ_d 100 ms	τ_d 200 ms	τ_d 0 ms	τ_d 100 ms	τ_d 200 ms
σ_e^2/σ_i^2	-	0.42	0.53	0.56	0.67	0.95	1.00
K_v	in/rad	0.6	0.24	0.32	0.3	0.20	0.02
τ_L	s	1.24	2.66	2.26	2.44	3	3
RMS_u	in	0.23	0.17	0.2	0.29	0.26	0.02
ω_c	rad/s	1.89	0.63	1.2	1.25	0.46	0.03
PM	deg	82.84	120	97	111.91	122.8	93.27

limited available error compensation parameter pairs for delayed configurations (see Figure 5.16). Pilot control activity does not show major deviations, except the 200 ms condition for the high bandwidth forcing function. Phase margins also stay in the interval of 82 to 122 degrees, for both forcing function bandwidths, which show that optimal performance points had a higher stability than the ones with the no remnant conditions (e.g., PM was almost 0 degrees for the low bandwidth forcing function cases as given in Table 5.3).

Crossover regression

When the pilot model contains remnant, the crossover frequencies of the optimum points with the CEs including 0, 100 and 200 ms of added time delays are shown in Figure 5.18.

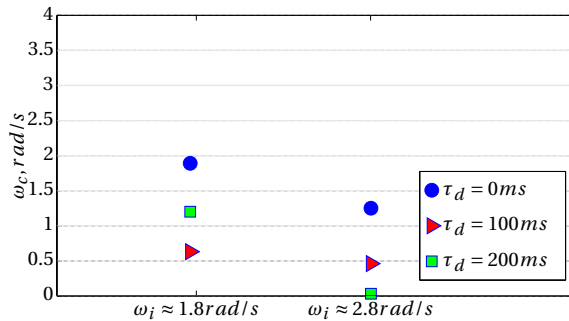


Figure 5.18: Crossover frequencies of open-loop systems with optimum performance pilot models with remnant and CEs with 0, 100 and 200 ms of time delays, when subjected to forcing function with discrete PSD with bandwidths of 1.8 and 2.8 rad/s.

As depicted in Figure 5.18, the configurations without time delay show a crossover regression tendency when forcing function is increased to $\omega_i \approx 2.8$ rad/s. This behaviour is similar to 'classical' crossover regression considerations. In addition, when 100 ms of time delay was introduced, further regression was noticed due to the additional time

delay, in both forcing function bandwidth conditions. However, for the low bandwidth configuration, 200 ms of added time delay resulted in a higher crossover frequency than the condition with 100 ms added time delay. When normalized error graphs of both conditions are compared (Figure 5.15-b and -c), optimum of the 200 ms of added time delay could be with a lower pilot visual gain and higher lead time constant if a higher parameter variation resolution (i.e., smaller than 0.02) could have been used. Thus, it could be possible that the resultant crossover frequency would then also be lower than 100 ms case. Nevertheless, a crossover regression tendency due to forcing function bandwidth and added time delay was observed for this configuration.

5.3.3. COMPREHENSIVE RESULTS

By using the values in Tables 5.3 and 5.4, and simulation framework results gathered from the analyses performed with a continuous PSD, the variation of resultant parameters (i.e., dependent measures) are depicted in Figure 5.19 for comparison purposes.

Figure 5.19 shows the complete overview of the results of the simulation framework which was carried out by using optimum performance points. Table 5.5 summarizes these results.

Table 5.5: General trends of parameter variation when time delay and task bandwidth are increased.

Increasing time delay:	Increasing task bandwidth:
<ul style="list-style-type: none"> • Mainly reduced pilot visual gains. • Mainly increased lead time constant in both bandwidths of forcing function. • Increased errors. • Slightly reduced control activity ($RMS(u)$) for low bandwidth case but drastic decrease for high bandwidth case. • Mainly increased phase margins. • Mainly reduced crossover frequencies. 	<ul style="list-style-type: none"> • Mainly reduced pilot visual gains. • Slightly increased lead time constants. • Increased errors. • Slightly reduced control activity ($RMS(u)$) for low bandwidth case but drastic decrease for high bandwidth case. • Slightly increased phase margins. • Mainly reduced crossover frequencies.

Overall, the major parameter variation (see Table 5.5) when time delay or task bandwidth were increased showed similar trends in all simulation cases. Eventually, increased task bandwidth (i.e., harder tasks) require higher pilot workload. Depending on the

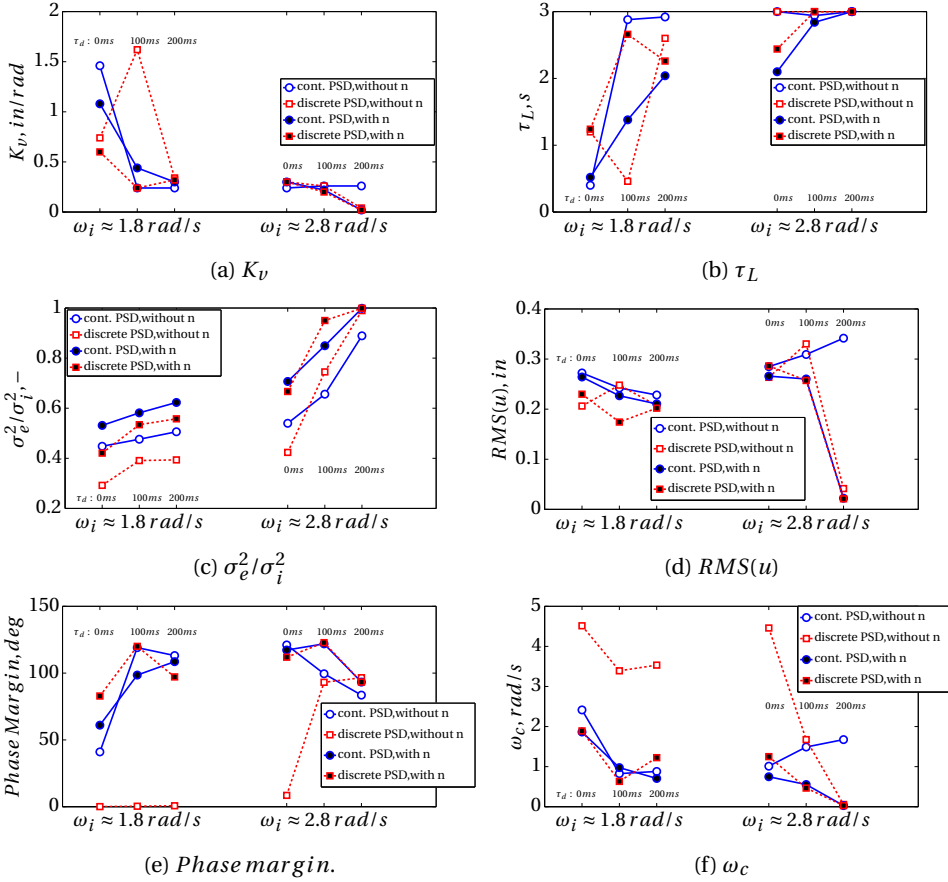


Figure 5.19: PVS parameters for the optimum performance points, for forcing functions with discrete and continuous PSDs and two bandwidths, CE with various time delays, and pilot model with or without the remnant.

controlled element, the pilot may prefer to 'back off', as in the definition of classical crossover regression. Similarly, pilot may need to back off if any added time delay threatens the system stability considerably. Therefore, a similar parameter variation trend in Table 5.5 indicates that there could be a crossover regression due to added time delay, as well as the classical regression due to forcing function bandwidth (i.e., task difficulty).

5.3.4. COMPARISON TO EXPERIMENT CONDITIONS

Since the forcing function is the element that defines the task in this simulation framework, the PSD distribution is a key variable, accompanying the bandwidth of the forcing function. Accompanying the discussion in section 5.3.1, in an offline simulation study, simulating a discrete PSD without pilot remnant has a drawback of finding the optimum performance with almost no stability margin, which does not match with the trends in

other configurations (see Figure 5.19). The explanation for this is the possibility of aligning the closed-loop resonance peak between powered frequencies, as described in Section 5.3.1. It can be seen from Figure 5.19 that adding pilot remnant reduced that effect, hence, discrete and continuous PSD with and without pilot remnant conditions show similar parameter variation trends.

It is worth mentioning that the optimum performance pilot settings, which were calculated in the simulation framework, may not in fact be achieved in experiment conditions. One of the reason is that the lowest task error can be achieved with a large set of possible pilot equalization terms (e.g., the flat isolines in normalized error variance figures). Therefore, a real human operator could prefer to achieve almost the same performance with a control behaviour that is in fact different from the 'numerically' optimal settings. In order to check this hypothesis, the simulation framework was prepared such that for each time delay condition, the pilot limitation terms and remnant power ratio were set according to the measured pilot specific values. For example, Figure 5.20 shows the PSD of error with calculated optimum, experiment and simulation framework results with the usage of pilot limitation parameters gathered from experiment.

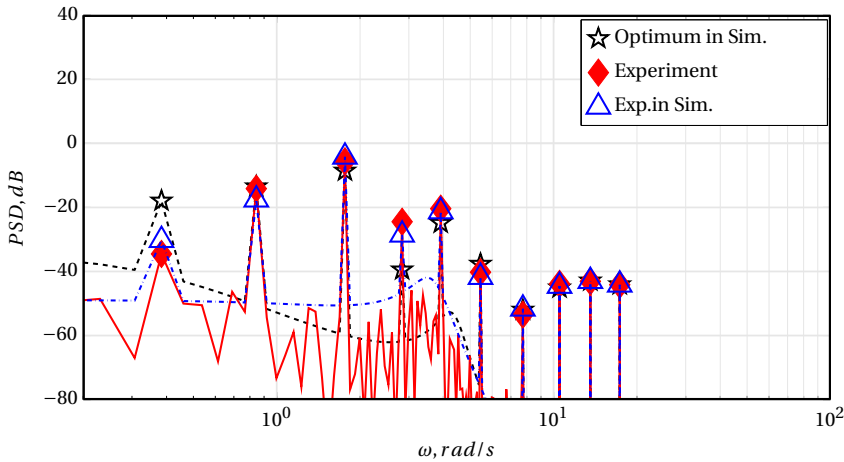


Figure 5.20: PSD of the error (e) calculated in the simulation frame for the optimal performance, measured from the preliminary identification experiment, and calculated in the simulation framework by using the experiment parameters.

Figure 5.20 illustrates that the optimal performance points calculated by the simulation framework (star markers in the figure) do not represent what actually happened in the sample experiment (diamond markers), which was taken from the preliminary identification experiments. There is a clear difference at the lowest frequency with power and, around 3 rad/s. In order to observe the validity of the simulation framework, measured experiment values were fed in to the simulation framework (triangular markers),

and it is resulted in very close representation of the measured response. This illustrates that, the simulation framework has potential to be used to analyse: 'What was the optimum during a sample experiment run with a human operator, and did he/she achieve the optimum performance?'

In addition to Figure 5.20 that showed a difference in the PSD of errors obtained from measurement data and the calculated optimal performance, Figure 5.21 shows the error isolines accompanying conditions in Figure 5.20.

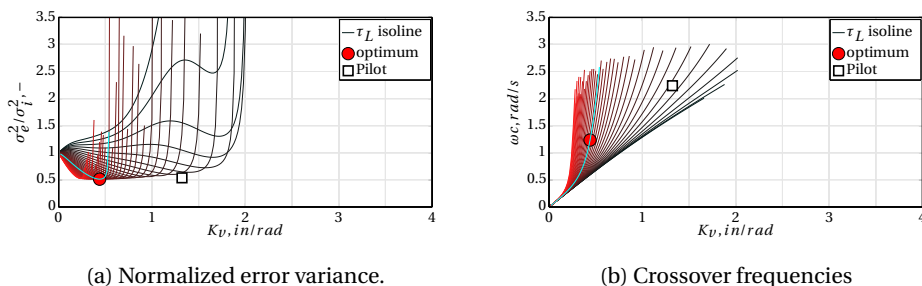


Figure 5.21: Normalized error variance and crossover frequency isolines adjusted by measured pilot data.

Figure 5.21 exemplifies for one of the pilots from the second experiment that he did not show the characteristics of the optimum. Instead, he exhibited a higher error, but also a higher crossover frequency. This example illustrates that pilots would not strictly aim for the optimum performance, but probably a more convenient strategy that they exhibit to attain system stability while considering the experiment conditions.

5.4. CONCLUSIONS

To investigate the crossover regression tendencies of a PVS subjected to various task difficulties and added time delay in the CE, a simulation framework was developed. The simulation framework contained a pilot model, and a CE in a compensatory task, based on the design of the MCIM, as described in Chapter 3. In the pilot model, all pilot limitation parameters (i.e., the pilot delay and neuromuscular system parameters) were kept constant based on the values measured in the preliminary identification experiment, as described in the previous chapter. Both pilot equalization parameters (K_v and τ_L) were varied in the simulation framework. If available, the pilot remnant was added to the pilot control signal with 10% of the pilot control signal power.

Task difficulty was varied by altering the bandwidth of the forcing function. Two bandwidth values were chosen to represent task difficulty while the higher bandwidth being the hardest task, and *visa versa*.

It was observed that an additional time delay caused pilot compensation similar to that found in preliminary identification experiments, such that reduced gains and higher leads provided the optimum performance points. Adding remnant to the pilot control

signal significantly changed the optimum points for the forcing function with discrete PSD. Classical crossover regression due to the task difficulty was observed, and additional regression due to the added time delay was apparent around 100 ms. Thus, by using crossover regression and accompanying system parameters, the simulation framework highlighted the HQ of the rotorcraft model would be limited around 100 ms for low bandwidth tasks, whereas the hard task already imposes regression without any added time delay.

Although the simulation framework aimed to cover a broad range of conditions, in experiment settings, the results would also depend on several other factors, primarily the perception and control strategy of the pilot. Therefore, it is planned to conduct a set of pilot model identification experiments as a following step to this simulation framework. The next chapter will describe the identification experiment which was designed, executed and analysed by the MCIM principles, and will discuss results of the adaptation of identified manual control behaviour when exposed to added time delay and varied task difficulty.

6

MANUAL CONTROL IDENTIFICATION METHOD (MCIM) EXPERIMENT

In the previous chapter, a simulation study was carried out in order to investigate the effects of task difficulty and the added time delay on pilot control behaviour, particularly resulting in the optimal task performance (i.e., the minimum tracking error). Although promising results were obtained during the simulation study (e.g., signatures of crossover regressions), it was also demonstrated that human operators were not able to attain the 'best' performance. While aiming for the optimal task performance, the simulation study required very high values of the lead compensation (i.e., very high pilot workload) which would not be preferred by the human operators during a demanding task. Instead, human operators have preferred slightly higher task errors with significantly lower lead time constant values. This difference between the simulated manual control and the identified human operator response is a good example of the drawback of some HQ criteria with 'paper' pilot models with restrictions and limitations, as discussed in Chapter 2. Therefore, it was concluded that the simulation study would not be representative of the control strategy choice of human operators in such demanding tasks.

This chapter continues with the complete application of the MCIM by conducting a human-in-the-loop experiment to identify the manual control behaviour. In this experiment, participants are exposed to nine different combinations of added time delay and task difficulty in a disturbance-rejection task in pitch-axis (both varied at three levels). There were nine configurations which were combinations of three levels of task difficulty and three levels of added time delay. Akin to the simulation study, task difficulty was varied by increasing the bandwidth of the disturbance forcing function, and the time delay was implemented as a transport delay in the CE. The experiment was conducted in the SRS at TU Delft with nine participants. As a part of the MCIM, frequency and time domain identifi-

ation methods are used to identify the parameters of the manual control behaviour from the measurement data. Changes of the identified parameters, task performance measures, open-loop crossover frequencies and phase margins are investigated for all task configurations. Corresponding RPC tendencies are elaborated by the detections tools in the MCIM.

6.1. INTRODUCTION

In the previous chapter, a computer simulation framework was used to investigate manual control behaviour that could result in the best task performance (i.e., minimum tracking error) when task difficulty and added time delay were varied. The simulation framework had two varying pilot equalization parameters (i.e., the pilot visual gain K_v and the lead time constant τ_L) to achieve the optimal task performance per each configuration. Particularly, crossover regression tendencies were examined for varied task difficulty and added time delay conditions, and results were discussed in the previous chapter.

Eventually, it is hypothesised that human operators can exhibit different control strategies than the computer simulation which was specifically utilized to achieve the optimal task performance in a simulated task. In this chapter, the experimental approach of MCIM is followed to investigate the manual control behaviour when participants were exposed to combinations of task difficulty and added time delay in the CE, as discussed in the MCIM development in Chapter 3. As a result, measured manual control behaviour will be identified for varied task configurations, and HQ deviations and adapted control strategy to avoid RPC occurrences will be investigated.

6

6.2. TASK DESIGN

This section describes the design of the conducted experiment, which is one of the fundamental elements of the MCIM. Section 6.2.1 defines the pitch control task in the experiment. Section 6.2.2 explains the CE (i.e., the rotorcraft model) in the disturbance-rejection task. Section 6.2.3 provides information about the participants and the apparatus used in the experiment. Finally, Section 6.2.4 describes the manual control behaviour model to be identified by using the measurement data.

6.2.1. PITCH CONTROL TASK

Similar to the second preliminary experiment and the simulation framework (Chapters 4 and 5, respectively), this experiment was conducted by using a disturbance-rejection task in the pitch-axis as described by the MCIM in Chapter 3.

As a part of the MCIM, three task difficulty levels were used in the final experiment: ET, MT and HT. These task difficulties are defined by the forcing function bandwidth values of $\omega_i \approx 0.8, 1.8$ and 2.8 rad/s, respectively, as summarized in Table 6.1.

Table 6.1: Task difficulty definitions.

Forcing Function Bandwidth (ω_i , rad/s)	Task Difficulty Abbreviation
0.84	ET : Easy Task
1.76	MT : Moderate Task
2.84	HT : Hard Task

6.2.2. ROTORCRAFT MODEL

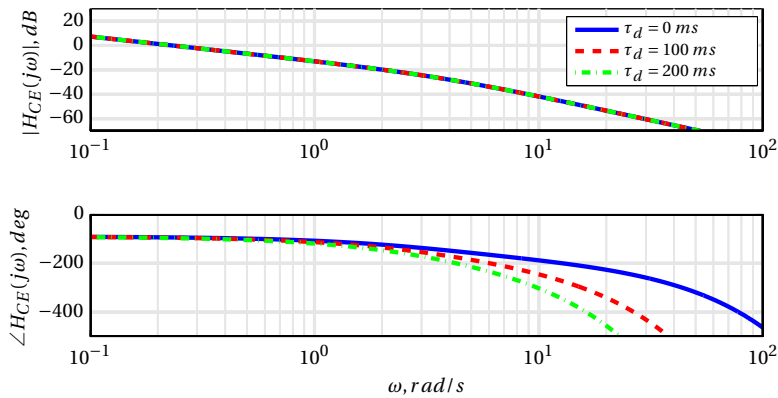
In this experiment, a pitch-axis rotorcraft model was used, as described in the MCIM. Similar to the simulation study, the CE is a single-to-double integrator form with an inherent delay representing the rotor dynamics, as discussed in Chapter 3. Parameter values of the CE model of a Bo-105 helicopter in hover¹¹¹, and the transfer function of the CE is given as:

$$\frac{\theta}{\delta_{lon}}(j\omega) = \underbrace{\frac{M_{\delta_{lon}}}{(j\omega)(j\omega + M_q)} e^{-\tau_s(j\omega)}}_{\text{Baseline CE}} \underbrace{e^{-\tau_d(j\omega)}}_{\text{Additional time delay}} \quad (6.1)$$

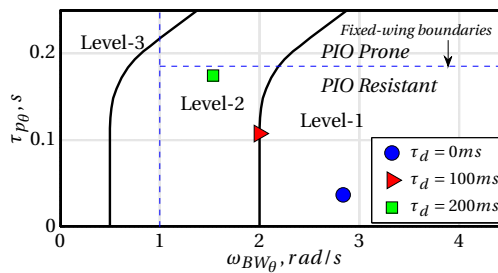
where the control authority term (i.e., longitudinal cyclic control derivative) $M_{\delta_{lon}} = 0.8693 \text{ rad}/(\text{in.}\cdot\text{s}^2)$, the aerodynamic pitch damping $M_q = -3.74 \text{ s}^{-1}$, and the inherent delay accounting for the rotor model $\tau_s = 50 \text{ ms}$. Three levels of added time delays (τ_d) were used in the experiment to consider different levels of HQ : 0, 100 and 200 ms. These added time delay values were also used in the second preliminary identification experiment (Chapter 4) and the simulation framework (Chapter 5). Bode plots of CEs with different levels of added time delay are depicted in Figure 6.1. As discussed in Chapter 3, BPD is used to assess the HQ of the CE as shown Figure 6.1.

As it can be seen from Figure 6.1, increasing added time delay results in more phase lag, while magnitude responses do not change. Corresponding BPD shows the degradation of the HQ (i.e., from Level-1 to Level-2) with increased time delay. As discussed in Chapter 2, the BPD criterion does not account for the task difficulty. In addition, PIO boundaries of fixed-wing aircraft are superimposed on the BPD chart with dashed lines for only comparison reasons. According to the fixed-wing boundaries, all added time delay conditions were predicted to be PIO resistant.

It can be noted that CEs of the simulation framework and this experiment were not exactly identical. First, the aerodynamic pitch damping of the CE was set to the Bo-105 helicopter value ($M_q = -3.74 \text{ s}^{-1}$)¹¹¹ in the experiment, whereas the simulation study used a generic high bandwidth value ($M_q = -3 \text{ s}^{-1}$). In addition, the gearing ($M_{\delta_{lon}}$) between the pilot longitudinal cyclic input to the pitch acceleration was defined by the characteristics of the cyclic in the SRS, accompanying the experiment set-up, whereas the simulation study used the value from the preliminary experiments conducted in HHS. Finally, the CE in the experiment included an inherent delay (50ms), represent-



(a) Bode plot of CEs.



(b) BPD criterion of CEs.

Figure 6.1: Bode diagram (a) and bandwidth phase delay criterion (b) of CEs with 0, 100 and 200 ms of added time delay.

ing the simplified effect of rotor dynamics whereas the simulation study was carried out by assuming a model without this delay term, as in the preliminary identification experiments.

Despite the listed differences, the overall CE responses have highly similar characteristics. Since the experiment was designed to investigate the effect of the time delay, the inherent delay in the CE of the experiment and the added time delay can simply be added together. Thus, the methods and interpretations are very similar for the two CEs of the simulation study and the experiment. Moreover, these two CEs possess the same HQ levels (see Figures 4.13 and 6.1b).

6.2.3. APPARATUS AND PARTICIPANTS

APPARATUS

The experiment was conducted in the SRS at TU Delft without physical motion. As it was shown in Chapter 4, a scaled-up attitude indicator was used as a compensatory dis-

play to indicate the pitch tracking error. The control inceptor was a central cyclic stick (Moog FCS[®]) with a control loading system which is particularly designed for rotorcraft simulations. Akin to the preliminary identification experiments (Chapter 4), during this simulator experiment, the breakout force and friction settings of the manipulator were disabled in order to keep the linearity in the control path. Participants could only control the pitch-axis of the cyclic during the experiment, and other axes were locked. The force gradient of the control loading system was set to 0.77 pound/inch in order to provide sufficient feel of a realistic central cyclic in longitudinal axis. This force gradient value corresponds to Level-1 in ADS-33 Handling Qualities specifications for allowable control force gradients in pitch-axis⁶.

PARTICIPANTS

The experiment was performed by nine participants, who were all Delft University of Technology students or staff members. All participants had prior experience with similar human-in-the-loop experiments with manual control tasks. Eight of the participants were male and one of the participants was female. Their ages ranged from 23 to 44 years, with an average age of 28.4 years. Three participants had pilot licences for single engine aircraft, and one participant was an active helicopter pilot.

6.2.4. PILOT MODEL

As described in Chapter 3, MCIM utilizes a simplified version of the precision pilot model. The same model was used for the identification of the manual control behaviour in preliminary experiments (Chapter 4), and the simulation framework (Chapter 5). In summary, the pilot visual gain (K_v) and the lead time constant (τ_L) parameters are the pilot equalization term, and the pilot delay (τ_p), the neuromuscular frequency (ω_{nms}) and the damping (ζ_{nms}) are the pilot limitation terms (see Equation 3.10). These parameters will be identified by using the measurement data gathered from the experiment, and their changes with varying experiment conditions will be discussed in this chapter.

6.3. INDEPENDENT VARIABLES

This experiment aimed to investigate the effects of task difficulty and the added time delay on the manual control behaviour. Hence, there were two independent variables in this experiment. First, three levels of time delay (i.e., 0, 100 and 200 ms) were added to the CE model, like in the second identification experiment (Chapter 4) and the simulation framework (Chapter 5). Second, the task difficulty was varied by changing the forcing function bandwidth, as described in Section 6.2.1. Thus, combinations of these two independent variables resulted in nine conditions in total, as given in Table 6.2.

Table 6.2: Experiment conditions.

Experiment Condition	Forcing Function Bandwidth	Added Time delay (ms)
1	ET ($\omega_i \approx 0.8$ rad/s)	0
2	ET	100
3	ET	200
4	MT ($\omega_i \approx 1.8$ rad/s)	0
5	MT	100
6	MT	200
7	HT ($\omega_i \approx 2.8$ rad/s)	0
8	HT	100
9	HT	200

6.4. EXPERIMENT PROCEDURES

Prior to the experiment, all participants were briefed about the objective of the experiment and the task (i.e., minimizing the displayed pitch error by using the longitudinal cyclic input). Details of the CE or task difficulty settings were not conveyed to the participants, to sustain compensatory control behaviour without pre-assigned, or biased control strategies.

Akin to the preliminary experiments (Chapter 4), the final experiment was designed by considering the application of an ANOVA. Therefore, the experiment execution order was designed as a Latin square sequence as listed in Table 6.3.

Table 6.3: Latin square experiment design.

Participants	Experiment Conditions								
I	8	1	2	6	9	4	5	7	3
II	7	9	1	5	8	3	4	6	2
II	2	4	5	9	3	7	8	1	6
IV	4	6	7	2	5	9	1	3	8
V	3	5	6	1	4	8	9	2	7
VI	5	7	8	3	6	1	2	4	9
VII	9	2	3	7	1	5	6	8	4
VIII	1	3	4	8	2	6	7	9	5
IX	6	8	9	4	7	2	3	5	1

As described in Chapter 3, there were two phases of the identification experiment. The familiarization phase consisted of two repetitions of each condition in Table 6.3. During this phase, each participant experienced all available conditions with increasing

difficulty, and they got familiarized with the task and the simulator environment, e.g., cyclic forces and the display. No data were recorded in this phase, and no performance measures were used as feedback to participants. The second experiment phase was the training and measurement phase, during which each participant repeated the condition assigned according to the Latin square designed experiment matrix, as shown in Table 6.3. Participants were not informed about the applied condition. They repeated each condition until they got steady scores for that condition, as described in Chapter 3.

During the training phase, all participants aimed to achieve their best performance (i.e., the highest score) for the configuration at hand. After achieving steady scores, four or five runs were recorded as the measurement data, which reflect the preferred control strategy of participants for the applied configuration. After completing each configuration, which approximately lasted 10 to 12 repetitions, a small break was provided in order to avoid fatigue. Furthermore, after two configurations, a longer break was given for each participant. The total execution of the experiment per participant was approximately six hours including all breaks.

6.5. DEPENDENT MEASURES

As described in Chapter 3, during the experiment, the pitch attitude of the CE, the displayed error, and the pilot control input were recorded. By using these measured data, several dependent measures were calculated. Similar to the preliminary identification experiments (see Section 4.2.4 and Section 4.3.4 in Chapter 4), the variances of the displayed error and the control input were interpreted as indications of the task performance and the control activity, respectively. Second, by using the identification methods, which were described in Chapter 3, parameters of the manual control behaviour were identified, and the manual control behaviour adaptation to varied experiment conditions were discussed.

In terms of PVS analysis, open-loop crossover frequencies and phase margins were calculated. Consequently, tendencies of crossover regression strategies were investigated. In addition, as a part of the MCIM, ROVER and PAC were utilized for RPC detection, by using the time traces of the pilot control input and the vehicle responses recorded for all conditions of the experiment.

6.6. HYPOTHESIS

This experimental approach is an extension of the preliminary identification experiments (Chapter 4) and the simulation study (Chapter 5). In summary, these chapters investigated the manual control behaviour and PVS characteristics with varied added time delay and forcing function bandwidth. Considering the findings of these chapters, a primary hypothesis can be formulated as ‘manual control behaviour of participants will show crossover regression tendencies because of individual and combined effects of the task difficulty and the added time delay’. Furthermore, HQ variation of the vehicle, as well the RPC tendency, can also be related to these crossover regression occurrences. As discussed in Chapter 2, it was proposed in MCIM that the crossover regression is an

indication of a ‘back-off’ control strategy, which ultimately aims to avoid any instability in the PVS.

6.7. METHODS USED FOR ANALYSING THE EXPERIMENT DATA

This section provides information about the identification methods, statistical tools, and RPC detection criteria that were used in the analysis of this experiment. Section 6.7.1 describes the application of identification techniques. Section 6.7.2 describes the ANOVA assumptions to be used while analysing statistical data. Section 6.7.3 provides information about the methods of RPC detection, and their settings.

6.7.1. IDENTIFICATION METHODS

In order to identify the manual control behaviour, two LTI identification methods were used as a part of the MCIM: the frequency-domain FCMwO and the time-domain MLE. Details of these methods were provided in Chapter 3. In summary, FCMwO method computes the Fourier coefficients in the data measured between displayed error (e), and the manual control input (u). Then, by using the predefined manual control model structure ($H_p(j\omega)$), an optimization is performed in the frequency-domain to find the model parameters. MLE uses the same control model structure, and the model parameters are identified in time-domain. The reader is advised to refer to Chapter 3 for details of these methods and their application in MCIM. Figure 6.2 shows a sample identification result for a participant, during the ET with 200 ms of added time delay condition.

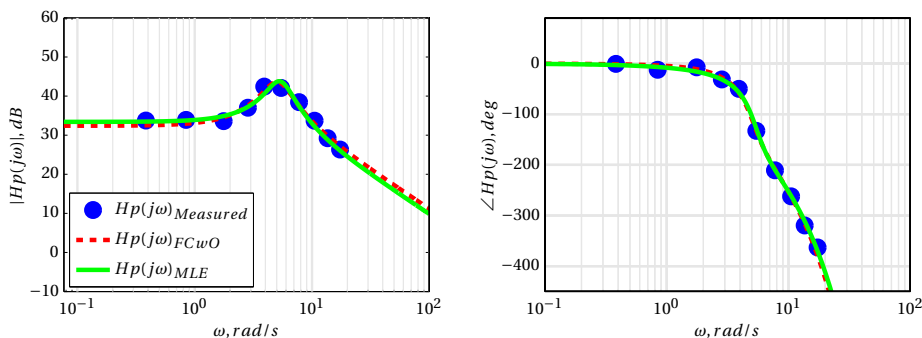


Figure 6.2: Frequency-domain results of two identification methods (i.e., FCMwO and MLE) on the measured data of the Participant 6, during the ET with 200 ms of added time delay condition.

Figure 6.2 exemplifies that both FCMwO and MLE techniques were able to describe the manual control behaviour that was measured during a sample experiment run, such that measured $H_p(j\omega)$ was very closely captured by both techniques. As described in Chapter 3, the VAF¹⁰⁵ was used to assess the accuracy of the described model. VAF=100% indicates that all the measured manual control can be presented by the estimated linear model, i.e., $H_p(j\omega)$. Thus, high values of VAF are required to claim that $H_p(j\omega)$ indeed describes the actual control behaviour that was measured during the experiment. For example, Figure 6.3 depicts a sample time history which shows both measured and

identified control signals with corresponding VAF values.

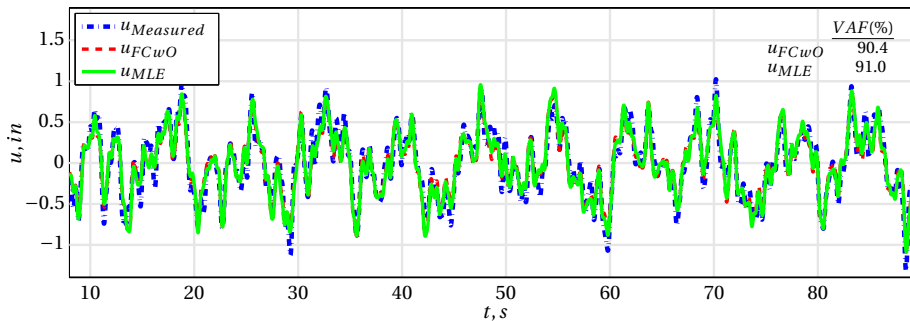


Figure 6.3: Time-domain results of two identification methods (i.e., FCMwO and MLE) on the measured data of Participant 6, during the ET with 200 ms of added time delay condition. VAF values of both methods are also given in the figure.

Similar to the frequency-domain comparisons (Figure 6.2), both identification methods showed good accuracy of estimation of the manual control behaviour in time-domain (Figure 6.3), as indicated by VAF values around 90%. These VAF values imply that the measured control behaviour can be modelled by the identified parameters in the estimated linear pilot model structure with an accuracy of $\approx 90\%$. The remaining $\approx 10\%$ reflects the remnant, resulting from all sorts of non-linearities, which can not be included in a LTI model, as discussed in Chapter 3.

6.7.2. STATISTICAL ANALYSES

In order to check the statistical significance of the variations among configurations, a two-way repeated-measures ANOVA is applied on the results of the experiment, as discussed in Chapter 3. The interval scale were satisfied for all dependent measures analysed with the two-way repeated-measures ANOVA. The normality assumption was rarely violated, but the ANOVA is fairly robust for such instances, as discussed in the Chapter 3. If the sphericity assumption was violated, the Greenhouse-Geisser correction was applied²⁰. Such occurrences are marked in the ANOVA tables of Section 6.8.

6.7.3. RPC DETECTION

As a part of the MCIM, ROVER and PAC were used for RPC detection. Details of these detections tools can be found in Chapter 3. These detection tools were used to investigate the correlation between identified manual control behaviour and RPC susceptibility of the PVS with added time delay and various task difficulties. In summary, ROVER uses the frequency of the vehicle response, amplitude of the control stick, the pitch rate and the phase between the control input and the pitch response. Then, ROVER assigns flags per each parameter depending on their thresholds. Based on the measured data, ROVER thresholds used in this experiment are given in Table 6.4.

Table 6.4: ROVER variables and their threshold values used in the experiment. Here, ω_q is the pitch rate frequency, θ_{long} is the cyclic stick deflection, q is the pitch rate response of the rotorcraft, and ϕ_θ is the phase between pilot control peaks and resultant body rate response (q).

Variables as ROVER flags		Threshold
Frequency	ω_q	8 rad/s
Stick amplitude	θ_{long}	0.95 in
Pitch rate	q	0.21 rad/s
Phase	ϕ_θ	85 deg.

As described in Chapter 3, PAC detects the control aggression and phase delay in the measured data, and locates these detected parameter pairs on a phase-aggression chart with PIO susceptibility boundaries, as described in the MCIM. In the following section, both ROVER and PAC results will be investigated.

6.8. RESULTS

This section provides the analysis of the obtained results. First, Section 6.8.1 will provide sample time histories of displayed error and pilot control inputs. Section 6.8.2 will show the control activity and the task performance achieved during the experiment. Pilot model identification results and corresponding identified pilot model parameters will be provided in Section 6.8.3. Then, the results of the open-loop crossover frequency and the phase margin will be elaborated in Section 6.8.4. Finally, the results of the RPC detection tools will be presented in Section 6.8.5.

6.8.1. SAMPLE TIME HISTORIES

Before performing any frequency-domain analysis, time traces of the measured data can provide an initial overview on the general control strategy approach of participants to the given task with varied configurations. Sample time histories of applied control and displayed error of a typical participant are shown in Figures 6.4 and 6.5, respectively.

Time histories of the control input (u), as shown in Figure 6.4, indicate that Participant 7 applied approximately equal control inputs for all three levels of added time delay conditions during the ET. However, when the task difficulty was increased to moderate (i.e., MT), the participant showed lower amplitude controls for the 200 ms added time delay condition than the ones with 0 and 100 ms added time delay. When the task difficulty was further increased (i.e., HT), amplitudes of the control input were the lowest of all task difficulty configurations. In summary, time histories of the control input (u) of Participant 7 indicate that:

- ET and MT tasks incited more control activity than the HT.
- Added time delay in the controlled element has the most noticeable deviation in the control activity during the MT, for the 200 ms of added time delay configuration.

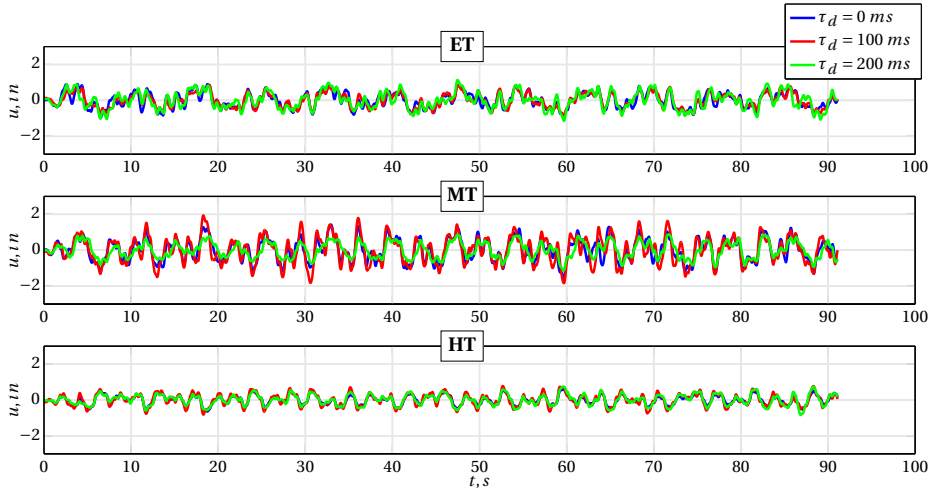


Figure 6.4: Control input time histories of the time-averaged measurement runs of Participant 7, with all combinations of varied task difficulty and added time delay configurations.

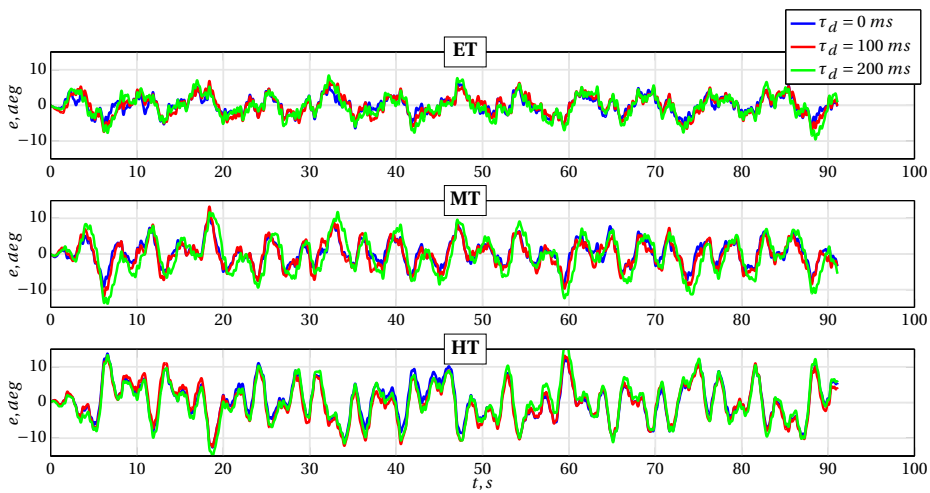


Figure 6.5: Displayed error time histories of the time-averaged measurement runs of Participant 7, with varied task difficulty and added time delay configurations.

Displayed pitch errors, which are also indication of the task performance, were inherently related to the forcing function bandwidth. This effect can be observed in the time histories which are depicted in Figure 6.5. In the ET condition, all three added time delay configurations showed nearly identical displayed errors. However, for the moderate task, 200 ms of added time delay condition resulted in higher displayed errors than seen for the 0 and 100 ms time delay conditions. The hardest task (i.e., HT) conditions showed the highest errors of all task difficulty configurations, as previously discussed in Chapter 5.

Similar to the easy task, the time traces of the error do not clearly show a remarkable difference between added time delay configurations. In summary, the displayed error time histories show that;

- Increasing the forcing function bandwidth resulted in increased displayed error.
- The effect of the added time delay was noticeable during the MT, particularly for the 200 ms added time delay condition.

6.8.2. TASK PERFORMANCE AND CONTROL ACTIVITY

The task performance was measured by the normalized error variance (σ_e^2/σ_i^2), and RMS of the control input (u) is used as a measure of manual control activity, as described in Chapter 3. Figure 6.6 depicts the task performance and the control activity, which are both calculated from the time averaged data of the measurement runs per participant per configuration.

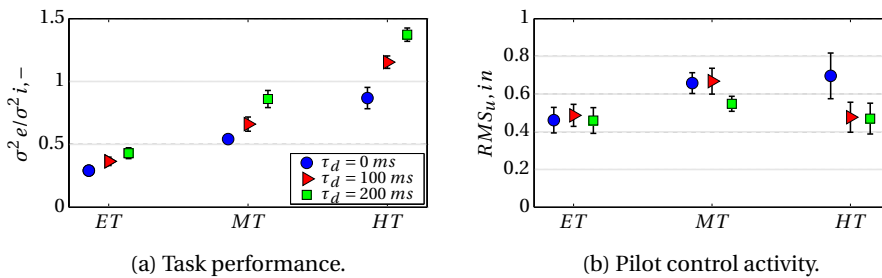


Figure 6.6: Mean and 95% confidence intervals of measured task performance (a) and control activity (b), all corrected for between-subject variability.

It can be seen from Figure 6.6 that increasing the task difficulty resulted in larger errors. This is expected since the task becomes harder to compensate with increased forcing function bandwidth, which represents the task difficulty in MCIM. For each task difficulty level, it can be observed that increasing the added time delay resulted in worse performance as well. This is due to the fact that the added time delay increases the phase lag of the CE, as shown in Figure 6.1.

Pilot control activity comparisons in Figure 6.6 shows a difference between task difficulties and added time delay configurations. One obvious deviation can be noticed between 100 and 200 ms of added time delay configuration in the MT. Another major deviation can also be seen in the HT between 0 and 100 ms of added time delay. Furthermore, it can be noted that confidence intervals of the control activity for the HT are bigger than the other task difficulties. This suggests that the control inputs for the HT varied the most between the participants, when compared to other task difficulties. For example, the time traces of the control input of Participant 7 (Figure 6.4) do not indicate this change in RMS_u for the HT. However, for the same participant, the noticeable deviation of the control activity in MT complies with change of the mean control activity for

all participants.

Table 6.5 shows the ANOVA results of the task performance and the control activity.

Table 6.5: Two-way repeated-measures ANOVA results for the control activity and task performance, where ** is highly significant ($p < 0.05$).

Dependent measures	Independent variable factors								
	ω_i			τ_d			$\omega_i \times \tau_d$		
	dF	F	Sig.	dF	F	Sig.	dF	F	Sig.
σ_e^2 / σ_i^2	2,16	457.96	**	2,16	103.72	**	4,32	11.38	**
RMS_u	2,16	6.50	**	2,16	10.05	**	4,32	4.29	**

The ANOVA results in Table 6.5 show that effects of the forcing function bandwidth and the added time delay on task performance are highly significant, $[F(2,16)=457.96, p < 0.05]$ and $[F(2,16)=103.72, p < 0.05]$, respectively. Moreover, the interaction between effects of the task difficulty and the added time delay is also found to be statistically highly significant $[F(4,32)=11.37, p < 0.05]$. Similar to the achieved task performance, both the task difficulty and the added time delay showed significant effect on pilot control activity, $[F(2,16)=6.5, p < 0.05]$ and $[F(2,16)=10.05, p < 0.05]$, respectively. In addition, highly significant interaction between the task difficulty and the added time delay was found for the control activity as well $[F(1.15,12,12)=4.3, p < 0.05]$. These statistical analyses indicate that both task performance and control activity are significantly affected by the added time delay, the task difficulty and their interactions.

6.8.3. IDENTIFIED PILOT MODEL PARAMETERS

The identification procedure described in Chapter 3 requires an LTI system, and the linearity of the pilot control behaviour was checked by the squared correlation coefficient (ρ^2), as described in Chapter 4. In summary, ρ^2 uses the ratio of the noise and manual control input periodograms to evaluate the linearity of the signal at the powered frequencies of the forcing function. In addition, the VAF can also be taken into account as an evaluation of the linearity of the system, depending on the accuracy of the estimated pilot model, as discussed in Chapter 3. An example of the average ρ^2 for one typical participant, and VAF values, which were corrected for between-subject variability for all experiment conditions, are shown in Figure 6.7.

It is depicted in Figure 6.7 that average ρ^2 values for a typical participant were generally found to be close to one, which indicates that manual control behaviour can be considered linear. In addition, VAF values obtained for all participants were between 82% to 92% with a grand-average of 88%, as shown in Figure 6.7. This indicates that the estimated describing function ($H_p(j\omega)$) with identified parameters captures almost 90% of the measured manual control behaviour in all experiment conditions. The remaining 10% are generally the non-linear control behaviour (i.e., remnant), which could not be

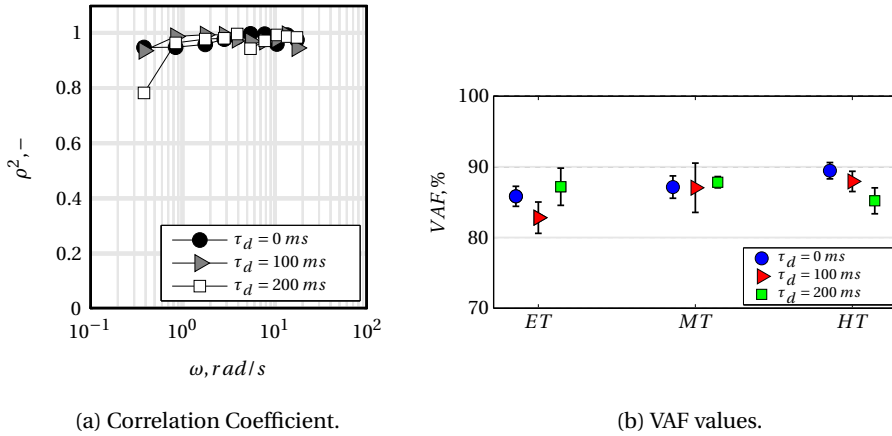


Figure 6.7: Average ρ^2 values for Participant 5 (a) during HT, and mean and 95% confidence intervals of VAF values, corrected for between-subject variability (b).

captured by an LTI oriented model.

6

High values of ρ^2 and VAF allow for high-accuracy identification using $H_p(j\omega)$. As described in the MCIM, $H_p(j\omega)$ contains equalization parameters (i.e., the pilot visual gain (K_v) and the lead time constant (τ_L)), and pilot limitation parameters (i.e., the pilot delay (τ_p), the neuromuscular damping (ζ_n) and natural frequency (ω_n)). After correcting for the between-subject variability, Figure 6.8 depicts the identified parameters with their mean values and 95% confidence intervals for each condition of the experiment.

In compliance with Figure 6.8, the results of a two-way repeated-measure ANOVA on pilot model parameters are given in Table 6.6.

Table 6.6: Two-way repeated-measures ANOVA results for the identified pilot model parameters, where ** is highly significant ($p < 0.05$), * is significant ($0.05 \leq p < 0.1$), - is not significant ($p \geq 0.1$) and gg is the Greenhouse-Geisser sphericity correction.

Dependent measures	Independent variable factors								
	ω_i			τ_d			$\omega_i \times \tau_d$		
	dF	F	Sig.	dF	F	Sig.	dF	F	Sig.
K_v	2,16	125.5	**	2,16	86.11	**	4,32	3.23	**
τ_L	2,16	48.39	**	2,16	12.32	**	1,7,13.8 ^{gg}	4.446	*
ω_{nms}	2,16	0.35	-	2,16	61.337	**	4,32	0.22	-
ζ_{nms}	2,16	5.28	*	2,16	4.417	*	2,16	4.49	-
τ_p	2,16	3.11	*	2,16	0.44	-	2,2,17.7 ^{gg}	2.522	-

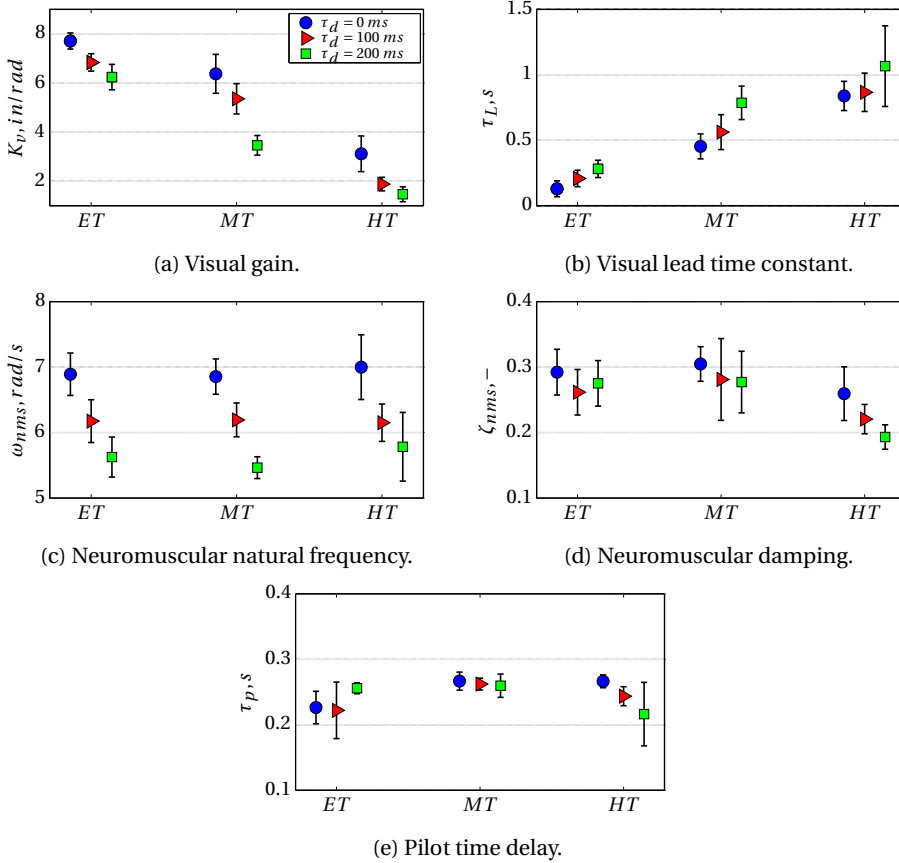


Figure 6.8: Mean and 95% confidence intervals of estimated pilot visual gain (a), lead time constant (b), neuromuscular natural frequency (c), damping (d), and pilot time delay (e) parameters, all corrected for between-subject variability.

Identified pilot visual gain (K_v) shows a dependence on the task difficulty and the added time delay, as shown in Figure 6.8. ANOVA also shows the high significance of the effect of task difficulty and the added time delay on K_v , $[F(2,16)=125.5, p<0.05]$ and $[F(2,16)=86.11, p<0.05]$, respectively. Moreover, the interaction of the task difficulty and the added time delay is found to be highly significant as well, $[F(4,32)=3.23, p<0.05]$. Similar to K_v , pilot lead time constant (τ_L) is found to be highly significantly affected by the task difficulty and the added time delay, $[F(2,16)=48.39, p<0.05]$ and $[F(2,16)=12.32, p<0.05]$, respectively. Figure 6.8 shows that during the condition with MT with 200 ms of added time delay, both K_v and τ_L resulted in a noticeable deviation when compared to the trends in other task difficulty conditions. A quantified comparison of the parameter deviations of K_v and τ_L for all task configurations are given in Figure 6.9.

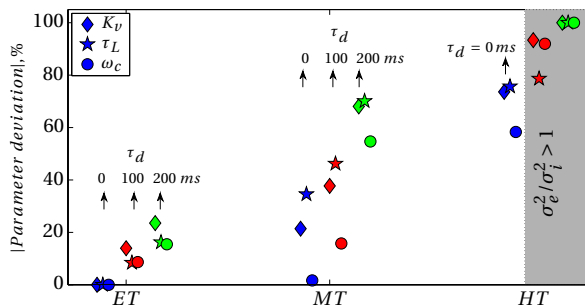


Figure 6.9: Absolute parameter deviations (%) of K_v , τ_L and ω_c based on the minimum and the maximum of each parameters mean values for all task configurations. Conditions with tracking error amplification (i.e., $\sigma_e^2/\sigma_i^2 > 1$) are greyed out in the figure.

Figure 6.9 shows that for the MT, K_v deviated from 21 % to 37 % between 0 and 100 ms of added time delay levels, respectively. However, when the added time delay was further increased to 200 ms, the deviation became recognizably higher as 68 %. A similar noticeable deviation for the 200 ms condition has occurred for the τ_L as well, such that 34 %, 46 % and 70 % deviations were observed for 0, 100 and 200 ms of added time delay levels, respectively. As it will be discussed in Section 6.8.4, the HT without added time delay condition is an example of a typical crossover regression due to the increased task difficulty, and the HT without added time delay condition showed very similar K_v and τ_L deviations to this crossover regression condition.

In Figure 6.8, neuromuscular natural frequencies (ω_{nms}) appear to be highly dependent on the added time delay but not on the task difficulty. The ANOVA results agree with the same observation, such that task difficulty showed no significant effect on ω_{nms} , whereas the added time delay affects ω_{nms} highly significantly [F(2,16)=61.33, $p < 0.05$]. The interaction between task difficulty and the added time delay did not show a significant effect on ω_{nms} . The neuromuscular damping (ζ_{nms}) parameter shows the largest confidence intervals of all identified pilot parameters. This indicates that the spread between participants is the highest for this parameter. Task difficulty and the time delay significantly affect the ζ_{nms} , [F(2,16)=0.35, $0.05 \leq p < 0.1$] and [F(2,16)=4.42, $0.05 \leq p < 0.1$], respectively. However, the interaction between the task difficulty and the added time delay does not have a significant effect on ζ_{nms} . Finally, pilot time delay (τ_p) is significantly affected by task difficulty only, [F(2,16)=3.11, $0.05 \leq p < 0.1$]. The added time delay or its interaction with task difficulty do not show any significant effect on τ_p .

Considering the identified pilot model parameters, one of the largest overall deviation in identified control behaviour was observed for the MT, particularly between 100 ms and 200 ms conditions. By using the means of the identified parameters, the resultant mean pilot describing functions for the MT are depicted in Figure 6.10.

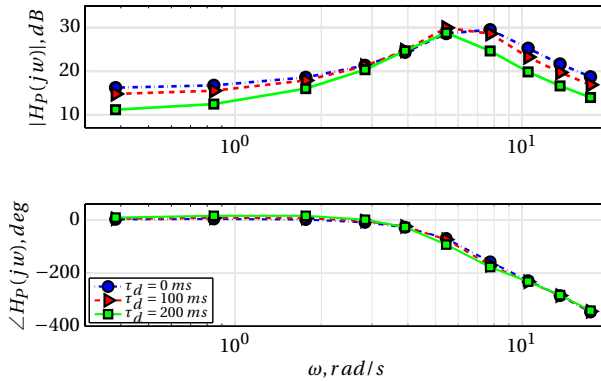


Figure 6.10: Mean pilot describing functions in the MT for 0, 100 and 200 ms of added time delays. Powered frequencies of the forcing function are emphasized by markers.

Figure 6.10 points out the noticeable pilot control behaviour change between 100 and 200 ms of added time delay in the MT. Basically, reduced K_v can be traced by the drop of magnitude of $H_p(j\omega)$ at low frequencies. Second, an increased lead time constant can be recognized by the initiation of the slope of the magnitude in low and mid-frequencies until 5 rad/s. Another indication of increased τ_L in Figure 6.10 is the positive phase, which suggests that participants tried to cope with the reduced stability due to added time delay by providing additional phase into the PVS at low frequencies. Although ω_{nms} also shows a decreasing trend with increasing added time delay, this trend is nearly identical for all task difficulties (Figure 6.8), and not particularly different for the MT.

In summary, the pilot equalization parameters, K_v and τ_L , show a noticeable deviation in their trends in MT between 100 and 200 ms of added time delay, as depicted in Figure 6.9. This deviation suggests that the crossover regression, or the pilot control strategy to avoid a possible RPC, may be observed in between these two configurations.

6.8.4. CROSSOVER FREQUENCIES AND PHASE MARGINS

By using the identified manual control behaviour in the previous section, the open-loop crossover frequencies and corresponding phase margins were obtained. In order to investigate the degradation of the handling qualities, the focus was on crossover regression occurrences. Figure 6.11 shows the crossover frequencies and the phases margins with means and 95% confidence intervals, corrected for between-subject variability. In order to evaluate the statistical significance of possible effects of task difficulty and added time delay on crossover frequency and phase margin, a two-way repeated-measures ANOVA was applied, and the results are listed in Table 6.7.

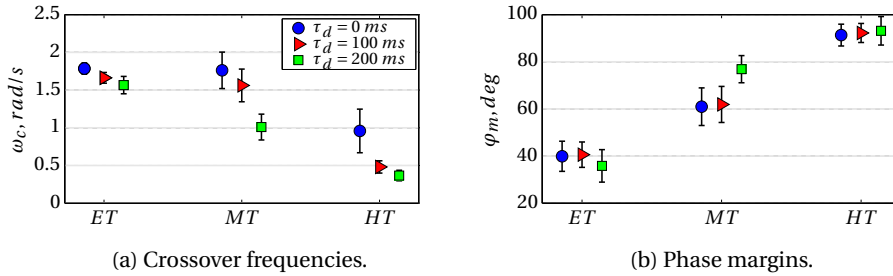


Figure 6.11: Mean and 95% confidence intervals of the crossover frequency(a) and the phase margin(b), all corrected for between-subject variability.

Table 6.7: Two-way repeated-measures ANOVA results for the crossover frequencies and phase margins, where ** is highly significant ($p < 0.05$).

Dependent measures	Independent variable factors								
	ω_i			τ_d			$\omega_i \times \tau_d$		
	dF	F	Sig.	dF	F	Sig.	dF	F	Sig.
ω_c	2,16	95.333	**	2,16	53.228	**	4,32	4.196	**
ϕ_m	2,16	143.605	**	2,16	4.54	**	4,32	5.631	**

It can be seen in Figure 6.11 that a noticeable crossover regression occurs in the MT between 100 and 200 ms added time delays. Moreover, further crossover regression can be observed between 0 and 100 ms of added time delay in the HT. Although the magnitude of the drop in ω_c is very close for these two occurrences (both approximately 0.5 rad/s), the regression in the MT is thought to be more important. The reason for this is due to the fact that the manual control compensation of the error in the HT was already hard, because of the high forcing function bandwidth even without the added time delay, as previously shown in Figure 6.9. It can be seen in Figure 6.11 that the ‘classical’ crossover regression due to the task difficulty has already been present between MT and HT for the conditions without the added time delay. The ANOVA results in Table 6.7 shows that task difficulty, the added time delay and their interaction all have highly significant effects on the crossover frequency, $[F(2,16)=95.33, p < 0.05]$, $[F(2,16)=53.23, p < 0.05]$ and $[F(4,32)=4.2, p < 0.05]$, respectively. Thus, the stated hypotheses in Section 6.6 is indeed fulfilled.

Not only crossover frequencies, but also phase margins were found to be significantly affected by the added time delay, the task difficulty and their interaction, $[F(2,16)=143.6, p < 0.05]$, $[F(2,16)=4.54, p < 0.05]$ and $[F(4,32)=5.63, p < 0.05]$, respectively. It can be seen in Figure 6.11 that the task difficulty determined some sort of regimes of the available phase margins. For the ET, phase margins ranging from 10 to 50 degrees were observed, whereas the MT showed a regime of phase margins ranging from 50 to 85 degrees. The

HT showed the highest phase margins with the smallest variation between 85 to 100 degrees, as depicted in Figure 6.11. Although the effect of the added time delay does not show a trend in Figure 6.11 within each task difficulty, the phase margin deviation is noticeably higher between 100 and 200 ms in MT.

6.8.5. ROVER AND PAC RESULTS

The algorithms of both ROVER and PAC were described in Chapter 3 in detail, and the settings used for their application here were given in Section 6.7.3. Mean and standard deviations of the detected ROVER flags are shown in Figure 6.12, and two-way ANOVA results are given in Table 6.8.

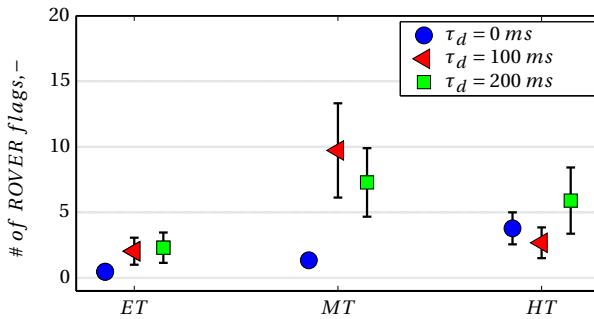


Figure 6.12: Mean and standard deviations of the detected ROVER flags for all experiment conditions.

Table 6.8: Two-way repeated-measures ANOVA results for the ROVER detections, where ** is highly significant ($p < 0.05$).

Dependent measures	Independent variable factors								
	ω_i			τ_d			$\omega_i \times \tau_d$		
	dF	F	Sig.	dF	F	Sig.	dF	F	Sig.
ROVER flags	2,16	3.74	**	2,16	3.98	**	4,32	3.17	**

Figure 6.12 indicates that for the ET, there is a slight increase in the number of detected ROVER flags for 100 ms and 200 ms of added time delay. However, given the spread in the data, it is hard to conclude on a certain trend among these configurations. On the other hand, the MT shows the most interesting differences among the added time configurations. When the added time delay was increased from 0 ms to 100 ms, an obvious increase of detected ROVER flags was observed, as shown in Figure 6.12. This suggests that the rotorcraft model features considerably higher RPC susceptibility with

this configuration. Increasing the added time delay to 200 ms made the CE more unstable and it could be expected to result in even more ROVER flag detections. However, RPC tendency is seen to decrease. This behaviour suggests that participants reverted to a less RPC-prone control strategy, such as the ‘back-off’ strategy to avoid RPC incipiences. This strategy reveals itself also in the HT, since all added time delay configurations during this task showed low RPC tendencies, when compared to 100 ms in MT.

In order to focus on the interesting RPC tendency in the MT, PAC was utilized. Figure 6.13 depicts PAC detection results of a typical participant data, for 0 ms, 100 ms and 200 ms of added time delay in the MT.

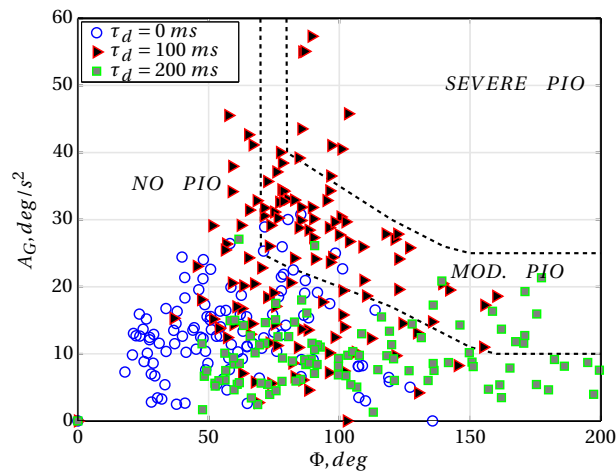


Figure 6.13: PAC detection results for Participant 7 during the MT with 0, 100 and 200 ms of added time delays.

It can be seen in Figure 6.13 that increasing the added time delay from 0 ms to 100 ms, both aggression and phase distortion detections increase and the task moves from ‘No PIO’ to ‘Moderate PIO’. As discussed in Chapter 3, these PIO boundaries can not be definite, but the PAC plots still provide the characteristics of the detected response of the vehicle. When the added time delay was further increased to 200 ms seconds, aggression became less, but the phase distortion became higher, bringing the task back to the ‘No PIO’ region. Similar to the ROVER results for the MT, this suggest a back-off control strategy to avoid higher RPC tendencies.

6.9. DISCUSSION

This chapter presented the results of the MCIM experiment, and only briefly discussed the results. This section provides a more detailed discussion of fundamental aspects of crossover regression and correlated adverse RPC tendencies. As a complete application of the MCIM, the main objective of this experiment was to detect configurations in which human operators exhibit crossover regression, e.g., ‘back-off’ strategy. Moreover, RPC susceptibility of the PVS was assumed to show a similar tendency, such that human operators would prefer to avoid higher risks of getting into adverse couplings, and adjust their control strategy accordingly.

It was found that task difficulty, the added time delay and their interaction had indeed highly significant effects on both the task performance and the control activity. When the task difficulty or the amount of added time delay was increased, task performance degraded. This could be predicted because both the stability of the CE and the number of powered sinusoids in the forcing function could result in larger errors in a disturbance-rejection task. Manual control activity, on the other hand, did not show such a clear trend with varied task configurations, despite being statistically significant. However, especially the reduction of the control activity in the MT between 100 ms and 200 ms of added time delays was noticeable. Similarly, a remarkable reduction in control activity was also observed in the HT between 0 ms and 100 ms of added time delay. These deviations could be an initial indication of a ‘back-off’ strategy, such that participants might have noticeably changed their control amplitudes. Although these recognizable control activity deviations did not result in a such a noticeable deviation in task performance. This may mean that participants consciously preferred to adapt their control strategy instead of completely ignoring the task.

As a part of the MCIM, both FCMwO and MLE were used to identify the manual control behaviour, and it was observed that the active compensation parameters, i.e., K_v and τ_L , were significantly affected by the added time delay, task difficulty and their interaction. This result was expected since these parameters define the active compensation, which was already seen to be varied for different configurations in preliminary identification experiments. With increasing added time delay and task difficulty, K_v reduces and τ_L increases. Considering the active compensation parameters, lead time constant (τ_L) is the only parameters that could provide additional positive phase to the PVS. Therefore, when the stability was threatened by added time delay, participants needed to exhibit higher lead to increase the stability. However, high lead compensation is known to be correspond to high pilot workload⁷⁵, and human operators can not keep the same visual gain and increase the lead at the same time. Moreover, the closed-loop resonance peak can be amplified with increased $K_v \times \tau_L$ which defines the the pilots’ magnitude responses around crossover.

Investigation of the pilot limitation terms in the pilot model showed that the added time delay had a highly significant effect on the neuromuscular frequency ω_{nms} . Very similar values of ω_{nms} were obtained for the task difficulty variable with the same added time delay configurations. From a stability point of view, lowering the ω_{nms} results in a

reduced phase margin, since the neuromuscular actuation was modelled as a second-order system. This behaviour of ω_{nms} deviation can be explained by the preference of the human control strategy, but as a side-effect while dealing with the demanding task, instead of a conscious decision. First of all, it must be noted that ω_{nms} can be related to the stiffness of the neuromuscular system, like the connection between the natural frequency and the spring constant in a typical second-order spring-damper system. During the no added time delay configurations, participants probably were more confident with the input-to-response characteristics, and this might encourage them to have a tighter neuromuscular system, regardless of the task difficulty. However, when the added time delay was increased, participants might have preferred to have a looser neuromuscular system simply because the response of the CE was less predictive. Thus, instead of a tightly settled limb muscle system, a more relaxed system could provide to correct possible overshoots originating from the added time delays. This neuromuscular system adaptation was applied almost equally during each task difficulty, suggesting no specific interaction with crossover regression tendency but an adaptation to increased time delay.

Both ζ_{nms} and τ_p observed to be not being highly significantly affected by any independent variable or their interactions. In general, HT resulted in lower ζ_{nms} and the means of τ_p varied between 0.21 s to 0.27 s. Statistically, ζ_{nms} was observed to be affected by the added time and the task difficulty, but not their interaction. τ_p was only affected by the task difficulty. None of these effects were highly significant, however. Especially, the regression candidate configurations, i.e., in the MT with 100 ms and 200 ms of added time delay conditions, showed very similar ζ_{nms} and τ_p values. Therefore, the variation in control behaviour *between these candidate configurations* did not include the deviation of ζ_{nms} and τ_p . Overall, it was shown that the manual control behaviour change is easily recognizable between 100 ms and 200 ms of added time delay conditions in the MT.

Another critical measure to observe a change in manual control behaviour is the open-loop crossover frequency and the corresponding phase margin. The results of the crossover frequency showed that increasing time delay in each task difficulty leads to reduced crossover frequencies. This is simply due to the fact that the CE with increased added time delay reduces the PVS stability. In the MT with 100 ms and 200 ms of added time delay conditions, the reduction was considered to be more important since the active participation of the pilot was more pronounced between these configurations. On the other hand, the manual control strategy was only able to amplify the error between 0 and 100 ms of added time delay in the HT.

In addition, the classical crossover regression tendency, which originates from increased task difficulty^{81,83}, was also observed in the experiment. This regression can be traced between MT and HT for no added time delay configurations. Obviously, added time delay on these configurations continued the reduction of the crossover frequency for each task difficulty, as discussed above.

Phase margin results showed that the task difficulty grouped the phase margins into three distinct ranges. ET ended up with the lowest phase margins, around 40 degrees. MT showed a variation approximately between 60 and 80 degrees. HT resulted in the highest phase margins, around 90 degrees. This variation of phase margins according to the task difficulty is an indication of how participants aimed to prioritize the PVS stability when it was threatened by added time delay and varied task difficulty. The most noticeable change in phase margins for each task difficulty were between 100 ms and 200 ms added time delay conditions in the MT. Unlike the crossover regression tendency, the deviation of phase delay was hardly recognizable between 0 and 100 ms of added time delay in the HT.

As discussed in detail in Chapter 2, adding a time delay is a well-known CAT.I RPC trigger in rotorcraft studies, e.g., additional time delay in BO-105 in Ockier's study¹⁰⁷. Moreover, the crucial interaction of the task difficulty accompanying the added time delay on exposing RPC was discussed as well, e.g., precision hover task in the ARISTOTEL project¹¹⁵. In this experiment, ROVER and PAC were used as two RPC detection tools as a part of the MCIM. Results of RPC detection tools on showed that in the MT, RPC tendency was noticeably increased when 100 ms of time delay was added. However, when the added time delay was further increased to 200 ms, RPC occurrences reduced. This suggests that participants adapted their control strategy in order to avoid great risk of getting into more RPC prone conditions during the task. In the HT, all conditions showed lower RPC tendencies than the 100 ms and 200 ms added delay conditions of the MT. This was also expected, such that when the task is the hardest (i.e., HT), human operators already exhibited 'classical' crossover regression for the no added time delay condition, solely due to the increased task difficulty. This means human operators were exhibiting a cautious control strategy from the start, to sustain the stability of the PVS, and RPC occurrences in these conditions were expected to be lower than the conditions when human operators were fully engaged without any crossover regression.

6.10. CONCLUSIONS

The previous chapter showed that the simulation framework had the disadvantage of the PVS constrain (i.e., the optimal task performance) which resulted in control behaviours that were not preferred by the human operators in experiment conditions. The main objective of the present chapter was to investigate the rotorcraft HQ degradation by objectively considering the manual control behaviour in an RPC-prone task in human-in-the-loop simulator experiments. It was ultimately aimed to find the task configurations that cause a clear deviation in manual control strategy, elaborated by using the identified pilot parameters and relevant PVS characteristics. This method, MCIM, was described in Chapter 3 in detail, and it was utilized for the identification experiment described in this chapter.

After identifying the manual control behaviour, the pilot equalization term was observed to be the primary term in the pilot model that reflected a clear variation in control behaviours for configurations with different task difficulties and added time delays. Therefore, the most crucial parameters of the pilot describing function were the visual

gain (K_v) and the lead time constant (τ_L). A sudden decrease in K_v and an increase in τ_L were the symptoms of a recognizable manual control behaviour change. Neuromuscular natural frequency (ω_{nms}) observed to be reduced with added time delay, independent of the task difficulty. Crossover frequencies showed three clear regression tendencies. First, a regression due to the added time delay, between 100 ms and 200 ms added time delay in the MT. Second, the 'classical' crossover regression between no added time delay conditions between MT and HT. Third, a regression due to 100 ms of added time delay in the HT, although this regression was already occurred in a 'classical' regressed condition. The most interesting regression is the first one, which is also the essence of the MCIM application. At this condition, phase margins also indicated a recognizable deviation. Moreover, applied RPC tools showed that RPC susceptibility of the rotorcraft model remarkably increases from 0 to 100 ms of added time delay. However, further added time delay (i.e., 200 ms of added time delay) demonstrated a sudden decrease of detected ROVER flags and transition from 'Moderate PIO' to 'No PIO' regions in PAC detection map. RPC investigations also suggest that human operators changed their control strategy to avoid increased RPC tendency of the closed-loop.

In this chapter, MCIM successfully demonstrated its ability to detect the configurations where the HQ and the RPC susceptibility of a designed rotorcraft recognizably deviate, by using objective measures such as the identified pilot model parameters. These findings of MCIM can determine how much time delay can lead to drastic changes of HQ and RPC tendencies, in which level of task difficulty, all from identified parameter perspectives. Unlike the HQ cliff phenomena⁵ discussed in Chapter 2, the variations of HQ were provided by objective measures of the MCIM, in addition to RPC susceptibility.

Next chapter will provide the conclusions of this dissertation, and the recommendations for the future work.

7

CONCLUSIONS AND RECOMMENDATIONS

7.1. CONCLUSIONS

7.1.1. THEORY

This study was initiated to investigate new objective measures of rotorcraft Handling Qualities (HQ) deficiencies and Rotorcraft Pilot Coupling (RPC) susceptibility during an early stage of a rotorcraft design. HQ deficiencies and RPC events are still a major threat to the operational safety of both fixed wing and rotorcraft operations. Generally, rotorcraft HQ and RPC susceptibility are assessed by subjective pilot ratings, such as Handling Qualities Ratings (HQR) and Pilot Induced Oscillations Ratings (PIOR), respectively. Such subjective pilot assessments mainly occur at later phases of a vehicle development program, when a prototype rotorcraft has already been built. Addressing any detected HQ deficiency at this late design stage may cause extra costs, delays in the development schedule, more flight tests and higher operational safety risks. Moreover, subjective pilot ratings during some HQ and RPC assessments are generally considerably scattered, which lead to unreliable determination of HQ deficiency and RPC proneness.

In addition to the subjective pilot ratings, there are several objective rotorcraft HQ criteria in the literature as well. One of the well-known HQ criteria for rotorcraft design is Bandwidth Phase Delay (BPD) criterion from the Aerodynamic Design Standard (ADS)-33. Despite its wide range of application in both fixed and rotary wing industries, the BPD criterion does not directly account for the pilot, who has a vital role in an RPC event. There are several other HQ criteria (e.g., the Neal-Smith criterion), however, which utilize 'paper' pilot models. Such paper pilot models are generally included in criteria requirements (e.g., the closed-loop resonance peak in Neal-Smith criterion). Such pre-determined assignments of pilot models may limit the understanding of the 'actual' manual control behaviour on the detail of model parameters.

Considering these drawbacks, this thesis aimed to fill the scientific gap on the objective criteria for rotorcraft HQ and RPC susceptibility assessments by utilizing identification of manual control behaviour.

7.1.2. DEVELOPMENT OF THE MANUAL CONTROL IDENTIFICATION METHOD (MCIM)

Human operators tend to sacrifice task performance and show a ‘back-off’ control strategy to avoid significant Pilot Vehicle System (PVS) instabilities, as described in Chapter 2. In this thesis, the idea behind the developed methodology (i.e., MCIM) is to use the identification of manual control behaviour for conditions that may cause these control strategies. This would allow us to objectively determine under which conditions a rotorcraft design may lead human operators to change their control strategy significantly. Parameters of identified models of the manual control behaviour, open- and closed-loop characteristics of the PVS can then be used as objective measures of HQ and RPC tendency of the design. Chapter 3 thoroughly describes the development of the MCIM, which consists of five steps.

The first step is the development of a rotorcraft model, which must be capable of including added time delay. The second step is the compensatory task, which must include a forcing function to determine the task difficulty with its bandwidth. The third step requires an MCIM identification experiment which must be designed considering the statistical requirements (e.g., Latin square test matrix), and the eligibility for Linear Time Invariant (LTI) identification procedures (e.g., removed non-linearities of the control manipulator). The fourth step is the analyses of the MCIM identification experiment, particularly focused on the identified pilot model parameters, crossover frequencies, and several other PVS characteristics (e.g., phase margins). The fifth step consists of applying RPC detection tools to the results of the MCIM identification experiment, and investigating the relation between the identified manual control behaviour and the RPC susceptibility.

Conditions of the MCIM identification experiment are determined by two independent variables: the task difficulty and the added time delay. Increased task difficulty is a well-known condition that may cause a ‘back-off’ control strategy (e.g., *crossover regression*⁸⁰). Moreover, increased added time delay is a typical trigger for a possible RPC event, because the reduced phase margin in the PVS forces the operator to reduce the control gain, i.e., to ‘back-off’, to avoid a potential loss of control. Therefore, by combining these two independent experiment variables, the MCIM can determine limiting conditions of a rotorcraft design in terms of HQ deficiency and RPC susceptibility.

7.1.3. APPLICATION OF THE MCIM

Two preliminary identification experiments were conducted, to identify possible changes in manual control behaviour under conditions with various levels of added time delay. Both experiments indicated that increasing the added time delay may result in a considerable reduction in the crossover frequency. Moreover, in the second identification experiment, between the 0 ms and 100 ms added time delay conditions, no crossover

regression was found, whereas the 200 ms condition did result in regression-like behaviour. This result suggests that added time delay may have boundaries that would limit the vehicle design in terms of added time delay. When the added time delay was increased, identified pilot model parameters indicated that human operators show lower visual gain and neuromuscular natural frequency, and higher lead compensation.

In the first experiment, the control manipulator gearing was also deliberately varied (e.g., configurations with a higher-sensitivity cyclic that could represent a different simulator control manipulator) to observe the resulting adaptation of the manual control behaviour. Increasing the control gearing sensitivity is equivalent to increasing the Controlled Element (CE) gain, which normally causes human operators to simply adapt their gains. Despite this well-known adaptation, particular interest was on the added time delay conditions. Identification results showed that human operators adapt only their gains, and the remaining identified parameters did not show any significant variation with the control gearing between same added time delay conditions.

In both experiments, existing RPC detection tools in the MCIM (i.e., Realtime Oscillation Verifier (ROVER) and Phase Aggression Criteria (PAC)) showed an increased RPC susceptibility with increased added time delay, and correlated well with the identified manual control behaviour. In the second experiment, both ROVER and PAC detected noticeably increased RPC proneness when added time delay was increased from 0 ms to 100 ms. However, when the added time was further increased to 200 ms, ROVER showed a relatively similar number of RPC detections, and PAC's detected RPC proneness shifted from the 'Moderate Pilot Induced Oscillations (PIO)' zone to the 'No PIO' zone. Thus, very similar to the identified manual control behaviour, RPC susceptibility also changed its trend when added time delay was further increased.

In the preliminary identification experiments of this thesis, MCIM showed that apart from the increased forcing function bandwidth (i.e., the 'typical' cause of a crossover regression), **only** added time delay can also lead human operators to exhibit a crossover regression behaviour, and the corresponding RPC susceptibility can be determined.

Considering the MCIM results of the preliminary identification experiments, a follow-up computer simulation study was performed. The developed simulation framework contained a pilot model, and a CE in a compensatory task, matching the MCIM experiments. The aim of the simulation study was to predict the manual control behaviour that yields the optimum task performance during conditions with combinations of the additional time delay **and** the task difficulty.

While keeping the pilot limitation parameters (i.e., the pilot delay and neuromuscular system parameters) constant, based on the values measured in the preliminary identification experiment, both pilot equalization parameters (i.e., visual gain and lead compensation) were varied in the simulation. Moreover, based on the simulation conditions, the pilot remnant was neglected or added to the pilot control signal. In addition, high and low bandwidth forcing functions, with discrete or continuous Power Spectral

Density (PSD), were applied to represent the task difficulty.

For each task difficulty condition with added time delay generally lower pilot visual gain and higher lead time constant were predicted to yield the optimum performance. This trend of parameter variation matches well with the identified pilot model parameters in the preliminary identification experiments. Moreover, crossover regressions were generally found when the added time delay was increased, and also when the task difficulty was increased.

It was demonstrated that when the exact same pilot limitation parameters from the preliminary experiment were used in the simulation study, human operators have preferred slightly higher tracking errors with higher visual gains and lower lead compensation when compared to the optimum performance parameters as predicted by the simulation study.

A clear difference between the optimum performance parameters of the simulation framework and the identified parameters was the lead time constant. The simulation study required considerably higher lead time constants when compared to the identified ones. Typically, the lead time constant is related to pilot workload⁷⁵, and the simulation would aim for very high workload for the best performance, whereas human pilot would prefer less workload in the real task. Akin to the 'paper' pilot limitations in some existing HQ criteria, the simulation study was considered to be not entirely representative of the preference of a human operator in a real tracking task with demanding conditions.

Finally, the MCIM was fully applied in a simulator experiment with combinations of three levels of added time delay (i.e., 0 ms, 100 ms and 200 ms) and three levels of task difficulty (i.e., easy, moderate and hard tasks, represented as Easy Task (ET), Moderate Task (MT) and Hard Task (HT), respectively). These task difficulties were determined by the forcing function bandwidth. The objective of this MCIM experiment was to find the task configurations that cause a clear deviation in manual control strategy, elaborated by using the identified pilot parameters and relevant PVS characteristics.

Experiment results showed that the visual gain and the lead time constant were the most crucial parameters that indicated the adaptation of the exhibited manual control behaviour for different task configurations. Akin to the preliminary experiments and the simulation study, a recognizable change in the trend of decreasing visual gain and increasing lead time constant characterized the major adaptation of the manual control strategy among experiment task conditions. Consequently, crossover frequencies indicated three clear regression tendencies.

The first crossover regression was due to the added time delay, between 100 ms and 200 ms conditions in the MT. A very similar observation was made also during preliminary identification experiments. The second was a 'classical' crossover regression due to increased task difficulty, mainly recognizable between MT and HT. The third crossover regression occurred in HT when added time delay was increased to 100 ms. Particularly

the first crossover regression is an excellent example of the fundamental objective of the MCIM.

At the conditions of the first crossover regression, it is worth noting that the conventional BPD criterion did not predict any RPC proneness based on either the internal PIO notification in the ADS-33, nor the superimposed fixed-wing PIO proneness boundary. Moreover, it does not also account for the task difficulty, such that the same HQ chart would be applicable to all task difficulties. However, the MCIM showed that when added time delay was increased to 100 ms, there was a clear increase in the RPC tendency. Next, when added time delay was further increased to 200 ms, RPC tendencies were reduced, which corresponds to the crossover regression found.

In other words, operators noticeably changed their control strategy to still perform the same disturbance rejection task when the added time delay increased from 100 ms to 200 ms. As mentioned before, identified parameters showed that their visual gains were noticeably reduced and lead time constants were increased. In return, they were able to avoid any further RPC tendencies that would jeopardize the task completion.

7.1.4. CONCLUSIONS ON THE MCIM STEPS

STEP 1: ROTORCRAFT MODEL

A single-axis rate-command rotorcraft model with inherent time delay (i.e., the 'conceptual handling qualities model'¹¹¹) was successfully used in the MCIM. The rotorcraft model had a relatively high pitch (or roll) damping value (i.e., high bandwidth) of a typical hingeless rotor type (e.g., Bo-105). In the MCIM, the bandwidth of the rotorcraft model defines the frequency at which the response characteristics of the model transforms from a single-integrator to a double-integrator, which causes an increased phase lag in the response (e.g., phase 'roll-off'). In addition, as a part of the MCIM, adding more time delay to the model increases this phase lag even further. Therefore, having a high-bandwidth rotorcraft model was beneficial to investigate the effects of the added time delay, because the phase 'roll-off' happened at high frequencies. This allowed human operators to apply control at a wide range of frequencies, without threatening the PVS stability. Moreover, the added time delay was easily added to the inherent delay, which accounts for the high-order rotor dynamics in the rotorcraft model. Thus, there was no need to change the structure of the model. This advantage significantly simplified the analysis of the rotorcraft model and the PVS response for all conditions.

STEP 2: TASK DIFFICULTY

A single-axis disturbance-rejection task was successfully applied in the MCIM by injecting a forcing function in the form of sum-of-sines. In the MCIM, the discrete power distribution of the forcing function was composed of two partitions: a high-amplitude low-frequency region and a low-amplitude high-frequency shelf. The forcing function bandwidth determines the frequency at which a transition between these two partitions occurs. Therefore, this power distribution of the forcing function design allows for direct

easy control of the task difficulty, i.e., by changing the forcing function bandwidth while keeping the same total power. As a result, the comparison of conditions with various task difficulties and corresponding PVS analyses were easily accomplished. Moreover, the participants in simulator experiments showed highly linear responses during various task difficulties, which indicates that the forcing function design was indeed adequate for these experiments even for the more demanding conditions with added time delay.

STEP 3: DISTURBANCE-REJECTION TASK

A disturbance-rejection task was designed for the MCIM and used in two simulators, the SIMONA Research Simulator (SRS) and the HeliFlight Helicopter Simulator (HHS), without motion feedback. The purpose of the task was to excite the PVS for manual control behaviour identification. This task was designed as a compensatory task, such that human operators were required to null the disturbance (i.e., difference between the forcing function and the vehicle response) that was displayed on scaled-up attitude indicators in both simulators, without any outer screen visual. Considering the noticeable differences between the simulators, the simplicity of the task allowed a quick integration in both simulators. Although these two simulators had different control manipulators (e.g., cyclic control), setting-up linear configurations (e.g., no breakout-force) minimized any effects of manipulator differences in terms of MCIM applications. Moreover, the MCIM experiments were conducted by professional helicopter pilots and participants without such a piloting profession, in different experiment campaigns. Since the MCIM mainly focuses on the 'variation' of the manual control strategy, it was shown that the MCIM was able to detect the same parameter variation trend for the added time delay conditions (i.e., reduced visual gain and increased lead time constant) for both participant groups, and in different simulators. Despite the limited number of experiment campaigns, this result was found to be promising for the robustness of the MCIM. During the MCIM training phases of the identification experiments, it was recognized that the Latin square test matrix, which was required for the Analysis of Variance (ANOVA) statistical analyses, required human operators to adapt to each condition in a mixed order, and prevented them to apply predicted control strategies. It was also noted that giving enough time breaks between experiment conditions improved the focus and the performance of human operators.

STEP 4: PVS ANALYSES

Based on the independent variables (i.e., the task difficulty and the added time delay), dependent measures were investigated during the PVS analyses. These dependent measures were task performance, control activity, pilot model parameters, crossover frequency and phase margin. These metrics were measured during identification experiments for all conditions. Task performance and control activity were calculated in the time domain. Each participant of an identification experiment was informed about his/her task performance in the form of a 'score', just after each experiment run. This score represented the ratio of the powers of the displayed error to the injected forcing function. Keeping track of these scores allowed tracing of general trends of task performance for different configurations *during* the experiment campaign, before performing

any *ad hoc* PVS analysis. Moreover, announcing the task performance after each experiment run helped participants to find their ‘best’ control strategy, i.e., the strategy that resulted in the highest score to be achieved by each participant.

Pilot model parameters, crossover frequency and phase margin were calculated in the frequency domain by analysing the measured data from the identification experiments, for all human operators who participated in all experiment conditions. These measured data were processed by two LTI identification techniques (i.e., Fourier Coefficients Method with Optimization (FCMwO) and Maximum Likelihood Estimation (MLE)), which were used in conjunction to mitigate possible optimization issues, e.g., converging to local minima. Pilot model parameters were based on the estimated manual control behaviour (i.e., the pilot model), and the identified parameters showed that the identification process using the estimated pilot model resulted in high values of Variance Accounted For (VAF) (i.e., the accuracy of the estimated output). Therefore, not only the LTI identification methodology, but also the estimated pilot model exhibited a good accuracy for capturing the manual control behaviour, including demanding experiment conditions (e.g., hard tasks with high added time delay conditions).

Variation of the pilot model parameters, crossover frequency and phase margin were examined with the ANOVA statistical method, which required a Latin square design for the execution of identification experiment conditions. ANOVA statistical results were correlated well with the observations on the change of dependent measures, and also provided insight on the ‘combined’ effects of task difficulty and added time delay.

STEP 5: RPC DETECTION

In the MCIM, although the BPD criterion of the ADS-33 was used for HQ considerations, the PIO notification of the BPD was not applicable to the rate-command rotorcraft model of the MCIM. Alternatively, two RPC detection tools were utilized: the ROVER and the PAC, for the determination of RPC tendencies. These tools are originally developed for warning the pilot ‘online’ about an incipience of an RPC event. However, in the MCIM they were used as ‘offline’ analyses tools to investigate the RPC susceptibility, based on the measured experiment data.

An enhanced version of the ROVER was utilized in the MCIM (e.g., improved peak-to-peak detection), and improvements on RPC detections during several irregular cases were examined during the Aircraft and Rotorcraft Pilot Couplings – Tools and Techniques for Alleviation and Detection (ARISTOTEL) project as well. A typical drawback of the ROVER is the determination of flag thresholds ‘prior’ to a flying task. Generally, historic data from similar flight conditions are used for these thresholds, before any flying task. However, these thresholds do not guarantee to cover the characteristics of the flying task, particularly when the vehicle is exposed to the task for the first time (e.g., a new design). In the MCIM, it was advantageous to use ROVER with measured data ‘after’ the experiment campaign. Therefore, the experiment data gathered from all conditions flown by all human operators lead to overview the overall MCIM experiment, in terms of ROVER threshold considerations.

The second RPC detection tool of the MCIM was the PAC, which was developed during the ARISTOTEL project. The PAC can be considered as an extension to the ROVER, with an aggression parameter accounting for the pilot control activity between detected peaks of vehicle rate response. Akin to the ROVER, PAC was primarily developed for 'online' RPC detection, whereas, MCIM utilized it for 'offline' analyses. Using the PAC extended the understanding of the manual control aggressiveness with respect to the phase delay, which was inherently altered with added time delay conditions. It was particularly useful while interpreting the hypothesized 'back-off' strategy when human operators aimed to avoid RPC occurrences.

7.1.5. GENERAL CONCLUSION

Considering the objective of this thesis, the MCIM was able to successfully determine the configurations where the HQ and the RPC susceptibility of a designed rotorcraft notably deviate, by using the identified parameters of manual control behaviour as **objective** measures. Therefore, it would be possible to elaborate the added time delay and task difficulty combinations that cause a recognizable change of HQ and RPC susceptibility. Such objective measures then could be used at an earlier stage of rotorcraft design, and both the added time delay and task difficulty limitations could be determined objectively without requiring any subjective rating or any constrained 'paper pilot' models.

7.2. RECOMMENDATIONS

In this section, the most important recommendations are categorized for each of the MCIM steps.

7

7.2.1. STEP 1: ROTORCRAFT MODEL

Considering the complicated flight dynamics of a rotorcraft, a very simple rate-response type was used in the MCIM, since it was aimed for the very early stages of the design. However, when the maturity of the vehicle increases with the later stages of the design, the MCIM could still be used if a proper linear vehicle model is provided. Therefore, the MCIM could be integrated to a comprehensive design development program (e.g., part of a development program milestone).

In the MCIM, the selection of the hingeless Bo-105 helicopter model, which was also used for RPC studies during the ARISTOTEL project, provided the ease of using a singular aerodynamic damping term (i.e., M_q). This assumption only holds for the hover and low speed regimes, and it becomes less accurate with increased speed (e.g., the pitch and the heave axes become strongly coupled). The rotorcraft dynamics model could be extended with higher fidelity terms, as exemplified in Section 3.2. Particularly, oscillatory rotor responses, which could couple with the body response within the interested frequency range of the MCIM, could be interesting to examine (e.g., coupling of the short-period mode with the regressive flap mode for moderate and high speed). However, it must be kept in mind that increased rotorcraft model fidelity could require more complex dynamics that would have to be identified. This should be carefully assessed since

the MCIM utilizes a parametric pilot model such that the manual control behaviour is represented by an estimated and identified parametric pilot model. In addition, addressing an articulated rotorcraft design at hover condition resembles the typical fixed-wing longitudinal modes (e.g., short-period and phugoid modes), thus, pilot models used in fixed-wing research could be applied, with appropriate adaptations.

Another approach to extend the application of the MCIM rotorcraft model would be investigating multi-axis tasks, while still using approximate body modes. In literature, there are examples of manual control behaviour identification performed in multi-axis, such as Ref. [9, 42, 149, 150]. For MCIM applications, this would require the rotorcraft model to include coupled or decoupled multiple modes (e.g., longitudinal and heave). Corresponding parametric pilot models must be carefully considered for modeling and identification purposes. Such attempts to extend the rotorcraft model fidelity could also benefit from the 'added dynamics' research in the literature, such as Ref. [72, 89]. Essentially, such studies aim to find which added dynamics could be recognized by human operators, and how they alter their control strategy accordingly. Combining with the scope of the MCIM, such studies could be beneficial to investigate the manual control behaviour for various rotorcraft models with added dynamics, and eventually the MCIM could guide the designer for a larger subset of rotorcraft models.

7.2.2. STEP 2: TASK DIFFICULTY

Akin to the added time delay, the task difficulty could also be applied with a higher precision (i.e., smaller frequency differences between task bandwidths of conditions) around candidate conditions at which crossover regression behaviour would possibly be observed. There are several approaches that could introduce a more realistic task design than the compensatory task that is used in the MCIM. For example, one approach could be using a pursuit task⁸⁰, during which both the reference signal and the rotorcraft state are displayed to the human operator. Then, the human operator can be considered as performing a 'pursuit' to match the rotorcraft response to the displayed reference signal, thus, inherently minimizing the tracking error.

Another approach to increase the realism of the task could be using a predictive tracking task, requiring another type of control: the precognitive control. During this control strategy, the human operator could use a feed-forward control as he/she predicts the rotorcraft response and the task to be flown²⁴. Particularly for RPC studies, this control strategy could potentially help to understand the incipience of an RPC event, during which the 'mental' model of the vehicle perceived by the pilot may change after a triggering condition. This transition is a complicated phenomenon of interest, which was pointed out by McRuer et al⁸⁵. Although such a task would not be applicable to the current LTI structure of the MCIM, it is a considerable potential for further RPC research.

An alternative other approach to could be designing multiple-axis tasks, which could be typical for rotorcraft operations, as discussed in the previous step. However, designing a multi-axis tracking task would require a task design with at least two signals to be

injected to the PVS^{101,147}. Therefore, considering a possible coupling of the manual control behaviour due to the divided attention between these axes, the PSD distribution and task bandwidths of all tasks shall be carefully designed in an RPC study, accompanying the rotorcraft model to be investigated.

A well-known flying task for PIO studies is the Boundary Avoidance Tracking (BAT)³¹, which was also investigated during the ARISTOTEL project¹¹⁵. In summary, the BAT suggests that when a pilot is performing a tracking task, if a task boundary is presented (e.g., high obstacles during a nap-of-the-earth helicopter flight), the pilot switches from the tracking task to a control strategy to prevent from hitting the boundary. Consequently, this means that the pilot utilizes a hybrid control strategy during such a task. Although the current LTI structure of the MCIM is not suitable for such hybrid control behaviour models for identification, extending the MCIM with Linear Time Varying (LTV) capability could bring a beneficial potential to be able use BAT tasks to investigate RPCs.

7.2.3. STEP 3: DISTURBANCE-REJECTION TASK

As mentioned in the previous steps, higher resolutions of added time delay and task difficulty may reveal the limiting conditions (i.e., when human operators exhibit crossover regression strategy) with higher precision, while focusing on a particular PVS design. It must be kept in mind that increasing the number of conditions would also require to increase the number of participants. Therefore, there could be several stages of a MCIM experiment campaign which may be arranged consequentially. For example, since the noticeable regression has occurred at MT with 100 ms of added time delay in the last MCIM experiment, with the same number of participants another MCIM experiment could be conducted by using two closer task difficulties to MT and higher resolution added time delay values between 100 ms and 200 ms (e.g., 100 ms, 150 ms and 200 ms). The limiting conditions could then be more precisely determined.

Although the MCIM utilizes a compensatory display, enabling the physical motion of the simulator may improve the perception of the task by human operators. Thus, corresponding changes of the manual control behaviour with motion may improve the understanding of the combined effects of the added time delay and the task difficulty. It must be noted that including the motion will also require extending the pilot model with the motion cue terms (e.g., the vestibular channel), thus, it would make the analyses more complicated than the current version of the MCIM. Moreover, with the motion cues being included, one must pay attention to the composition of a tracking and a disturbance-rejection task²⁰. For example, the motion cues could be considered as a turbulence field in a disturbance rejection task, whereas in a compensatory task it represents the response of the rotorcraft to a given control input.

A key parameter of the MCIM is the added time delay, which is included as a delay at the control input of the human operator to the rotorcraft model. During the MCIM simulator experiments, possible inherent delays due to control manipulator hardware, real-time software execution and attitude indicator displays were neglected (i.e., we assumed an ideal simulator without any delay). However, such delays could potentially

build-up to considerable values that would affect the PVS analyses, as exemplified for the visual delay in the SRS in Ref. [129]. A remedy would be identifying all sources of such delays in the simulator environment prior to the identification experiments of MCIM, and including these delays in the identification experiment design, and PVS analyses.

7.2.4. STEP 4: PVS ANALYSES

As mentioned in the previous steps, an important limitation of the MCIM is that it uses LTI models. This means that the MCIM cannot function well with strong non-linearities in the PVS, such as a transition from a steady flight to a full-blown PIO. Therefore, the MCIM is limited to pre- and post-PIO conditions, both considered applicable to linear analysis. However, triggering conditions would easily create a transition, which can be only captured by LTV methods. For example, Mitchell and Klyde⁸⁹ discussed the use of wavelet-based scalograms to identify the effects of added dynamics on rotorcraft-pilot interaction, in both the frequency and time domain. Such an LTV approach could be integrated in the MCIM with an appropriate pilot modeling technique, such as the LTV model used in Ref. [101, 139, 148, 150]. It would enhance the capability of the MCIM to capture the transient manual control behaviour during the incipience and development of a full RPC event.

The estimated pilot model in the MCIM contains a second order system, which lumps the neuromuscular system and the control manipulator dynamics. Starting with McRuer⁸⁰, this model has been widely used in pilot model identifications studies^{24,104}. This modeling technique requires as linear as possible control inceptor dynamics (e.g., excluding the friction and the breakout force) for LTI studies (i.e., minimized non-linearity), as described in this thesis. In terms of helicopter controls, Mitchell et al.⁹⁴ state that '*... the low effective mass of the cockpit controls makes the feel-system frequency less important (p. 10).*' Besides, with the fly-by-wire (or -light) technology, and active side-stick control manipulators becoming more common in helicopter control^{30,34}, some RPC studies have been addressing them. For example, Klyde et al.⁶⁰ investigated PIO events with a fly-by-wire system, by using a scalogram-based PIO metric. Considering the future applications of the MCIM, the control inceptor dynamics shall be reconsidered based on the adapted control mechanisms (e.g., decoupling of the neuromuscular system and control manipulator dynamics).

7.2.5. STEP 5: RPC DETECTION

An enhanced version of the ROVER, and the PAC are used in the MCIM as RPC detection tools, which are used for post experiment analyses to determine the RPC susceptibility. An interesting application of MCIM would be designing experiment conditions with 'online' warning ability of these tools, and then comparing the differences between identified manual control behaviours. Therefore, one can objectively assess the effectiveness these RPC warning systems, and understand the conditions that human operators prefer to alter their control strategy. A further improvement would be having a time-variant identification, such that the transition in the control strategy could be captured.

In the PAC, an approximation of average gain response of the vehicle (i.e., H_s) is used as default. Considering the MCIM rotorcraft model, this approximation could be improved by combining the break frequency (i.e., M_q in MCIM) with the corresponding control input frequency. Therefore, particularly high frequency input conditions would be represented more accurately. One could expect that the aggression terms of the PAC would have lower values for such high frequency inputs.

During the ARISTOTEL project, the novel PIO rating scale, Adverse Pilot Coupling Scale (APCS)⁵⁴, showed promising improvements on the common PIO rating scale. Although such subjective rating scales are not in the scope of MCIM, objective measures of the MCIM could still be cross-checked with such ratings, which shall be provided by trained human operators.

REFERENCES

- [1] International Helicopter Safety Team. URL www.ihst.org.
- [2] Butterworth Filter Design. URL <https://mathworks.com/help/signal/ref/butter.html>.
- [3] lsqnonlin - MathWorks. URL <https://www.mathworks.com/help/optim/ug/lsqnonlin.html>.
- [4] Andrews, H. Technical Evaluation Report on the Flight Mechanical Panel Symposium on Flying Qualities. In *AGARD*, AGARD-AR-311, Paris, France, apr 1992.
- [5] Anon. Handling Qualities of Unstable Highly Augmented Aircraft. *AGARD AR-279*, may 1991.
- [6] Anon. ADS-33E-PRF, Handling Qualities Requirements for Military Rotorcraft. Technical Report March, U.S. Army AMCOM, Redstone, AL, mar 2000.
- [7] Anon. Flying Qualities Testing. Technical report, USAF Test Pilot School, Air Force Flight Test Center, Edwards Air Force Base, 2002.
- [8] Aponso, B. L., Mitchell, D. G., and Hoh, R. H. Simulation Investigation of the Effects of Helicopter Hovering Dynamics on Pilot Performance. *Journal of Guidance, Control and Dynamics*, 13(1), 1987.
- [9] Barendswaard, S., Pool, D. M., and Mulder, M. Human Crossfeed in Dual-Axis Manual Control with Motion Feedback. In *Proceedings of the 13th IFAC/IFIP/IFORS/IEA Symposium on Analysis, Design, and Evaluation of Human-Machine Systems*, Kyoto, Japan, 2016.
- [10] Bellera, J. and Varra, G. NH90 ADS-33 Handling Qualities Level 1 Methodology of a Success. In *Royal Aeronautical Society Conference Proceedings: "Rotorcraft Handling Qualities"*, Liverpool, UK, nov 2008.
- [11] Berg, B. A. Locating Global Minima in Optimization Problems by a Random-Cost Approach. *Nature*, (361):708–710, 1993.
- [12] Blanken, C. L. and Pausder, H. J. Investigation of the Effects of Bandwidth and Time Delay on Helicopter Roll Axis Handling Qualities. *Journal of the American Helicopter Society*, 39(3):24–33, 1994.
- [13] Blanken, C. L., Lusardi, J. A., and Al, E. An Investigation of Rotorcraft Stability-Phase Margin Requirements in Hover. In *American Helicopter Society 65th Annual Forum*, Texas,US, 2009.

- [14] Blanken, C. L., Lusardi, J. a., Ivler, C. M., Tischler, M. B., Höfingler, M. T., Decker, W. a., Berger, T., and Tucker, G. E. An Investigation of Rotorcraft Stability-Phase Margin Requirements in Hover. *AHS Forum Handling Qualities Session*, 33 (October 2016), 2009.
- [15] Bottasso, C., Croce, A., Leonello, D., and Riviello, L. Rotorcraft Trajectory Optimization with Realizability Considerations. *Journal of Aerospace Engineering*, 18 (3):146–155, 2005.
- [16] Carlson, R. M. Helicopter Performance-Transportation's Latest Chromosome. *Journal of the American Helicopter Society*, 47(3-17), 2002.
- [17] Cook, M. V. *Flight Dynamics Principles*. Butterworth Heinemann, Burlington,UK, 1st edition, 1997.
- [18] Cooke, A. K. and Fitzpatrick, E. W. H. *Helicopter Test and Evaluation*. AIAA Education Series, Reston, Virginia, US, 2002.
- [19] Cooper, G. E. and Harper, R. P. J. The Use of Pilot Rating in the Evaluation of Aircraft Handling Qualities. *AGARD AR-567*, jul 1969.
- [20] Damveld, H. J. *A Cybernetic Approach to Assess the Longitudinal Handling Qualities of Aeroelastic Aircraft*. Ph.D. thesis, Delft University of Technology, The Netherlands, 2009.
- [21] Dodge, J. S. Incorporating Practical Experience with Aeronautical Design Standard 33 in the United States Naval Test Pilot School Rotary Wing Curriculum. M.Sc. thesis, University of Tennessee-Knoxville, US, 2004.
- [22] Dornheim, M. A. Report Pinpoints Factors Leading to YF-22 Crash. *Aviation Week & Space Technologies*, pages 53–54, nov 1992.
- [23] Drezner, J. A., Smith, G. K., Horgan, L. E., Rogers, C., and Schmidt, R. Maintaining Future Military Aircraft Design Capability. *US R-4199-AF*, pages 1–86, 1992.
- [24] Drop, F. *Control-Theoretic Models of Feedforward in Manual Control*. Ph.D. thesis, Delft University of Technology, The Netherlands, 2016.
- [25] Efremov, A. V., Korovin, A. A., and Koshelenko, A. V. Modification of the approaches to flying qualities and PIO event prediction . In *Proceedings of the EuroGNC 2013, 2nd CEAS Specialist Conference on Guidance, Navigation & Control*, Delft, Netherlands, apr 2013.
- [26] Elkind, J. J. *Characteristics of Simple Manual Control Systems*. Ph.D. thesis, Massachusetts Institute of Technology, 1956.
- [27] Flynn, W. A. and Lee, R. E. AGARD. *AGARD*, CP-560:23(1)–23(6), 1995.

- [28] Forrest, J. S., Kaaria, C. H., and Owen, I. Determining the Impact of Hangar-Edge Modifications on Ship-Helicopter Operations using Offline and Piloted Helicopter Flight Simulation. In *American Helicopter Society 66th Annual Forum & Technology Display*, Phoenix, US, 2010.
- [29] Fox, R. G. The History Of Helicopter Safety. In *International Helicopter Safety Symposium*, pages 1–19, Quebec, Canada, 2005.
- [30] Gibson, J. C. *Development of a methodology for excellence in handling qualities design for fly by wire aircraft*. Ph.D. thesis, Delft University of Technology, The Netherlands, 1999.
- [31] Gray, W. R. Boundary Avoidance Tracking: A new Pilot Tracking Model. In *AIAA Atmospheric Flight Mechanics Conference*, AIAA 2005-5810, San Francisco, CA, US, 2005.
- [32] Gray, W. R. Handling Qualities Evaluation at the USAF Test Pilot School. In *AIAA Atmospheric Flight Mechanics Conference*, AIAA-2009-6317, Chicago, Illinois, aug 2009.
- [33] Ham, J. A. and Tischler, M. B. Flight Testing and Frequency Domain Analysis for Rotorcraft Handling Qualities Characteristics. In *NASA/AHS Specialist Meeting*, NASA-CP-3220, jan 1993.
- [34] Hamel, P. *In-Flight Simulators and Fly-by-Wire/Light Demonstrators: A Historical Account of International Aeronautical Research*. Springer International Publishing, Gewerbestrasse 11, Cham (ZG), Switzerland, 1 edition, 2017.
- [35] Hamel, P. G. Rotorcraft-Pilot Coupling. *AGARD CP-592*, pages 235–243, apr 1997.
- [36] Heffley, R. K. and Al, E. A Compilation and Analysis of Helicopter Handling Qualities Data, Volume One: Data Compilation, Volume Two: Data Analysis. Technical Report NASA Contractor Reports 3144 & 3145, NASA, aug 1979.
- [37] Hess, R. A. The Effects Of Time Delays On Systems Subject To Manual Control. *Journal of Guidance, Control and Dynamics*, 7(4):416–421, 1984.
- [38] Hess, R. A. A Model-Based Theory for Analyzing Human Control Behavior. *Advances in Man- Machine Systems Research*, 2(1):129–175, 1985.
- [39] Hess, R. A. Unified Theory for Aircraft Handling Qualities. *Journal of Guidance, Control and Dynamics*, 20(6):1141–1148, 1997.
- [40] Hess, R. A. Obtaining multi-loop pursuit-control pilot models from computer simulation. *Journal of Aerospace Engineering*, 222(189), 2008.
- [41] Hess, R. A. Analytical Assesment of Performance, Handling Qualities, and Added Dynamics in Rotorcraft Flight Control. *IEEE Transactions on Systems, Man, and Cybernetics-Part A:Systems and Humans*, 39(1):262–271, 2009.

- [42] Hess, R. A. Modeling Pilot Control Behavior with Sudden Changes in Vehicle Dynamics. *Journal of Aircraft*, 46(5):1584–1592, 2009.
- [43] Hodgkinson, J., Rossitto, K. F., and Kendall, E. R. The Use and Effectiveness of Piloted Simulation in Transport Aircraft Research and Development. Technical Report ADP006872, Douglas Aircraft, Long Beach, CA, US, feb 1992.
- [44] Hoh, R. H. New Developments in Flying Qualities Criteria with Application to Rotary Wing Aircraft. In *Specialists Meeting on Helicopter Handling Qualities*, NASA-CP-2219, page 247, California, US, 1982. NASA.
- [45] Hoh, R. H. Dynamic Requirements in the New Handling Qualities Specification for US Military Rotorcraft. In *Helicopter Handling Qualities and Flight Control, RAeSoc International Conference*, London, UK, 1988.
- [46] Hoh, R. H. Lessons learned concerning the interpretation of subjective Handling Qualities Pilot Rating Data. In *AIAA Atmospheric Flight Mechanics Conference*, Portland, US, aug 1990.
- [47] Hoh, R. H. and Ashkenas, I. L. Development of VTOL Flying Qualities Criteria for Low Speed and Hover. Technical Report TR-1116-1, Systems Technology Inc., California, US, 1979.
- [48] Hoh, R. H. and Heffley, R. K. Development of Handling Qualities Criteria for Rotorcraft with Externally Slung Loads. In *American Helicopter Society 58th Annual Forum*, Montreal, Canada, jun 2002.
- [49] Hoh, R. H. and Mitchell, D. G. The Role of Handling Qualities Specifications in Flight Control System Design. In *Flight Mechanics Panel Symposium*, Turin, Italy, may 1994.
- [50] Hoh, R. H., Mitchell, D. G., Aponso, B. L., Key, D. L., and Blanken L., C. Background Information and User's Guide for Handling Qualities Requirements for Military Rotorcraft. Technical report, U.S. Army Aviation Systems Command, Moffett Field, CA, dec 1989.
- [51] Hosman, R., Abbink, D. A., and Cardullo, F. M. The Neuromuscular System. In *AIAA Modeling and Simulation Technologies Conference 2010*, pages 1–13, Toronto, Italy, 2010.
- [52] Jones, M., Jump, M., and Lu, L. Development of the Phase-Aggression Criterion for Rotorcraft—Pilot Coupling Detection. *Journal of Guidance, Control, and Dynamics*, 36(1):35–47, 2013.
- [53] Jones, M. G. *Prediction, Detection, and Observation of Rotorcraft Pilot Couplings*. Ph.D. thesis, University of Liverpool, UK, 2015.
- [54] Jones, M. G. and Jump, M. New Methods to Subjectively and Objectively Evaluate Adverse Pilot Couplings. *Journal of the American Helicopter Society*, 60(1):1–13, 2015.

- [55] Kaletka, J. and Gimonet, B. Identification of Extended Models from BO 105 Flight Test Data for Hover Flight Condition. In *European Rotorcraft Forum*, 21, pages VII/7.1–7.16, Saint Petersburg, Russia, 1995.
- [56] Kaletka, J., Grünhagen, W. V., Tischler, M. B., and Fletcher, J. W. Time and Frequency-Domain Identification and Verification of Bo 105 Dynamic Models. In *European Rotorcraft Forum*, Amsterdam, The Netherlands, 1989.
- [57] Kay, S. M. *Fundamentals of Statistical Signal Processing; Estimation Theory*. Prentice-Hall Signal Processing Series. Prentice-Hall, Inc., 1 edition, 1993.
- [58] Kirby, M. R. *A Methodology For Technology Identification, Evaluation, And Selection In Conceptual And Preliminary Aircraft Design*. Ph.D. thesis, Georgia Institute of Technology, US, 2001.
- [59] Kleinman, D. L., Baron, S., and Levison, W. H. An Optimal Control Model of Human Response Part I : Theory and Validation. *Automatica*, 6(1):357–369, 1970.
- [60] Klyde, D. H., Schulze, P. C., Mello, R. S., and Mitchell, D. Assessment of a Scalogram-Based PIO Metric with Flight Test Data. In *AIAA Atmospheric Flight Mechanics Conference*, AIAA 2017-1641, Texas, US, 2017.
- [61] Kok, J. and Wijk, R. van. *Evaluation of models describing human operator control of slowly responding complex systems*. Ph.D. thesis, Delft University of Technology, The Netherlands, 1978.
- [62] Kumar, M. V., Prasad, S., Suresh, S., Omkar, S. N., and Ganguli, R. Design of a Stability Augmentation System for a Helicopter Using LQR Control and ADS33 Handling Qualities Specifications. *Aircraft Engineering and Aerospace Technology: An International Journal*, 80(2):111–123, 2008.
- [63] Kun, Z., Lixin, W., and Xiangsheng, T. Flying qualities reduction of fly-by-wire commercial aircraft with reconfiguration flight control laws. *Procedia Engineering*, 17: 179–196, 2011.
- [64] Lawler, M. A., Ivler, C. M., Tischler, M. B., and Shtessel, Y. B. System Identification of the Longitudinal/Heave Dynamics for a Tandem-Rotor Helicopter Including Higher-Order Dynamics. In *AIAA Atmospheric Flight Mechanics Conference*.
- [65] Lawrance, B. and Padfield, G. D. Handling Qualities Analysis of the Wright Brothers' 1902 Glider. *Journal of Aircraft*, 42(1):224–236, 2005.
- [66] Levine, W. S., editor. *The Control Handbook*. IEE and CRC press, 1 edition, 1996.
- [67] Levison, W. H. and Papizian, B. The Effects of Time Delay and Simulator Mode on Closed-loop Pilot/Vehicle Performance - Model Analysis and Manned Simulation Results. In *Flight Simulation Technologies Conference*, Monterey, CA, US, 1987.
- [68] Lone, M. M. and Cooke, A. K. Development of a Pilot Model Suitable for the Simulation of Large Aircraft. In *27th International Congress of the Aeronautical Sciences*, pages 1–15, Nice, France, sep 2010.

- [69] Lone, M. M. and Cooke, A. K. Review of pilot modeling techniques. In *48th AIAA Science Meeting Including the New Horizons Forum and Aerospace Exposition*, AIAA-2010-297, Orlando, Florida, US, jan 2010.
- [70] Lone, M. M. and Cooke, A. K. Pilot-model-in-the-loop simulation environment to study large aircraft dynamics. *Proceedings of the Institution of Mechanical Engineers, Part G: Journal of Aerospace Engineering*, 227(3):555–568, mar 2012.
- [71] Lone, M. M. and Cooke, A. K. Review of pilot models used in aircraft flight dynamics. *Aerospace Science and Technology*, 34(1):55–74, 2014.
- [72] Lu, T., Pool, D. M., Paassen, M. M. van, and Mulder, M. Quantifying the Effects of Added Dynamics with Human Operator Control Behavior Measurements and Simulations. In *Proceedings of the AIAA Modeling and Simulation Technologies Conference*, AIAA-2017-3667, Denver, US, 2017.
- [73] Mackenzie, R. *Flight of the V-22 Osprey DVD*. Discovery Communications LLC, 2012.
- [74] Mariano, V. and Guglieri, G. Application of pilot induced oscillations prediction criteria to rotorcraft. In *American Helicopter Society 67th Annual Forum*, Virginia Beach, US, 2011.
- [75] McDonnell, J. D. Pilot Rating Techniques for the Estimation and Evaluation of Handling Qualities. Technical Report AFFDL-TR-68-76, Air Force Flight Dynamics Laboratory, dec 1968.
- [76] McRuer, T. D. Pilot-Induced Oscillations and Human Dynamic Behavior. Technical Report July, NASA, 1995.
- [77] McRuer, D. T. Human Dynamics in Man-Machine Systems. *Automatica*, 16(1): 237–253, 1980.
- [78] McRuer, D. T. Active Control Technology and Interdisciplinary Interactions. *AGARD*, CP-560:K1–1, K1–9, 1994.
- [79] McRuer, D. T. and Graham, D. Pilot-vehicle control systems analysis. In Langford, R. C. and Mundo, C. J., editors, *AIAA Guidance and Control Conference*, Cambridge, 1963. AIAA Academic Press.
- [80] McRuer, D. T. and Jex, H. R. A Review of Quasi-linear Pilot Models. *IEEE Transactions on Human Factors in Electronics*, HFE-8(3):231–249, 1967.
- [81] McRuer, D. T. and Krendel, E. S. Dynamic Response of Human Operators. *WADC-TR-56-524*, 1957.
- [82] McRuer, D. T. and Krendel, E. S. Mathematical Models of Human Pilot Behaviour. *AGARD*, (AGARD-AG-188):1–92, jan 1974.

- [83] McRuer, D. T., Graham, D., Krendel, E. S., and Reisener Jr., W. Human Pilot Dynamics in Compensatory Systems. Theory, Models and Experiments with Controlled Element and Forcing Function Variations. *AFFDL-TR-65-15*, 1965.
- [84] McRuer, D. T., Clement, W. F., Thompson, P. M., and Magdaleno, E. Minimum Flying Qualities Volume II: Pilot Modeling for Flying Qualities Applications. Technical report, Flight Dynamics Laboratory, Wright Research and Development Center, Ohio, US, Jan 1990.
- [85] McRuer, T. D., Droste, C. S., Hess, R. A., LeMaster, D. P., Mathhews, S., McDonnel, J., McWhae, J., Melvin, W. W., and Pew, R. W. *Aviation Safety and Pilot Control: Understanding and Preventing Unfavorable Pilot-Vehicle Interactions*. National Academy Press, Washington DC, US, 1997.
- [86] Michel, M., Hijum, M. van, and Al, E. The European Helicopter Safety Team (EHST): 2008/2009 Achievements. In *35th European Rotorcraft Forum (ERF)*, pages 1–14, Hamburg, Germany, Sep 2009.
- [87] Mitchell, D. G. Identifying the Pilot in Pilot-Induced Oscillations. In *AIAA Atmospheric Flight Mechanics Conference*, AIAA-2000-3985, Denver, US, Aug 2000.
- [88] Mitchell, D. G. and Hoh, R. Development of Methods and Devices to Predict and Prevent Pilot-Induced Oscillation. *AFRL-VA-WP-TR-2000-3046*, 2000.
- [89] Mitchell, D. G. and Klyde, D. H. Recommended Practices for Exposing Pilot-Induced Oscillations or Tendencies in the Development Process. In *USAF Developmental Test and Evaluation Summit - U.S. Air Force T&E Days Conferences*, AIAA 2004-6810, California, US, 2004.
- [90] Mitchell, D. G. and Klyde, D. H. Testing for Pilot-Induced Oscillations. In *AIAA Atmospheric Flight Mechanics Conference and Exhibit*, San Francisco, CA, US, 2005.
- [91] Mitchell, D. G. and Klyde, D. H. Identifying a PIO Signature - New Techniques Applied to an Old Problem. In *AIAA Atmospheric Flight Mechanics Conference and Exhibit*, Keystone, Colorado, US, 2006.
- [92] Mitchell, D. G. and Klyde, D. H. Identifying a Pilot-Induced Oscillation Signature: New Techniques Applied to Old Problems. *Journal of Guidance, Control, and Dynamics*, 31(1):215–224, 2008.
- [93] Mitchell, D. G., Hoh, R. H., Jr, A. A., and Key, D. L. Ground based simulation evaluation of the effects of time delays and motion on rotorcraft handling qualities. Technical Report AD-A256 921, US Army Aviation Systems Command-Aeroflightdynamics Directorate, Moffett Field, CA, US, Jan 1992.
- [94] Mitchell, D. G., Aponso, B. L., and Klyde, D. H. Feel Systems and Flying Qualities. In *AIAA 20th Atmospheric Flight Mechanics Conference*, Baltimore, MD, US, 1995. AIAA.

- [95] Mitchell, D. G., Arencibia, A. J., and Munoz, S. Real-Time Detection of Pilot-Induced Oscillations. In *AIAA Atmospheric Flight Mechanics Conference*, Providence, US, 2004.
- [96] Mitchell, D. G., Doman, D. B., Key, D. L., Klyde, D. H., Leggett, D. B. Moorehouse, D. J., Mason, D. H., Raney, D. L., and Schmidt, D. K. Evolution, Revolution and Challenges of Handling Qualities. *Journal of Guidance, Control and Dynamics*, 27 (1):12–28, 2004.
- [97] Mitchell, D. G., Nicoll, T. K., Fallon, M. P., and Roark, S. H. Rotorcraft Handling Qualities for Shipboard Operations. In *AIAA Atmospheric Flight Mechanics Conference*, August, pages 1–10, Chicago, Illinois, US, aug 2009.
- [98] Mitchell, D. G., Nicoll, T. K., Klyde, D. H., and Schulze, C. Determining Effects of Time-Varying Rotorcraft Dynamics on Pilot Control. In *AIAA Atmospheric Flight Mechanics Conference*, August, pages 1–9, Chicago, Illinois, 2009.
- [99] Morgan, J. M. and Baillie, S. W. ADS-33C Related Handling Qualities Research Performed using the NRC Bell 205 Airborne Simulator. Technical report, NASA Ames Research Center, San Francisco, CA, US, jan 1993.
- [100] Mulder, M. *Cybernetics of tunnel-in-the-sky displays*. Ph.D. thesis, Delft University of Technology, The Netherlands, 1999.
- [101] Mulder, M., Pool, D. M., Abbink, D. A., Boer, E. R., Zaal, P. M. T., Drop, F. M., El, K. van der, and Paassen, M. M. van. Manual Control Cybernetics: State-of-the-Art and Current Trends. *IEEE Transactions on Human-Machine Systems*, pages 1–18, 2017.
- [102] Muscarello, V., Masarati, P., and Quaranta, G. Multibody analysis of rotorcraft pilot coupling. In *Proceedings of the second joint international conference on multibody system dynamics*, IMSD 2012, Stuttgart, Germany, 2012.
- [103] Neal, T. P. and Smith, R. E. An In-flight Investigation to Develop Control System Design Criteria for Fighter Airplanes. *AD880426*, nov 1971.
- [104] Nieuwenhuizen, F., Beykirch, K. A., Mulder, M., and Bulthoff, H. H. Identification of Pilot Control Behaviour in a Roll-Lateral Helicopter Hover Task. In *AIAA Modeling and Simulation Technologies Conference and Exhibit*, South Carolina, US, 2007.
- [105] Nieuwenhuizen, F. M., Zaal, P. M. T., Mulder, M., Van Paassen, M. M., and Mulder, J. A. Modeling Human Multichannel Perception and Control Using Linear Time-Invariant Models. *Journal of Guidance, Control, and Dynamics*, 31(4):999–1013, jul 2008.
- [106] NTSB. National Transportation Safety Board (Aircraft Accident Report). Technical Report NTSB/AAR-00/02 (DCA97MA055), Washington DC, US, 1997.
- [107] Ockier, C. J. Pilot Induced Oscillations in Helicopters - Three Case Studies. Technical Report IB 111-96/12, DLR, Braunschweig, Germany, 1996.

- [108] Ockier, C. J. Pilot Induced Oscillations in Helicopters - Three Case Studies. Technical Report 111-96/12, DLR-IB, 1996.
- [109] Ockier, C. J. and Pausder, H. J. Experiences with ADS-33 Helicopter Specification Testing and Contributions to Refinement Research. *AGARD*, (CP-560):1-4,4-20, 1995.
- [110] O'Rourke, R. V-22 Osprey Tilt-Rotor Aircraft: Background and Issues for Congress. *Congressional Research Service*, (7-5700 RL31384), 2009.
- [111] Padfield, G. D. *Helicopter Flight Dynamics*. Blackwell Publishing Ltd, Oxford, UK, 2nd edition, jan 2007.
- [112] Padfield, G. D. Rotorcraft Handling Qualities Engineering: Managing the Tension between Safety and Performance. *Journal of the American Helicopter Society*, 58 (1):1-27, jan 2013.
- [113] Padfield, G. D., Charlton, M. T., and Kimberley, A. K. Helicopter Flying Qualities in Critical Mission Task Elements; Initial Experience with the DRA Bedford Large Motion Simulator. In *18th European Rotorcraft Forum*, Avignon, France, sep 1992.
- [114] Pavel, M. D. *On the Necessary Degrees of Freedom for Helicopter and Wind Turbine Low-Frequency Mode Modeling*. Ph.D. thesis, Delft University of Technology, The Netherlands, 2001.
- [115] Pavel, M. D., Jump, M., Dang-Vu, B., Masarati, P., Gennaretti, M., Ionita, A., Zaichik, L., Smaili, H., Quaranta, G., Yilmaz, D., Jones, M., Serafini, J., and Malecki, J. Adverse rotorcraft pilot couplings—Past, present and future challenges. *Progress in Aerospace Sciences*, 62:1-51, oct 2013.
- [116] Perhinschi, M. and Prasad, J. V. R. Analytical Investigation of Helicopter Handling Qualities Criterion using a Structural Pilot Model. In *AIAA 20th Atmospheric Flight Mechanics Conference*, AIAA-95-3456-CP, Baltimore, MD, US, 1995.
- [117] Phillips, W. H. Flying qualities from early airplanes to the Space Shuttle. *Journal of Guidance, Control and Dynamics*, 12(4):449-459, 1989.
- [118] Pintelon, R. and Schoukens, J. *System Identification, A Frequency Domain Approach*. IEEE Press, 445 Hoes Lane, Piscataway, New Jersey, US, 2001.
- [119] Pool, D. M., Zaai, P. M. T., Van Paassen, M. M., and Mulder, M. Identification of Multimodal Pilot Models Using Ramp Target and Multisine Disturbance Signals. *Journal of Guidance, Control and Dynamics*, 34(1):86-97, 2011.
- [120] Pratt, R. *Flight Control Systems, practical issues in design and implementation*. IEE, Control Engineering Series 57, Herts., UK, 2000.
- [121] Prouty, R. W. *Helicopter Aerodynamics*. Eagle Eye Solutions, LLC, 1st edition, 2009.

- [122] Rohlf, M., Grünhagen, W., and Kaletka, J. Nonlinear Rotorcraft Modeling and Identification. In *RTO SCI Symposium*, May, pages 5–7, Madrid, Spain, 1998. RTO MP-11.
- [123] Roscoe, A. H. and Ellis, G. A. A Subjective Rating Scale for Assessing Pilot Workload in Flight: A Decade of Practical Use. Technical Report TR-90019, Royal Aerospace Establishment, Hampshire, UK, mar 1990.
- [124] Sébastien, K. and Mathieu, M. Mathematical Study of Linear and Nonlinear Rotorcraft Pilot-Induced Oscillations. In *ICAS 27th International Congress of the Aeronautical Sciences*, pages 1–7, Nice, France, 2010.
- [125] Shafer, M. E. and Steinmetz, P. Pilot-Induced Status Oscillation at the End of the Century. *NASA/CP-2001-210389*, 2, 2001.
- [126] Slack, M. The Probability Distributions of Sinusoidal Oscillations Combined in Random Phase. *Journal of the Institution of Electrical Engineers. Part 3. Radio and communication engineering*, 93(22):76–86, 1946.
- [127] Smith, R. E. A Unifying Theory for Pilot Opinion Rating. In *12th Annual Conference on Manual Control*, NASA-TM-73, pages 542–558, may 1976.
- [128] Smith, R. E. and Sarrafian, S. K. Effect of Time Delay on Flying Qualities: An Update. Technical report, NASA, California, US, aug 1986.
- [129] Stegeman, B. Effects of Visual Delay on Manual Control in Flight Simulators. M.Sc. thesis, Delft University of Technology, The Netherlands, 2013.
- [130] Suliman, S. M. T. Apply the Real-time Oscillation VERifier (ROVER) to detect Rotorcraft Pilot Couplings (RPCs). M.Sc. thesis, Delft University of Technology, The Netherlands, 2012.
- [131] Suliman, S. M. T., Yilmaz, D., and Pavel, M. D. Harmonizing Real - Time Oscillation Verifier (Rover) with Handling Qualities Assessment for Enhanced Rotorcraft Pilot Couplings Detection. In *38th European Rotorcraft Forum (ERF)*, Amsterdam, The Netherlands, 2012.
- [132] Thompson, P. and McRuer, D. T. Comparison of the human optimal control and crossover models. In *AIAA Guidance, Navigation and Control Conference*, AIAA-88-4183, Reston, Virginia, US, aug 1988. doi: 10.2514/6.1988-4183.
- [133] Tischler, M. B. and Cauffman, M. G. Frequency-Response Method for Rotorcraft System Identification: Flight Applications to BO 105 Coupled Rotor/Fuselage Dynamics. *Journal of the American Helicopter Society*, 37(3), 1992.
- [134] Tischler, M. B. and Remple, R. K. *Aircraft and Rotorcraft System Identification*. AIAA Education Series, 2nd edition, 2012.
- [135] Tischler, M. B., Fletcher, J. W., and Morris, P. M. Applications of Flight Control System Methods to an Advanced Combat Rotorcraft. In *USAASCOM Conference*, 89-A-002, California, US, jul 1989.

- [136] U.S. Department of Defense. Flying Qualities of Piloted Aircraft. *MIL-STD-1797A*, pages 1–717, aug 1997.
- [137] U.S. JHSAT. The Compendium Report: The U.S. JHSAT Baseline of Helicopter Accident Analysis, Volume-I. jul 2011.
- [138] U.S. JHSAT. The Compendium Report: The U.S. JHSAT Baseline of Helicopter Accident Analysis, Volume-II. aug 2011.
- [139] Grootheest, A. van, Pool, D. M., Paassen, M. M. van, and Mulder, M. Identification of Time-Varying Manual Control Adaptations with Recursive ARX Models. In *Proceedings of the AIAA Modeling and Simulation Technologies Conference, Kissimmee (FL)*, AIAA-2018-0118, Florida, US, 2018.
- [140] Van Lunteren, A. *Identification of Human Operator Describing Function Models with One or Two Inputs in Closed Loop Systems*. Ph.D. thesis, Delft University of Technology, The Netherlands, 1979.
- [141] Vreeken, J. and Stevens, J. European Helicopter Safety Team (EHST): Technological Solutions Mitigating Helicopter Safety Issues. In *38th European Rotorcraft Forum (ERF)*, pages 1–11, Amsterdam, The Netherlands, 2012.
- [142] Weber, G., Efremov, A. V., and Ogloblin, A. V. Development of Criteria for Flying Qualities Prediction Using Structural Modelling of Human Pilot Behaviour in the Longitudinal Precise Tracking Task. In *European Conference for Aerospace Sciences (EUCASS)*, France, 2005.
- [143] Webster, F. and Smith, T. D. Flying Qualities Flight Testing of Digital Flight Control Systems. *AGARD RTO-AG-300*, 21(December), 2001.
- [144] White, T. N. *Human supervisory control behavior: Verification of a cybernetic mode*. Ph.D. thesis, Delft University of Technology, The Netherlands, 1983.
- [145] Williams, J. N., Ham, J. A., and Tischler, M. B. Flight Test Manual: Rotorcraft Frequency Domain Flight Testing. Technical report, U.S. Army Aviation Technical Test Center, Airworthiness Qualification Test Directorate, sep 1995.
- [146] Wilson, D. J. and Riley, D. R. Cooper-Harper Rating Variability. In *Atmospheric Flight Mechanics Conference*, Boston, US, aug 1989.
- [147] Zaal, P. M. T. *Pilot Control Behavior Discrepancies Between Real and Simulated Flight Caused by Limited Motion Stimuli*. Ph.D. thesis, Delft University of Technology, The Netherlands, 2011.
- [148] Zaal, P. M. T. Manual Control Adaptation to Changing Vehicle Dynamics in Roll-Pitch Control Tasks. *Journal of Guidance, Control, and Dynamics*, 39(5):1046–1058, 2016.
- [149] Zaal, P. M. T. and Mobertz, X. R. I. Effects of Motion Cues on the Training of Multi-Axis Manual Control Skills. In *Proceedings of the AIAA Modeling and Simulation Technologies Conference*, AIAA-2017-3473, Denver, US, 2017.

-
- [150] Zaal, P. M. T. and Sweet, B. Identification of Time-Varying Pilot Control Behavior in Multi-Axis Control Tasks. In *AIAA Modeling and Simulation Technologies Conference, Guidance, Navigation, and Control*, pages 1–20, Minnesota, US, 2012.
 - [151] Zaal, P. M. T., Pool, D. M., Mulder, M., and Paassen, M. M. van. New Types of Target Inputs for Multi-Modal Pilot Model Identification. In *AIAA Modeling and Simulation Technologies Conference and Exhibit*, Honolulu, 2008.
 - [152] Zaroni, A., Masarati, P., and Quaranta, G. Rotorcraft pilot impedance from biomechanical model based on inverse dynamics. In *IMECE*, Houston, Texas, 2012.
 - [153] Zaychik, K. B., Cardullo, F. M., and George, G. A Conspectus on Operator Modeling : Past , Present and Future. In *AIAA Modeling and Simulation Technologies Conference and Exhibit*, August, pages 1–17, Keystone, Colorado, US, aug 2006.

A

SUBJECTIVE RATING SCALES

This appendix provides the subjective rating scales that have been referred to in the thesis. The first section provides the HQR for handling qualities assessment. The second section presents the PIO rating scale. The third section provides the APCS subjective rating scale which was developed and tested during the ARISTOTEL project. The last section describes the BedfordWork Loading Scale Ratings (Bedford Work Loading Scale Ratings (WLR)) to assess the pilot workload.

A.1. HANDLING QUALITIES RATING SCALE

Cooper-Harper handling qualities rating scale¹⁹, i.e., HQR, is shown in Figure A.1.

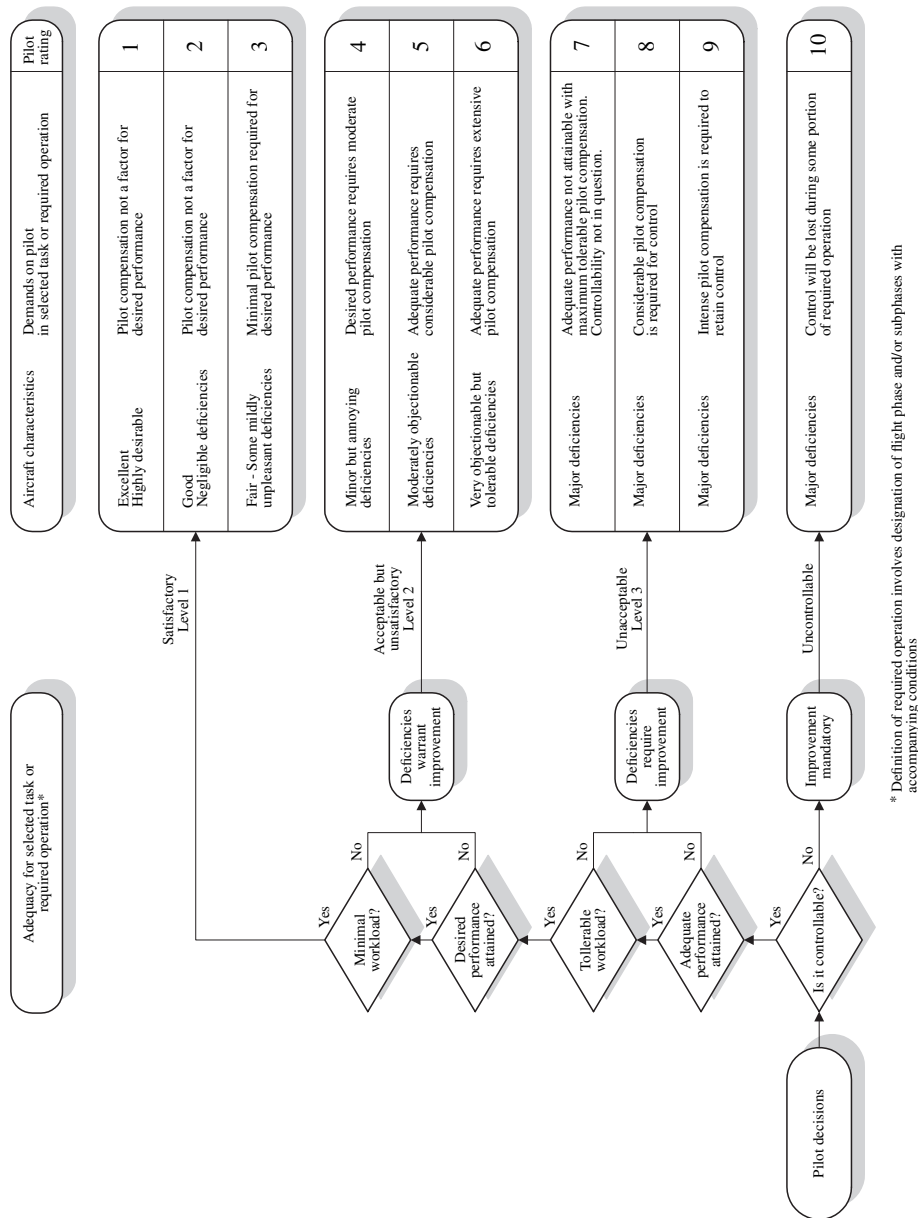


Figure A.1: Cooper-Harper handling qualities ratings scale¹⁹, adapted from Ref. [20].

A.2. PILOT INDUCED OSCILLATIONS RATING SCALE

Pilot induced oscillations rating scale¹³⁶, i.e., PIOR, is shown in Figure A.2.

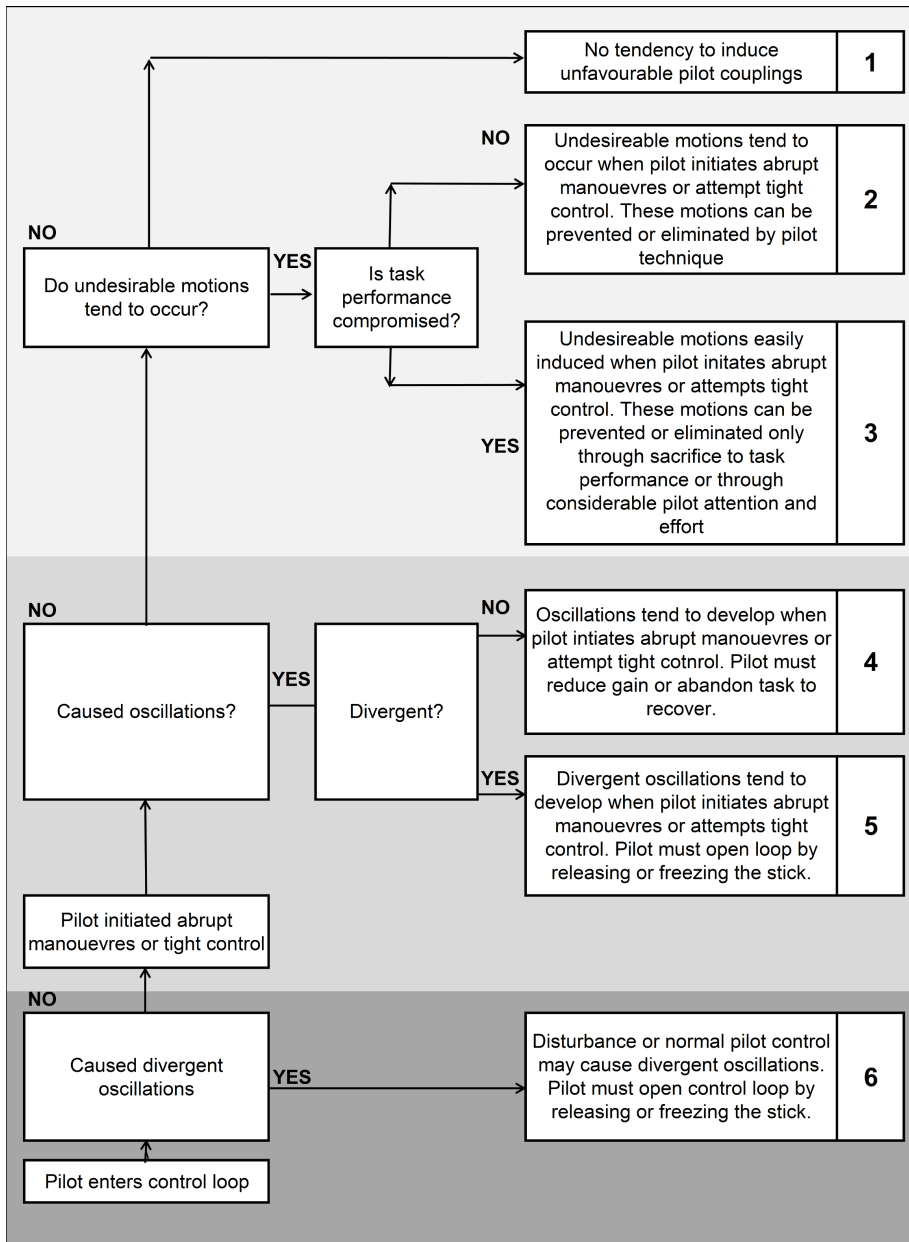


Figure A.2: PIOR scale, adapted from Ref. [136]

A.3. ADVERSE PILOT COUPLING SCALE

The APCS⁵⁴, which was developed and used in the flight simulator test campaigns of ARISTOTEL, is provided in Figure A.3.

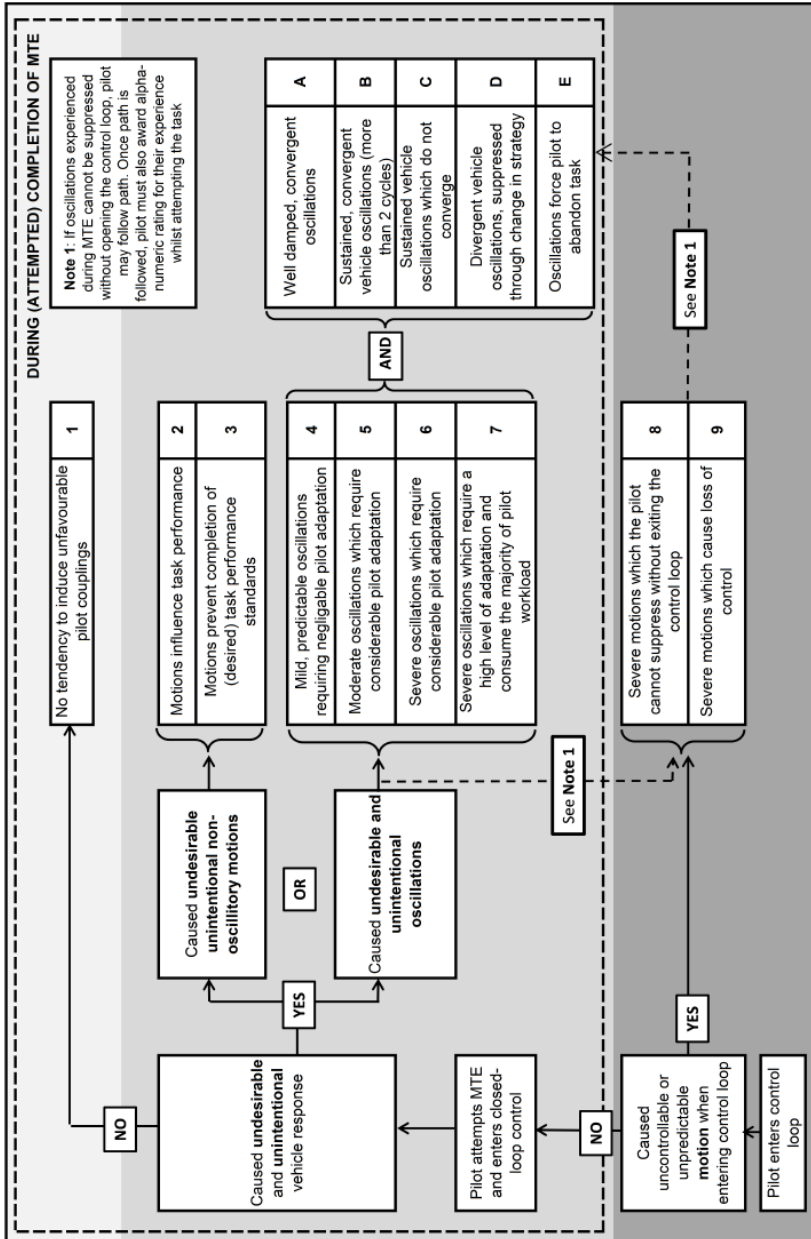


Figure A.3: APCS, adapted from Ref. [54]

A.4. WORKLOAD RATING SCALE

The Bedford workload ratings scale¹²³ is a 10-point subjective rating scale, which reflects the pilot's spare capacity to perform additional tasks. In WLR, a rating of one is assigned to tasks that present the least difficulty, and higher ratings represent increasing task difficulty such that pilot's capacity to perform additional tasks diminishes, as shown in Figure A.4. WLR is based on the established HQR^{19,28}.

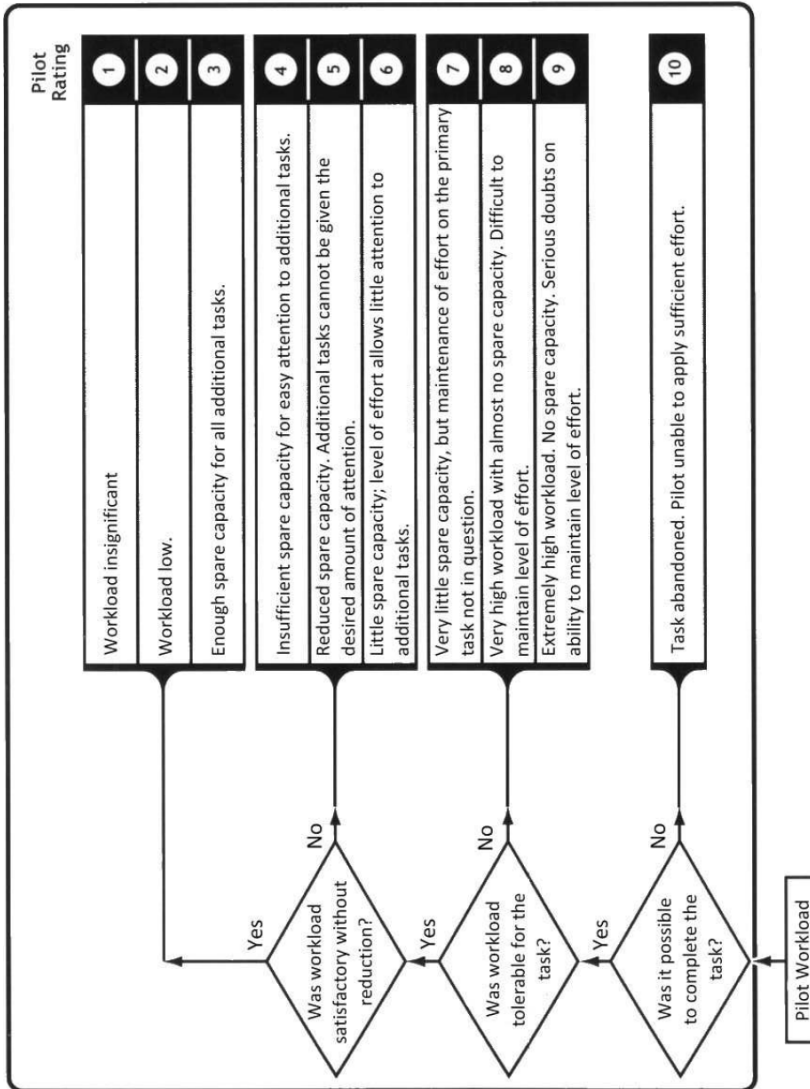


Figure A.4: WLR scale, adapted from Ref. [123]

ACRONYMS

A/RPC	Aircraft / Rotorcraft Pilot Couplings	2
RPC	Rotorcraft Pilot Coupling	173
PIO	Pilot Induced Oscillations	175
ARISTOTEL	Aircraft and Rotorcraft Pilot Couplings – Tools and Techniques for Alleviation and Detection	179
HQ	Handling Qualities	173
ADS	Aerodynamic Design Standard	173
MTE	Mission Task Element	6
ACAH	Attitude Command/Attitude Hold	
SCAS	Stability Control Augmentation System	21
ROVER	Realtime Oscillation Verifier	175
PAC	Phase Aggression Criteria	175
PIW	Pilot Inceptor Workload	85
DC	Duty Cycle	85
A_G	Aggression term	85
BPD	Bandwidth Phase Delay	173
OCM	Optimal Control Model	28
BAT	Boundary Avoidance Tracking	182
HQSF	Handling Qualities Sensitivity Function	7
HQDT	Handling Qualities During Tracking	44
PAO	Pilot Assisted Oscillations	34
FBW	Fly By Wire	16
DLR	German Aerospace Center	3
DoF	Degree of Freedom	59
IHST	International Helicopter Safety Team	1
SAS	Stability Augmentation System	2
USAF-TPS	United States Air Force - Test Pilot School	17
SRS	SIMONA Research Simulator	178
UoL	University of Liverpool	74
HHS	HeliFlight Helicopter Simulator	178

HFR	HeliFlight-R Helicopter Simulator	46
HQR	Handling Qualities Ratings	173
PIOR	Pilot Induced Oscillations Ratings	173
APCS	Adverse Pilot Coupling Scale	184
WLR	Bedford Work Loading Scale Ratings	197
RMS	Root Mean Square	76
MLE	Maximum Likelihood Estimation	179
ET	Easy Task	176
MT	Moderate Task	176
HT	Hard Task	176
ANOVA	Analysis of Variance	178
MCIM	Manual Control Identification Method	174
EBMM	Experimental Behavior Measurement Method	53
PSD	Power Spectral Density	175
CE	Controlled Element	175
PVS	Pilot Vehicle System	174
LTI	Linear Time Invariant	174
LTV	Linear Time Varying	182
FCM_{wO}	Fourier Coefficients Method with Optimization	179
VAF	Variance Accounted For	179
LQR	Linear Quadratic Regulator	63
SISO	Single Input Single Output	67

LIST OF SYMBOLS

Roman symbols

$H_{CE}(j\omega)$	Controlled element linear response dynamics
$H_{OL}(j\omega)$	Open-loop linear response
$H_P(j\omega)$	Pilot linear response dynamics
H_s	Average gain response of the vehicle in PAC, [rad/(s.in)]
K_n	Remnant filter gain, [in/rad]
K_v	Pilot visual gain, [in/rad]
$L\delta_{lat}$	Lateral control term, [rad/(s ² in)]
L_p	Roll aerodynamic damping, [1/s]
$M\delta_{lon}$	Longitudinal control term, [rad/(s ² in)]
M_q	Pitch aerodynamic damping, [1/s]
n	Remnant in pilot control input, [in]
p	Rotational rate around body-x axis, [rad/s]
PM	Phase Margin, [deg]
q	Rotational rate around body-y axis, [rad/s]
RMS_e	Root mean square of displayed error, [rad]
RMS_u	Root mean square of pilot control, [in]
s	Laplace operator, [rad/s]
t	Time, [s]
T_{sim}	Simulation time, [s]
u	Pilot control input, [in]

Greek symbols

δ_{lat}	Lateral cyclic input, [in]
δ_{lon}	Longitudinal cyclic input, [in]

$\tau_{p\theta}$	Phase delay, [s]
Φ	Phase in PAC, [deg]
ϕ	Roll attitude, [deg]
φ_m	Phase Margin, [deg]
ϕ_θ	Phase in ROVER, [deg]
ω_q	Body rate frequency in ROVER, [rad/s]
θ	Pitch attitude, [deg]
τ_L	Pilot lead time constant, [s]
τ_p	Pilot time delay, [s]
σ_e^2	Variance of error, [rad ²]
σ_i^2	Variance of forcing function, [rad ²]
σ_n^2	Variance of remnant, [rad ²]
σ_u^2	Variance of pilot control input, [in ²]
ω_{180}	Phase crossover frequency [rad/s]
ω_{BW_θ}	Vehicle pitch bandwidth, [rad/s]
ω_c	Crossover frequency, [rad/s]
ω_i	Forcing function bandwidth [rad/s]
ω_{nms}	Neuromuscular system natural frequency, [rad/s]
ω_{un}	Remnant filter natural frequency, [rad/s]
ρ^2	Correlation coefficient, [-]
ζ_{nms}	Neuromuscular system damping, [-]
ζ_{un}	Remnant filter damping, [-]

Subscripts

d	Disturbance forcing function
t	Tracking forcing function
n	Remnant

ACKNOWLEDGEMENTS

The long journey to complete this thesis has been an outstanding experience. Both the scientific and the personal aspects of this period in my life have shaped me forever. Considering the duration, the multidisciplinary content and the international aspects of this journey, there are a lot of people to whom I am deeply thankful. Their academic and personal support made it possible.

This journey has initiated with the efforts of Mrs Pavel, after our first project with a Nuffic scholarship. I have learnt a lot about the rotorcraft discipline from her during my thesis. She has always supported me, and provided me different perspectives and challenges to improve myself while helping me to cope with all the tough stages of this journey. Performing SIMONA helicopter practicals, giving lectures, etc. had always been enjoyable. Also, we had the privilege to successfully complete an international EU project (i.e., ARISTOTEL project) together. I feel extremely lucky to have such a brilliant person to be involved in my academic and personal development.

When I first stepped into the Control and Simulation Division, the cybernetics discipline was a complete new field for me, and my promoter Max have helped me enormously in this alien territory. I can not thank him enough for his endless support, invaluable feedbacks and his dedication to me during this journey. Likewise, my copromoter Daan has probably spent as much time as me with this thesis, with endless reviews, brain storms, discussions, translations, etc. Without his efforts, this thesis could not see the sunlight. During my process of building up the cybernetic perspective of this thesis, I would like to specifically thank Herman Damveld and Rene van Paassen, with their priceless inputs.

I had the best opportunity to work together with awesome Ph.D. colleagues in the department. I honestly miss those times, with a lot of eye-opening discussions, fruitful sessions and a super friendly environment. I was lucky to share a flat with Laurens from the office. Jia was my 'only' colleague in the office working with rotorcraft, and we had great time together (e.g., we have been in the TU Delft magazine, twice). Actually, we had great fun with all my colleagues; Ligua, Wouter, Jamie, Thomas, Sophie, Yazdi, Dyah, Tao, and many others. With Jan Comas, I had the privilege to not only share the office, but later also worked together side-by-side in my next job after leaving the department. In the department, we had a squash group (i.e., Coen, Erik and Joost) who had taught me how to play this game. I am very thankful to their patience and continuous support, accompanying a lot of academic and personal chats. The SIMONA in the department was our 'simulator' contribution to the ARISTOTEL project, and this contribution could not be possible without the valuable help of Olaf. We have conducted a lot of test campaigns, experiments and simulator practicals with his endless support. I also had a lot of motivation from visiting friends during my stay in the department. I would like to thank Lisette for her support (e.g., bringing home-made cookies), and Ruxy for boosting my morale during her visit. To sum up, my period in the department was an excellent aca-

demic experience with the guidance of the pioneers in their fields, within a very friendly atmosphere.

The funding of this thesis was from the ARISTOTEL project, which helped me to gain a lot of international working experience in EU. I would like to thank all my colleagues in the project, from Italy, UK, Netherlands, Russia, France, Romania and Germany. It had always been a pleasure to collaborate together, and I enjoyed all project events in various countries. One particular person from this wonderful crowd requires a special recognition: Mike from Liverpool. As we have stayed in our houses when we had the simulator test campaigns in the Netherlands and UK, we had a lot of technical and personal collaborations (e.g., we happened to be the 'best man' in each others weddings). I would like to thank him again for his priceless friendship. Linghai from Liverpool also visited me in Netherlands several times, and I am so glad to have his companionship and technical discussions. Overall, ARISTOTEL project helped me to see the practical aspects of the RPC in full flight simulators with hands-on experience. I would like to thank Mrs Pavel again for introducing me into this special project.

After the thesis, while working in Sim Industries->Lockheed Martin->CAE CFT->CAE Germany, I have collected great friendships in my working environment, while I was still writing this thesis. First of all, having Hilal on my side was a blessing, since we have been friends started back in our graduate years in Turkey. We reminded ourselves the sense of humour from our homeland, and we were supporting each other in good and bad times. Guido was also another special friend from the company, who accompanied me to many metal festivals in Europe (e.g., Stockholm, Madrid, and a lot German cities). Another special friend from the company is Alexia, who had helped me a lot to see various perspectives, and we had deep brain storming sessions about the life itself. Anabel has been a wonderful friend as well, and we shared a lot of our cat-ownership issues. In the work environment, I had the chance to observe several other dimensions of the modeling and simulation fields, and many colleagues have helped me to improve my technical skills in various disciplines (e.g., flight performance, landing gear modeling, system modeling, control loading systems, team management) during the Ph.D. thesis writing period of this journey. I would like to highlight that the company management had always been supportive to provide me enough flexibility.

In the personal side, my dear wife Özlem is the person who have suffered with me during all the stages of this journey. For example, our vacations always had a flavour of my laptop for my Ph.D. work, and she did not complain once. Without her unconditional support, this thesis could never come through. In the darkest hours, during the most chaotic times (e.g., while changing job, house, country), her moral boost kept me going. She has patiently reviewed, discussed, and commented on almost every part of the thesis. I truly believe she deserves the title as much as I do. Her personal support is not possible to put into words. I can not even begin to think how to thank her enough.

This thesis is dedicated to her.

My family have provided their support in all these years. During my visits to them, I often worked in the balcony during the night, and always a plate with a piece of cake with the best wishes was coming in the middle of the night. Whenever in doubt, they always knew the right words to say, and helped me to continue in all though times. I would like to thank my family for being always on my side. Same for my parents-in-

law, for their continuous support in these years. As a part of my family in Netherlands, I would like mention the contribution(!) of our cats: Kediman (R.I.P) and Çirkin. They actually jeopardize the Ph.D. thesis writing process by simply laying on my lap while I was writing the thesis, but also accompanied me during long busy nights.

I consider my dear friends Deniz and Banu as a part of my family too. Their support is priceless. Since they are from the academic world, their ideas and reviews had been very valuable. When I needed a place to work on my thesis, they opened their house countless times. Moreover, during the transition period to our house, we (i.e., me, Özlem, our turtle Paşa and our cat Çirkin) have been staying in their house together for months, and yet still feeling at home. I can not describe how much I appreciate their support.

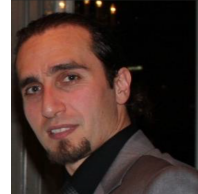
During this journey, one of my main distractions was attending to metal festivals for couple of days to clear my mind. I want to mention here that in these years, I have collected invaluable friendships with strong bonds. I can not name them all but some special ones I want to thank for joining me: Laura, Magchiel, Pascal, Arthur, Deb, all my Dutch tribe members, Nathalie, Eline, Seb, Franzi, Julie, Barth, Jas, Sam, Basak, Oliver, Guido, Manu, Hagen, Laura (Gr), Konnie, Michail, Chris, Dona, Stef, etc. Travelling, camping, BBQ, headbanging, and listening to music in huge crowds in isolated landscapes had been a wonderful experience with these friends, and it helped me to refresh my mind during this journey.

Deniz Yılmaz

Maastricht, October 2018

CIRRICULUM VITAE

Deniz Yılmaz was born on April 26, 1980 in Samsun, Turkey. He studied in Yomra Fen Lisesi (Scientific High School) in Trabzon, Turkey, and in 1999 he enrolled as a student at the Faculty of Aerospace Engineering at the Middle East Technical University (METU) in Ankara, Turkey. As a part of his Aerospace Engineering studies, he performed an internship on the Elastomeric Articulation helicopter rotor hubs at 5th Main Maintenance Command Centre, where full spectrum maintenance, modernization, ground and flight testing of the complete helicopter fleet of the Turkish Army is performed. During his last two years of Bachelor studies, he worked as a software developer of the Sikorsky S-70 and the Bell AB-206 helicopter simulators, in Gate Elektronik.



After his graduation, in 2005 he started his M.Sc. studies on the 'Evaluation and Comparison of Helicopter Simulation Models with Different Fidelities', which has been granted by the TUBITAK (The Scientific and Technological Research Council of Turkey). During his first year of M.Sc. studies, he also worked as a certified flight simulator developer and operator for Cessna C-172S FNPTII (Flight Navigation and Procedure Trainer) in Sindel Aviation Flight Academy. During his M.Sc. studies, he has also participated in several part-time jobs in both helicopter and simulation fields, such as development of a real-time Stability Augmentation algorithm for a big scale rotorcraft UAV, and flight model enhancement for Sikorsky S70-A Black Hawk level-D simulators.

In 2008 he started his Ph.D. research at the Faculty of Aerospace Engineering at Delft University of Technology (TU Delft), granted with a Nuffic HSP scholarship (the Dutch organisation for internationalisation in education). His research project, with the title 'Increasing Safety of Helicopter Operations', involved investigating new Handling Qualities criteria focusing on vibrational loads and rotorcraft performance. After one year of the research, he had to return to Turkey for the mandatory military service that lasts six months, and the Nuffic scholarship could not continue to support the Ph.D. research afterwards. After the military service, in March 2010 he started to work as a lead research engineer in the MODSIMMER (Modeling and Simulation Research Centre) in METU, with his project on developing a multi-purpose simulator with a motion base (i.e., configurable simulation base and cockpit to be used for land, air and marine vehicle simulations). In December 2010, he has started his Ph.D. project in TU Delft, in the ARISTOTEL (Aircraft and Rotorcraft Pilot Couplings - Tools and Techniques for Alleviation and Detection) project, which is an EU 7th Framework program. His research, as described in this thesis, involved the development of an objective method (i.e., a cybernetic approach) for assessing rotorcraft handling qualities and adverse rotorcraft pilot couplings based on measurements of human operators' manual control behaviour.

In 2015 he has started to work in the Flight Simulation Division of the US defence company Lockheed Martin (LM) in Sassenheim, The Netherlands, as a software engineer on flight performance and system design for level-D Boeing 787 flight simulators. A year later Canadian simulation and training company CAE acquired this LM division, and he continued on working in level-D Citation-M2 simulator, as a team leader for ancillary system design and development. After completing the Citation-M2 project, he worked as a product owner/team leader for the Boeing 737 control loading development project in the same company. In January 2018, Deniz started to work in CAE Elektronik GmbH in Stolberg, Germany, as a software developer. He is currently involved in a project with Eurocopter EC-135 helicopter simulators.

PUBLICATIONS

19. M.D.Pavel, D.Yilmaz, M. Jump, L. Lu, et al., *Practices to identify and prevent adverse aircraft-and-rotorcraft-pilot couplings—A ground simulator perspective*, Journal Progress in Aerospace Sciences, volume 77, 54-87, 2015.
18. M.D.Pavel, D.Yilmaz, M. Jump, L. Lu, et al., *Practices to identify and preclude adverse Aircraft-and-Rotorcraft-Pilot Couplings – A design perspective*, Journal Progress in Aerospace Sciences, volume 76, 55-89, 2015.
17. L. Lu, D.Yilmaz, M. Jump., et al., *Comparison of Simulator Platform and Flight Tasks on Adverse Rotorcraft Pilot Coupling Prediction*, 70th AHS (American Helicopter Society) Conference, Montreal, Canada, 2014.
16. M.D.Pavel, D.Yilmaz, B. D. Vu, M. Jump., L. Lu, M. Jones, *Adverse Rotorcraft Pilot Couplings-Modeling and Prediction of Rigid Body RPC*, 39th European Rotorcraft Forum, Moscow, Russia, 2013. [Selected as 'The Best Paper', achieved the Cheeseman Award, and re-presented in the 70th AHS Conference, Montreal, Canada, 2014.]
15. D.Yilmaz, M. Jones, B. D. Vu, *Rotorcraft Pilot Coupling Susceptibility Accompanying Handling Qualities Prospects In Preliminary Rotorcraft Design*, 39th European Rotorcraft Forum, Moscow, Russia, 2013.
14. M. Jump, L. Lu, M. Jones, D.Yilmaz, et al., *Exposing Rotorcraft Pilot Couplings Using Flight Simulation*, 39th European Rotorcraft Forum, Moscow, Russia, 2013.
13. M.D.Pavel, D.Yilmaz, M. Jump, L. Lu, et al., *Adverse Rotorcraft Pilot Couplings-Past, Present and Future Challenges*, Journal Progress in Aerospace Sciences, volume 62, 1-51, 2013.
12. D.Yilmaz, M.D.Pavel, M.Jones, M. Jump, L. Lu, *Identification of Pilot Control Behavior During Possible Rotorcraft Pilot Coupling Events*, 38th European Rotorcraft Forum, Amsterdam, Netherlands, 2012.
11. S.Suliman, D.Yilmaz, M.D.Pavel, *Harmonizing Real-Time Oscillation Verifier (Rover) With Handling Qualities Assessment For Enhanced Rotorcraft Pilot Couplings Detection*, 38th European Rotorcraft Forum, Amsterdam, Netherlands, 2012.
10. J.Venrooij, D.Yilmaz, M.D.Pavel, G.Quaranta, M. Jump, M. Mulder, *Measuring Biodynamic Feedthrough in Helicopters*, 37th European Rotorcraft Forum, Gallarate, Italy, 2011.
9. B.van der Meer, D.Yilmaz, J.A.A.M Stoop, M.D.Pavel, *Helicopter Safety: A contradiction in terms? An overview of the status at the beginning of the 21st century*, 37th European Rotorcraft Forum, Gallarate, Italy, 2011.
8. D.Yilmaz, A.Yilmaz, A.M. Senyigit, B.K. Gorur, V.Isler, *Development of a Multi-Purpose Generic Research Simulator*, Ulusal Savunma Uygulamaları Modelleme ve Simülasyon Konferansı USMOS (National Modeling and Simulation Symposium),Ankara, Turkey, June 2011

7. I. Yavrucuk, D.Yilmaz, O. Tarimci, *A New Helicopter Simulation and Analysis Tool: HeliDYN+*, 36th European Rotorcraft Forum, Paris France, 2010 .
6. D.Yilmaz, M.D. Pavel,İ. Yavrucuk, *Helicopter Design for Handling Qualities Enhancements*, 35th European Rotorcraft Forum, Hamburg Germany, 2009.
5. D.Yilmaz, I. Yavrucuk, M.D. Pavel, *Development of Complementary Helicopter Handling Qualities Criteria Based on Performance and Vibratory Loads*, 5th Ankara International Aerospace Conference (AIAC), Ankara, August 2009.
4. D.Yilmaz, I. Yavrucuk, O. Tarimci, *A low cost flight simulator using virtual reality tools*, AIAA Modeling and Simulation Technologies Conference, Chicago, August 2009.
3. O. Tarimci, D.Yilmaz, Yavrucuk, I., *On the Level of Center of Gravity Modeling Error in Neural Network Based Adaptive Controller Design*, 34th European Rotorcraft Forum, Liverpool, UK, 2008.
2. D.Yilmaz, O.Uzol, I. Yavrucuk, *Simulation of Helicopter Dynamics in Engine Related Emergency Scenarios*, applied to 64th AHS Forum, April 29 - May 1 2008.
1. D.Yilmaz, Dr. I. Yavrucuk, *Development of a flight dynamics model for a UH-1H helicopter simulator*, Ankara International Aerospace Conference (AIAC), September 2007.

ገገገገ

ISBN 978-94-6186-966-1



9 789461 869661